

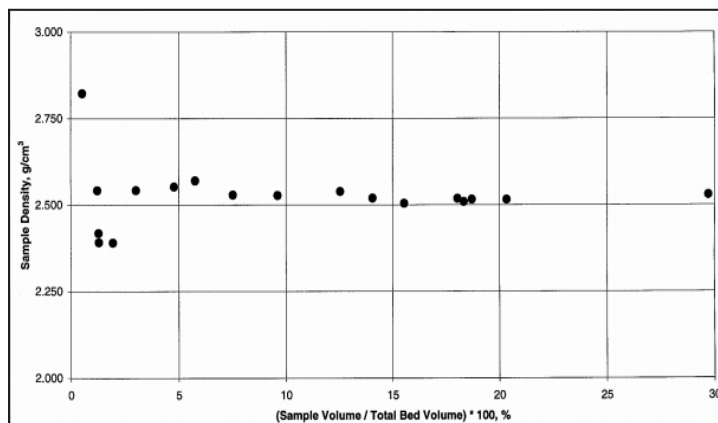
New Capability for the GeoPyc Makes Visible the Percent of the DryFlo Bed Occupied by the Sample

If too little sample is used with the GeoPyc® Envelope Density Analyzer, poor reproducibility of results will occur. The instrument is simply unable to distinguish between a DryFlo® bed with sample and one without sample when the sample volume occupies too small a percentage of the total bed. For optimum performance, the sample should occupy a minimum of 20% of the DryFlo bed. A larger percentage of sample is preferable as long as it can be surrounded sufficiently by DryFlo. To make the sample percent visible, Micromeritics has incorporated into version 2.00 of the GeoPyc software a calculation for the percent of bed volume occupied by the sample.

Utilizing this capability requires that each sample cell be calibrated without DryFlo or sample to determine the “zero bed” volume. This information is stored internally and thereafter the percent sample volume is reported with each analysis. The operator can then use this number to optimize the quantity of sample necessary to meet a specific reproducibility criteria.

The table and graph shows the typical effect of sample quantity on the reproducibility of results. The sample used in this example was composed of varying quantities of nonporous glass spheres 6 mm in diameter. The analyses were conducted using a 25.4-mm diameter sample cell. The absolute density of the spheres was 2.5202 g/cm³ as measured by Micromeritics' AccuPyc 1330. Being nonporous, the envelope density of the spheres was also 2.5202 g/cm³. As shown, this value is achieved within 1% when the sample occupies more than 7.5% of the total bed volume. Other materials will exhibit similar behavior but may not follow this exact pattern.

| % Sample Volume | Envelope Density | % Error |
|-----------------|------------------|---------|
| 0.537 | 2.8223 | +11.99 |
| 1.228 | 2.5416 | +0.85 |
| 1.284 | 2.4177 | -4.07 |
| 1.299 | 2.3913 | -5.11 |
| 1.944 | 2.3903 | -5.15 |
| 3.012 | 2.5419 | +0.86 |
| 4.782 | 2.5518 | +1.25 |
| 5.761 | 2.5699 | +1.97 |
| 7.523 | 2.5288 | +0.34 |
| 9.616 | 2.5269 | +0.27 |
| 12.547 | 2.5386 | +0.73 |
| 14.063 | 2.5193 | -0.04 |
| 15.538 | 2.5041 | -0.64 |
| 18.039 | 2.5184 | -0.07 |
| 18.335 | 2.5089 | -0.45 |
| 18.706 | 2.5155 | -0.19 |
| 20.333 | 2.5153 | -0.19 |
| 29.708 | 2.5289 | +0.35 |



Attaining Envelope Density Reproducibility and Accuracy with Your GeoPyc

This application note contains guidelines for attaining reproducible and accurate envelope density measurements with your GeoPyc®.

Reproducibility

Achieving high reproducibility in any analytical measurement often requires performing tests in an identical manner using a single instrument, fixed instrument parameters, and the same quantity of test material. This is particularly true with the GeoPyc technique because it is very sensitive to procedural variations and deviations in test parameters. Reproducibility of results of approximately $\pm 1.0\%$ can be expected when parameters are controlled to the fullest extent possible. A description of these parameters and the criteria that must be observed to achieve this level are described below.

Envelope density is calculated from specimen mass and envelope volume, that is, volume including both open and closed pores. This volume is measured using a non-intruding, free-flowing, dry powder medium called DryFlo®, which is confined in a cylindrical sample chamber having one of five diameters from 12.7mm (0.5 in.) to 50.8 mm (2.0 in.). The volume of the specimen is determined by subtracting the volume of consolidated DryFlo (blank run) in a sample chamber from the volume of the same consolidated DryFlo in the same chamber with the specimen included (test run). The medium bed is agitated through rotation and vibration, and the consolidation force is gradually increased to the same set value in both phases of a test.

1. The first criterion for a GeoPyc analysis is that the DryFlo consolidate identically in the blank and test runs. Repeated testing of the medium alone has shown that, almost without exception, it actually consolidates with a reproducibility of $\pm 0.34\%$ or better in all size sample chambers for bed depths of one-half to twice the chamber diameter. Somewhat better reproducibility of $\pm 0.25\%$ is typically achieved when the bed depth is restricted to approximately the chamber diameter. In any event, between one-third and one-quarter of the minimal overall error of $\pm 1.0\%$ is due to the nonideal behavior of DryFlo.

Guideline 1. Start an analysis with a DryFlo bed depth a little less than the chamber diameter.

2. Sample quantity plays the most significant role in reproducibility. Obviously, the specimen extracted from a larger quantity of material must be of sufficient quantity to be representative of the whole. The quantity of sample determines the minimum sample chamber size required for analysis. A chamber should be selected in which the sample constitutes a minimum of 20% of the total sample-plus DryFlo volume when consolidated. A larger percentage of sample is preferable; however, keep in mind that the sample must always be surrounded sufficiently by DryFlo.

Every envelope density result is derived from the difference in two volumes, the consolidated DryFlo and the consolidated DryFlo with sample. That difference should be as large as possible simply for mathematical significance.

For example, in one series of tests on a typical granular product where the product volume relative to the bed volume was varied from 6.9 to 41.7%, there was almost a 9.0% variability in envelope density. At the highest percentage, the sample quantity may have been sufficient for bridging of sample pieces to interfere with medium consolidation. At the lower percentage, small errors in consolidation were magnified in the difference value. However, the envelope volume within a $\pm 1.3\%$ error band was registered when the sample volume ranged from 30 to 35%. The current program for the GeoPyc automatically calculates the sample volume percentage. This percentage is a useful guide to optimum performance and should always be considered when assessing the validity of results.

Guideline 2. Select sample chamber dimensions, DryFlo volume, and specimen quantity to yield a sample volume percentage of at least 20%.

3. The error band was reduced to $\pm 0.95\%$ when another series of tests was run with the material used in the above guideline and both DryFlo and sample weights were held constant to the third decimal place. The reported sample-to-bed volume varied only between 32.1 and 33.4% in this case. Such control is not practical or even feasible in many instances, but this technique should be considered when possible.

Guideline 3. Maintain constant all parameters susceptible to control for optimum reproducibility.

4. Both the blank and test steps of an envelope density determination consist of an equal number of preparation and analysis cycles.

Preparation cycles are unrecorded, repetitious, agitation and consolidation attempts intended to orient the DryFlo grains and the specimen into a uniformly mixed bed. Analysis cycles follow the preparation cycles and yield statistical information on consolidated volumes. The bed is expected to become more and more consolidated during the preparation cycles, but little or no consistent increase or decrease in value should be evident in the analysis cycles. Diminishing information can be gleaned once the cycles exceed a certain number. The results presented above were primarily obtained with 10 preparation and 5 analysis cycles. Some specimens require more, but fewer are adequate in other cases; 10 preparation and 5 analysis cycles are good starting numbers.

Guideline 4. Choose the number of preparation and analysis cycles such that little or no consistent increase or decrease in value is revealed by the recorded data.

Accuracy

Make sure you follow the guidelines for reproducibility described earlier in this application note. Those guidelines must be followed, in conjunction with the guidelines listed below, to produce accurate envelope density measurements.

1. Sample shape influences GeoPyc results, but the effect cannot be rigorously quantified because shape itself is subject to infinite variation. The GeoPyc handles this problem by calibration. Two calibration values for each sample chamber, referred to as conversion factors, are noted in the operator's manual included with the GeoPyc.

The first conversion factor (calculated factor) is simply derived from geometry and mechanical couplings and relates the plunger movement to chamber volume as if there were no sample shape influence. The second factor (adjusted factor) is modified to include an average shape influence experimentally determined from many different shapes. Neither is likely to apply precisely to any particular specimen. True calibration for shape can be achieved only when the predetermined envelope density of a representative specimen of the material in question is used.

The representative specimen preferably is one from an evaluation procedure that was being followed before GeoPyc introduction. GeoPyc results can be expected then to track prior records. A completely nonporous specimen of the same shape as the material in question affords a degree of calibration but, because it is nonporous, cannot have the same surface texture and cannot be as satisfactory. Because in the final analysis the GeoPyc operates best as a comparison device, there is no real substitute for a truly representative specimen for calibration. A GeoPyc user should set aside enough of the selected calibration material to be able to recheck the calibration from time to time.

Guideline 1. Select for calibration a quantity of the material in question and determine its envelope density by the prior test procedure or some other method.

2. Calibration itself will only be reproducible to the degree the guidelines given earlier for reproducibility are followed. Accordingly, the weight of the representative sample, the quantity of DryFlo, and the sample chamber size should be selected on the basis of the amount of sample to be used later.

Also, all calibration tests should be made with the same consolidation force and the same number of preparation and test cycles to be used in analyses.

Guideline 2. Conduct calibration tests using parameters identical to those to be used in analyses.

3. Finally, a number of calibration tests should be made and the median selected as the conversion factor.

Guideline 3. Use the median value from a number of calibration tests as the conversion factor for the material to be analyzed.

Optimize Free-Space Correction for Low Surface Area Samples Using the Gemini Analyzer

The unique balanced measurement method used in the Gemini permits small amounts of surface area to be measured with nitrogen gas that otherwise would be measurable only with krypton. Low surface area samples often displace many times more nitrogen than they adsorb, especially if composed of low-density materials of large particle size. The standard, built-in, helium free-space difference measurement and mathematical compensation routine typically can remove the effects of more than 99% of this sample displacement, but the small amount remaining uncompensated can still be significant.

A technique for adding a compensating volume with negligible surface area into the balance tube has been developed. It can reduce the size of the initial imbalance to low levels and allow precise measurement of adsorbed gas. Either straight-wall or bulbous sample tubes may be used. Hanging filler rods are recommended but not required.

1. Load the sample tube with an appropriate quantity of sample.

2. Load the balance tube with glass beads that have a total volume approximately the same as the sample volume.

a. Determine the volume (v) of the sample in cm^3 :

$$v = w \div \rho$$

Where:

w = mass of sample (g)

ρ = density of sample (g/cm^3); if density is unknown, refer to your laboratory handbook

b. Determine the number (n) of glass beads needed to equal the sample volume:

$$n = v \div 0.014 \text{ cm}^3$$

Where:

0.014 cm^3 = approximate volume of one bead

3. Outgas the sample in the sample tube at an appropriate temperature for an appropriate amount of time.
4. Install the sample tube (containing the outgassed sample) onto the analysis port and the balance tube (containing the glass beads) onto the balance port. Use hanging filler rods for best results.
5. Set up the Gemini for a one-point measurement ($P/P_0 = 0.05$ to 0.1) so that the initial free-space measurement can quickly be determined; then perform the measurement.

$$\frac{\text{free space cm}^3 \times 2.515 \text{ g/cm}^3}{3.53} = \text{mass of glass beads (g)}$$

6. Using the “measured free space” absolute value and the following relationship, determine the mass of glass beads to remove from (or add to) the balance tube to reduce the free-space imbalance:

Where:

2.515 g/cm^3 = density of glass beads

3.53 = thermal correction (no units)

Note that the volume of one glass bead is approximately 0.014 cm^3 . Therefore, if the measured free space is less than 0.02 cm^3 , it is unnecessary to correct the free space.

APPLICATION NOTE 112

7. Use a beaker of warm water to bring the balance tube to room temperature before removing it from the balance port of the Gemini to remove (or add) glass beads. This prevents condensation of moisture from the laboratory atmosphere onto the cold glass beads.

8. Remove the balance tube:

- If the measured free space is negative (-), add the calculated mass of glass beads into the balance tube.

- If the measured free space is positive (+), remove the calculated mass of glass beads from the balance tube.
9. Reinstall the balance tube onto the balance port of the Gemini analyzer and proceed with the analysis.

For subsequent samples of the same material, you may simply use the same weight of sample that was used for the initial sample so that the original bead quantity may be left undisturbed on the balance port.

The Effect of Particle Size on the Manufacture of Chocolate Products



The taste and texture of chocolate candies and cakes depend to a great extent on the particle size of the ingredients used to make them. Chocolate manufacturers characterize their products by what they describe as “mouth feel.” If the product is too coarse, the taste testers describe the product as tasting “gritty.” If the product is made too fine, the end product may be described as “sticky.”

Particle size analysis can place numerical parameters on these descriptions and use it to guide the chocolate producers in their efforts to make the best consumer-acceptable product.

In this study, we purchased three different commercially available chocolate products to see what sort of variations

in particle size might occur. The three products tested were of increasingly more expensive offerings from a typical “chocolate candy bar” to a block of “higher grade” chocolate.

The chocolate was extracted with ethanol and then analyzed with a Saturn DigiSizer® 5200. Figure 1 shows the results of this analysis. The particle size distribution curve seen in this figure shows three distinct and separate size distributions. These samples were also involved in a “blind” taste test. The taste test results ranked the chocolate with the finest size distribution as having the best taste and “mouth feel.” The other two samples were ranked in the same order as the particle size distributions with the coarsest size distribution having the least appealing taste.

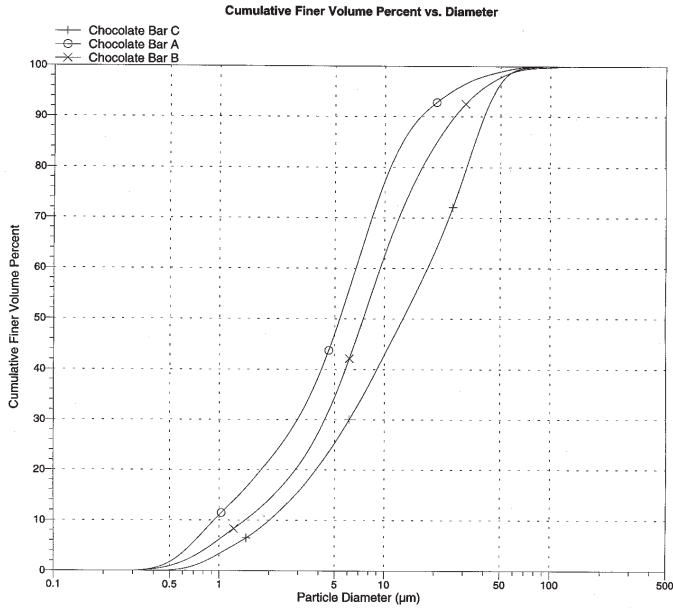


Figure 1. Three different chocolate types analyzed under the same conditions

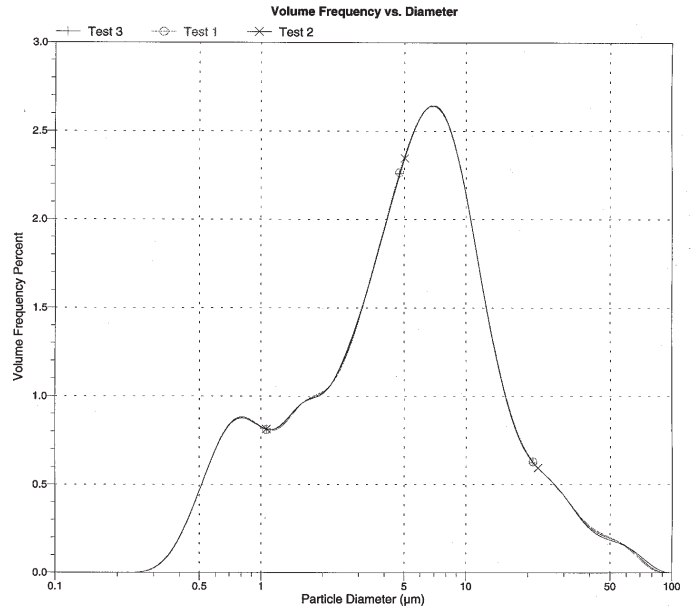


Figure 2. Three different tests of the same chocolate sample

Also of interest is the repeatability of the particle size analysis results. Figure 2 shows the results of three analyses of one of the chocolates. The results from these three analyses overlay each other so completely that it is hard to see that there are three different plots.

In conclusion, it has been shown that manufacturers of chocolate products may use particle size analysis to assist them in the production of the chocolate product they desire. This can be done with consistency and reliability from location to location when the particle size analysis is determined using the Saturn DigiSizer.

Acid Site Characterization of H⁺ Y (SiO₂/Al₂O₃:80/1): A Pulse Chemisorption and TPD Application for the AutoChem

The Brønsted acidity of zeolites and other catalysts is of keen interest, as this affects the kinetics of reactions. Characterization of these sites is consequently very important and is often performed according to the ASTM D 4824 ammonia chemisorption method. An alternative, but comparable, characterization method involves pulse chemisorption of propylamines followed by a temperature-programmed desorption (TPD) combined with a mass spectrometry analysis of propylene (see Figure 1). A complete characterization analysis can be performed using the AutoChem analyzer with the mass spectrometer and vapor generator accessories.

Materials

The zeolite used in this application contained hydrogen cations and had a silica-to-alumina ratio of 60:1. Isopropylamine (> 99.5% GC) and propylamine (> 99.0% GC) were used, separately, as reagents. Propylene (> 99%) was also used for calibration purposes.

Preparation

A Y zeolite sample can contain various cations, including ammonium and hydrogen. Cations in these compounds can be converted into hydrogen cations by means of a temperature ramp. The sample was activated first by heating to 500 °C at 10 °C/min in an inert helium environment, then cooling to 200 °C, the analysis temperature.

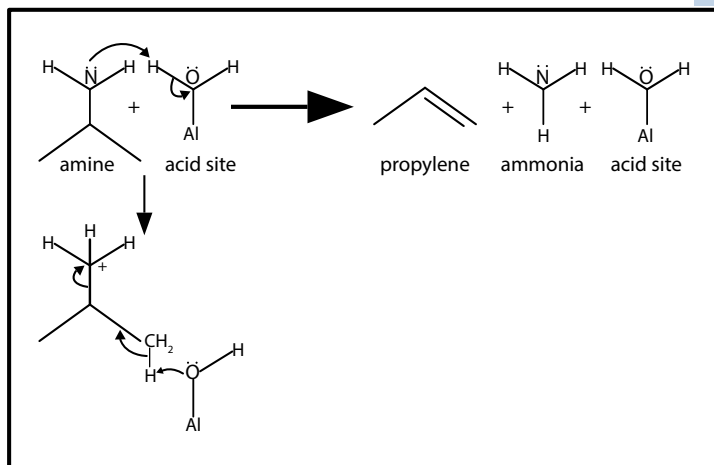


Figure 1. The amine reacts with acid sites to decompose into propylene and ammonia via a mechanism analogous to Hofmann Elimination.

Analysis

The activation of the Y zeolite was followed by pulse chemisorption. During this step, ten injections of propylamine vapor were dosed onto the sample (to ensure the sample was saturated) by means of an inert gas, helium, flowing through a 5-cm³ loop. The last part of the analysis involved a temperature-programmed desorption (TPD). At this step in the analysis, the mass spectrometer began scanning for propylene, the product of interest. Data were collected during a temperature ramp from 200 °C to 500 °C

APPLICATION NOTE 147

Data

To obtain quantitative data, the mass spectrometer must be calibrated by injecting a known volume of the gas to be detected (propylene), V_{cal} , through the septum with a high-precision syringe. The peak area of the mass spectrometer signal can be obtained using the AutoChem peak-editing software. To increase the accuracy of the calibration, injections may be made until peaks are similar in area. The areas can then be averaged to give a general conversion factor between mass spectrometer peak area and actual gas volume, allowing for the acidity of zeolites to be calculated. Figure 2 gives an example of this procedure.

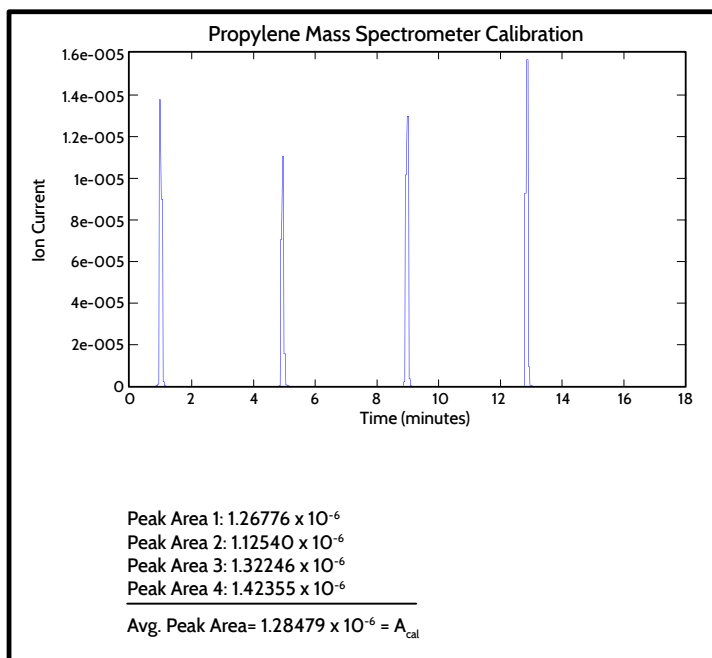


Figure 2. Example of mass spectrometer signal during an area-volume calibration.

Additionally, Figures 3 and 4 show that a thermal conductivity detection method includes residual amine and ammonia from the chemisorption, whereas mass spectrometer detection isolates the propylene signal, allowing the concentration of acid sites to be calculated.

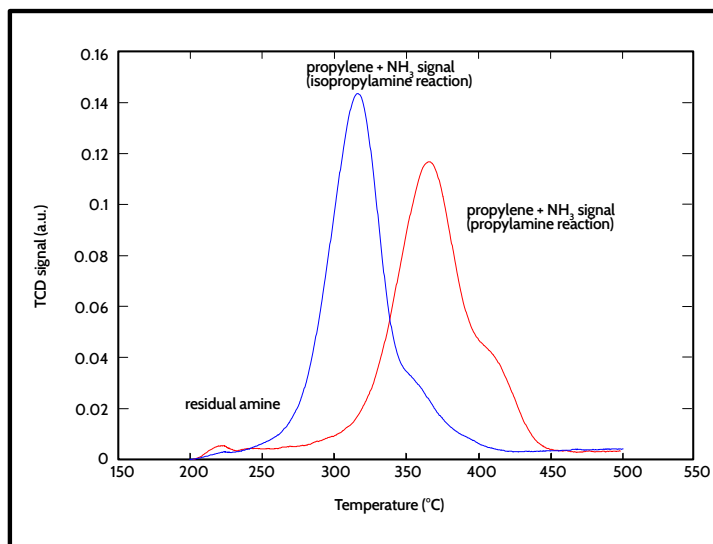


Figure 3. Thermal conductivity data from the AutoChem.

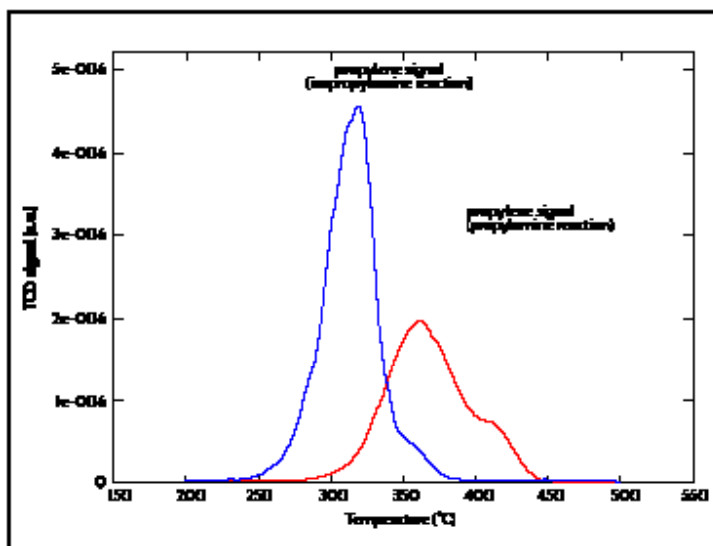


Figure 4. Mass spectrometer peak results.

After obtaining the peak area by integration of the propylene signal from Figure 4, A_{pms} , the acid site concentration, N_{as} , can be calculated as follows:

$$N_{as} = A_{pms} \left(\frac{V_{cal}}{A_{cal}} \right) \left(\frac{L}{10^3 cc} \right) \left(\frac{\text{mole}}{22.414 L @ STP} \right) \left(\frac{10^6 \mu\text{moles}}{\text{mole}} \right)$$

Below are calculated values that correspond to the data in Figure 4. The concentration values are expressed in units of micromoles of acid sites per gram of zeolite characterized.

$$N_{as}^{\text{isopropylamine}} = 676.31 \mu\text{moles/g}$$

$$N_{as}^{\text{propylamine}} = 448.00 \mu\text{moles/g}$$

Acid Site Characterization of H⁺ Y (SiO₂/Al₂O₃:80/1): A Pulse Chemisorption and TPD Application for the AutoChem

The Brønsted acidity of zeolites and other catalysts is of keen interest, as this affects the kinetics of reactions. Characterization of these sites is consequently very important and is often performed according to the ASTM D 4824 ammonia chemisorption method. An alternative, but comparable, characterization method involves pulse chemisorption of propylamines followed by a temperature-programmed desorption (TPD) combined with a mass spectrometry analysis of propylene (see Figure 1). A complete characterization analysis can be performed using the AutoChem analyzer with the mass spectrometer and vapor generator accessories.

Materials

The zeolite used in this application contained hydrogen cations and had a silica-to-alumina ratio of 80:1. Isopropylamine (>99.5% GC) and propylamine (>99.0% GC) were used, separately, as reagents. Propylene (>99%) was also used for calibration purposes.

Preparation

A Y zeolite sample can contain various cations, including ammonium and hydrogen. Cations in these compounds can be converted into hydrogen cations by means of a temperature ramp. The sample was activated first by heating to 500 °C at 10 °C/min in an inert helium environment, then cooling to 200 °C, the analysis temperature.

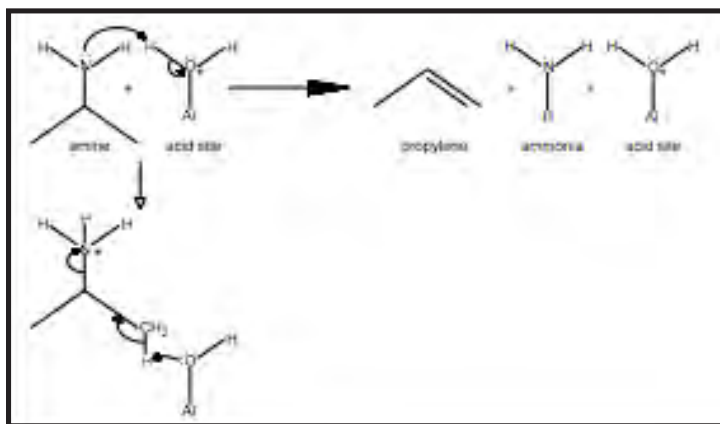


Figure 1. The amine reacts with acid sites to decompose into propylene and ammonia via a mechanism analogous to Hofmann Elimination.

Analysis

The activation of the Y zeolite was followed by pulse chemisorption. During this step, ten injections of propylamine vapor were dosed onto the sample (to ensure the sample was saturated) by means of an inert gas, helium, flowing through a 5-cm³ loop. The last part of the analysis involved a temperature-programmed desorption (TPD). At this step in the analysis, the mass spectrometer began scanning for propylene, the product of interest. Data were collected during a temperature ramp from 200 °C to 500 °C.

Data

To obtain quantitative data, the mass spectrometer must be calibrated by injecting a known volume of the gas to be detected (propylene), V_{cal}, through the septum with a high-precision syringe. The peak area of the mass spectrometer signal can be obtained using the AutoChem peak-editing software. To increase the accuracy of the calibration, injections may be made until peaks are similar in area. The areas can then be averaged to give a general conversion factor between mass spectrometer peak area and actual gas volume, allowing for the acidity of zeolites to be calculated. Figure 2 gives an example of this procedure.

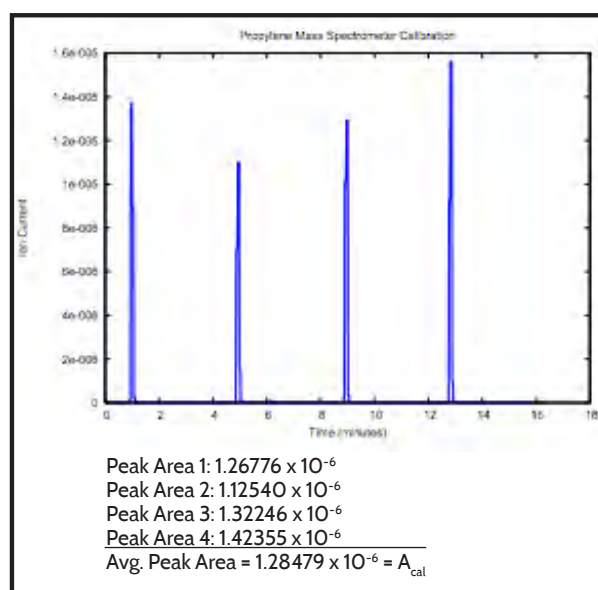


Figure 2. Example of mass spectrometer signal during an area-volume calibration.

APPLICATION NOTE 147

Additionally, Figures 3 and 4 show that a thermal conductivity detection method includes residual amine and ammonia from the chemisorption, whereas mass spectrometer detection isolates the propylene signal, allowing the concentration of acid sites to be calculated.

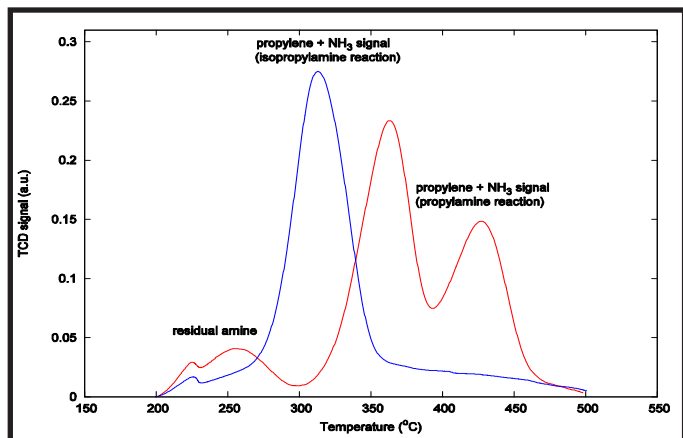


Figure 3. Thermal conductivity data from the AutoChem.

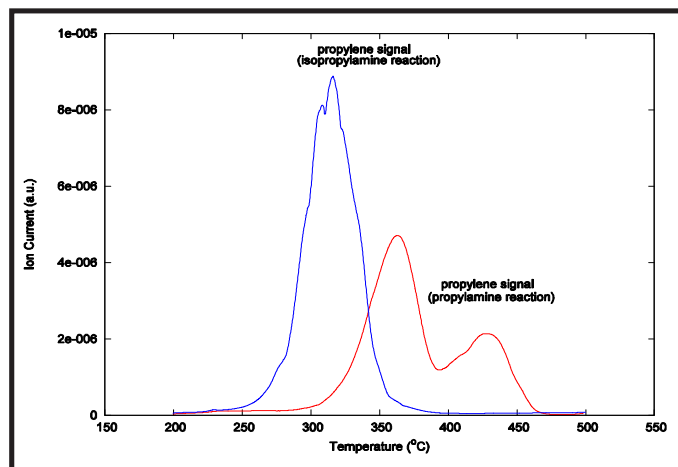


Figure 4. Mass spectrometer peak results.

After obtaining the peak area by integration of the propylene signal from Figure 4, A_{pms} , the acid site concentration, N_{as} , can be calculated as follows:

$$N_{as} = A_{pms} \left(\frac{V_{cal}}{A_{cal}} \right) \left(\frac{L}{10^3 cc} \right) \left(\frac{mole}{22.414 L @ STP} \right) \left(\frac{10^6 \mu moles}{mole} \right)$$

Below are calculated values that correspond to the data in Figure 4. The concentration values are expressed in units of micromoles of acid sites per gram of zeolite characterized.

$$N_{as}^{isopropylamine} = 241.67 \mu moles/g$$

$$N_{as}^{propylamine} = 164.61 \mu moles/g$$

Acid Site Characterization of H⁺ β (SiO₂/Al₂O₃:75/1): A Pulse Chemisorption and TPD Application for the AutoChem

The Brønsted acidity of zeolites and other catalysts is of keen interest, as this affects the kinetics of reactions. Characterization of these sites is consequently very important and is often performed according to the ASTM D 4824 ammonia chemisorption method. An alternative, but comparable, characterization method involves pulse chemisorption of propylamines followed by a temperature-programmed desorption (TPD) combined with a mass spectrometry analysis of propylene (see Figure 1). A complete characterization analysis can be performed using the AutoChem analyzer with the mass spectrometer and vapor generator accessories.

Materials

The zeolite used in this application contained hydrogen cations and had a silica-to-alumina ratio of 75:1. Isopropylamine (>99.5% GC) and propylamine (>99.0% GC) were used, separately, as reagents. Propylene (>99%) was also used for calibration purposes.

Preparation

A Beta zeolite sample can contain various cations, including ammonium and hydrogen. Cations in these compounds can be converted into hydrogen cations by means of a temperature ramp. The sample was activated first by heating to 500 °C at 10 °C/min in an inert helium environment, then cooling to 200 °C, the analysis temperature.

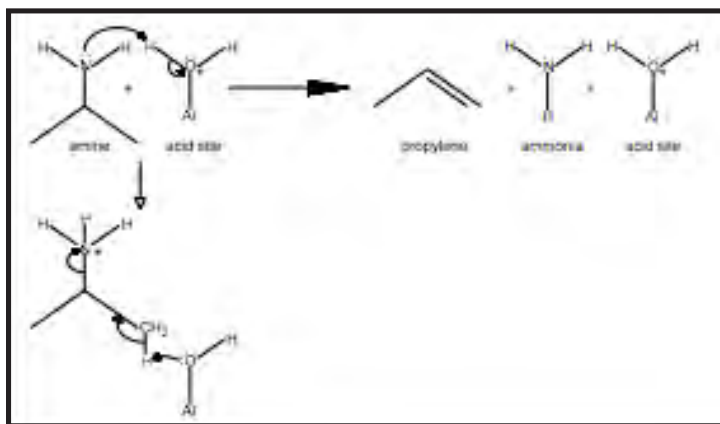


Figure 1. The amine reacts with acid sites to decompose into propylene and ammonia via a mechanism analogous to Hofmann Elimination.

Analysis

The activation of the Beta zeolite was followed by pulse chemisorption. During this step, ten injections of propylamine vapor were dosed onto the sample (to ensure the sample was saturated) by means of an inert gas, helium, flowing through a 5-cm³ loop. The last part of the analysis involved a temperature-programmed desorption (TPD). At this step in the analysis, the mass spectrometer began scanning for propylene, the product of interest. Data were collected during a temperature ramp from 200 °C to 500 °C.

Data

To obtain quantitative data, the mass spectrometer must be calibrated by injecting a known volume of the gas to be detected (propylene), V_{cal}, through the septum with a high-precision syringe. The peak area of the mass spectrometer signal can be obtained using the AutoChem peak-editing software. To increase the accuracy of the calibration, injections may be made until peaks are similar in area. The areas can then be averaged to give a general conversion factor between mass spectrometer peak area and actual gas volume, allowing for the acidity of zeolites to be calculated. Figure 2 gives an example of this procedure.

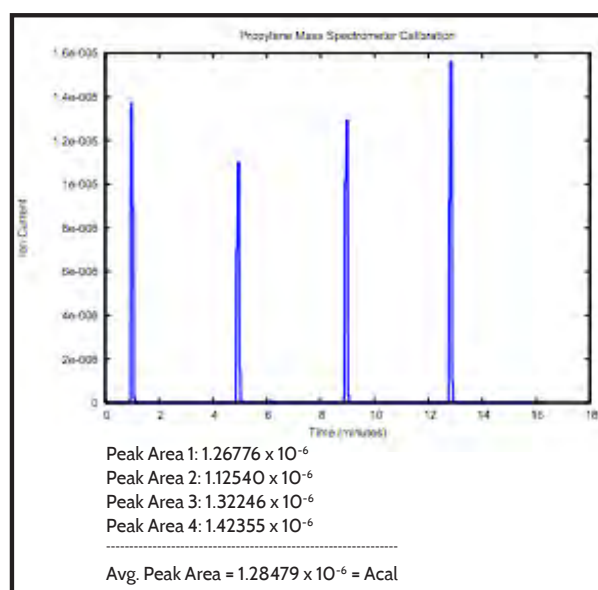


Figure 2. Example of mass spectrometer signal during an area-volume calibration.

APPLICATION NOTE 148

Additionally, Figures 3 and 4 show that a thermal conductivity detection method includes residual amine and ammonia from the chemisorption, whereas mass spectrometer detection isolates the propylene signal, allowing the concentration of acid sites to be calculated.

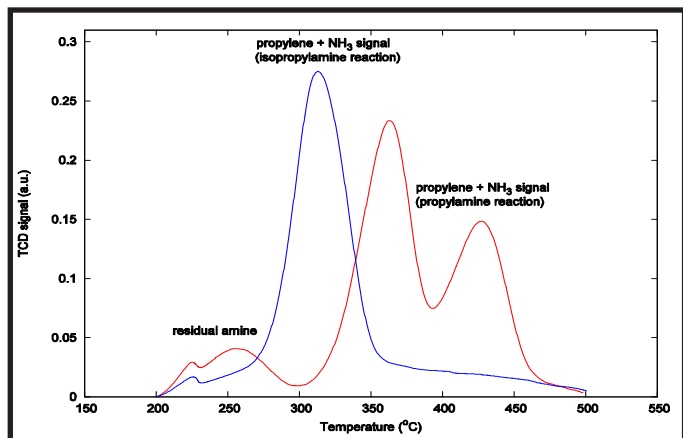


Figure 3. Thermal conductivity data from the AutoChem.

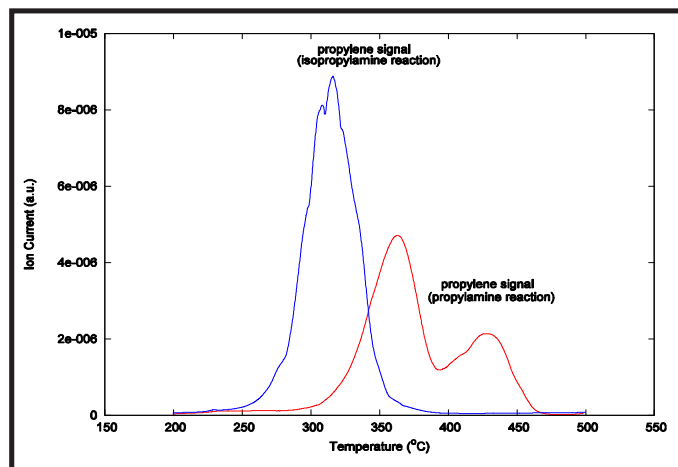


Figure 4. Mass spectrometer peak results.

After obtaining the peak area by integration of the propylene signal from Figure 4, A_{pms} , the acid site concentration, N_{as} , can be calculated as follows:

$$N_{as} = A_{pms} \left(\frac{V_{cal}}{A_{cal}} \right) \left(\frac{L}{10^3 cc} \right) \left(\frac{\text{mole}}{22.414 L @ STP} \right) \left(\frac{10^6 \mu\text{moles}}{\text{mole}} \right)$$

$$N_{as}^{\text{isopropylamine}} = 999.57 \mu\text{moles/g}$$

$$N_{as}^{\text{propylamine}} = 907.23 \mu\text{moles/g}$$

Acid Site Characterization of NH₄⁺ ZSM-5 (SiO₂/Al₂O₃:30/1): A Pulse Chemisorption and TPD Application for the AutoChem

The Brønsted acidity of zeolites and other catalysts is of keen interest, as this affects the kinetics of reactions. Characterization of these sites is consequently very important and is often performed according to the ASTM D 4824 ammonia chemisorption method. An alternative, but comparable, characterization method involves pulse chemisorption of propylamines followed by a temperature programmed desorption (TPD) combined with a mass spectrometry analysis of propylene (see Figure 1). A complete characterization analysis can be performed using the AutoChem analyzer with the mass spectrometer and vapor generator accessories.

Materials

The zeolite used in this application contained hydrogen cations and had a silica-to-alumina ratio of 30:1. Isopropylamine (>99.5% GC) and propylamine (>99.0% GC) were used, separately, as reagents. Propylene (>99%) was also used for calibration purposes.

Preparation

A ZSM-5 sample can contain various cations, including ammonium and hydrogen. Cations in these compounds can be converted into hydrogen cations by means of a temperature ramp. The sample was activated first by heating to 500 °C at 10 °C/min in an inert helium environment, then cooling to 200 °C, the analysis temperature.

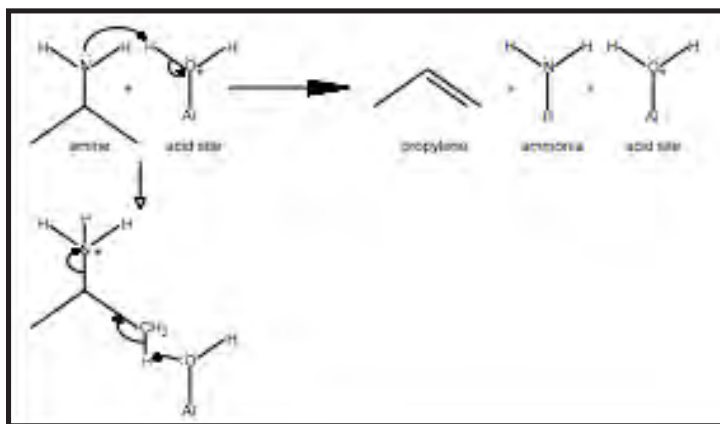


Figure 1. The amine reacts with acid sites to decompose into propylene and ammonia via a mechanism analogous to Hofmann Elimination.

Analysis

The activation of the ZSM-5 was followed by pulse chemisorption. During this step, ten injections of propylamine vapor were dosed onto the sample (to ensure the sample was saturated) by means of an inert gas, helium, flowing through a 5-cm³ loop. The last part of the analysis involved a temperature-programmed desorption (TPD). At this step in the analysis, the mass spectrometer began scanning for propylene, the product of interest. Data were collected during a temperature ramp from 200 °C to 500 °C.

Data

To obtain quantitative data, the mass spectrometer must be calibrated by injecting a known volume of the gas to be detected (propylene), V_{cal}, through the septum with a high-precision syringe. The peak area of the mass spectrometer signal can be obtained using the AutoChem peak-editing software. To increase the accuracy of the calibration, injections may be made until peaks are similar in area. The areas can then be averaged to give a general conversion factor between mass spectrometer peak area and actual gas volume, allowing for the acidity of zeolites to be calculated. Figure 2 gives an example of this procedure.

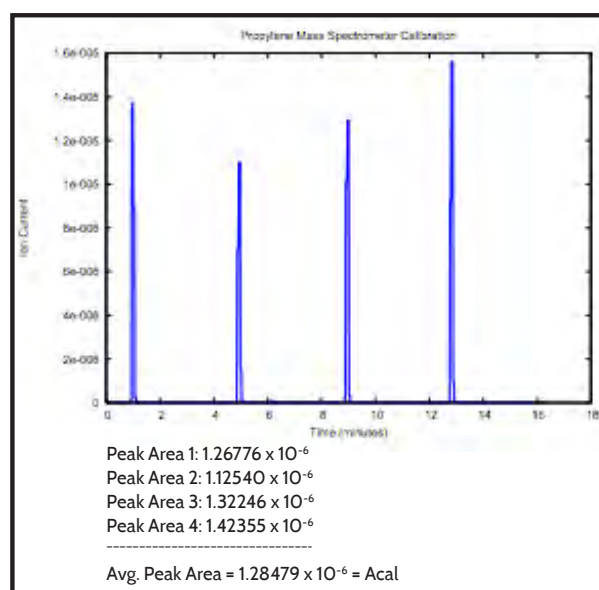


Figure 2. Example of mass spectrometer signal during an area-volume calibration.

APPLICATION NOTE 149

Additionally, Figures 3 and 4 show that a thermal conductivity detection method includes residual amine and ammonia from the chemisorption, whereas mass spectrometer detection isolates the propylene signal, allowing the concentration of acid sites to be calculated.

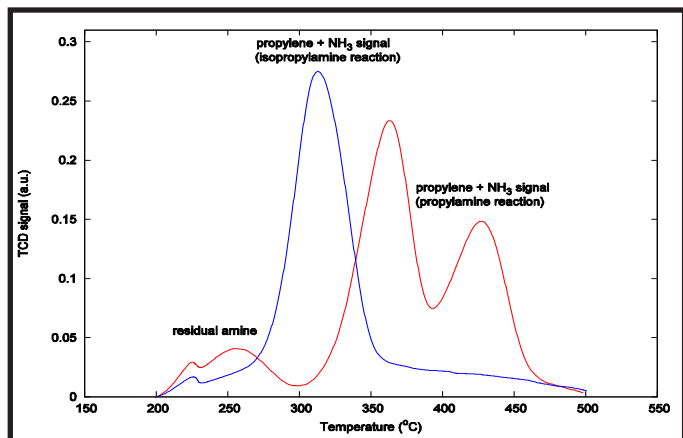


Figure 3. Thermal conductivity data from the AutoChem.

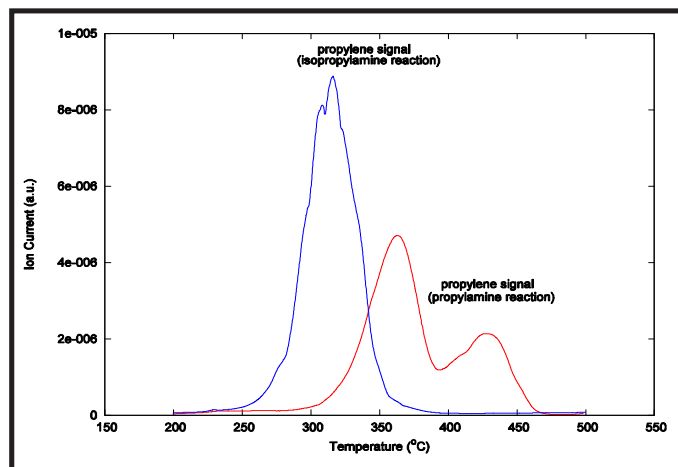


Figure 4. Mass spectrometer peak results.

After obtaining the peak area by integration of the propylene signal from Figure 4, A_{pms} , the acid site concentration, N_{as} , can be calculated as follows:

$$N_{as} = A_{pms} \left(\frac{V_{cal}}{A_{cal}} \right) \left(\frac{L}{10^3 cc} \right) \left(\frac{\text{mole}}{22.414 L @ STP} \right) \left(\frac{10^6 \mu\text{moles}}{\text{mole}} \right)$$

$$N_{as}^{\text{isopropylamine}} = 1384.36 \mu\text{moles/g}$$

$$N_{as}^{\text{propylamine}} = 1050.06 \mu\text{moles/g}$$

Acid Site Characterization of NH₄⁺ ZSM-5 (SiO₂/Al₂O₃:50/1): A Pulse Chemisorption and TPD Application for the AutoChem

The Brønsted acidity of zeolites and other catalysts is of keen interest, as this affects the kinetics of reactions. Characterization of these sites is consequently very important and is often performed according to the ASTM D 4824 ammonia chemisorption method. An alternative, but comparable, characterization method involves pulse chemisorption of propylamines followed by a temperature-programmed desorption (TPD) combined with a mass spectrometry analysis of propylene (see Figure 1). A complete characterization analysis can be performed using the AutoChem analyzer with the mass spectrometer and vapor generator accessories.

Materials

The zeolite used in this application contained hydrogen cations and had a silica-to-alumina ratio of 50:1. Isopropylamine (> 99.5% GC) and propylamine (>99.0%GC) were used, separately, as reagents. Propylene (>99%) was also used for calibration purposes.

Preparation

A ZSM-5 sample can contain various cations, including ammonium and hydrogen. Cations in these compounds can be converted into hydrogen cations by means of a temperature ramp. The sample was activated first by heating to 500 °C at 10 °C/min in an inert helium environment, then cooling to 200 °C, the analysis temperature.

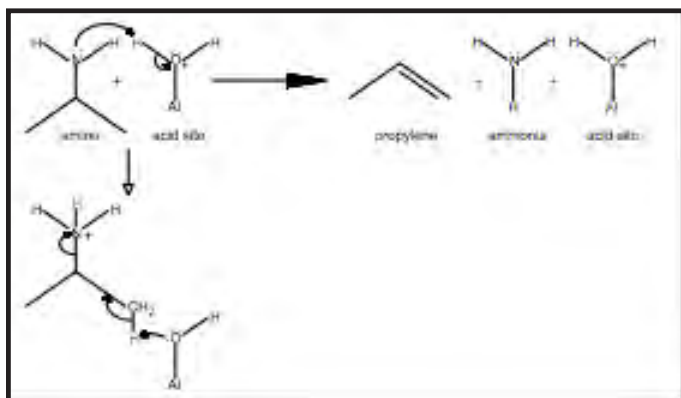


Figure 1. The amine reacts with acid sites to decom- pose into propylene and ammonia via a mechanism analogous to Hofmann Elimination.

Analysis

The activation of the ZSM-5 was followed by pulse chemisorption. During this step, ten injections of propylamine vapor were dosed onto the sample (to ensure the sample was saturated) by means of an inert gas, helium, flowing through a 5-cm³ loop. The last part of the analysis involved a temperature-programmed desorption (TPD). At this step in the analysis, the mass spectrometer began scanning for propylene, the product of interest. Data were collected during a temperature ramp from 200 °C to 500 °C.

Data

To obtain quantitative data, the mass spectrometer must be calibrated by injecting a known volume of the gas to be detected (propylene), V_{cal}, through the septum with a high-precision syringe. The peak area of the mass spectrometer signal can be obtained using the AutoChem peak-editing software. To increase the accuracy of the calibration, injections may be made until peaks are similar in area. The areas can then be averaged to give a general conversion factor between mass spectrometer peak area and actual gas volume, allowing for the acidity of zeolites to be calculated. Figure 2 gives an example of this procedure.

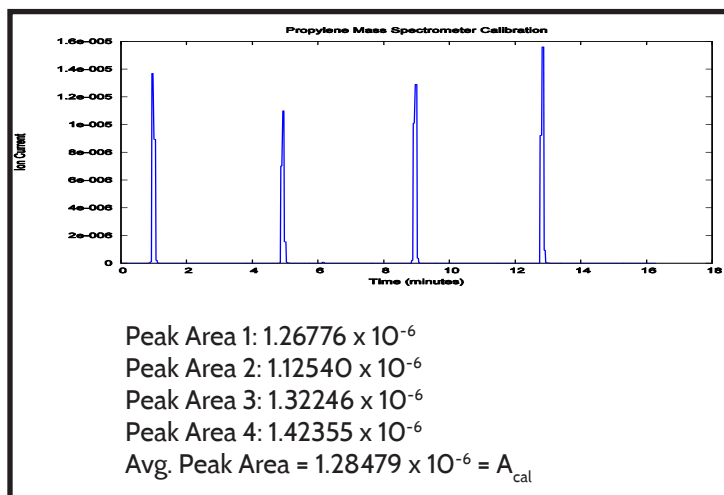


Figure 2. Example of mass spectrometer signal during an area-volume calibration.

APPLICATION NOTE 150

Additionally, Figures 3 and 4 show that a thermal conductivity detection method includes residual amine and ammonia from the chemisorption, whereas mass spectrometer detection isolates the propylene signal, allowing the concentration of acid sites to be calculated.

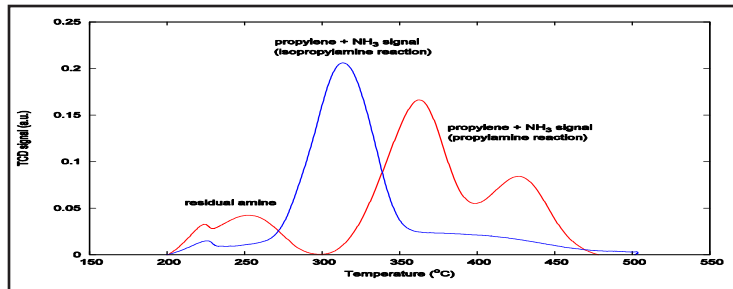


Figure 3. Thermal conductivity data from the AutoChem.

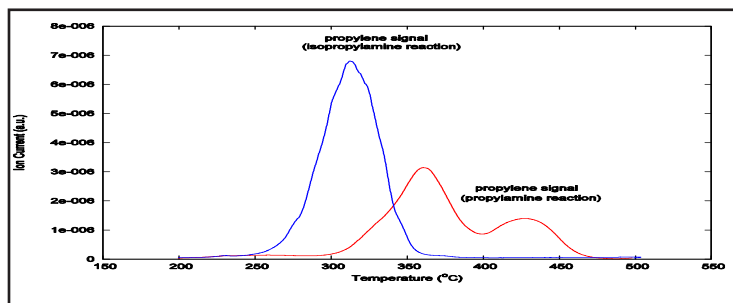


Figure 4. Mass spectrometer peak results.

After obtaining the peak area by integration of the propylene signal from Figure 4, A_{pms} , the acid site concentration, N_{as} , can be calculated as follows:

$$N_{as} = A_{pms} \left(\frac{V_{cal}}{A_{cal}} \right) \left(\frac{L}{10^3 \text{ cc}} \right) \left(\frac{\text{mole}}{22.414 \text{ L@STP}} \right) \left(\frac{10^6 \mu\text{moles}}{\text{mole}} \right)$$

Below are calculated values that correspond to the data in Figure 4. The concentration values are expressed in units of micromoles of acid sites per gram of zeolite characterized.

$$N_{as}^{\text{isopropylamine}} = 106.17 \mu\text{moles/g}$$

$$N_{as}^{\text{propylamine}} = 759.32 \mu\text{moles/g}$$

Acid Site Characterization of NH_4^+ ZSM-5 ($\text{SiO}_2/\text{Al}_2\text{O}_3:80/1$): A Pulse Chemisorption and TPD Application for the AutoChem

The Brønsted acidity of zeolites and other catalysts is of keen interest, as this affects the kinetics of reactions. Characterization of these sites is consequently very important and is often performed according to the ASTM D 4824 ammonia chemisorption method. An alternative, but comparable, characterization method involves pulse chemisorption of propylamines followed by a temperature-programmed desorption (TPD) combined with a mass spectrometry analysis of propylene (see Figure 1). A complete characterization analysis can be performed using the AutoChem analyzer with the mass spectrometer and vapor generator accessories.

Materials

The zeolite used in this application contained hydrogen cations and had a silica-to-alumina ratio of 80:1. Isopropylamine (>99.5% GC) and propylamine (>99.0% GC) were used, separately, as reagents. Propylene (>99%) was also used for calibration purposes.

Preparation

A ZSM-5 sample can contain various cations, including ammonium and hydrogen. Cations in these compounds can be converted into hydrogen cations by means of a temperature ramp. The sample was activated first by heating to 500 °C at 10 °C/min in an inert helium environment, then cooling to 200 °C, the analysis temperature.

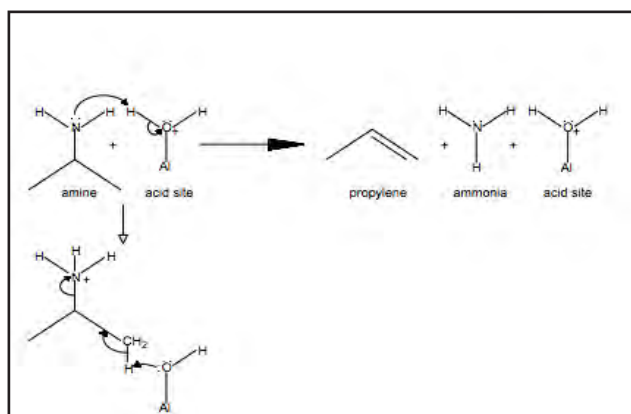


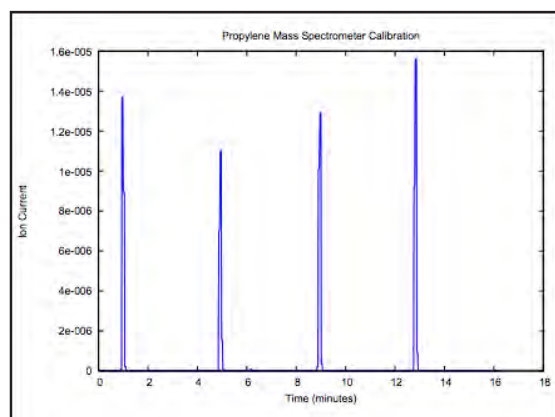
Figure 1. The amine reacts with acid sites to decompose into propylene and ammonia via a mechanism analogous to Hofmann Elimination.

Analysis

The activation of the ZSM-5 was followed by pulse chemisorption. During this step, ten injections of propylamine vapor were dosed onto the sample (to ensure the sample was saturated) by means of an inert gas, helium, flowing through a 5-cm³ loop. The last part of the analysis involved a temperature-programmed desorption (TPD). At this step in the analysis, the mass spectrometer began scanning for propylene, the product of interest. Data were collected during a temperature ramp from 200 °C to 500 °C.

Data

To obtain quantitative data, the mass spectrometer must be calibrated by injecting a known volume of the gas to be detected (propylene), V_{cal} , through the septum with a high-precision syringe. The peak area of the mass spectrometer signal can be obtained using the AutoChem peak-editing software. To increase the accuracy of the calibration, injections may be made until peaks are similar in area. The areas can then be averaged to give a general conversion factor between mass spectrometer peak area and actual gas volume, allowing for the acidity of zeolites to be calculated. Figure 2 gives an example of this procedure.



Peak Area 1: 1.26776×10^{-6}
 Peak Area 2: 1.12540×10^{-6}
 Peak Area 3: 1.32246×10^{-6}
 Peak Area 4: 1.42355×10^{-6}

Avg. Peak Area = $1.28479 \times 10^{-6} = A_{\text{cal}}$

Figure 2. Example of mass spectrometer signal during an area-volume calibration.

APPLICATION NOTE 151

Additionally, Figures 3 and 4 show that a thermal conductivity detection method includes residual amine and ammonia from the chemisorption, whereas mass spectrometer detection isolates the propylene signal, allowing the concentration of acid sites to be calculated.

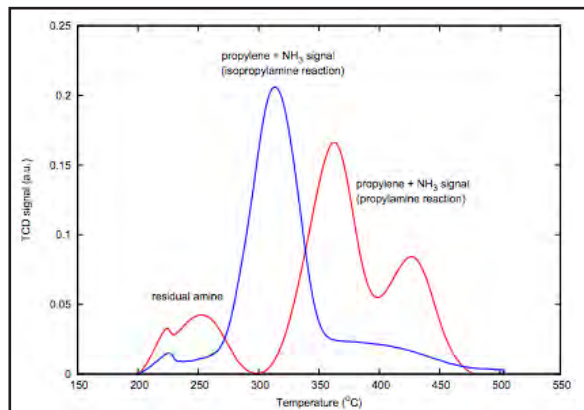


Figure 3. Thermal conductivity data from the AutoChem.

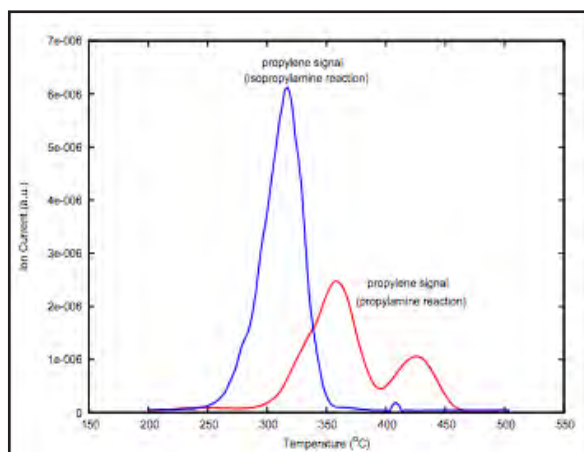


Figure 4. Mass spectrometer peak results.

After obtaining the peak area by integration of the propylene signal from Figure 4, A_{pms} , the acid site concentration, N_{as} , can be calculated as follows:

$$N_{as} = A_{pms} \left(\frac{V_{cal}}{A_{cal}} \right) \left(\frac{L}{10^3 cc} \right) \left(\frac{\text{mole}}{22.414 L @ STP} \right) \left(\frac{10^6 \mu\text{moles}}{\text{mole}} \right)$$

Below are calculated values that correspond to the data in Figure 4. The concentration values are expressed in units of micromoles of acid sites per gram of zeolite characterized.

$$N_{as}^{\text{isopropylamine}} = 841.88 \mu\text{moles/g}$$

$$N_{as}^{\text{propylamine}} = 583.26 \mu\text{moles/g}$$

Acid Site Characterization of NH₄⁺ ZSM-5 (SiO₂/Al₂O₃:280/1): A Pulse Chemisorption and TPD Application for the AutoChem

The Brønsted acidity of zeolites and other catalysts is of keen interest, as this affects the kinetics of reactions. Characterization of these sites is consequently very important and is often performed according to the ASTM D 4824 ammonia chemisorption method. An alternative, but comparable, characterization method involves pulse chemisorption of propylamines followed by a temperature-programmed desorption (TPD) combined with a mass spectrometry analysis of propylene (see Figure 1). A complete characterization analysis can be performed using the AutoChem analyzer with the mass spectrometer and vapor generator accessories.

Materials

The zeolite used in this application contained hydrogen cations and had a silica-to-alumina ratio of 280:1. Isopropylamine (>99.5% GC) and propylamine (>99.0%GC) were used, separately, as reagents. Propylene (>99%) was also used for calibration purposes.

Preparation

A ZSM-5 sample can contain various cations, including ammonium and hydrogen. Cations in these compounds can be converted into hydrogen cations by means of a temperature ramp. The sample was activated first by heating to 500 °C at 10 °C/min in an inert helium environment, then cooling to 200 °C, the analysis temperature.

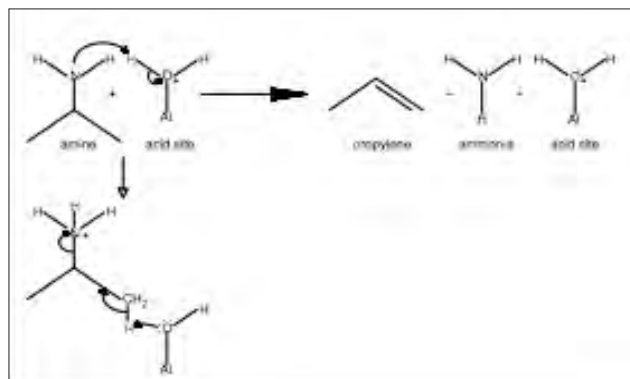


Figure 1. The amine reacts with acid sites to decompose into propylene and ammonia via a mechanism analogous to Hofmann Elimination.

Analysis

The activation of the ZSM-5 was followed by pulse chemisorption. During this step, ten injections of propylamine vapor were dosed onto the sample (to ensure the sample was saturated) by means of an inert gas, helium, flowing through a 5-cm³ loop. The last part of the analysis involved a temperature-programmed desorption (TPD). At this step in the analysis, the mass spectrometer began scanning for propylene, the product of interest. Data were collected during a temperature ramp from 200 °C to 500 °C.

Data

To obtain quantitative data, the mass spectrometer must be calibrated by injecting a known volume of the gas to be detected (propylene), Vcal, through the septum with a high-precision syringe. The peak area of the mass spectrometer signal can be obtained using the AutoChem peak-editing software. To increase the accuracy of the calibration, injections may be made until peaks are similar in area. The areas can then be averaged to give a general conversion factor between mass spectrometer peak area and actual gas volume, allowing for the acidity of zeolites to be calculated. Figure 2 gives an example of this procedure.

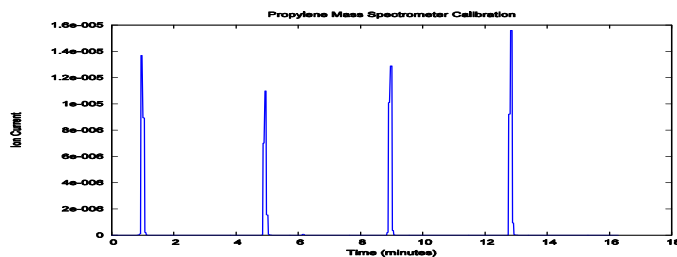


Figure 2. Example of mass spectrometer signal during an area-volume calibration.

APPLICATION NOTE 152

Additionally, Figures 3 and 4 show that a thermal conductivity detection method includes residual amine and ammonia from the chemisorption, whereas mass spectrometer detection isolates the propylene signal, allowing the concentration of acid sites to be calculated.

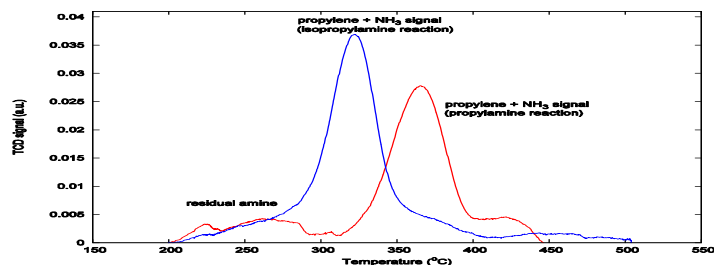


Figure 3. Thermal conductivity data from the AutoChem.

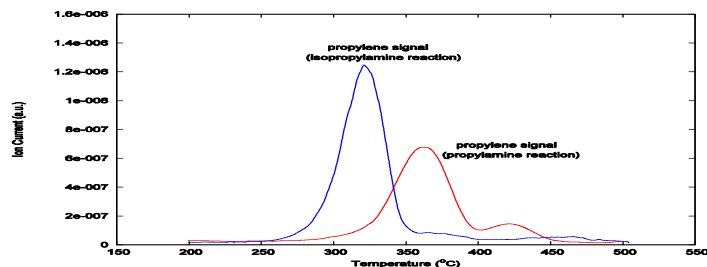


Figure 4. Mass spectrometer peak results.

After obtaining the peak area by integration of the propylene signal from Figure 4, A_{pms} , the acid site concentration, N_{as} , can be calculated as follows:

$$N_{as} = A_{pms} \left(\frac{V_{cal}}{A_{cal}} \right) \left(\frac{L}{10^3 cc} \right) \left(\frac{\text{mole}}{22.414 L @ STP} \right) \left(\frac{10^6 \mu\text{moles}}{\text{mole}} \right)$$

Below are calculated values that correspond to the data in Figure 4. The concentration values are expressed in units of micromoles of acid sites per gram of zeolite characterized.

$$N_{as}^{\text{isopropylamine}} = 152.86 \mu\text{moles/g}$$

$$N_{as}^{\text{propylamine}} = 119.93 \mu\text{moles/g}$$

The Measurement of Pharmaceutical Lubricants Using the TriStar II Krypton Option

A major advantage for using the TriStar II with the Krypton Option is the ability to measure low surface areas. Although the TriStar II standard nitrogen system can measure surface areas as low as 0.01 m²/g, the Krypton Option enables you to measure areas as low as 0.001 m²/g and provides increased accuracy for materials under 1.0 m²/g. Krypton is also useful for analyzing materials that are difficult to sample or have very low density; pharmaceutical lubricants, for example.



resulting in increased error. Normally for materials with low surface areas, the amount of material is maximized in order to increase this difference ($V_i - V_e$). Unfortunately this approach has an upper limit depending on the size of the sample tube and the physical properties of the material. Another approach is to use an alternate analysis gas.

Krypton is an excellent choice for low surface area measurements. Nitrogen at 77 K has a saturation pressure of 760 torr, whereas krypton has a saturation pressure of only 2.5 torr. Since pressure is proportional to the number of moles or molecules in a set volume*, there are ~ 300 molecules of nitrogen for every 1 molecule of krypton. When the quantity adsorbed is significantly small, lowering the amount of molecules present by a factor of 300 substantially reduces the amount of error.

Advantages of Using Krypton

Isotherms are collected by measuring the amount of gas adsorbed by a material over a range of pressures at a constant temperature. The quantity of gas adsorbed by a material is determined by taking the original quantity of gas dosed into a tube (V_i) and subtracting the amount of gas remaining in the tube after equilibrium is reached (V_e). For materials with low surface areas, the difference between the original amount of gas and the amount remaining after equilibrium ($V_i - V_e$) can be substantially small and difficult to measure,

Analysis Parameters

Pharmaceutical lubricants are added to reduce the friction between a tablet and the process utilized to shape the tablets. Calcium, magnesium, and sodium stearates are typical pharmaceutical lubricants and have been chosen for analysis using the Krypton Option since they can be difficult to measure

| | |
|--------------------|---|
| Test Amount | ~ 0.3 gram of each material; less than this amount produced too much variability. |
| Preparation | Degassed for 48 hours at ~ 25 °C. USP method <846> suggests outgassing magnesium stearate for two hours at 40 °C; however, a lower temperature for a longer amount of time was utilized for all materials to minimize temperature damage to the materials and to ensure that all impurities were removed. |
| Free Space | Measured |
| Relative Pressures | 0.05 to 0.15 |
| Equilibration | Relative pressure of 1.0 with an equilibration interval of 10 seconds |
| Backfill | Start of analysis only; not at conclusion |

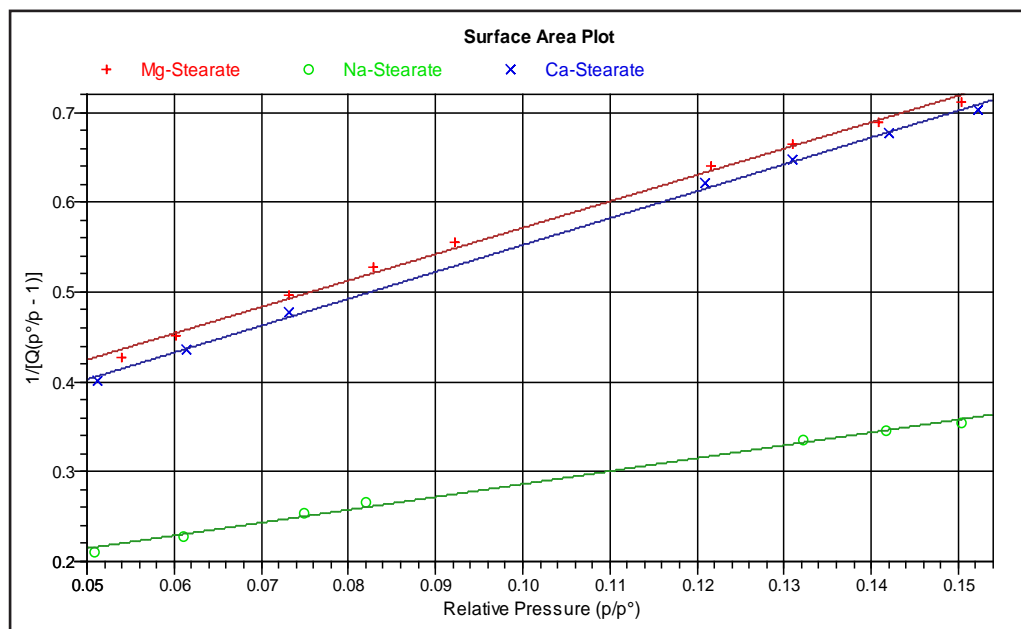
*Liquid nitrogen temperatures; a non-ideality factor must be used for Krypton.

APPLICATION NOTE 153

Analysis Results

Surface area for the three stearates was determined using the BET multipoint analysis. One of the advantages of the TriStar II unit is the ability to run three analyses concurrently. The results for all tests are shown below. Also shown are BET plots for one of the tests.

| Test | Surface Area (m ² /g) | | |
|--------------------|----------------------------------|---------|---------|
| | MMC | Lactose | Gelatin |
| 1 | 1.7862 | 3.7979 | 1.7444 |
| 2 | 1.7597 | 3.9357 | 1.8402 |
| 3 | 1.7487 | 3.5191 | 1.8051 |
| 4 | 1.8089 | 3.6376 | 1.9575 |
| 5 | 1.7891 | 3.4044 | 2.0575 |
| 6 | 1.8865 | 3.7537 | 2.3472 |
| Average | 1.7965 | 3.6747 | 1.9587 |
| Standard Deviation | 0.0491 | 0.1940 | 0.2210 |



The Measurement of Pharmaceutical Binders Using the TriStar II Krypton Option

The TriStar II's Krypton Option can measure materials with surface areas as low as 0.001 m²/g and is ideal for difficult-to-measure pharmaceutical binders. Pharmaceutical binders such as micro-crystalline methylcellulose (MMC), lactose, and gelatin typically have surface areas under 2 m²/g and, therefore, are perfect candidates for krypton adsorption with the TriStar II analyzer.



order to increase this difference ($V_i - V_e$). Unfortunately this approach has an upper limit depending on the size of the sample tube and the physical properties of the material. Another approach is to use an alternate analysis gas.

Krypton is an excellent choice for low surface area measurements. At 77 K, nitrogen has a saturation pressure of 760 torr, whereas krypton has a saturation pressure of only 2.5 torr. Since pressure is proportional to the number of moles or molecules in a set volume*, there are ~ 300 molecules of nitrogen for every 1 molecule of krypton. When the quantity adsorbed is significantly small, lowering the amount of molecules present by a factor of 300 substantially reduces the amount of error.

Advantages of Using Krypton

Isotherms are collected by measuring the amount of gas adsorbed by a material over a range of pressures at a constant temperature. The quantity of gas adsorbed by a material is determined by taking the original quantity of gas dosed into a tube (V_i) and subtracting the amount of gas remaining in the tube after equilibrium is reached (V_e). For materials with low surface areas, the difference between the original amount of gas and the amount remaining after equilibrium ($V_i - V_e$) will be small and difficult to measure accurately, resulting in increased error. Normally for materials with low surface areas, the amount of material is maximized in

Analysis Parameters

USP method <846> Specific Surface is based on low-temperature gas adsorption and the BET surface area calculation. The relative pressure (P/P_0) range used for the isotherms for this testing was restricted to 0.05 < P/P_0 < 0.15. USP <846> also calls for a correlation coefficient (or goodness of fit) larger than 0.9975. All of the data presented meet this criteria.

| | |
|--------------------|--|
| Test Amount | ~ 0.3 gram of each material |
| Preparation | Degassed for 48 hours at ~ 40 °C. Subsequent degassing performed for two hours at 40 °C. |
| Free Space | Measured |
| Relative Pressures | 0.05 to 0.3 (results taken from 0.05 to 0.15) |
| Equilibration | Relative pressure of 1.0 with an equilibration interval of 10 seconds |
| Backfill | Start of analysis only; not at conclusion |

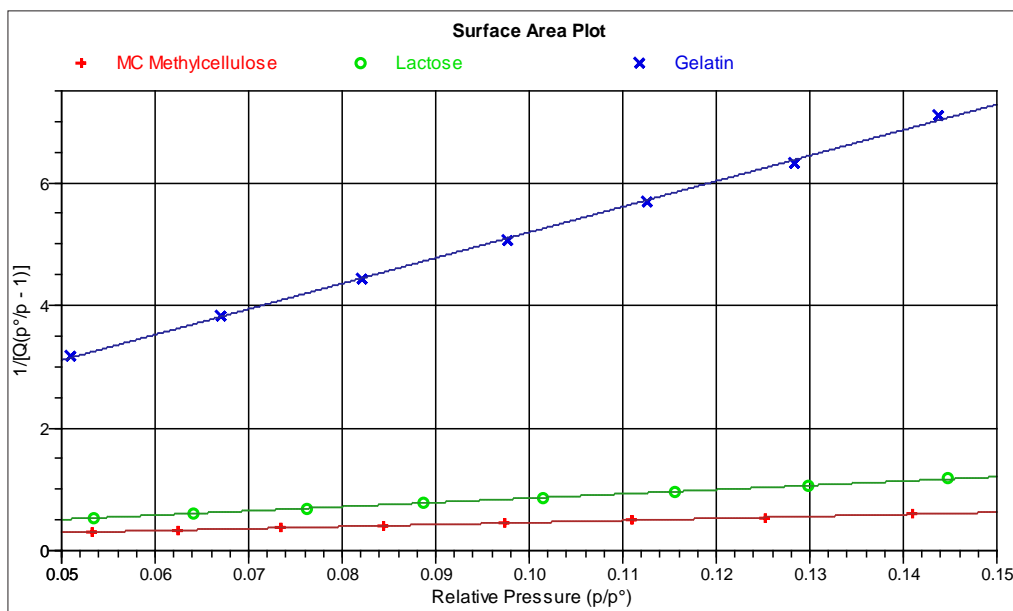
*At liquid nitrogen temperatures, a non-ideality factor must be used for krypton.

APPLICATION NOTE 154

Analysis Results

Surface area for the three samples was determined using the BET multipoint analysis. The results for all tests are shown below. Also shown are plotted isotherms for one of the tests.

| Test | Surface Area (m ² /g) | | |
|--------------------|----------------------------------|---------|---------|
| | MMC | Lactose | Gelatin |
| 1 | 1.6398 | 0.7945 | 0.1319 |
| 2 | 1.6426 | 0.7767 | 0.1171 |
| 3 | 1.6245 | 0.7681 | 0.1132 |
| 4 | 1.6228 | 0.7597 | 0.1040 |
| 5 | 1.6185 | 0.7554 | 0.0987 |
| 6 | 1.5787 | 0.7488 | 0.0920 |
| 7 | 1.5989 | 0.7396 | 0.1076 |
| 8 | 1.5794 | 0.7348 | 0.0912 |
| Average | 1.6132 | 0.7597 | 0.1070 |
| Standard Deviation | 0.0249 | 0.0198 | 0.0137 |



Improved BJH Pore Size Distribution Using the Maximum Volume Increment Option

Pore size distribution is usually determined by gas adsorption techniques from the gas adsorption isotherm. For samples with 2 to 50-nm pore structure, BJH is the most commonly used method for calculating pore size distribution.

In order to get good results, sufficient isotherm sorption points are needed. However, the adsorbed volume at a certain relative pressure usually cannot be predicted before measurement, resulting in insufficient points for the BJH pore size distribution calculation.

If additional data points need to be collected between target pressures, a feature in Micromeritics software named Maximum Volume Increment can be used. When using this feature, if the maximum increment has been adsorbed since the last collected data point, then another point is equilibrated and collected.

The Silica-Alumina sample illustrates how the Maximum Volume Increment feature works. In Figure 1, the isotherm shows only a few collected points in the relative pressure range of hysteresis. Therefore, there are fewer points in the BJH pore size distribution.

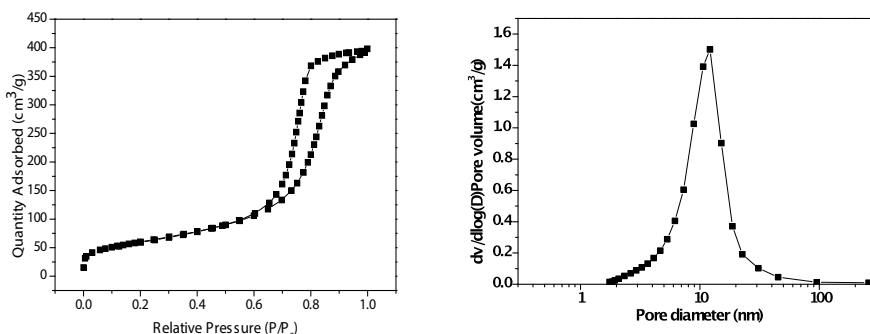


Figure 1. The isotherm and BJH pore size distribution of Silica-Alumina sample with pressure targets

Contrast this result with the effect of using the Maximum Volume Increment feature shown in Figure 2. In this experiment, maximum volume increment is 15 cm³/g. The isotherm seen in the resulting data plot has more points in the relative pressure range of hysteresis. The greater number of data points automatically collected

by the Maximum Volume Increment feature provides increased isotherm definition leading to significantly better resolution of the BJH pore size distribution

The Maximum Volume Increment capability is an exclusive feature of Micromeritics gas adsorption instruments.

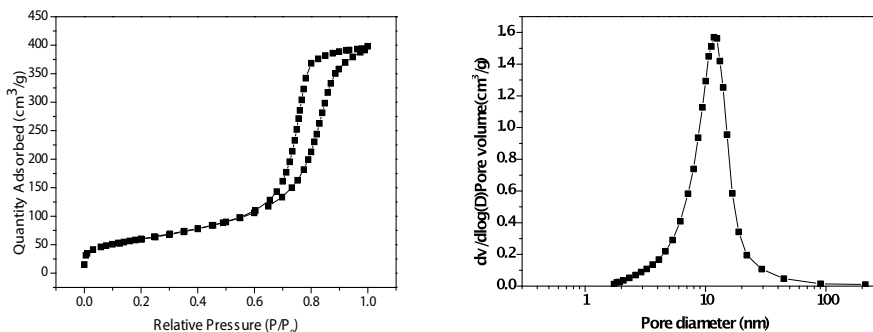


Figure 2. The isotherm and BJH pore size distribution of Silica-Alumina sample with pressure targets plus Maximum Volume Increment

The Effect of Particle Shape on Particle Size Measurement

Particle size analysis has a broad range of applications encompassing virtually all industries. Numerous automated techniques exist for measuring particle size distribution and virtually all report particle size in units of equivalent spherical diameter. This is necessary because of the ambiguity of describing the diameter of an irregularly shaped particle, and of constraints inherent in the instrument detection system.

Different measurement techniques that report in equivalent spherical diameter produce somewhat different particle size distributions when particles are non-spherical. Understanding what each particle size technique actually measures, how it performs the measurement, and how it transforms the quantity measured into equivalent spherical diameters are crucial when selecting the most appropriate particle sizing technique for your sample or application. To demonstrate this, we analyzed samples of glass beads, garnet, and wollastonite (because of their shape differences). The analytical techniques employed are static laser light scattering, electrical sensing zone (Coulter Principle), X-ray sedimentation, and dynamic image analysis. The effect particle shape has on the reported particle size is discussed for each of these materials and techniques.

Laser Light Scattering

The basic assumption of laser light scattering is that spherical particles of different sizes scatter light in patterns of intensity versus the scattering angle that are specific to the diameter of the particle. The scattering patterns are additive when particles of different sizes are involved. The particle sizes reported by this technique are the diameters of spheres in an assemblage of spherical particles that produce the same, or most nearly the same, scattering pattern as that detected by the instrument.

Electrical Sensing Zone

The electrical sensing zone technique measures the difference in electrical signal strength end-to-end across an orifice filled only with electrolyte to the signal strength when a non-conducting particle is present in the electrolyte as it passes through the orifice. From this measurement, the volume of electrolyte displaced by a particle, and therefore the volume of the particle, is determined. The particle size reported by this technique is essentially the diameter of a sphere that displaces the same volume of electrolyte as the detected particle.

Sedimentation

Particle size by sedimentation is determined by measurement of the terminal velocities of particles settling in a fluid medium. The particle size reported by this technique is the diameter of a sphere of the same material that settles at the same terminal velocity as the test particle in the same fluid and under the influence of the same force.

Dynamic Image Analysis

Dynamic image analysis acquires images of particles as they pass through the detection zone. Linear dimensions of the cross-sectional shape of each image are analyzed using a variety of shape parameters. The particle size reported by this technique is in terms of these linear dimensions.

Analytical Technique Properties

The table below lists the analytical techniques, the fundamental property determined, and the Micromeritics analyzer that employs each technique and which were used to generate data used in this study.

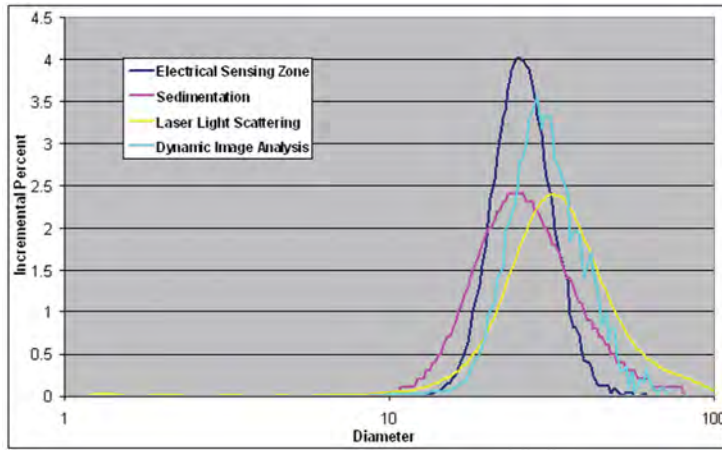
| Analytical Technique | Basic Measurement | Particle Variables Affecting Measurement | Micromeritics Analyzer |
|-------------------------|--|--|------------------------|
| Laser light scattering | Light intensity versus scattering angle | Refractive index, shape, orientation | Saturn® DigiSizer II |
| Electrical sensing zone | Change in electrical signal across a conducting orifice | Porosity, conductivity E | Elzone® II |
| Sedimentation | Settling velocity | Density, shape | SediGraph® III |
| Dynamic image analysis | Linear dimensions of projected cross-section of particle | Particle orientation | Particle Insight |

APPLICATION NOTE 158

Testing Results

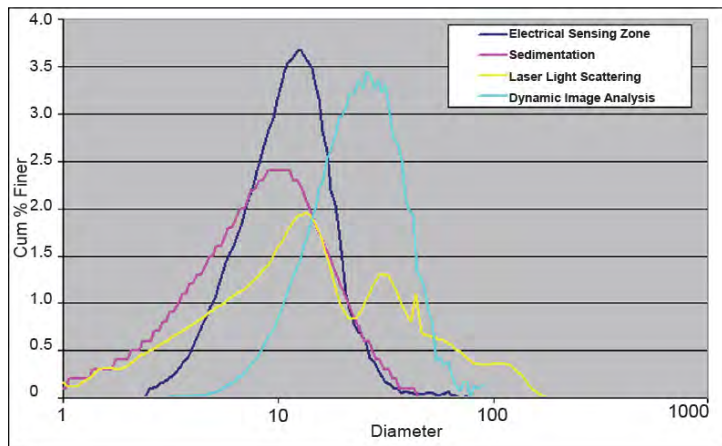
Garnet

Garnet crystals approximate cubic shapes. Since the diagonal of a cube is approximately 30% longer than a sphere of the same volume, larger particle size is reported by methods that take orientation into account (laser light scattering and dynamic image analysis).



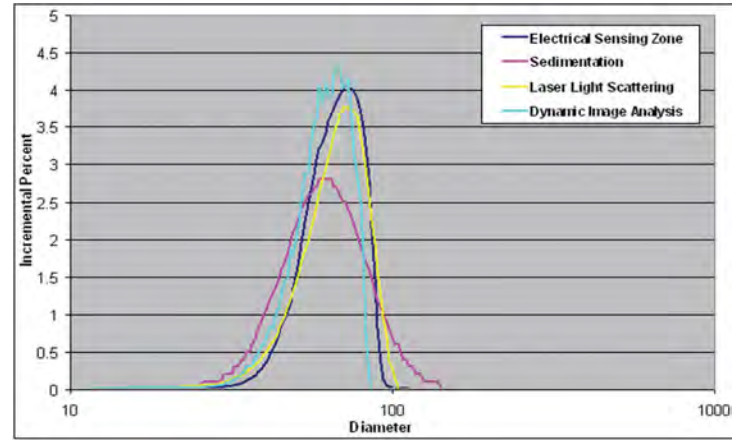
Wollastonite

Wollastonite particles are rod-shaped. Since the apparent dimensions of a rod-shaped particle can vary drastically depending on its orientation, the detection methods that were affected by particle orientation (laser light scattering and dynamic image analysis) exhibited larger particle size measurements and broader peaks.



Glass Spheres

Glass spheres, as expected, produced the most consistent results for the different techniques. Since the particles are spherical, their orientation has no effect on their measurement. Microscopy of the sample indicated that the glass spheres contained air bubbles in variable sizes, reducing somewhat the density of some of the spheres. Because of this, the SediGraph detects some of the particles as being undersized and, therefore, widens the distribution and shifts it to a slightly finer size.



Degas Options for Sample Preparation

Introduction

A degas study was conducted to determine the effectiveness of flow versus vacuum degas. An amorphous silica-alumina and a microporous zeolite were prepared by both techniques and then nitrogen isotherms were collected for both materials. The resulting isotherms established equivalence between vacuum versus flow degas.



Theory

Typical degas options include vacuum or flowing degas. The basic concept of degas is quite simple. The sample material is placed in an inert environment. This inert environment exploits chemical potential and creates a favorable state for an adsorbed molecule, perhaps water or carbon dioxide to shift from an adsorbed state to the inert environment. We can justify this theory by assuming a finite concentration of adsorbed molecules on the surface versus zero concentration in the inert environment. This assumption allows us to use Le Chatelier's principle which establishes that the equilibrium must shift. Hence the adsorbed molecules will change concentration (desorb) to reach a new chemical equilibrium.

To assist the shift from the adsorbed molecule to an inert environment, the temperature of the surface may be increased. Increasing temperature will increase the rate of desorption. This establishes two key requirements of degassing:

1. Inert environment – shift from adsorbed phase to inert.
2. Heat – increase the rate.

Vacuum versus Flowing Degas Methods

In the present study we accept that temperature may be controlled by various methods and that commercial temperature controllers provide repeatable performance. Rather than studying temperature control, this document will evaluate the topic of vacuum versus flowing degas.

1. Vacuum degas utilizes mass action as the only method for shifting the chemical equilibrium. An adsorbed molecule has a concentration on the surface, C and a negligible pressure, $P=0$ in the vapor phase. The pressure is maintained near zero since the sample is in a vacuum. Heating the sample increases the rate of transfer from the adsorbed molecules to the inert environment.
2. Flowing degas also utilizes mass action by constant inert purge. The desorbed molecules are swept from the system via the continuous inert gas flow and the partial pressure of the desorbed molecules in an inert stream approaches zero in a manner similar to the vacuum technique. Heating the sample also increases the rate of desorption. However, the inert purge method also has another driving force.

For example, nitrogen or helium molecules are continuously striking the surface of the material. During this process, momentum from the molecules striking the surface is transferred to adsorbed molecules. The inert gas method benefits from additional energy input and, as a result, a faster rate of degassing.

APPLICATION NOTE 160

Analysis

Based on these fundamental actions of vacuum and flowing degas, we can assume that both techniques provide a comparable result. An amorphous silica-alumina and microporous zeolite (13X) was used to explore the various degas options available to gas adsorption instrument users.

To establish the performance of both degassing techniques, a sample of silica alumina was prepared using the matrix of instruments and degas given in Table 1.

| FLOW | VACUUM | DEGAS DEVICE | ANALYSIS |
|------|--------|----------------|-----------|
| X | | FlowPrep | TriStar |
| | X | ASAP 2420 | ASAP 2420 |
| X | X | FlowPrep/3FLEX | 3Flex |

Table 1: Degas matrix for the preparation and analysis of amorphous silica-alumina

Nitrogen isotherm data were collected and the results are presented in Figure 1. This simple study establishes the equivalence of flow versus vacuum degas options for non-microporous materials.

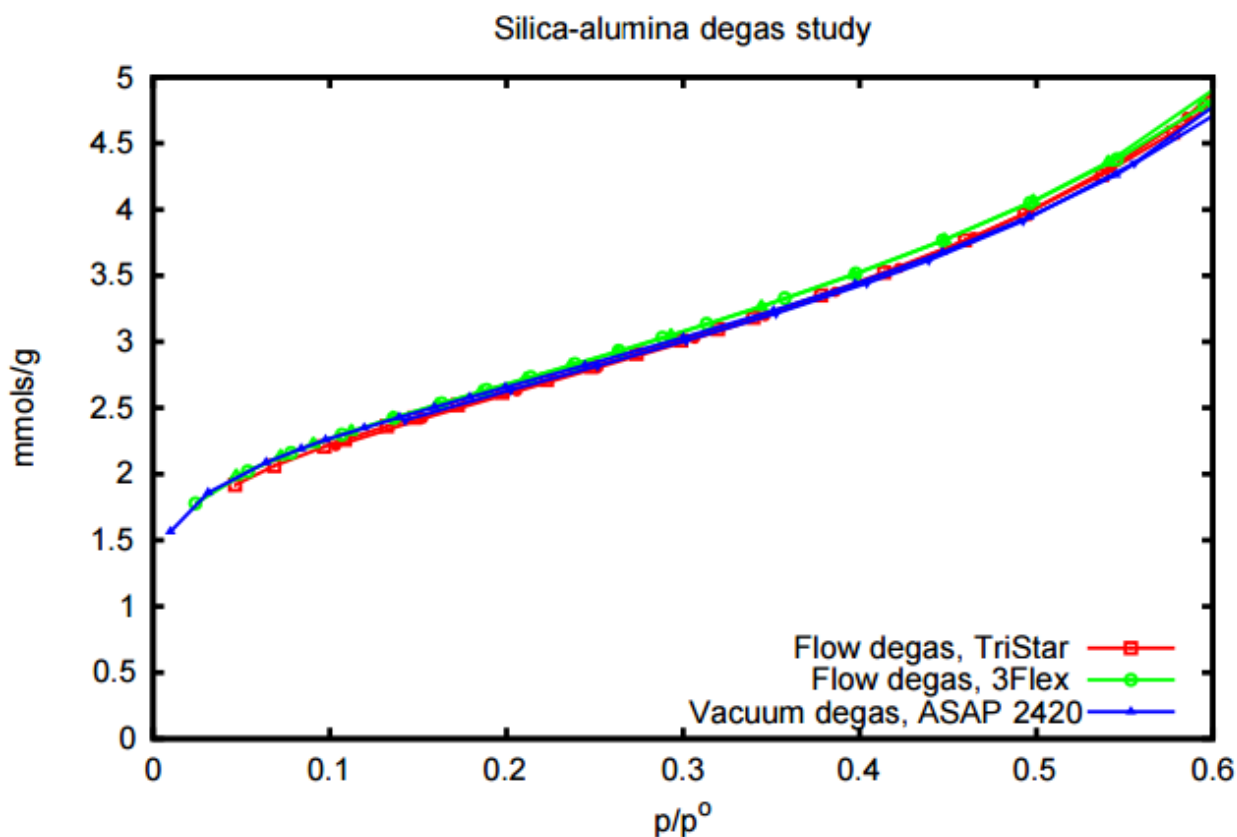


Figure 1: Nitrogen adsorption isotherm for silica-alumina vacuum degassed on the ASAP 2420 (blue), flow degassed on the TriStar 3020 (red), and flow degassed followed by vacuum on-port degas on the 3Flex (green). Equivalence is observed for all methods.

APPLICATION NOTE 160

The study was then expanded to investigate the use of flow versus vacuum degas and demonstrate the utility of a secondary on-port degas to establish an ultra clean sample prior to adsorption analyses.

The micropore zeolite was chosen because of the nature of these materials to adsorb small quantities of stray gas. The results of this study are presented in Figure 2.

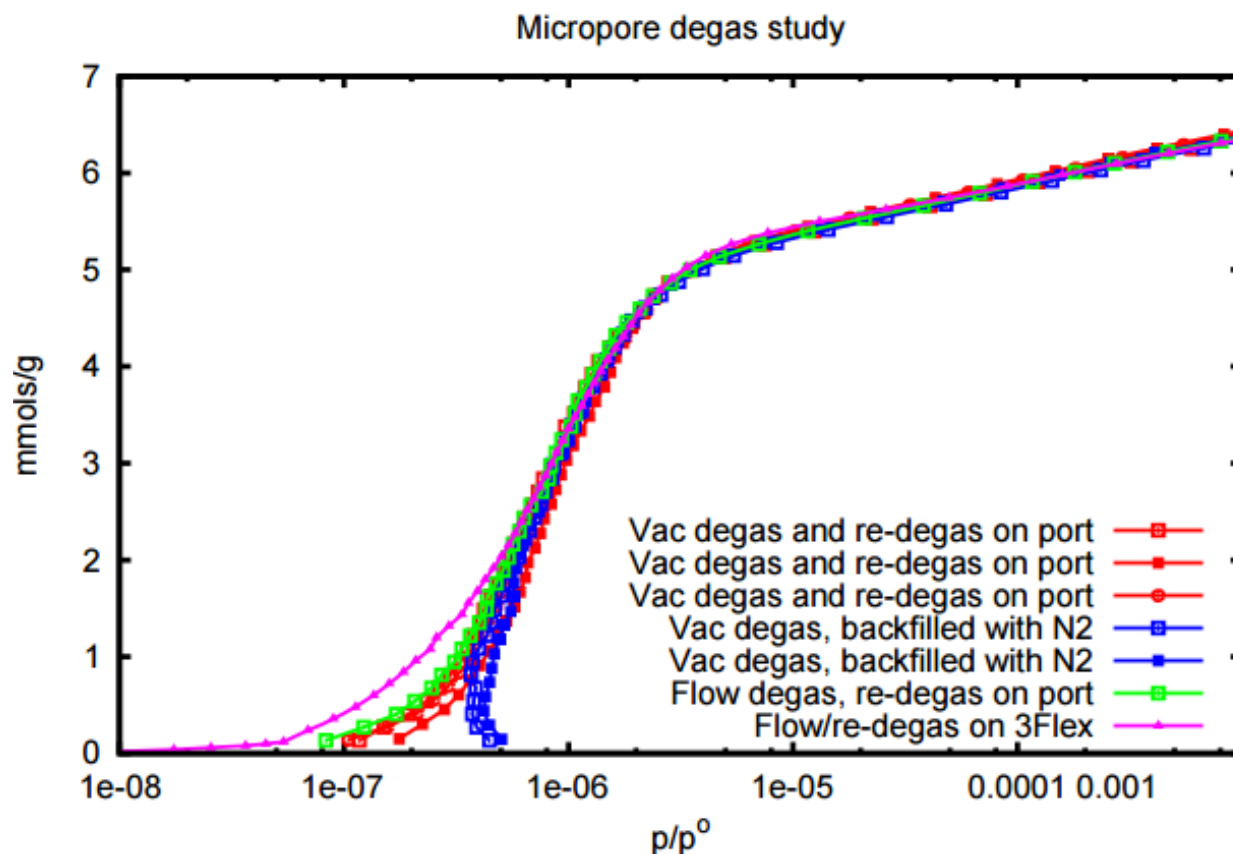


Figure 2: Nitrogen adsorption isotherms collected for zeolite 13X. Results in red were obtained using an ASAP 2020 and vacuum degassing followed by "on-port" degassing, the data in blue are obtained from ASAP 2020 vacuum degassing and nitrogen backfill without "on-port" degassing, the green and magenta isotherms were obtained by flow degassing and subsequent "on-port" degassing.

The isotherms collected using nitrogen and the 13X demonstrate two clear trends:

1. Flow degassing or vacuum degassing combined with on-port degassing provides the highest quality isotherm
2. Vacuum degassing does not provide the same high quality result as vacuum degassing plus a subsequent on-port degas.

Conclusion

Either flow or vacuum degassing provides a clean surface for adsorption. This conclusion is established by comparing the nitrogen isotherms obtained on an amorphous silica alumina and the 13X zeolite. The addition of on-port degas provided an ultra-clean sample devoid of any stray gas, weakly sorbed molecules, or molecules that are diffusion limited and difficult to quickly remove from the surface. On-port degassing also eliminated any possibility of contamination arising from transport of the sample from degas to the analysis station.

APPLICATION NOTE 160

External Sample Preparation units available from Micromeritics:

FlowPrep O60 – [click here for link to webpage](#)

The FlowPrep applies both heat and a stream of inert gas to the sample for removal of adsorbed contaminants from the surface and pores. With six degassing stations, this sample preparation unit lets you choose the temperature, gas, and flow rate best suited for your sample material and application. Needle valves allow the user to introduce the flowing gas slowly to prevent fluidization of samples.



VacPrep O61 – [click here for link to webpage](#)

The VacPrep offers two methods for removing adsorbed contaminants. In addition to flowing gas, this sample preparation unit provides vacuum to prepare samples by heating and evacuation. The VacPrep offers the user a choice of vacuum or gas flow on each of the six degassing stations. Needle valves allow the user to introduce the flowing gas or vacuum slowly to prevent fluidization of samples.



SmartPrep O65 – [click here for link to webpage](#)

The SmartPrep applies a stream of flowing gas over the sample at elevated temperatures to remove adsorbed contaminants. Temperature, ramp rates, and soak times are individually controlled on the six degassing stations by a computer. This sample preparation unit contains 2 serial ports, one for connecting to the computer and the other for connection to an additional SmartPrep. Up to five ramps and soaks are allowed. All degas information is integrated into the sample data file for future reference.



Specific Surface Area Measurement of Intact Lyophilized Cakes

Introduction and Significance

As physical characterization of pharmaceuticals becomes more of a focus, analytical techniques must be able to provide data that is representative of the materials being analyzed. Companies are implementing Quality by Design (QbD) and Process Analytical Technologies (PAT) initiatives to ensure robustness of formulas, processes, and products. Lyophilized products have key areas where these initiatives can play roles in product and process knowledge. Measurement of the surface area of lyophilized cakes provides valuable information on process capability and product consistency. BET surface area analysis of lyophilized products currently requires manipulation of the cake prior to testing to introduce the sample into the instrument sample tubes. This type of sample preparation technique for BET surface area testing may introduce error resulting in the lack of repeatability and robustness of the analysis and possible misrepresentation of the true surface area of the sample. Also, since manipulation is destructive to the sample, no further testing can be performed.

Possible variability stemming from non-standardized extraction techniques for removing cakes from their vials may lead to less reliable surface area data. We have developed a special prototype lyophilization vial holder apparatus that attaches to the Micromeritics ASAP 2420 Surface Area and Porosity Tester that will allow for non-destructive, intact lyophilized cake testing of surface area. In this preliminary study, we have found that surface area measurements of intact lyophilized cakes are approximately 35 - 55% less than the surface area of the same samples that have been manipulated during preparation. Further development of this product enhancement will lead to an invaluable characterization technique for lyophilized products during product development, scale-up, and as an implementable PAT tool for control of this critical process parameter.

Lyophilization Method

Full chamber loads of model product in 20cc tubing vials were processed in a 48 square foot lyophilizer within a GMP aseptic environment. The product selected for the purposes of the preliminary BET testing was amorphous sucrose. Lyophilization cycles utilized either a standard freezing technique or employed a controlled nucleation methodology using rapid depressurization of the product chamber.

Specific Surface Area Method of Analysis

In the present study we accept that temperature may be controlled by various methods and that commercial temperature controllers provide repeatable performance. Rather than studying temperature control, this document will evaluate the topic of vacuum versus flowing degas.

The vial is placed onto the sample holder and the sample holder/vial combination is then placed on the analysis port of the ASAP 2420 using a ferrule, frit and o-ring.

A step-wise manual evacuation is performed on each sample. The samples are left on the analysis port under evacuation with no added external heat for 16 hours to ensure any possible contaminants have been removed prior to beginning the test.

Sample analysis is started at liquid nitrogen temperatures with no backfill at the start of analysis. The sample is run using krypton over a ranges of relative pressures from 0.045-0.24 P/PO.



APPLICATION NOTE 161

Results

Results are presented for 5 separate analyses. Specific Surface Area (SSA) is reported for samples of intact cakes, tested in their lyophilization vials and samples that have been

manipulated (broken into pieces and removed from their vials and introduced into instrument-specific sample tubes.).

| SAMPLE | TYPE | SS (M ² /G) MANIPULATED CAKES | SS (M ² /G) INTACT CAKES | % DIFFERENCE |
|--------|---------|--|--|--------------|
| 1 | Sucrose | 0.8663 | 0.5481 | -36.7 |
| 2 | Sucrose | 0.8030 | 0.5167 | -35.7 |
| 3 | Sucrose | 0.4384 | 0.2060 | -53.0 |
| 4 | Sucrose | 0.3704 | 0.1868 | -49.6 |
| 5 | Sucrose | 0.8854 | 0.4609 | -47.9 |

Conclusion

Data presented from this preliminary study show a significant difference in specific surface area of lyophilized cakes when the cakes are tested intact versus non-intact. This research demonstrates important and useful advances being made for surface area analysis for lyophilized samples. We are currently continuing to develop this technology through iterations of the sample vial holder and analysis conditions.

Once implemented, this technology will allow for a more convenient, direct, and efficient means of obtaining surface area measurements of intact lyophilized cakes while still allowing further physical characterization testing of intact cakes following surface area measurement.

Expanding the Material Characterization “Toolbox” for Excipient and Active Pharmaceutical Ingredient (API) Vendor Qualification



Physical characterization of pharmaceutical excipients is not only a requirement but can also provide data that can be predictive in nature regarding the performance of final dosage forms including tablets, capsules, inhaled dosage forms, transdermals, and others. Manufacturers generally provide some of this physical testing data, such as particle size. In the case of particle size data, the manufacturer's specification may be wider than is actually acceptable for a particular process or product. Additionally, other tests may not be reported such as surface area, density, or porosity. In some cases, this data may provide insight into how a particular material will behave in a given process (flow, blending, compression) or final dosage form (disintegration, dissolution, bioavailability).

With implementation of Quality by Design, design space, risk analysis, and control strategies as outlined in ICH Q8, Q9, and Q10, increasing the knowledge base around excipients and APIs can aid in a company's ultimate understanding of their materials and what effect they may have in a formulation.

Lactose and microcrystalline cellulose are two of the most common excipients used in solid oral dosage forms.

Lot-to-lot or supplier-to-supplier variation in either of these materials, particularly when they comprise the bulk of a formulation, could lead to unwanted issues. In this example, both of these excipients have been subjected to a battery of tests to demonstrate the degree of consistency of the materials. Three lots of each material were tested to simulate a raw material vendor qualification study. Anhydrous lactose (SuperTab 21AN), spray-dried lactose (SuperTab 11SD), and microcrystalline cellulose (Pharmacel 101) were provided by DFE Pharma. Each material was tested for the following characteristics:

- True or skeletal density by helium pycnometry on the AccuPyc 1340
- Porosity by mercury intrusion porosimetry on the AutoPore IV 9500
- BET specific surface area using krypton gas on the ASAP 2420 Surface Area Analyzer
- Particle size distribution by laser light scattering on the Saturn DigiSizer II

APPLICATION NOTE 163

The following table summarizes the data generated for each test listed above. Depending on a company's application or internally developed specification, the data may be utilized to show lot-to-lot similarity or may show that additional controls are needed to ensure the material is acceptable for use in a specific application. There is no generic wrong or right data set for every process or product. What the data means to you is application-dependent. If qualifying a new raw material supplier, does this data show equivalence?

Or is there a critical parameter that needs tighter control due to unwanted effects on a product performance characteristic such as dissolution rate? Clearly, the data generated for this study is more comprehensive than reliance on vendor specifications alone. This data in combination with corresponding product performance data can increase the assurance level that the product being manufactured will be more consistent, robust, and perform as intended once administered to the patient.

| MATERIAL | LOT | DENSITY | POROSITY | SURFACE AREA (M ² /G) |
|---------------|----------|---------|----------|----------------------------------|
| SuperTab 21AN | 10678881 | 1.5821 | 8.5783 | 0.3490 |
| | 10640579 | 1.5810 | 8.5917 | 0.3442 |
| | 10680069 | 1.5798 | 11.1114 | 0.3452 |
| | Mean | 1.5810 | 9.4271 | 0.3461 |
| | %RSD | 0.07 | 15.5 | 0.73 |
| SuperTab 11SD | 10614997 | 1.5389 | 3.4083 | 0.2172 |
| | 10643209 | 1.5391 | 2.8102 | 0.2207 |
| | 10641963 | 1.5384 | 3.0303 | 0.1892 |
| | Mean | 1.5388 | 3.0829 | 0.2090 |
| | %RSD | 0.02 | 9.8 | 8.26 |
| Pharmacel 101 | 00100016 | 1.5495 | 18.6942 | 1.3805 |
| | 00100014 | 1.5545 | 16.3986 | 1.3345 |
| | 00100018 | 1.5527 | 16.9754 | 1.3792 |
| | Mean | 1.5522 | 17.3561 | 1.3647 |
| | %RSD | 0.16 | 6.9 | 1.92 |

APPLICATION NOTE 163

| MATERIAL | LOT | PARTICLE SIZE (VOLUME DISTRIBUTION) | | | |
|---------------|----------|-------------------------------------|---------|---------|--------|
| | | MEAN | D90 | D50 | D10 |
| SuperTab 21AN | 10678881 | 132.874 | 299.980 | 118.163 | 1.286 |
| | 10640579 | 123.902 | 278.460 | 111.046 | 1.184 |
| | 10680069 | 137.314 | 298.012 | 128.024 | 1.399 |
| | Mean | 131.363 | 292.151 | 119.078 | 1.290 |
| | %RSD | 5.2 | 4.1 | 7.2 | 8.3 |
| SuperTab 11SD | 10614997 | 59.168 | 117.334 | 53.639 | 4.146 |
| | 10643209 | 67.634 | 124.826 | 65.090 | 11.091 |
| | 10641963 | 69.883 | 136.195 | 64.786 | 7.324 |
| | Mean | 65.562 | 126.118 | 61.172 | 7.520 |
| | %RSD | 8.6 | 7.5 | 10.7 | 46.2 |
| Pharmacel 101 | 00100016 | 51.810 | 98.606 | 49.353 | 7.824 |
| | 00100014 | 55.109 | 103.303 | 53.231 | 9.020 |
| | 00100018 | 57.587 | 105.306 | 56.397 | 11.028 |
| | Mean | 54.835 | 102.405 | 52.994 | 9.291 |
| | %RSD | 5.3 | 3.4 | 6.7 | 17.4 |

Conclusion

Monitoring raw materials is an important part of the overall control strategy in pharmaceutical formulations. Knowledge of physical characteristics can be beneficial when developing a design space or control strategies to ensure quality is built into processes and products and, in combination with final product performance, can help to identify critical process parameters and critical quality attributes of starting materials and final dosage forms.

The additional testing demonstrated in this study have shown that a more thorough examination of materials may help ensure consistency of material from a particular

supplier, provides a battery of testing that can be performed to qualify new material suppliers, and may generate data that could be predictive in nature regarding process and/or product performance. By building this knowledge base around your starting materials, many instances of undesirable process or product performance that may occur will result in troubleshooting with more “tools” in your “toolbox”.

Asphalt Density Using AccuPyc II TEC

Abstract

Measuring asphalt density per ASTM Test Method D70-09 requires the use of a glass pycnometer and very tedious analysis conditions. Using this ASTM method as a guide, the density of asphalt is measured using an AccuPyc II TEC and 3.3-cc disposable aluminum cups. The density results of four different asphalt samples using the AccuPyc are compared to results obtained by a third party using the ASTM glass pycnometer method. Results from the two methods ranged from a 0.003% to 0.026% difference.

Introduction

Asphalt density is used in the calculation to determine the quality and amount of asphalt needed to pave roads. The quality and uniformity of the mixture determines whether a road will be paved evenly and if the thickness of the pavement at different points is also uniform.

The density of asphalt is currently determined by using a glass pycnometer as described by ASTM Test Method D70-09. The pycnometer must be cleaned thoroughly and have no defects or weaknesses. Using an analytical balance and a water bath, the density of water is first obtained using the pycnometer. Then the asphalt sample is heated until it is viscous enough to pour. The glass pycnometer is filled about three-fourths full and weighed, then filled to full with water and weighed. The final calculation described in the ASTM method allows the analyst to determine the density of the asphalt at 25 °C. If anything happens to compromise the pycnometer, such as breakage, the entire procedure must be repeated using a new pycnometer.

The goal of this application note is to obtain the same density values for four (4) asphalt samples, Sample A, Sample B, Sample C, and Sample D, using the AccuPyc II TEC and disposable sample cups, a much cleaner and easier method. For scientific quality, a third party lab withheld the actual density values collected using the ASTM pycnometer method until the project was completed.



Experimental

Materials

- AccuPyc II TEC with 3.3-cc disposable aluminum sample cups and nitrogen gas
- Analytical balance
- Laboratory oven
- Disposable plastic pipettes

Procedure

For each sample, twelve (12) 3.3-cc disposable aluminum cups are labeled. The first eleven cups are labeled sequentially from 1 to 11 and the 12th cup is labeled "cal cup." The "cal cup" is the cup that will be used to calibrate the AccuPyc. Its mass and volume are used to correct for the volume of the other eleven sample cups used on the day of analysis and under the same conditions.

Once all twelve cups are labeled, they are placed in a preheated laboratory oven at not less than (NLT) 163 °C for NLT 30 minutes. This is the conditioning step. The cups are then removed from the oven and allowed to cool to room temperature and weighed, including the "cal cup." Cups 1 thru 11 are then placed back into the oven until the asphalt is ready to be sampled. The "cal cup" is taken to the AccuPyc and used for the calibration.

The bulk container of sample asphalt is placed in the oven at NLT 163 °C for about an hour or until the asphalt is soft enough to be drawn into a disposable plastic pipette. Once the asphalt is ready, small aliquots are placed into cups 1 thru 11 using the disposable pipettes. Each cup is filled about half way to three-fourths full, being careful not to get asphalt on the side of the cup. Once the cups are filled, the cups with the asphalt aliquots are placed back in the oven for about an hour to remove any air pockets that may have formed. The cups are then removed from the oven, allowed to cool to room temperature, and a final weight is taken.

The AccuPyc is set up with the following conditions:

- Gas: Nitrogen
- Number of Purges: 2

APPLICATION NOTE 164

- Purge Fill Pressure: 19.500
- Number of Cycles: 99
- Cycle Fill Pressure: 19.500
- Equilibration Rate: 0.0050
- Peltier Temperature setting: 25.0 °C

The “Cal Cup” is then placed into the AccuPyc and the standard procedure used to calibrate the volume is used. A 2.5-cm steel ball standard with a volume of 1.7671 cc is used as the calibration standard. Once the calibration is complete, a sample file labeled “check standard” is created using the same parameters to be used on the asphalt aliquots. The steel ball is then analyzed as a sample to verify the volume measured. Each asphalt aliquot is analyzed and the data files created are labeled with the sample identification number and the cup number.

Once all the data are collected, the volume of each aliquot cup is corrected by taking the difference in the weights between the empty aliquot cup and the “cal cup,” then dividing by 2.7 g/cc (density of aluminum). The sample weight is then divided by the corrected cup volume to calculate the density of the sample.

Results

The results for each asphalt sample submitted are displayed in the following table.

| Asphalt Sample | Average Density (n=11) (g/cc) | % Relative Standard Deviation (n=11) | ASTM Method Density (g/cc)* | % Difference Between Methods |
|----------------|-------------------------------|--------------------------------------|-----------------------------|------------------------------|
| Sample A | 1.02543 | 0.03 | 1.02536 | 0.0067 |
| Sample B | 1.01845 | 0.06 | 1.01848 | 0.0031 |
| Sample C | 1.01821 | 0.07 | 1.01848 | 0.0263 |
| Sample D | 1.02563 | 0.09 | 1.02576 | 0.0125 |

* Density of asphalt sample from third party laboratory using glass pycnometer method

Conclusion

Accurately measuring the density of asphalt is crucial to the quality of paved roadways. It is possible to obtain accurate asphalt density values using an AccuPyc II TEC and 3.3-cc disposable aluminum cups. The average results of 11 test samples agree with results collected by a third-party laboratory using the glass pycnometer method described in ASTM Test Method D70-09 on the same batch of asphalt.



AccuPyc II TEC

Adding a Custom Model to the NLDFT Library: A CO₂ GCMC Model for Carbons

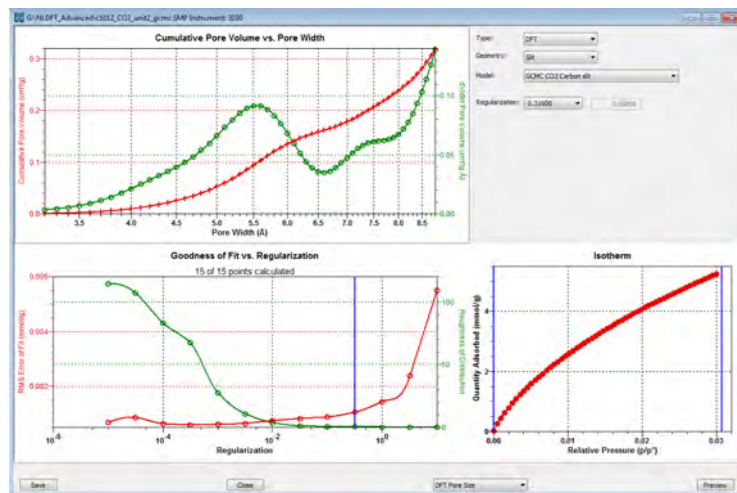
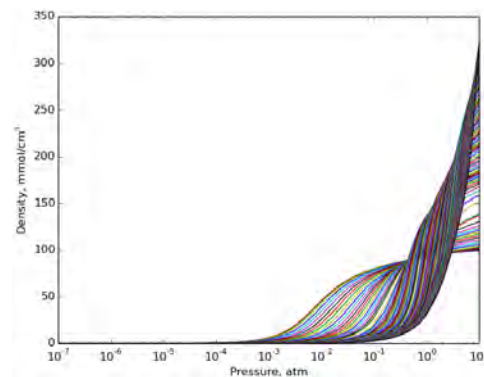
New models for determining the pore volume and pore size distribution of porous solids may be easily added to MicroActive™. These kernels developed using NLDFT, GCMC and other variants have been available for more than 20 years. Traditionally instrument manufacturers have supplied these proprietary models. To introduce new powerful capabilities for users, Micromeritics has developed a simple program to convert model isotherms (a kernel) to a model file that can be easily used with MicroActive. This provides users the full capabilities of the MicroActive user interface and advanced deconvolution techniques. A full description of the model requirements and conversion process are provided below and include an example using a GCMC kernel for carbon slit-shaped pores and CO₂ adsorption. The GCMC kernel used in this example was developed by Inmondo Tech. For user calculated kernels the following general specifications should be observed:

1. Each model isotherm should be calculated using a common pressure table and the minimum pressure should be less than 5e-9 atmospheres (or relative pressure).
2. A minimum of 15 points per decade of pressure and the pressures should be logarithmically spaced and the vector or pressures should be saved in a text file as **pVector.txt**.
3. Pore widths may start at a minimum of 0.32 nm and may have a spacing of 0.01 nm. The vector of pore widths should be saved in a text file as **width.txt**.
4. The kernel shall contain isotherms with each column corresponding to the pore width found in the file **width.txt** and adsorption densities in each row corresponding to pressures in **pVector.txt**. The kernel should be saved in text file as **kMatrix.txt**.

Using the three files, **width.txt**, **pVector.txt**, and **kMatrix.txt** a kernel compatible with MicroActive may be created using Python 3.x and a custom library from Micromeritics (**dftmodel.py**).

The example kernel, CO₂ adsorption and carbon slit-shaped pores is shown below.

The new model may be copied to the models directory in MicroActive and is immediately available for use. Simply open a file containing adsorption data and select DFT pore size and the new model appears in the selection list as shown below.



For a additional information on adding new models to MicroActive or a copy of the example used to create the GCMC kernel please [contact](#) your local Micromeritics representative.

The Principles and Theory of the Isothermal Jacket for Free Space Control in Gas Adsorption

Introduction

It has been 55 years since the first commercially available transportable static-volumetric gas adsorption instrument was invented by Dr. Clyde Orr and Mr. Warren Hendrix at the Georgia Institute of Technology (Georgia Tech). Of course, this is the invention which began Micromeritics Instrument Corporation in 1962. Since that time, significant and numerous advances have taken place as the “State-of-the-Art” has progressed.

This paper is a review of what Micromeritics engineers and researchers have learned about how to optimize instrument performance through improvements in freespace control.

Freespace, when used in this context is the volume of the sample holder (sample tube) below the valve which connects it to the dosing manifold of a gas adsorption instrument which is not displaced by the sample. It is important in a volumetric system to precisely know this volume and for this volume to remain stable throughout an analysis, despite evaporating cryogen. It is measured at room temperature and then after the Dewar is raised, at the liquid cryogen temperature. This latter measurement is known as cold freespace. Changes in cold freespace can contribute significantly to gas inventory calculation errors in even the most sophisticated instruments.

Micromeritics first introduced and patented the Isothermal Jacket for temperature control of cold freespace in the mid 1980's. The following is a product bulletin which describes the significant advantages of this device taken from that time.

1987 Isothermal Jacket Product Bulletin

The BET[®] technique for surface area and other models for pore size distribution evaluation employing low temperature gas adsorption requires precise measurement of gas quantities.

Accurate gas quantity measurement is possible only if pressure, volume, and temperature are accurately known in all parts of the measurement system. Since adsorption onto the material being tested must occur at cryogenic temperature and practical considerations dictate that the remainder of the system be at or near room temperature, it becomes imperative, especially in the space connecting the sample at low temperature to the remainder of the system, that temperature stability be maintained. This most critical interconnecting space presents a special challenge because of its large temperature gradient and the fact that cryogenic fluid evaporation will change the size of the zone if not properly controlled.

If, as illustrated below, a sample is simply immersed in a bath of liquid nitrogen (LN₂) and connected by tubing to other thermostated components, the gradient zone increases in length as the LN₂ evaporates and its level falls. This gives rise to an increasing volume within the tubing of uncertain temperature distribution—one segment of the connecting tubing being exposed to the ambient air and the remainder coming more and more under the influence of the evaporated but still chilled nitrogen gas.

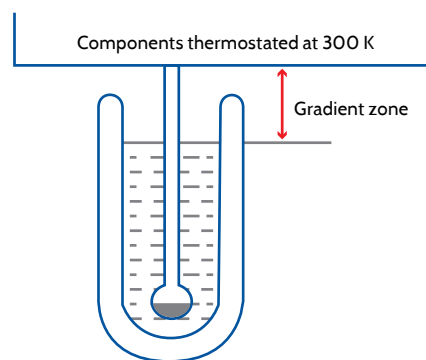


Illustration 1

*Brunauer, S.; Emmett, P.H.; and Teller, E. "The Adsorption of Gases in Multimolecular Layers" J. Am. Chem. Soc. 60, 309-19 (1938)

APPLICATION NOTE 167

Some instrument manufacturers attempt to rectify this situation by causing the LN₂ Dewar to rise as the liquid level falls. This indeed fixes the volume immersed but the length of tubing exposed to ambient conditions has to be greater initially and the connecting tube length contacted by chilled nitrogen gas of intermediate temperature thereafter increases as exposure to the ambient environment decreases as shown by Illustration 2. Because of this shift, the temperature distribution between the gradient extremes still changes and only partial compensation for evaporation is achieved.

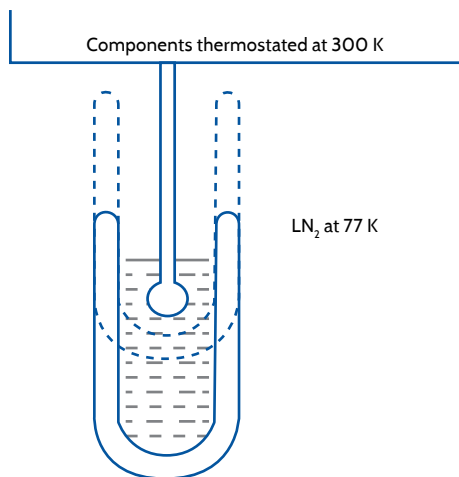


Illustration 2

In the mid 1980's, Micromeritics had for a decade employed the classical procedure of transferring fresh LN₂ from a large storage reservoir to the sample Dewar as evaporation proceeds in order to hold the liquid level fixed and the gradient constant, Illustration 3. This provides excellent stability but requires a somewhat involved LN₂ transferring mechanism.

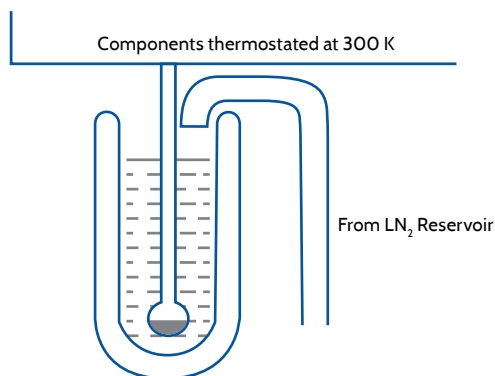


Illustration 3

Now (in 1987) Micromeritics has developed a very simple device described as an Isothermal Jacket® for which a patent is pending and which also provides excellent stability. The new device consists basically of a material having interconnecting

pores encased in an impervious outer shell which simply fits around the tube connecting the sample space with other system components. As long as the lower end of this composite is submerged in LN₂, the porous material remains saturated with LN₂ throughout its entire length, evaporation taking place only from its upper exposed end. The level of LN₂ about the connecting tube thus remains constant until only a very little LN₂ remains in the Dewar. The Dewar can be replenished with LN₂ just before depletion or at other convenient times, to provide temperature constancy for as long as needed. Use does not degrade the jacket and there is nothing to wear out. The Isothermal Jacket, Illustration 4, is truly a unique solution to what has long been a control problem.

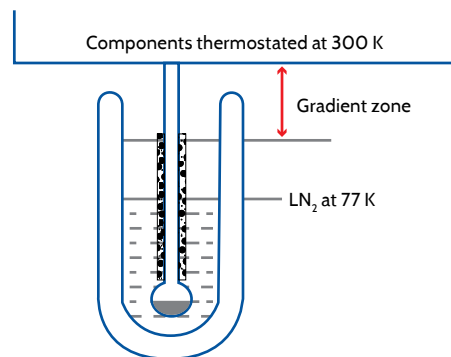


Illustration 4

Duplicate measurement systems, one corresponding to Illustration 4 and one to Illustration 1, and consisting of a pressure transducer, a bulb immersed in a 1-liter Dewar of LN₂, and connecting tubing serve to illustrate the stability provided by an Isothermal Jacket.

When the tubing within the Dewar was surrounded with a Jacket (Illustration 4) and the system partially filled with helium, the pressure held between 357.78 and 357.85 mmHg over an 8-hr period. During this time the LN₂ level fell 150 mm. The experiment without the Jacket (Illustration 1) resulted in the pressure changing very nearly linearly from to 373.34 mmHg during the same period. 359.19

What follows is a study performed some years later to demonstrate very clearly the direct effect in performance of different freespace control systems.

In gas adsorption studies of powder and granules such as adsorbents and catalysts for the purpose of evaluating their surface area and pore structure, ever-present requirements are maintaining the sample at constant temperature, typically that of the cryogen liquid nitrogen (LN₂), and maintaining other conditions fixed so that gas pressures about the sample can be accurately assessed. A problem arises because the LN₂, even when contained in the highest

APPLICATION NOTE 167

quality Dewar, evaporates and its level decreases with time. Because of this level change, if no means of compensation is provided, a segment of any access channel leading to the sample from instrumentation at laboratory temperature is exposed to a changing temperature environment, meaning the gas pressure about the sample is also changing.

At least three means of providing compensation for LN₂ evaporation have been devised. These include (1) frequently replacing the lost LN₂ in small increments, (2) raising the Dewar as the LN₂ level decreases, and (3) providing a special wick about the access channel to confine evaporation to one fixed point on the channel. The first requires a means for pumping LN₂ into the Dewar each time the level drops an increment and a means for sensing the LN₂ level in small increments. The second requires starting with the sample immersed only minimally in the Dewar contents and then raising the Dewar mechanically in response to the LN₂ level decrease. It also requires a sensor to track the LN₂ level. The third is passive and is called an isothermal jacket; it depends only on the natural surface tension of the LN₂. The Isothermal Jacket is patented.

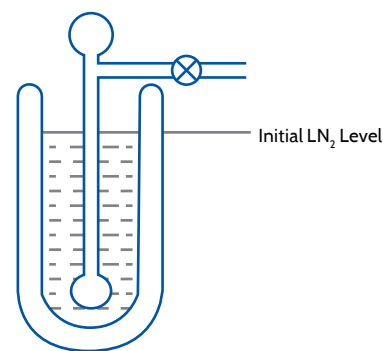
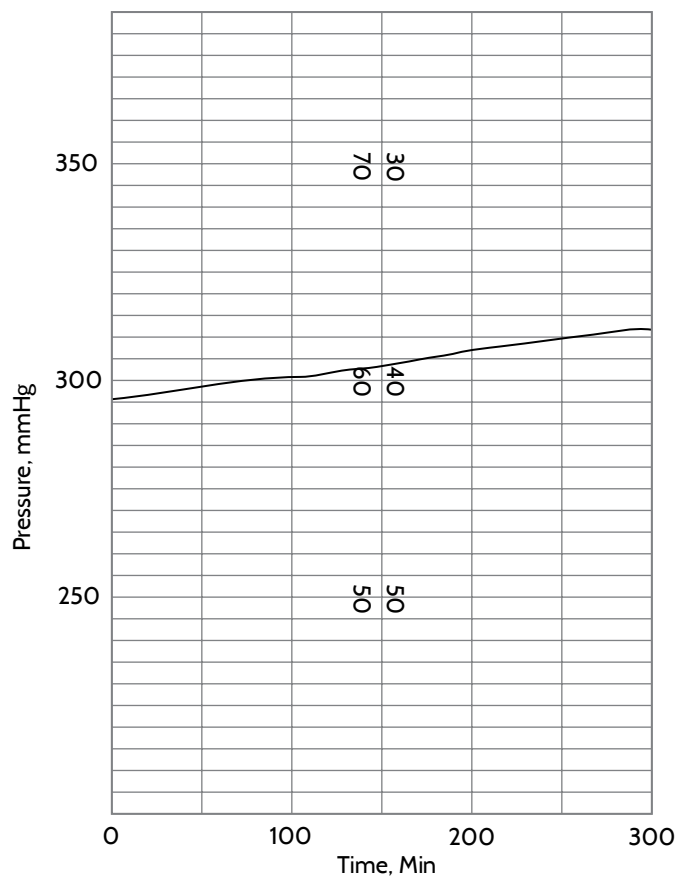
This report gives the results obtained with the three- enumerated means of control using a simple experimental arrangement of a sample bulb with a valve for admitting a gas, a transducer to follow the gas pressure as a function of time, and a Dewar to contain the LN₂.

1. An LN₂ pump and level detector were added when performing the level control experiment.
2. A motorized mechanical jack and the same LN₂ level detector were used in the rising Dewar test, but the experimental arrangement remained otherwise identical.
3. An isothermal jacket was merely slipped about the tube joining the sample bulb and pressure transducer when performing the third test.

The experimental system was purposely constructed to magnify equally deficiencies in the performance of the three techniques. Toward that end, the tube connecting the sample bulb, which would be immersed in LN₂, and the pressure transducer at ambient temperature was 20 cm long and 9 mm in internal diameter. A wide-mouth, 1-liter Dewar was employed as the LN₂ reservoir.

Four tests were performed. All tests were begun with the sample bulb immersed in LN₂ and with nitrogen gas at a pressure of approximately 300 mmHg in the sample tube. The pressure change with time was followed on a chart recorder. The experimental set-ups are diagrammed below and a representative recording is shown beside it.

The first test was made with no compensation at all.



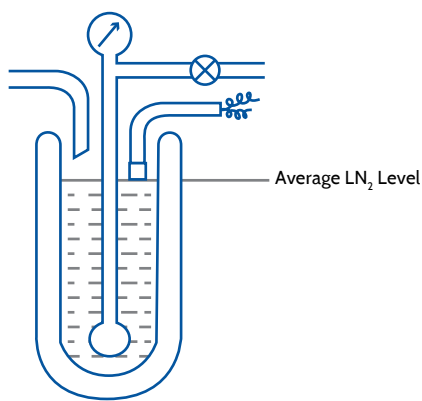
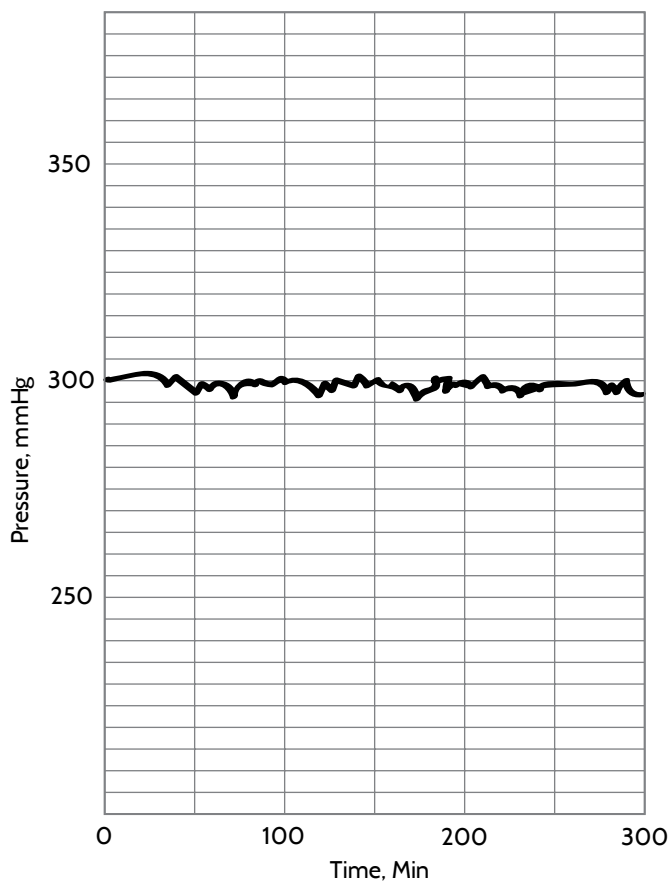
Test 1. No Control

Without compensation for LN₂ level decrease, the pressure in the system would be expected to increase with time because more of the stem leading to the sample bulb and its gas content are exposed to ambient temperature influences. This behavior is exactly what the recording to the right of the diagram shows.

Level control added to the system, as diagrammed below, would be expected to maintain stable conditions within narrow limits. As shown by the accompanying pressure-time recording,

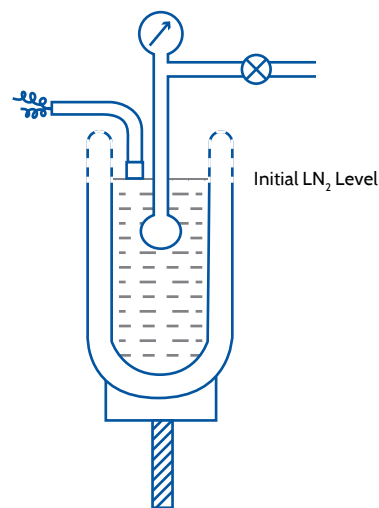
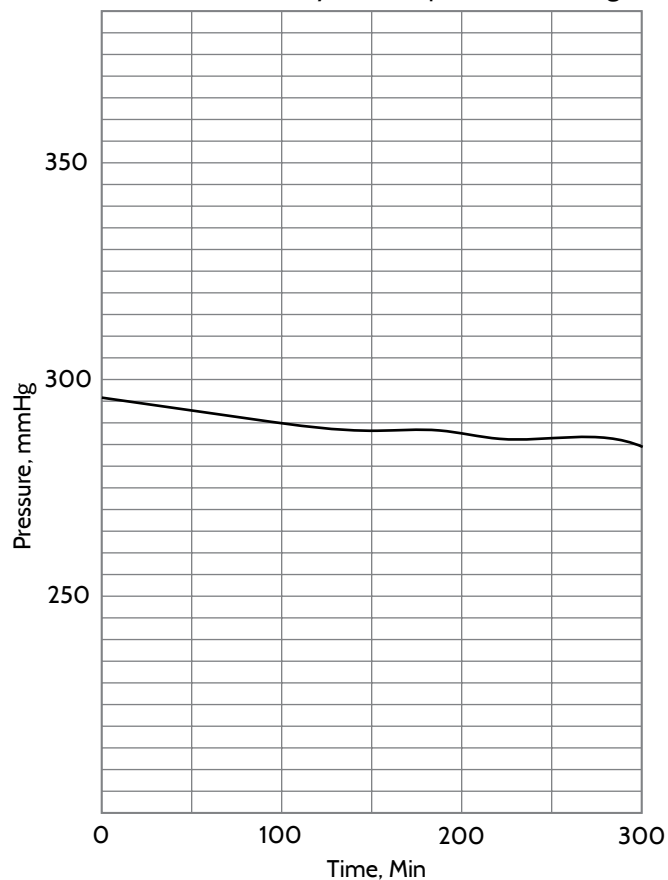
APPLICATION NOTE 167

it does this with minor fluctuations arising due to LN₂ surface disturbances as each increment of new liquid is added. This system accomplishes its intended goal and is attractive for very long analysis time situations. If the time is too long however, ice extracted from the water vapor in the ambient atmosphere will build up choking off access to the entire system. It also requires somewhat expensive peripheral equipment.



Test 2. LN₂ Level Control

Raising the Dewar to compensate for evaporation, as shown by the next diagram, inserts more of the stem leading to the sample and the gas contained in the stem into the expanding cold vapor zone deeper and deeper within the Dewar. This would be expected to produce a decrease in gas pressure, as indeed it does as is revealed by the companion recording.



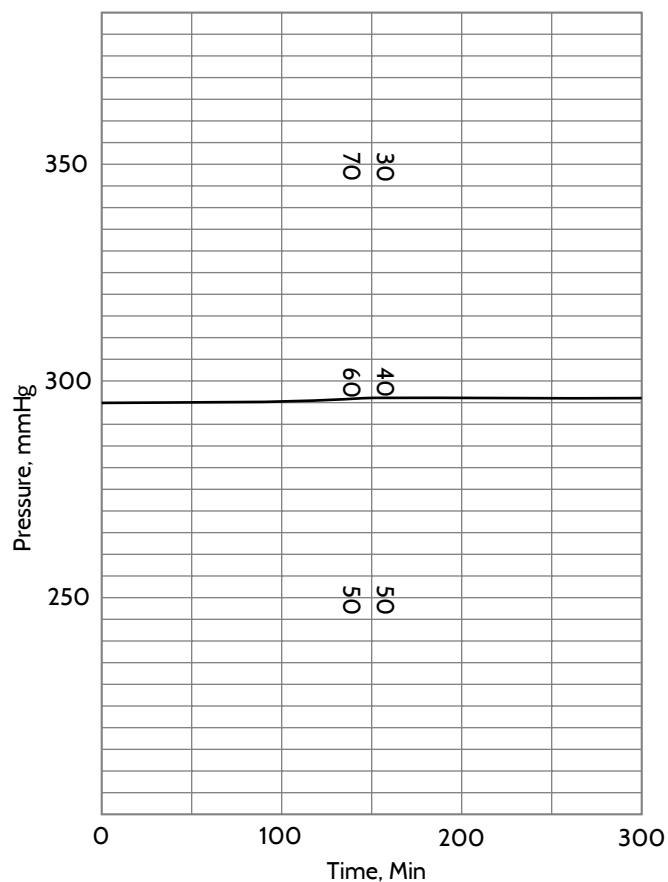
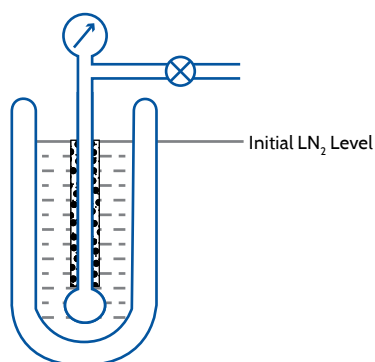
Test 3. Rising Dewar

APPLICATION NOTE 167

Of course, this effect can be mitigated by making the stem of small internal diameter so that less gas is contained therein and by inserting some kind of filling rod to take up much of the remaining volume. A small diameter stem creates difficulties in getting a sample in and out of the sample space; a close-fitting filler rod decreases the rate at which a sample can be evacuated when that step is required by an analytical procedure and it provides an added heat conduction path from the cold zone to the warm zone. As with level control, peripheral equipment adds to the initial expense and maintenance costs. Examining the recording for no control and the recording for the rising Dewar suggests that using a small diameter connecting stem from the sample bulb and no compensation would each produce about equally satisfactory results.

The final diagram and companion recording pertains to the Isothermal Jacket system. A bit of explanation is in order here. Isothermal Jackets are tubes of about 2.5 cm outside diameter and up to 18 cm in length. Their inside diameter ranges from 1.25 to 0.5 cm. Their outer shell is a thin nearly impervious layer inside which is a porous layer. They are designed to fit snugly about the stem of a sample tube. When their lower extremity is inserted in a cryogenic fluid such as LN_2 , the LN_2 rises by capillary action to the upper extremity to which evaporation is now largely restricted. The jacket thus bathes the stem in LN_2 and continues to do so until the level in the LN_2 bath falls below the lower extremity. Since the stem leading from the sample bulb is surrounded over a fixed length by LN_2 regardless of the LN_2 level in the Dewar, no change in gas pressure inside the stem would be expected until the Dewar is nearly empty. The recording shows this is indeed the case.

Their inside diameter ranges from 1.25 to 0.5 cm. Their outer shell is a thin nearly impervious layer inside which is a porous layer. They are designed to fit snugly about the stem of a sample tube. When their lower extremity is inserted in a cryogenic fluid such as LN_2 , the LN_2 rises by capillary action to the upper extremity to which evaporation is now largely restricted. The jacket thus bathes the stem in LN_2 and continues to do so until the level in the LN_2 bath falls below the lower extremity. Since the stem leading from the sample bulb is surrounded over a fixed length by LN_2 regardless of the LN_2 level in the Dewar, no change in gas pressure inside the stem would be expected until the Dewar is nearly empty. The recording shows this is indeed the case.



Test 4. Isothermal Jacket

In summary, this investigation has shown that stable conditions are achieved only when the liquid nitrogen level about the stem is maintained constant and that this situation is achieved by just two techniques—level control and Isothermal Jackets. The Isothermal Jacket, being inexpensive, reusable, and simple to use in addition to providing the best stabilization clearly is the obvious choice.

Through 55 years of product development, and having tried many different approaches, Micromeritics has learned that Isothermal Jackets are the best option for our users. They are simple, inexpensive devices which require no maintenance, will work with a wide range of cryogenes, require no electronic circuits to control, are guaranteed for the life of the instrument against failure and provide the most stable freespace and thus the highest quality data collection.

Analysis of Separator and Binder Materials in Lithium Ion Batteries

Binder materials are responsible for holding the active material particles within the electrode of a lithium-ion battery (LIB) together to maintain a strong connection between the electrode and the contacts. These binding materials are normally inert and have an important role in the manufacturability of the battery.

Binders must be flexible, insoluble in the electrolyte, chemically and electrochemically stable and easy to apply to the electrodes. Binders for the positive cathode also need to be resistant to oxidation. A common binder material for the cathode is polyvinylidene fluoride, whereas a common anodic binder material is styrene-butadiene copolymer. As electrode materials advance, binder materials that improve the performance of the new electrode materials are also required.

Separators are a class of membranes which allow for the physical separation of the anode and the cathode, allowing the ions within the electrolyte to flow between the two electrodes whilst blocking the electrons to prevent short-circuiting. By nature, separators are required to be highly porous, a good electronic insulator and a good ionic conductor. They are also commonly made from polymers such as polyolefins, ceramics or polymer/ceramic blends. Separators also act as a safety device within LIBs by stopping the ion flow when a battery is overheating.

The development and advancement of separators and binders have received less attention than electrode material development in LIBs, despite their properties being a crucial factor in the overall performance and safety of the battery. In a previous article, we outlined the important microstructural properties of electrode materials for LIBs and how to analyze them. This article outlines the analysis of separator and binder material properties and how the properties of these materials can be controlled to optimize battery manufacturability and performance using a range of methods.



Analysis of Porosity

High porosity is an important and desirable property in LIBs, as it provides a constant ion flow and allows the separator to act as an electrolyte reservoir- this is known to increase the amount of electrolyte held by the separator and provides an increase in the energy density and a reduction of the heat generated within the LIB. However, the porosity can't be too high, as the pores need to be small enough to close when the battery is overheating, and thus, allowing the separator to act as a safety shutdown. In typical battery system, the LIB separators have a porosity of 40%.

Porosity can be measured using both liquid and gas absorption methods. Micromeritics offers a number of instrument solutions for measuring the porosity of separator materials. These include the AccuPyc 1340, the TriStar II Plus and the AutoPore V which use gas displacement, gas adsorption and mercury displacement methods, respectively, to measure the porosity in the material(s).

Analysing Pore Size and Shape

To prevent the particles within the electrodes from entering the separator, the pores of the separator need to be smaller than the size of the particles in the electrodes. As such, separators commonly possess pores on the sub-micron scale. Small and tortuous pores also prevent dendritic lithium penetration.

Lithium dendrites are undesirable and are a common cause of short-circuiting within a battery, as their growth can lead to a connection between the electrodes. It is suspected that Samsung Galaxy note 7 fires in 2016 were caused by dendritic lithium growth.

A uniform pore size throughout helps to prevent an uneven ion flow and fluctuations in the current density of the electrode. These can be an issue as they cause parts of the battery to work more than others, causing the lifetime of the battery to be decreased.

Micromeritics offers pore size distribution measurements using mercury porosimetry in the form the AutoPore V (3.6 μm pores) and the TriStar Plus for even smaller pore sizes. Micromeritics also offers the Phenom Pro Scanning SEM as an ideal desktop SEM instrument to measure the size and structure of pores.

Analysing the Zeta Potential

Zeta potential offers an insight into the amount of electrostatic repulsion between adjacent particles of like charge. In LIBs, the zeta potential measured the affinity between the separator and the electrolyte, as well as the overall stability of the system, with the zeta potential impeding or aiding the flow of the electrolyte the separator. Therefore, zeta potential measurements can be used to understand the transport mechanisms of the separator and tune it to improve the cycle life of the battery.

Micromeritics offers the NanoPlus HD to determine the particle size and zeta potential of a wide range of materials with outstanding performance.

Conclusion

Whilst separators and binder materials are commonly used in LIB applications, there is still a great need for further research to increase their performance, increase battery lifetime and reduce costs.

Researchers who are developing new materials in this field require equipment that quickly and accurately assesses the relevant material properties, such as the porosity, pore size and shape and zeta potential. Micromeritics possesses a wide-ranging portfolio of instruments to meet these needs and help researchers to optimize their materials and develop the next generation of batteries.

References

Yoshio M, Brodd RJ, Kozwa A, "Lithium-Ion Batteries: Science and Technologies" Springer, 2009.

http://www.micromeritics.com/Repository/Files/battery_brochure_2016_v2.pdf Accessed August 3rd, 2017.

Arora P, Zhang Z, "Battery Separators" Chem. Rev, 104:4419-4462, 2004.

Zhang SS, "A review on the separators of liquid electrolyte Li-ion batteries" Journal of Power Sources, 164:351-364, 2007.

http://www.electronicproducts.com/Power_Products/Batteries_and_Fuel_Cells/What_are_dendrites_and_why_do_they_cause_fires_in_lithium_batteries.aspx Accessed August 3rd, 2017

Electrode Material Analysis in Lithium Ion Batteries

The electrode materials used in lithium-ion batteries (LIBs) enable them to have much higher energy densities than alkaline batteries and other rechargeable batteries, allowing them to store more energy in a smaller space.¹

Consumers want devices that are small, powerful, durable, long-lasting, charge quickly, and need charging less frequently. The performance and manufacturability of LIBs are determined by the materials that are used in the battery. Controlling porosity, pore size and shape, particle size and shape, surface area, and density of electrode materials is vital to optimize the performance of LIBs. This article outlines the important microstructural properties of electrode materials and the analysis solutions offered by Micrometrics.^{2,3}

Measuring Electrode Porosity

Electrode materials must be porous to allow electrolyte to transport lithium-ions to and from the active materials of the electrode. Controlling porosity increases the contact between the electrode and the conductive diluent, thereby increasing intra-electrode conductivity, and ensuring adequate lithium-ion intercalation.²

Promising electrode materials including tin, iron, and cobalt oxides have previously been limited in their applications as volume changes resulting from intercalation can cause severe electrode degradation. Increasing the porosity of electrode materials using nanostructures allows the pores to act as buffers for the volume changes, improving battery performance and demonstrating the importance of porosity in electrode material development.⁴

Porosity is typically measured by determining the volume of gas or liquid that can flow into the electrode material, filling the space that was previously empty. Micrometrics offers a number of equipment solutions for measuring the porosity of electrode materials including the AccuPyc 1340, which use gas displacement to measure porosity; and AutoPore V, which use mercury displacement.²



Measuring Particle Size and Shape

The size and shape of the particles that constitute the electrode materials impact the final performance of LIBs in a number of ways including influencing packing density, porosity, ion diffusion, and intercalation. It has been noted that reducing particle size can reduce volume changes upon intercalation, reducing mechanical stress and the risk of fracture. It has also been reported that it is possible to tune electrode materials to have a high energy density or high power based on their particle size distribution, as simulations have shown that broad particle size distributions can provide up to twice the energy density of electrodes with a monodisperse size particle distribution, while monodisperse size particle distributions deliver the highest energy and power density for high discharge rates.^{1,5,6,7}

The Sub-Sieve AutoSizer and Saturn DigiSizer II from Micrometrics provide particle size measurements using air-permeability and light scattering analysis techniques, respectively, while the Particle Insight is a state-of-the-art dynamic image analyzer that offers particle shape analysis.²

Measuring Particle Surface Area

Electrode materials with high surface areas reduce diffusion distances and facilitate ion exchange between the electrode and the electrolyte, improving the efficiency of the

electrochemical reactions. However, greater surface areas can cause problems due to degradation of the electrode surface by the electrolyte, resulting in reduced thermal stability and capacity loss. Furthermore, lower surface area materials often provide improved cycling performance and longer battery life. It is therefore important to optimize the electrode material surface area to provide the correct balance of properties.^{2,3}

The TriStar II Plus from Micromeritics provides single and multipoint BET surface area measurements for electrode materials using N₂ physisorption. Measuring the surface area of electrode materials using N₂ physisorption can provide insights into performance variables such as capacity, impedance, and rate capability.^{2,3}

Measuring Density and Tap Density

The true or absolute density of electrode materials indicates the electrochemical performance of the materials by providing a measure of internal pore density, which has been correlated with irreversible capacity. Tap density gives a measure of the volumetric energy density of the material. Energy density is considered an important property of LIBs, as there is a constant drive to make batteries that hold the same amount of energy in a smaller space. The GeoPyc 1365 Envelope and Tap Density Analyzer from Micromeritics determines the bulk density, tap density, and envelope volume of electrode materials.^{2,8}

Measuring Pore Size, Shape and Tortuosity

The size, shape, and tortuosity of the electrode material pores significantly affect the transport of lithium ions through the electrolyte and in turn, has a direct influence on energy density, power, lifetime, and reliability of LIBs. An understanding of the interconnectivity of adjacent pores, closed pores, and channels of the electrode material helps to ensure optimal electrolyte and electrode interaction.

The Micromeritics AutoPore series of mercury intrusion instruments provide pore size measurements and tortuosity. Scanning electron microscopy, such as the Phenom Pro SEM from Micromeritics permits visual inspection of the surface of the electrode with magnifications up to 130,000x.

Conclusion

Researchers who are developing new electrode materials for LIBs need access to equipment that can quickly and accurately assess relevant properties including porosity, pore size and shape, particle size and shape, surface area, and density.

Micromeritics provide a portfolio of instruments that can meet these needs and allow researchers to optimize their electrode materials and develop the next generation of batteries.

References

1. <http://www.azom.com/article.aspx?ArticleID=13695> Accessed August 3rd, 2017.
2. http://www.micromeritics.com/Repository/Files/battery_brochure_2016_v2.pdf Accessed August 3rd, 2017.
3. Wasz ML, "Electrode surface area characteristics of batteries" 7th International Energy Conversion Engineering Conference, AIAA 2009-4503, 2009.
4. Goripart ia G, Mielea E, De Angelisa F, Di Fabrizioc E, Zaccariaa RP, Capigliaa C "Review on recent progress of nanostructured anode materials for Li-ion batteries" *Journal of Power Sources*, 257:421-443, 2014.
5. Chung DW, Shearing PR, Brandon NP, Harris SJ, Garcia RE, "Particle Size Polydispersity in Li-Ion Batteries" *Journal of the Electrochemical Society*, 161(3):A422-A430, 2014.
6. Röder F, Sonntag S, Schröder D, Krewer U, "Simulating the Impact of Particle Size Distribution on the Performance of Graphite Electrodes in Lithium-Ion Batteries", *Energy Technology*, 4(12):1588-1597, 2016.
7. Magasinki A, Dixon P, Hetzberg B, Kvit A, Ayala J, Yushin G, "High-performance lithium-ion anodes using a hierarchical bottom-up approach" *Nature Materials*, 9:353:358, 2010.
8. Smekens J, Gopalakrishnan R, Van den Steen N, Omar N, Hegazy O, Hubin A, Van Mierlo J "Influence of Electrode Density on the Performance of Li-Ion Batteries: Experimental and Simulation Results" *Energies*, 9(2) 104, 2016.

Zeta Potential Analysis of Lithium Ion Battery Electrolytes



The lithium ions within a lithium ion battery (LIB) migrate back and forth between the two electrodes during charging and discharging. The ions travel between the anode and the cathode via a separator by an electrolyte commonly composed a lithium salt (e.g. LiPF₆) in an organic solvent.

The electrolyte solution plays a critical role within LIBs by enabling an effective conduction of the lithium ions between the electrodes. Additives are commonly added into the electrolyte solution to improve performance, enhance stability, prevent solution degradation and prevent dendritic lithium formation. The prevention of dendritic lithium formation is key to achieving battery safety as the lithium dendrites establish a connection between the electrodes, causing the battery to overheat and become a potential fire hazard.

The electrolytes and their additives are commonly used in LIBs to identify the current density, stability and the reliability of the final battery. The properties of the electrolyte are therefore critical to the overall performance of the battery. Electrolytes must possess a good ionic conductivity and be electrically insulating, they should have a wide electrochemical window, they must be inert to other battery components and they must be chemically and thermally stable. In addition, electrolytes of a high purity (free from contamination) help to prevent oxidation at the electrode and promote a good cycle life.

The electrolyte requires the ability to form a stable solution with lithium ions and be able to pass through the separator with ease. Charge separations occur at the separator-electrolyte interface causing an electro-kinetic phenomenon that either impedes or aids the transportation of the electrolyte across the separator. The electro-kinetic potential caused by this phenomenon is termed the zeta potential.

What is Zeta Potential?

Zeta potential describes the electrokinetic potential in colloidal dispersions and is the potential difference between the dispersion medium and the stationary fluid attached to a dispersed particle. Zeta potential corresponds to the energy required to detach the particle and its inner layer of counter-ions from the bulk.

Zeta potential is the measurement of the electrostatic repulsion between particles and can indicate surface charges, electrolyte stability, interactions between battery components and the overall stability of the battery system. A large zeta potential, regardless of whether it is positive or negative, can help researchers to identify which components will work well together within the battery, thus, reducing the time and cost of testing and ensuring that the final battery is stable.

Zeta potentials are usually measured using electrophoresis, where electrodes are inserted into the suspension and a voltage is applied, upon which the charged particles migrate to the electrode with opposite charge. Light scattering techniques are commonly used to quantify the zeta potential-dependent electrophoretic mobility, or the velocity of the particles.

By measuring the electrophoretic mobility, it enables the zeta potential of the particle(s) to be deduced using the Henry or Van Smolukoski equations. However, non-aqueous solutions present a challenging environment for zeta potential measurements due to low particle mobilities, so highly sensitive and accurate analysis equipment is required to measure battery components.

The NanoPlus HD Zeta Potential Analyzer

Micromeritics offers the NanoPlus HD instrument, which is a zeta potential analyser that provides outstanding performance, sensitivity, a compact benchtop footprint, and intuitive software, making the instrument of choice for measuring the zeta potential of a wide range of materials.

The NanoPlus HD utilises dynamic light scattering (DLS) and electrophoretic light scattering (ELS) techniques to measure the particle size, zeta potential and molecular weight of materials. The NanoPlus HD also offers highly accurate measurements for concentrated solutions, based on the true determination of electrophoretic mobility. This makes the NanoPlus HD an ideal instrument for measuring the zeta potential of battery components in electrolyte solutions using a wide range of measuring cells, including a unique cell for flat surface and membrane research.

Conclusion

Researchers who are developing new materials for LIB applications require access to instrumentation that can quickly and accurately assess properties, such as zeta potential, to help them make an informed decision about which components will work well together and be stable within a battery system.

The NanoPlus HD zeta potential analyser from Micromeritics is the ideal solution to the meet needs and demands of researchers who are developing the next generation of batteries.

References

http://www.micromeritics.com/Repository/Files/battery_brochure_2016_v2.pdf Accessed August 14th, 2017.

Zhang SS 'A review on electrolyte additives for lithium-ion batteries' *Journal of Power Sources*, 165:1379-1394, 2006.

Li Q, Chen J, Fan L, Kong X Lu Y, 'Progress in electrolytes for rechargeable Li-based batteries and beyond' *Green Energy & Environment* 1(1):18-42, 2016.

Li J, Armstrong BL, Kiggans J, Daniel C, Wood DL, 'Optimization of LiFePO₄ Nanoparticle Suspensions with Polyethyleneimine for Aqueous Processing' *Langmuir* 28(8):3783-3790, 2012.

Li J, Armstrong BL, Kiggans J, Daniel C, Wood DL, 'Lithium Ion Cell Performance Enhancement Using Aqueous LiFePO₄ Cathode Dispersions and Polyethyleneimine Dispersant' *Journal of The Electrochemical Society* 160(2):A201-A206, 2013.

Bhattacharjee S 'DLS and zeta potential – What they are and what they are not?' *Journal of Controlled Release* 235(10):337-351, 2016.

<https://www.azom.com/article.aspx?ArticleID=935> Accessed August 14th, 2017.

Materials Characterization and Failure Analysis in Lithium Ion Battery Manufacturing



Characterizing and analyzing the failure of materials is a vital procedure towards optimizing the manufacturing processes of lithium-ion batteries (LIBs). By mixing active materials together with a series of binders, additives and solvents, a slurry can be formed and coated onto a current collector foil and dried, to produce LIB porous electrodes.

Throughout the whole process, that is from the raw material stage up until the actual electrode manufacturing process and assembly, materials characterization provides much needed critical control parameters to ensure that the final battery performance meets expectations.

Failure analysis also provides an insight as to why the performance of a battery degrades over time, whilst ensuring that the manufacturing process to fabricate the battery is optimized to minimize performance degradation. Herein, we discuss the analysis of key materials characterization parameters throughout the LIB manufacturing and failure analysis processes, whilst outlining the analysis solutions offered by Micromeritics.

Particle size and shape

The size and shape of the particles in the raw materials of the manufacturing of LIBs have a significant influence on the packing density of the produced electrode, which in turn affects the electrodes thickness and energy density. Particles which are too large can induce large volume changes whilst cycling, thus, increasing the potential for fracture to occur, producing a limiting effect on the battery lifetime.

The particle size distribution within graphite anodes is also known to affect the electrochemical performance of the cell, therefore, it is essential to ensure that the raw materials used in the manufacturing of an electrode possess the correct particle size.

Micromeritics offers a number of solutions for measuring a material's particle size. The Sub-Sieve AutoSizer, for example, allows for the determination of particles within the range of 0.2-75 μm using air-permeability. On the other hand, the Saturn DigiSizer II is the first commercially available particle sizing instrument that uses light scattering techniques to produce a particle size analysis with a high resolution, accuracy, repeatability and reproducibility. Another instrument, the Particle Insight, provides a combination of particle size measurements and shape analyses, using dynamic image analysis, for particles 3-300 μm in size.

Solid Fraction Determination

The process of passing electrode sheets through rollers to compact them is commonly known as calendaring and increases the energy density by reducing the thickness and porosity of the electrode. By exposing the electrode to calendaring process, the pore structure of the electrode changes and in turn impacts the wetting behavior of the electrode film through the electrolyte.

Calendaring is seen as a critical step in the production high performance electrode and by increasing the calendaring you decrease the porosity of the electrode. This means that too much calendaring can have a negative effect on the electrode and induce capacity loss, high cycling rates and a poor longevity in the cycle performance of the final battery. The determination of the solid fraction, or relative density, of the electrodes can be used as a useful control parameter to identify the ideal setting for optimal calendaring, and thus, allowing for a consistent calendaring and electrochemical performance from batch to batch.

Calculating the solid fraction parameter is obtained through the simple division of the envelope density of the electrode by the absolute density—meaning both the envelope and absolute density values are required to perform the solid fraction calculation.

Micromeritics offers the ideal solution for solid fraction determination, in the form of the AccuPyc 1340 and GeoPyc 1365 Instrument Porosity Bundle. The combination of both instruments provides all of the necessary information to calculate the solid fraction, with the AccuPyc 1340 determining the absolute density using gas pycnometry and the GeoPyc 1265 determining the envelope density using quasi-fluid displacement.

Performance Degradation

It is a fact that the electrochemical performance of LIBs degrades over time. The drop in performance is often recognized through capacity fade during charge and discharge cycles, or by a reduction in the shelf life. The reasons for capacity fade and impedance are complex, but material characterization techniques can help to understand and limit the performance degradation.

The analysis of the surface area, porosity, pore size distribution, and morphology of both fresh and aged battery components can provide insights as to why the battery performance degrades with time, and enables the manufacturing process to be optimized to limit performance degradation within the battery.

The expansion and contraction of the electrode during battery cycling can cause stresses that affect the battery's performance, particle density and porosity, with the possibility of delamination and a reduction in the contact between the electrode and current collector occurring. Changes in these properties, caused by volume changes during the cycling process, can be monitored by comparing the properties of both aged and newly produced materials.

Micromeritics offers several key instruments for the physical evaluation of new and degraded battery materials. The AccuPyc 1340 and GeoPyc 1365, TriStar II Plus, and AutoPore V provide pore size and porosity measurements, whilst Phenom Pro SEM can be used to determine the whole surface morphology and pore size of electrode materials.

Conclusion

Utilizing material characterization techniques before, during and after battery manufacturing is a crucial process which ensures that the manufacturing process is optimized and the performance of the final battery meets expectations.

Micromeritics offers a number of instruments which meet the analysis needs of LIB manufacturers.

References

http://www.micromeritics.com/Repository/Files/battery_brochure_2016_v2.pdf Accessed August 14th, 2017.

Daniel C 'Lithium Ion Batteries and their Manufacturing Challenges' Available from <https://www.nae.edu/19582/Bridge/133842/134258.aspx> Accessed August 14th, 2017.

Chung DW, Shearing PR, Brandon NP, Harris SJ, Garcia RE, "Particle Size Polydispersity in Li-Ion Batteries" Journal of the Electrochemical Society, 161(3):A422-A430, 2014.

Röder F, Sonntag S, Schröder D, Krewer U, "Simulating the Impact of Particle Size Distribution on the Performance of Graphite Electrodes in Lithium-Ion Batteries", Energy Technology, 4(12):1588-1597, 2016.

APPLICATION NOTE 171

Magasinki A, Dixon P, Hetzberg B, Kvit A, Ayala J, Yushin G, "High-performance lithium-ion anodes using a hierarchical bottom-up approach" *Nature Materials*, 9:353:358, 2010.

<https://www.azom.com/article.aspx?ArticleID=13573>

Accessed August 14th, 2017.

Wolter M, Leiva D, Fritsch M, Borner S, 'Process development and optimization for Li-ion battery production' EVS27 International Battery, Hybrid and Fuel Cell Electric Vehicle Symposium, Barcelona Spain, 2013.

Cheng X, Pecht M, 'In Situ Stress Measurement Techniques on Li-ion Battery Electrodes: A Review' *Energies*, 10:591, 2017.

Agubra V, Fergus J, 'Lithium Ion Battery Anode Aging Mechanisms' *Materials (Basel)* 6(4):1310-1325, 2013.

Wang X, Sone Y, Segami G, Naito H, Yamada C, Kibe K 'Understanding Volume Change in Lithium-Ion Cells during Charging and Discharging Using In Situ Measurements' *Journal of The Electrochemical Society* 154(1):A12-A21, 2007.

Fine Powder Design – Flow Rate Control

By: Dr. Kerry Johanson Material Flow Solutions, Inc.

Engineers must often control the mass flow rate from a handling system by using a volumetric feed device. This poses several problems. Accurate control requires three conditions: consistent bulk density, geometries that are not flow rate limited, and orifice sizes greater than cohesive hang-up conditions. Flow rate limitations are often severe and it is difficult to tell the difference between a slow flow rate limited condition and a cohesive hang-up.

Fine powders have two flow modes under gravity feed conditions. If there is enough gas entrained in the material, then the bulk solid becomes semi-fluidized and behaves as a liquid flowing from a container. In this case, the flow rate limitation is governed by acceleration of the semi-fluidized bulk material through the container. An active flow channel forms around an orifice with a conical shape or conforms to the shape of the container if the wall friction angle is small enough to induce mass flow. In either case, convergence of the flow channel controls acceleration or increase in velocity through the outlet. This limitation results in very fast flow rates through containers.

There is another reason for flow rate limitations in process equipment. Fine materials consolidate as they flow through a bin. If consolidation occurs slowly, then gas contained in interstitial pores of the bulk material leaves the bulk material through the top material surface. As this compressed and de-aerated material approaches the hopper outlet, it expands to flow from the outlet. This expansion results in a negative gas pressure formation near the hopper outlet (Figure 1). Gas attempts to rush in to equalize this negative gauge pressure. If the permeability is low, this process takes time. The negative gas pressure gradient then persists, resulting in partial support of material flowing from the outlet and creating a very slow flow rate through the hopper. Both the compressibility and permeability of the bulk material are required to compute the value of this rate limitation.

Permeability is the superficial velocity of gas or fluid passing through bulk material when the pressure drop across the bulk material equals the weight density of the bulk. It can be thought of as an incipient fluidization velocity, except it is measured as a function of the stress applied to the bulk material. However, the value of the permeability extrapolated to zero stress is identically equal to the incipient fluidization velocity. Permeability data is used to determine pressure drops in packed bed operation. It is also used to determine limiting flow rates where the resistance to gas flow is the key limiting factor to solids flow.

The other property used to compute this limiting flow rate is the bulk density. Bulk density may seem like an intrinsically simple property. It is the weight of the particles divided by the combined volume of the particles and the interstitial voids surrounding the particles. However, it is a function of the stress level and strain history of the material. We measure it using uniaxial compression of a loosely packed bulk material.

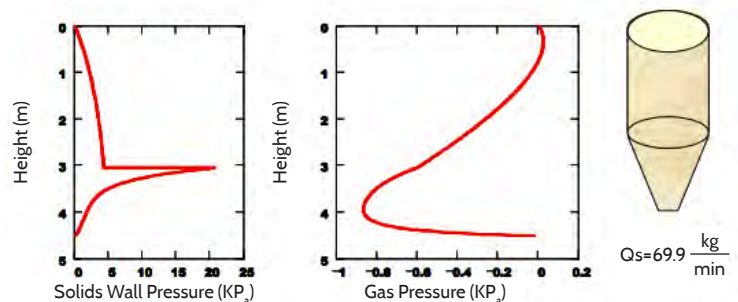


Figure 1. Gas pressure in process equipment resulting in flow limitations

APPLICATION NOTE 012

Compression of material during flow causes a change in the material porosity. This porosity change dictates the quantity of gas that must be injected into the bulk material to overcome negative gas pressure within the solids during flow. Permeability governs how fast this quantity of gas can pass through the bulk material. The combination of both these effects governs how fast a fully de-aerated material will flow from an outlet. Generally, this is at least an order of magnitude less than the acceleration limit. The solution to this problem is to inject gas at the right location and limit the right flow rate and pressure (Figure 2).

The amount of gas needed is only that required to match the gas squeezed out of the material during normal flow. The location and amount of gas injection are critical to proper operation. Too much gas aerates the material and results in uncontrolled flooding and flushing. Too little gas or gas injected in the wrong location will be insufficient to overcome flow rate limitations. Sometimes multiple injection locations must be used to achieve reliable flow. The degree of material cohesion and how close the material is to arching over outlets will also affect flow rates from the process vessel. In some instances, gas injection will change the mass flow and hang-up characteristics of the process vessel and this must be evaluated to assure gas injection will not cause other flow problems.

We use our proprietary computer program to compute limiting flow rates from bins, hoppers, blenders, feeders, and other process equipment. This program will examine your particular process vessel geometry and use measured flow properties to compute the expected flow rate limitations as well as the optimal gas injection placement and quantity to achieve reliable flow. It will determine if gas injection will initiate funnel flow or hang-up behavior and provides a means of solving your flow rate limitation problem.

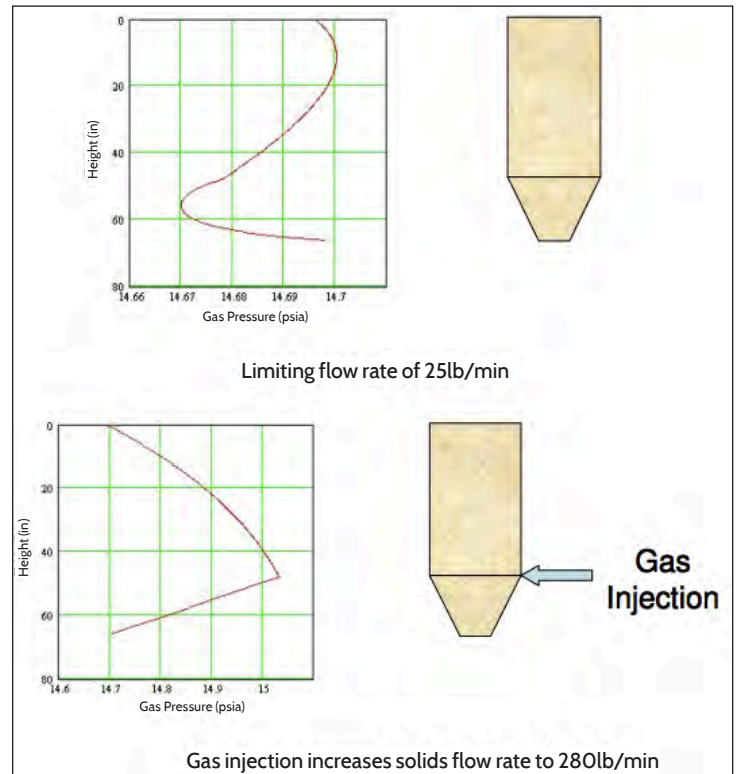


Figure 2: Example of how gas injection solves flow rate limitations

Sometimes the problem is too much gas entrained in the system. In this case, we can use our proprietary computer programs to compute the de-aeration time, maximum throughput or residence time required to de-aerate material during process operations. These calculations are based on measured flow properties and your particular geometry. Unit operations where deaeration is important and can be evaluated are bins, hoppers, screws, roll presses, belt feeders, table feeders, tablet or package fill stations, tablet press operation, and die filling operations. Controlling the mass flow rate is often the critical step required to create robust process control. Let us help you optimize your process and bring it under control using scientifically proven principles of operation.

Using a Tester to Accurately Predict Hang-Up Issues In Process Equipment

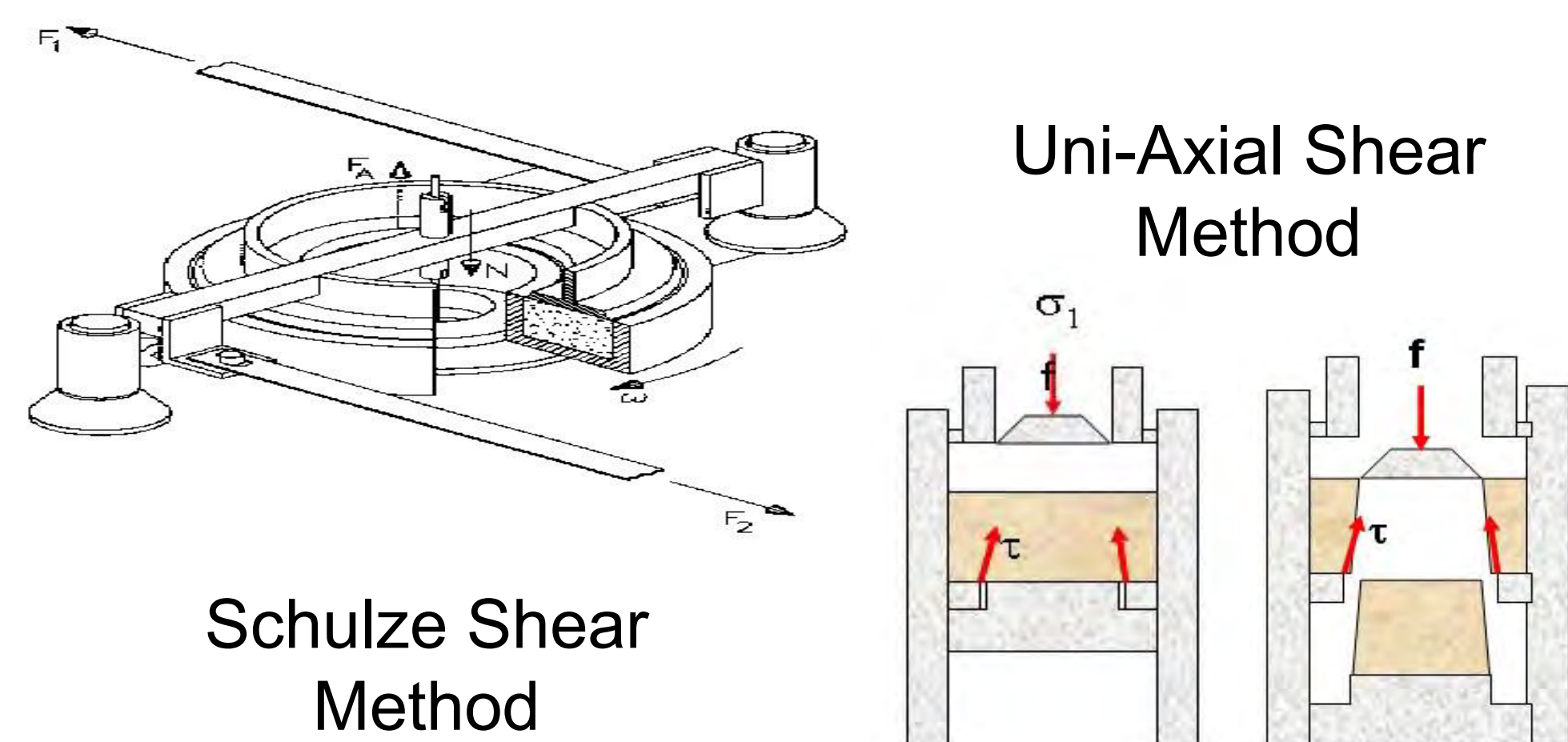
Authors: Max Groom* and Dr. Kerry Johanson**

* Particulate Systems (a subsidiary of Micromeritics) ** Material Flow Equipment, LLC

Full Abstract

Unconfined yield strength, measured as a function of major principle stress, is responsible for most process arches and hang-ups. However, traditional measurements of cohesive flow properties often result in poor process predictions, especially in small diameter hoppers. The major principle stress in a hopper is directly proportional to the hopper span. Thus, stress levels near small hopper outlets are very small – so small that traditional measurement techniques cannot quantify the bulk unconfined yield strength at stress levels corresponding to those expected near the hopper outlet. We postulated that the inability to predict this process behavior in small bins is because most current methods cannot measure strength values at low enough stresses to be useful. Recent advances in technology allow measurement of unconfined yield strength of fine powders at very low stress levels. To prove the technology, bulk strength values were measured using both traditional methods and the new methodology. Critical arching dimensions were computed using data from both methods and compared to direct measurements of arches in small diameter hoppers. Traditional measurement required data extrapolation to predict arching in small hoppers and resulted in arching estimates two or three times those measured in actual hoppers. Conversely, using the new method to compute critical arching dimensions resulted in predictions within 20% of actual measured arching dimensions. Thus, this new technology and test method provide prediction of process behavior significantly superior to all previous methods.

Unconfined Yield Strength Measured by Traditional Methods



There are several apparatus and methodologies available to measure material bulk strength. Most involve placing a material sample into a test cell, adding compaction pressure and rotating (or shearing) the apparatus until the material fails (falls out of the test cell):

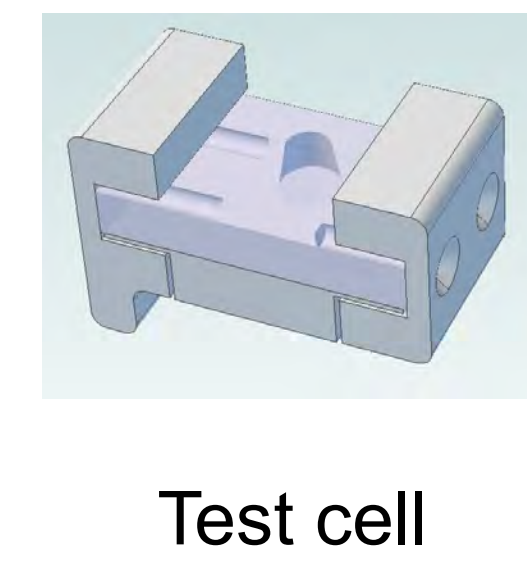
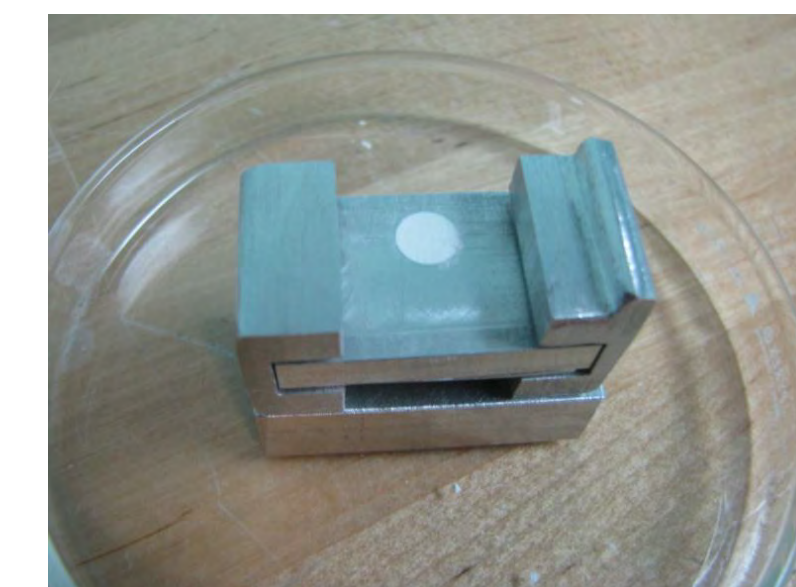
- Most bulk strength testers based on material shear require multiple tests to garner a single data point
- Most bulk strength testers require 300 or more grams of material to produce a full flow function
- Most bulk strength testers can measure only at pressures near or above 1KPa
- Real process pressures are more on the order of 300-400 Pa
- Extrapolation is messy – and does not correlate to small-scale geometries
- Small-scale designs based on traditional strength test methods

Recent advances in technology allow measurement of unconfined yield strength of fine powders at very low stress levels

Measurement Methodology

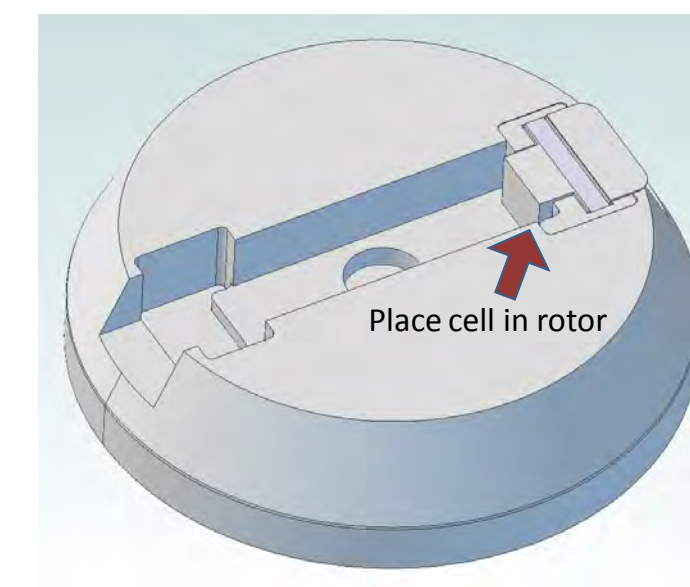
The test technique is to place a small quantity of material into an enclosed conical cavity; consolidate it using centrifugal force; remove the obstructions at the bottom of the conical cavity and use centrifugal force to cause material to fail, yield or extrude from the cavity. The process is summarized in steps 1 through 4 pictured below.

Step 1



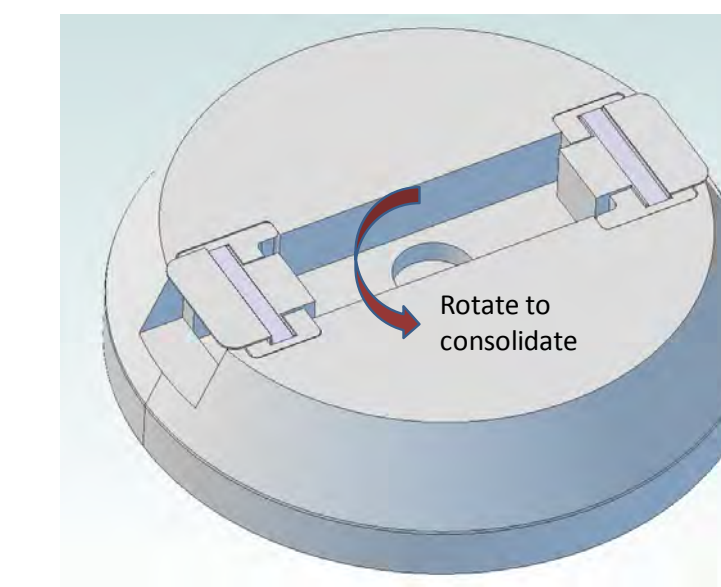
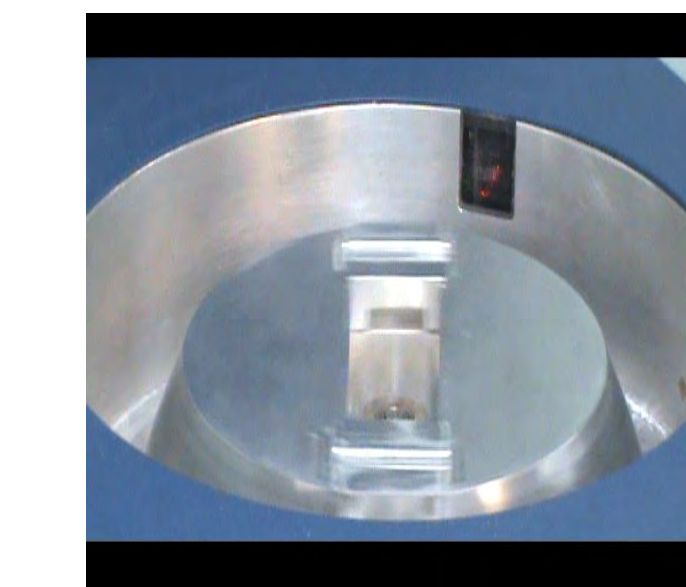
- Fill test cell with material: less than one (1) gram required

Step 2



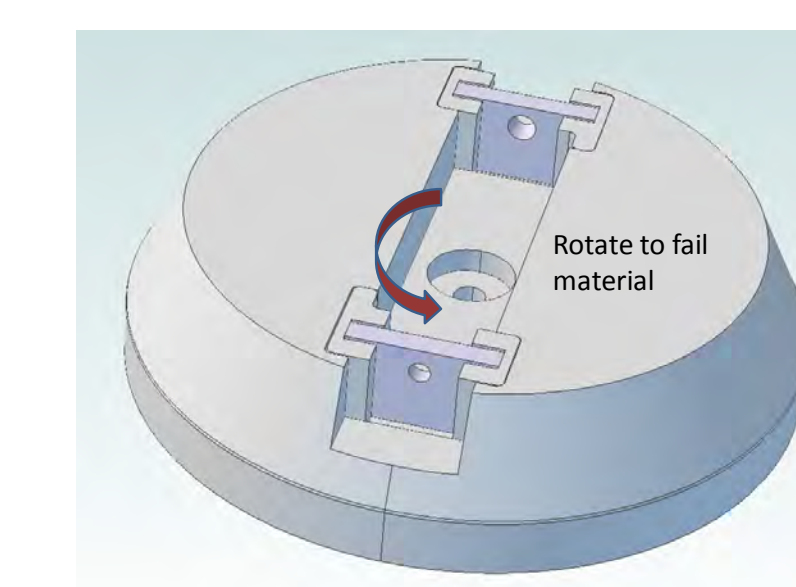
- Place test cell in rotor holder
- Centrifugal force used to both consolidate and fail material

Step 3



- Place full cell in rotor
- Spin rotor to compact material in cell
- Compute the major principle stress

Step 4



- Remove retaining gates
- Spin rotor to drive material from cell
- Laser detects free path
- Compute unconfined yield strength

Case Study – Comparison of New Method with Schulze Shear Method

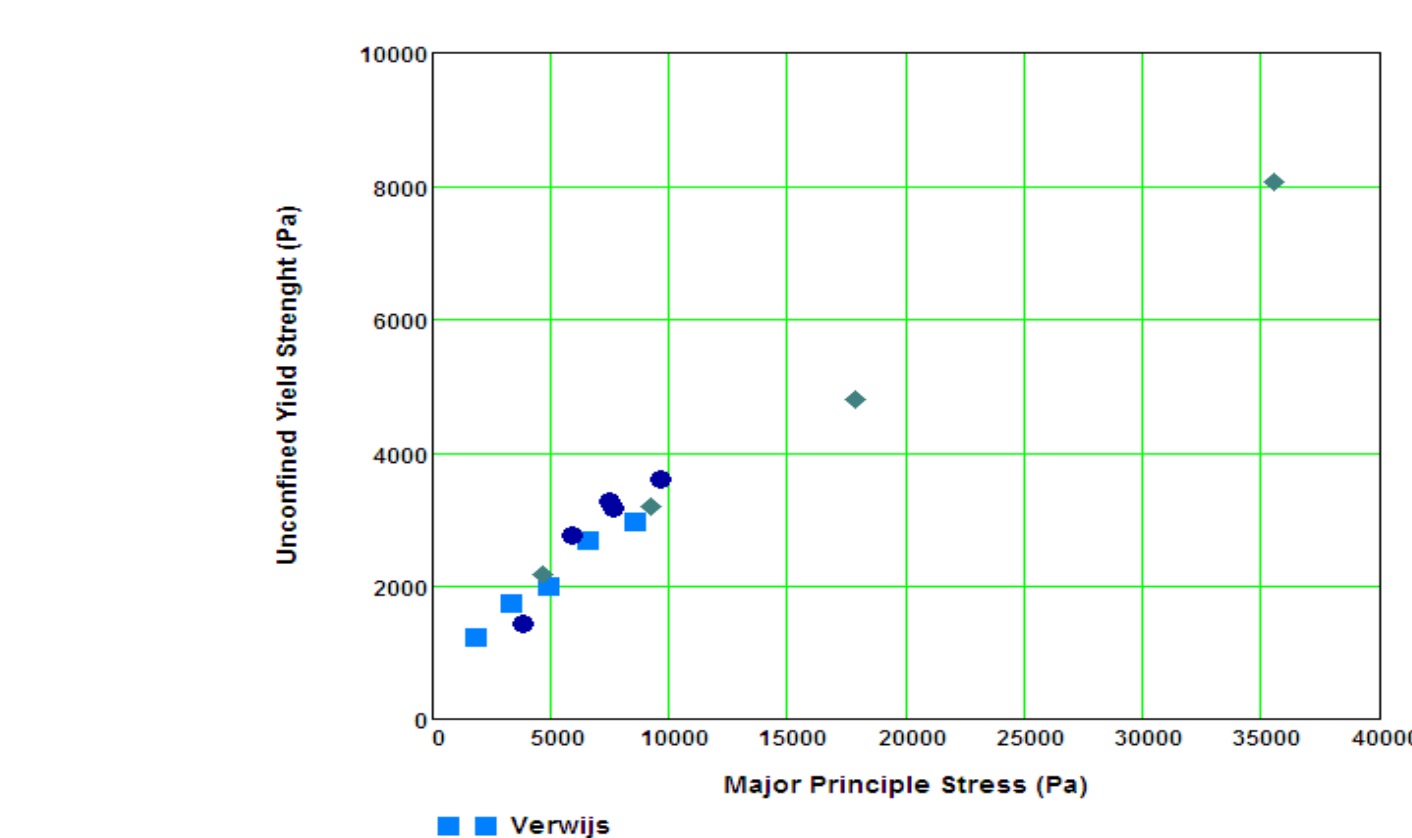


Figure 1. Comparison of BCR Limestone data generated from three different studies

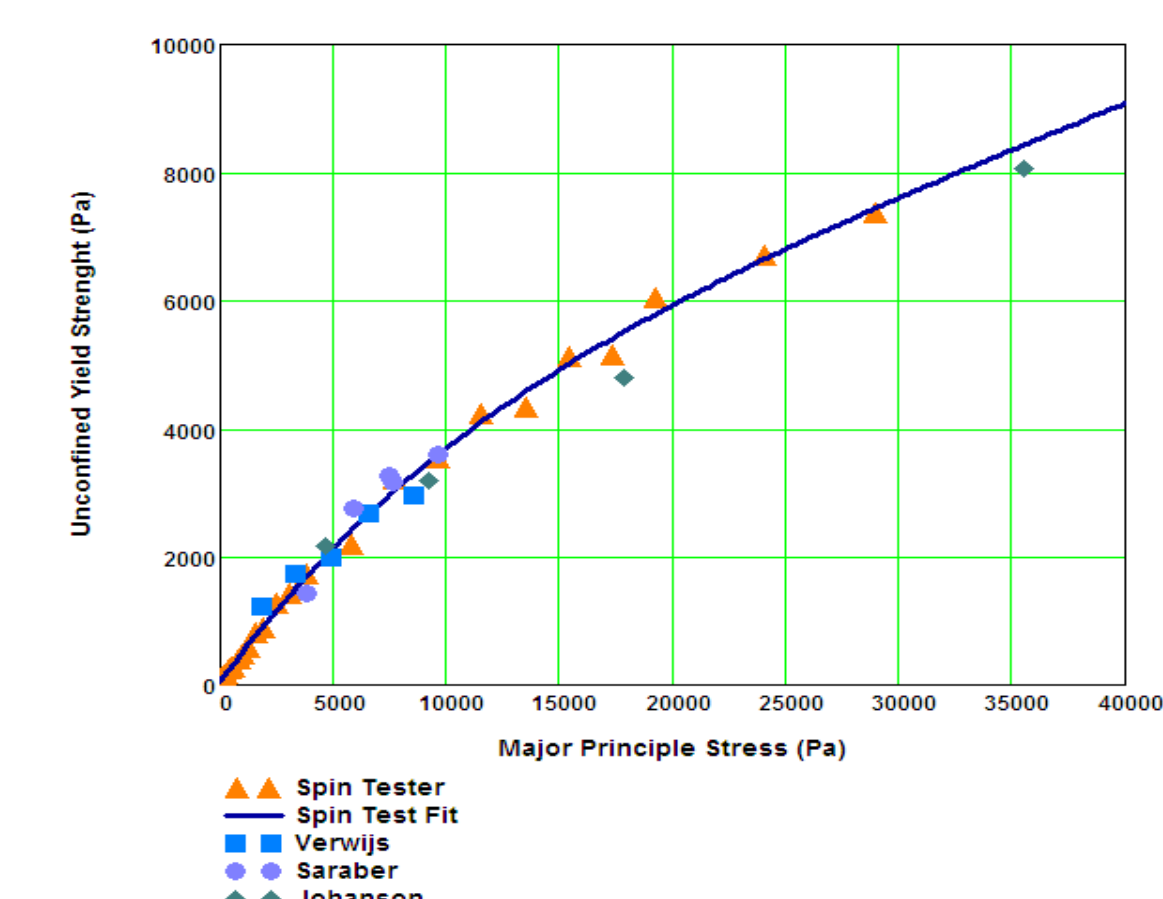


Figure 2. Comparison of BCR limestone data generated from three different studies and new test technique (SSSpinTester)

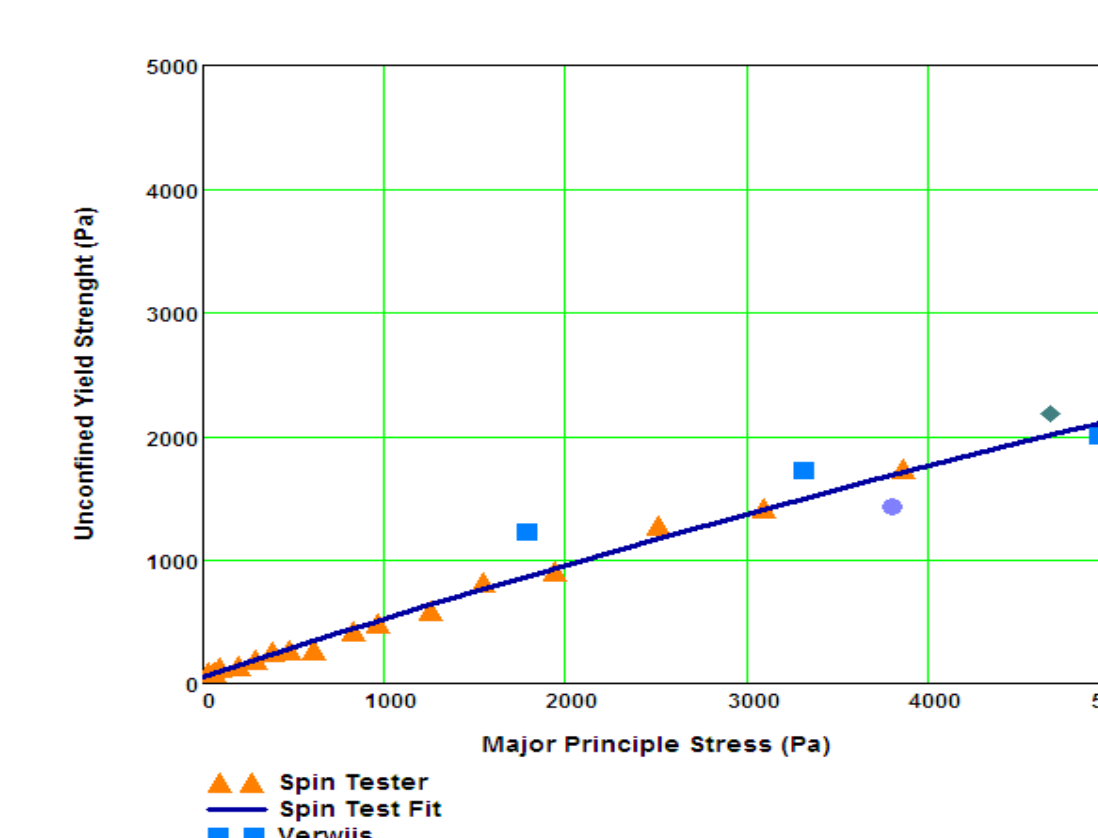


Figure 3. Comparison of low stress level BCR limestone data generated from three different studies and new test technique (SSSpinTester)

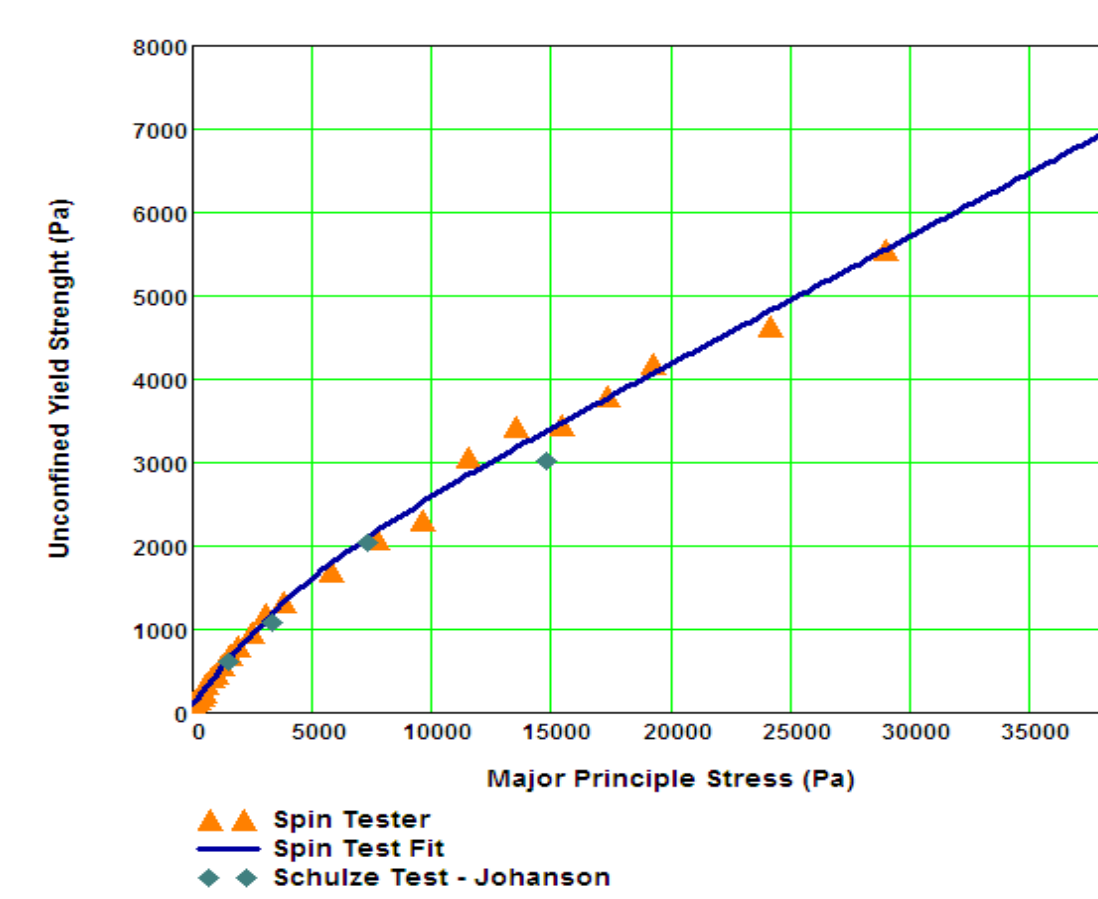


Figure 4. Comparison of the unconfined yield strength of Argo cornstarch measured with the Schulze direct shear method and the new test technique (SSSpinTester)

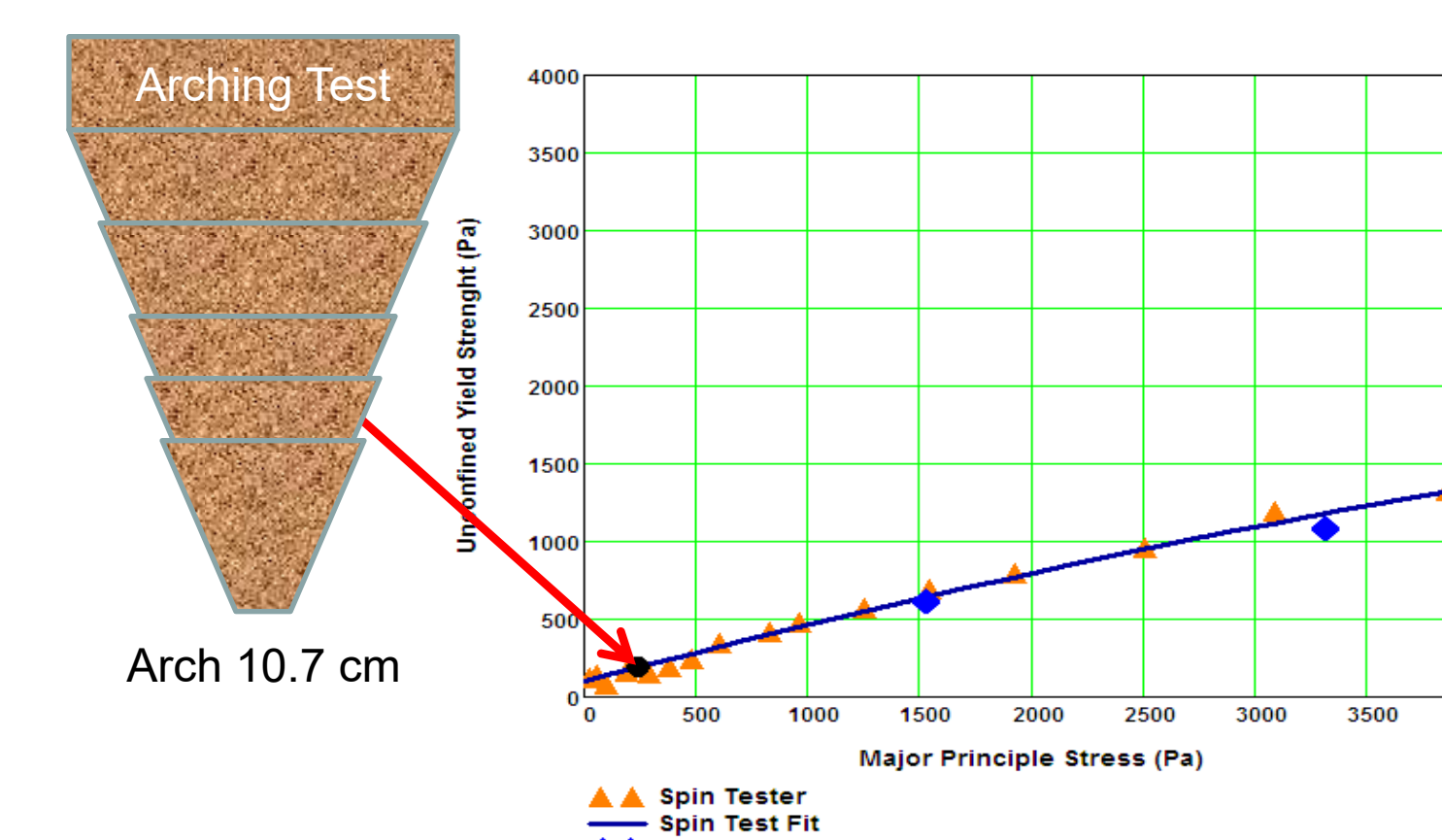


Figure 5. Comparison of the lower stress level unconfined yield strength of Argo corn starch measured with the Schulze direct shear method and the new test technique (SSSpinTester)

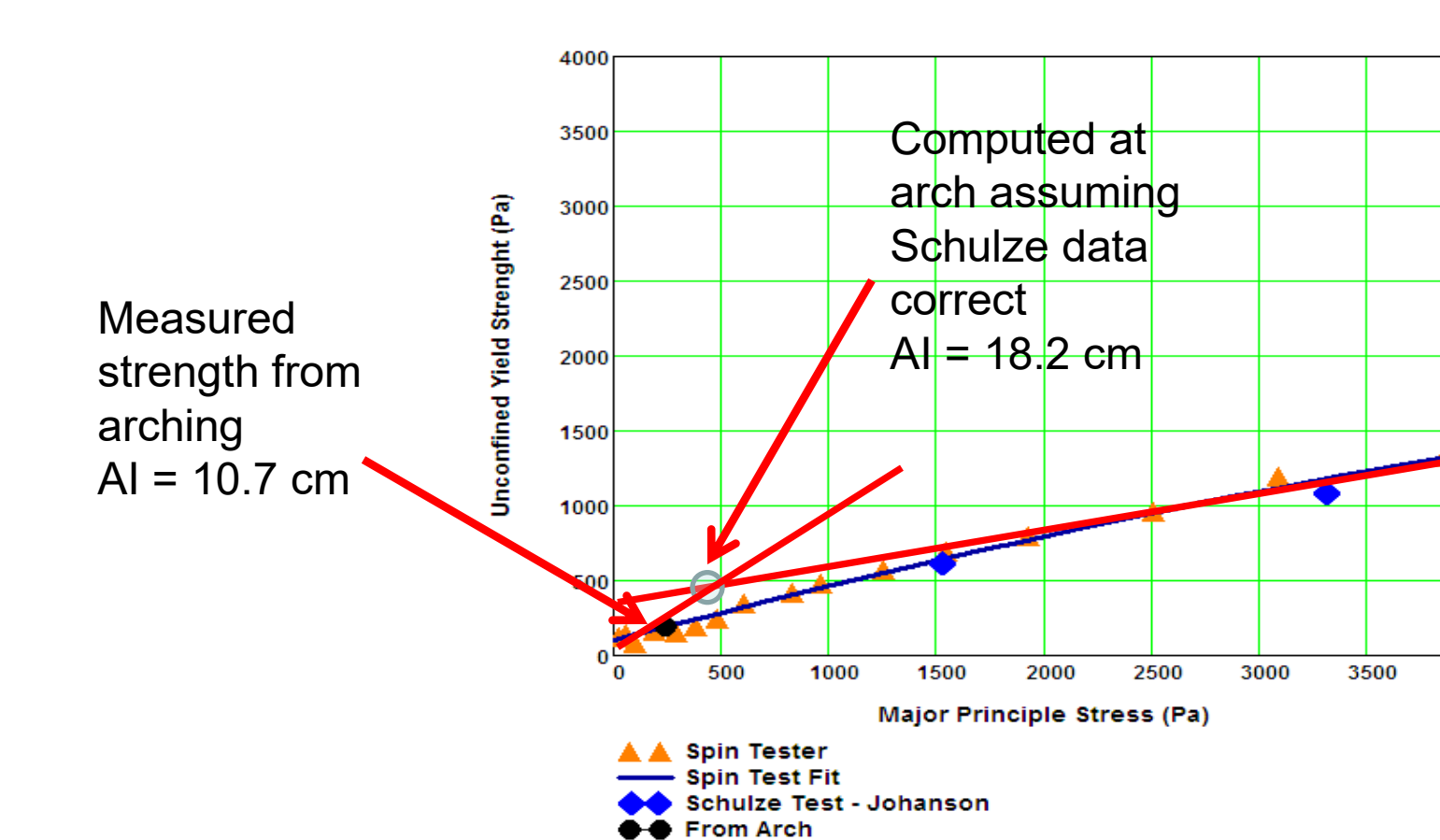


Figure 5. Comparison of the lower stress level unconfined yield strength of Argo corn starch measured with the Schulze direct shear method and the new test technique (SSSpinTester)

Conclusions

- New test method can measure strength at low stress values comparable to those near small diameters hopper outlets
- Can interpolate to get arching instead of extrapolate
- Strength is measured with very little material: Good for expensive and hard to get materials
- Low pressure strength can be applied to segregation on piles, capsule filling, tablet feed, fluidization, dispersion models and other low pressure unit operations or formulation needs



The Importance of Random Orientation When Measuring Particle Shape

Irregularly shaped particles require analysis with random orientation to ensure accurate results.

Introduction

Particle shape is becoming more and more recognized in industry as a desirable way to monitor many industrial materials and processes. In many applications, the circularity of particles can affect both performance and flowability in manufacturing. In some cases, for example, measuring surface smoothness can impact how abrasives will perform. For those who have realized that irregularity of their particles impact both manufacturability and efficacy, microscopy for shape analysis, historically, has been the solution. Microscopy (also known as static image analysis) orients particles so that the largest area of the particle faces the viewing point. This technique may be sufficient for providing a general idea of particle shape, but is insufficient when using particle shape analysis as a means to control a process.

Obtaining data from forced oriented particles provides only a portion of the information required for a full understanding of how particles will perform. Instrumentation providing limited information can lead to incorrect assumptions about raw material and, in turn, impact performance of the final product.

Therefore, a particle shape system being used for process control must be capable of fully analyzing all dimensions of particles.

Figure 1 shows a polystyrene latex bead, which is spherical, and a particle that is a flat disc. To a static image analysis system or microscope that orients the largest area of the particle toward the viewing point, these particles are reported as the same and render similar equivalent spherical size data. However, by the very nature of their shape, these particles would flow differently in a manufacturing process and have a different impact on the final product.



Figure 1: Although both yield similar results in equivalent spherical diameter, the sphere on the left is actually quite different from the flat disc on the right. A system that orients the largest area of the particle at the viewing point would be unable to see all dimensions of the particle.

Figure 2 shows a crystal-like sample, which is flat and hexagonal in shape. These sample characteristics have been determined using the Particle Insight Dynamic Image analyzer, which is designed for random particle orientation. The Particle Insight also recirculates the sample similar to a traditional Laser Diffraction system.

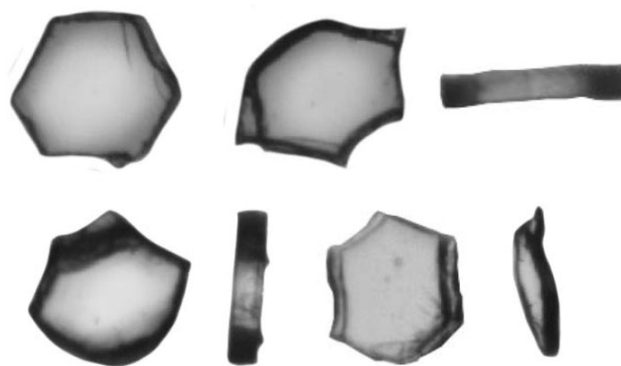


Figure 2: Typical particle thumbnails from a Dynamic Image Analysis system. Notice random orientation allows the analysis of all dimensions of the particle, not just the largest area.

Random orientation (for capturing true particle dimension) and recirculation of the sample (for statistical accuracy) are two features which have been instrumental in standardizing laser diffraction in process control for many raw materials worldwide.

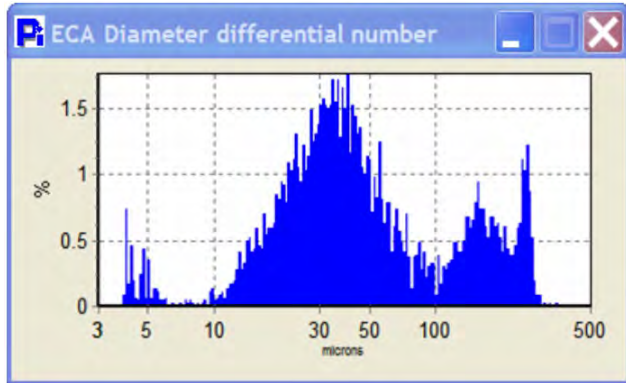


Figure 3: Statistical results for flat particles. Note the peaks above 100 μm are the particles that had their largest area oriented toward the viewing point. The particles under 100 μm are variations of particles being analyzed on their other orientations.

Figure 3 displays plotted results of the sample crystals shown in Figure 2.

Conclusion

The purpose of any particle shape analyzer is to provide the user with accurate results so that their process can be monitored or adjusted. By having such a system, the user can rest assured that the data being obtained are a true representation of their sample.

In this application, it is evident that random orientation provides a better representation of the sample and is the preferred method when true particle shape is critical to the efficacy of the final product.

The Particle Insight Analyzer from Particulate Systems employs two important features: random orientation and recirculation of the sample. These two features help to ensure a true representation of the sample and accurate data.

Uniformity of Particle Shape for Chromatography Packing Materials Used in HPLC

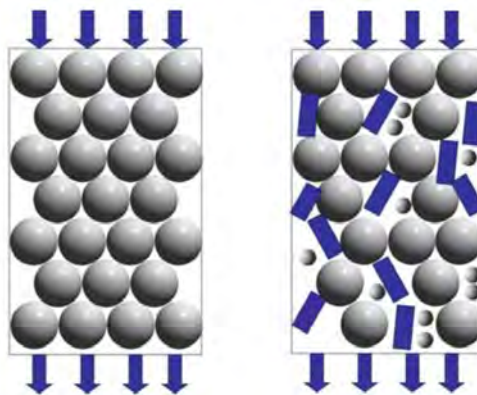
Introduction

High Performance Liquid Chromatography (or High Pressure Liquid Chromatography) is a separation technique used in many areas of analytical chemistry to separate, identify, and qualify various compounds in a specific solution. HPLC utilizes a column that holds chromatographic packing material that retains molecules as they are pumped through the column, the retention time being dependent on the packing material, the carrier liquid (solvent), and the specific type molecule. Each chemical species in the injected sample is most commonly identified by UV and Mass Spec detection.

Most traditional analytical HPLC packing materials have an average diameter of approximately 2 to 30 microns and are typically a silica-based or alumina-based material. The particle size of the packing material is usually measured using methods that assume all particles are uniformly spherical. This may not be the case, as in manufacture of the silica and bonding, fines and irregular shaped particles can be a percentage of the final product. As particle size decreases, the effect of fines and irregular shaped particles demands a greater degree of control on incoming quality of the silica material. Variation in particle shape can directly affect reproducible performance. Filling stage backpressure of the column can vary greatly depending on the shape of the HPLC particles.

The flow of a packed HPLC sample column using perfectly spherical particles has a very predictable performance when used to separate molecules. In addition, the manufacturing of a column with only truly spherical particles would be predictably consistent. However, in many situations, some of the particles used for HPLC column packing are irregular in shape or exist as fines. As a result, the packing geometry can become irregular and it may express as non-uniform performance of the final product from column to column, lot to lot.

The percentage of irregular packing and fines can alter the consistency of performance of the column and make HPLC columns much more expensive to manufacture because of the additional care and expertise required in



A column packed with uniform spherical beads is easier to manufacture and yields consistent and uniform results.

The same column containing irregular particles and fines will present manufacturing challenges as well as end-user concerns with respect to consistency.

achieving consistency in production. Possible downtime in production can result if incoming lots of materials contain varying percentages of irregular particles.

Ideally, if there was a method for the packing material manufacturer to specify shape characteristics and for column manufacturers to inspect incoming materials against those specifications, manufacturing of HPLC columns would become more predictable, less costly and exhibit consistent performance. Recent advancements in Image Analysis could provide the answer.

The analytical technique used in the experiment outlined in this application note is Dynamic Image Analysis. With Image Analysis, images are captured and analyzed as particles pass through a detection zone. ISO 13322-2 is used as the guideline for all Dynamic Image Analysis instruments available on the market today. The key benefit of using Image Analysis for HPLC column packing materials is to enable the identification and quantification of the different particle shapes present in incoming materials.

APPLICATION NOTE 003

Experiment

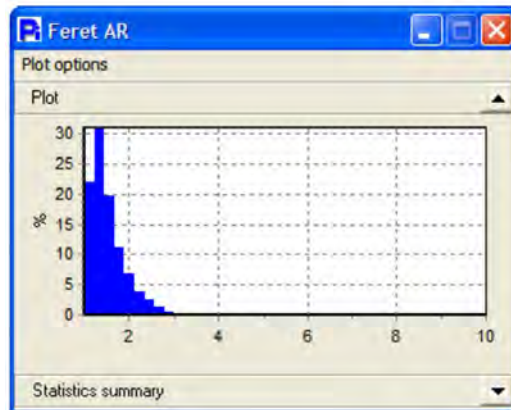
Inconsistent packing pressures observed during the manufacture of specific HPLC columns and a wide variation in their performance prompted the analysis of this particular sample.

For this experiment, the Particle Insight Particle Shape Analyzer measured incoming HPLC materials used to pack Size Exclusion Chromatography columns. Proper sampling of the incoming materials was made to ensure a homogeneous sub-sample was taken. The sample was then suspended in water and analyzed. The Particle Insight system recirculates the sample much like laser diffraction systems. All particles are measured and randomly oriented to measure all dimensions, not just two sides.

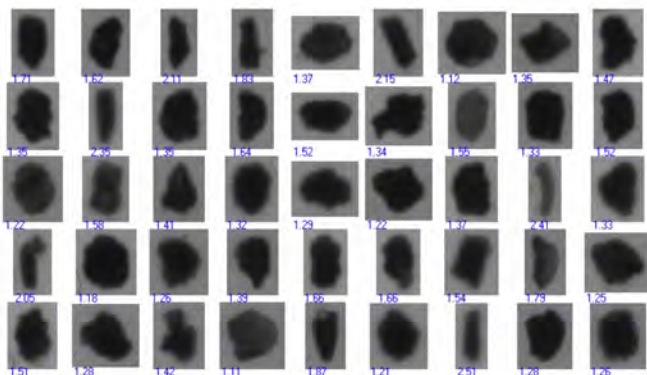
Results and Discussion

After analysis and a review of all particle thumbnail images, it was evident that this alumina sample had two distinct shape populations. One was rod-shape and the other had an aspect ratio near unity, but the particles were not round. Had the sample been analyzed using a sizing technique that assumes all particles to be spherical, these rod-like and irregular particles could not be differentiated.

In developing a method for this sample, particles with an aspect ratio greater than 1.9 were considered to be rod-like and more likely to negatively impact the packing efficiency of the column. This aspect ratio value threshold was derived from sample lots that did and did not exhibit the problems previously described.

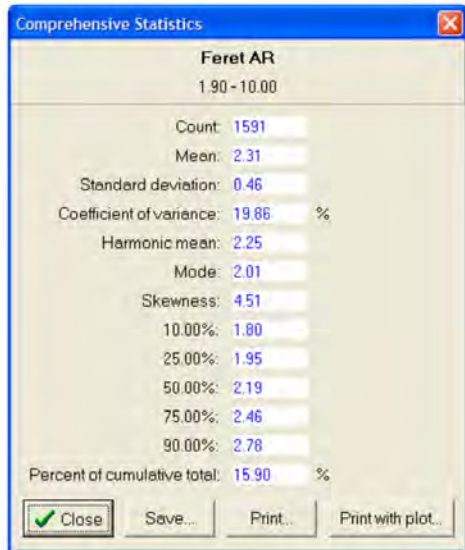


As shown in the histogram and statistical data, the percentage of rod-like particles in this column packing material was 15.90% of the total distribution which, compared to the historical lot of good material, proved to be excessive for the particular application of the column.

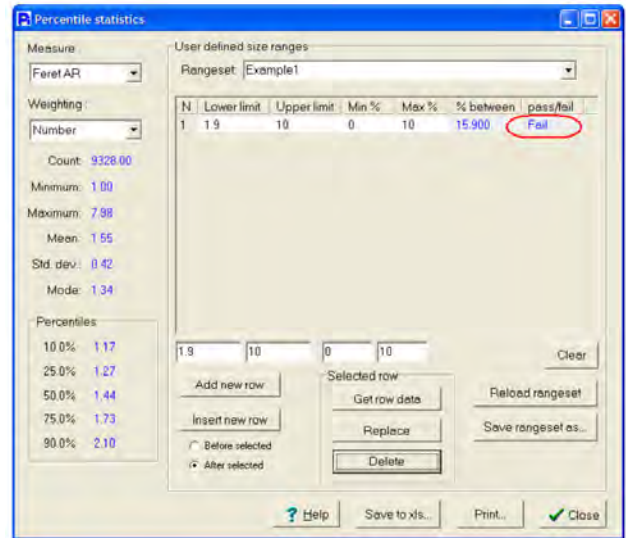


Random thumbnail images of the alumina sample from the 10,000 captured in just over one minute. The value under each thumbnail represents the Feret Aspect Ratio of each particle.

APPLICATION NOTE 003

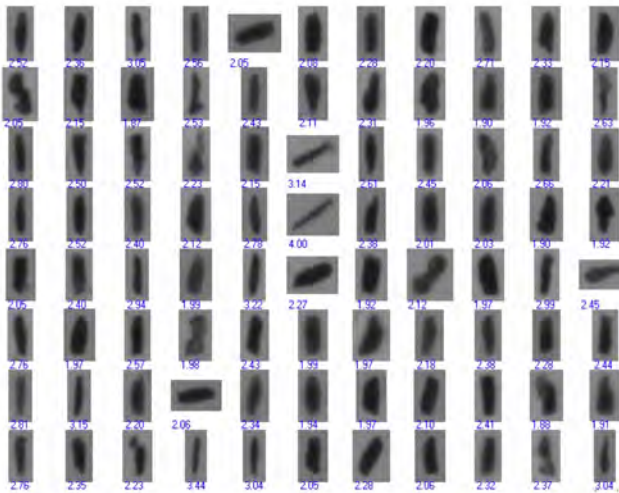


Comprehensive Statistics for the alumina sample.



The Percentile Statistics feature enables you to see particle statistics and pass/fail criteria.

A review of the thumbnails for only those particles that have a Feret Aspect Ratio greater than 1.9 gives a better perspective on what these particles actually look like.



A sampling of the thumbnails of the 1,591 particles found to have an aspect ratio greater than 1.9.

With a method established to determine that the Feret Aspect Ratio of incoming alumina packing material had no more than 10% rod-like particles, the end-user was able to create a simple process control indicator with the Particle Insight.

Using the Percentile Statistics feature, incoming quality control can determine easily and quickly if a lot of material passes or fails the criteria established by management.

Conclusion

The Particle Insight with its Dynamic Image Analysis technique can help reduce costs by finding HPLC packing material inconsistencies prior to reaching column manufacturing. The manufacturer is still responsible for determining the acceptable percentage of non-spherical particles for incoming materials. Once the manufacturer establishes incoming quality control criteria, the Particle Insight can be used as a pass/fail inspection tool to determine the percentage of spherical to non-spherical particles. Solving this potential problem early in the process improves production and helps to ensure consistent HPLC column quality and performance.

Using the HPVA to Analyze High-Pressure Carbon Dioxide Capture on Porous Carbons

The Particulate Systems HPVA (High Pressure Volumetric Analyzer) can evaluate the adsorption and desorption isotherms of carbons, metal organic frameworks (MOFs), and other materials at pressures up to 200 bar using a variety of gases. One application of the HPVA that is of particular interest in today's push for greener manufacturing and industrial processes is measuring carbon dioxide capture on carbons. Carbons can be used in stack scrubbers to capture the carbon dioxide produced by fossil fuel burning power plants and chemical refineries. The high-pressure system of the HPVA can also simulate conditions similar to the conditions underground where carbon dioxide can be stored using sequestration.

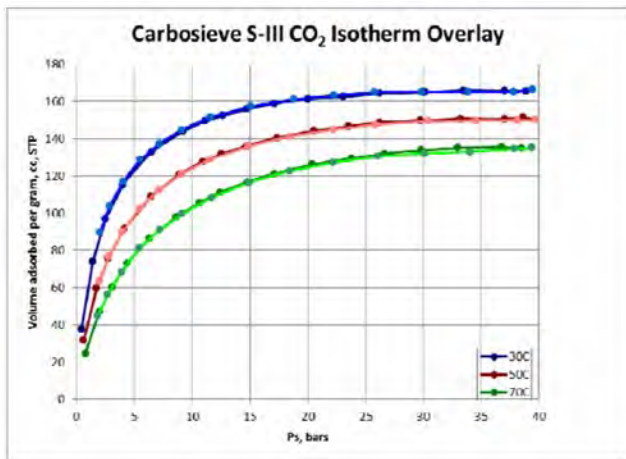


Figure 1: The carbon dioxide excess adsorption/desorption isotherms of carbon S-III. For differentiation purposes, the desorption curve is a lighter shade than the adsorption curve

The HPVA was used to evaluate the amount of carbon dioxide that can adsorb onto two porous carbons – Carbosieve S-III and Ultra Microporous Carbon (UMC) at pressures up to 40 bars. The carbon sample was placed in a sample tube and installed on the degas port of the HPVA, where it was evacuated under vacuum and heated to 350 °C. To ensure the removal of all water vapor and adsorbed gases, the sample was kept at 350 °C for a period of 20 hours. After 20 hours the sample was brought back to room temperature and moved to

the analysis port of the HPVA. An isolation valve on the sample stem prevents any atmospheric gases and water vapor from contaminating the sample after degassing. Once on the sample port, the carbons were analyzed at three temperatures: 30 °C, 50 °C, and 70 °C. The analysis temperature was held constant by means of a re-circulating temperature control bath. The analysis temperature was held to ± 0.1 °C throughout each analysis, with the exact sample temperature measured by an RTD integrated into the

HPVA system. Each isotherm experiment took approximately 24 hours to complete. The isotherms are shown in Figures 1 and 2.

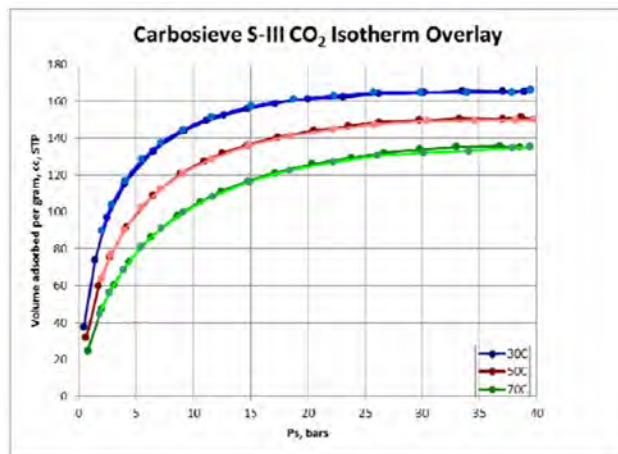


Figure 2: The carbon dioxide excess adsorption/desorption isotherms of carbon DW509. For differentiation purposes, the desorption curve is a lighter shade than the adsorption curve.

Due to the non-ideal nature of carbon dioxide at elevated pressures, the volumetric calculations are corrected using the compressibility factor (z) of carbon dioxide as a function of temperature and pressure. The compressibility factor at each temperature and pressure is determined using the National Institute of Standards and Technology (NIST) Reference Fluid Thermodynamic and Transport Properties Database (REFPROP), Version 8.0, 2007.

Using the HPVA to Analyze Hydrogen Storage Potential of Metal Organic Frameworks at High Pressures

Determining the hydrogen storage capabilities of materials such as Metal Organic Frameworks (MOFs) and other highly microporous materials is an important undertaking in the modern push for a hydrogen economy. An efficient method of hydrogen storage is a critical aspect in the development of hydrogen fuel cells. Hydrogen gas has a high energy density by mass but a low energy density by volume when stored as a compressed gas, making it unfavorable for hydrogen storage. Maintaining hydrogen in a liquid state (20 K at atmospheric pressure) also is not energy efficient. Storing hydrogen in a solid material by adsorption is the best alternative, requiring less volume than compressed gaseous hydrogen and consuming far less energy than required to liquefy hydrogen. Dosing high pressure hydrogen onto high surface area MOFs for storage as an adsorbed gas is a highly desirable process due to the high hydrogen energy density obtained and the availability of reversible adsorption.

Four commercially available MOFs produced by BASF were analyzed with Particulate Systems' High Pressure Volumetric Analyzer (HPVA) to determine their hydrogen storage potential. Those MOFs are: Basolite C300, a copper-based organic framework; Basolite F300, an iron-based organic framework; Basolite Z1200, a zinc-based organic framework; and Basolite A100, an aluminum-based organic framework. Approximately 500 mg of each MOF was placed under vacuum and slowly heated up to 200 °C for a period of 12 hours (Z1200 was only heated to 100 °C to prevent degradation of the sample) using the HPVA degas port. All four samples were analyzed at liquid nitrogen temperature (77 K) in a liquid nitrogen bath, utilizing the cryogenic option for the HPVA, up to pressures of 100 bar. An isothermal jacket was used to maintain the cryogenic temperature zone of the samples during analysis. At 77 K, each MOF showed different amounts of hydrogen uptake; C300 adsorbed the most while F300 adsorbed the least. A plot of the isotherms generated from the analyses is shown in Figure 1.

The isotherms displayed in Figure 1 exhibit a phenomenon in which the adsorption reaches a maximum and then declines as the pressure increases. This phenomenon is due to the increasing density of the hydrogen in the pores of the material

at elevated pressures. The density of the adsorbing gas (H₂) inside the pores (a function of pore size) is far greater than the density of a non-adsorbing gas (He). Since the calculated amount of gas in the sample cell is based on the density of helium and its resulting free-space volume (including the volume inside the pores), the amount of free gas in the sample cell is overestimated. When using the static volumetric method, like that of the HPVA, a maximum in the isotherm may be observed. This is used to create the excess isotherm as shown in Figure 1. To generate the absolute isotherm, the density of the gas and the volume

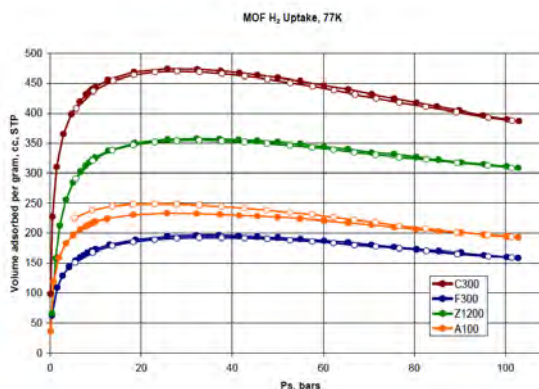


Figure 1: An overlay of the excess isotherms generated from the analysis of various MOFs with hydrogen at 77 K. The solid circles represent the adsorption isotherms and the hollow circles represent the desorption isotherms.

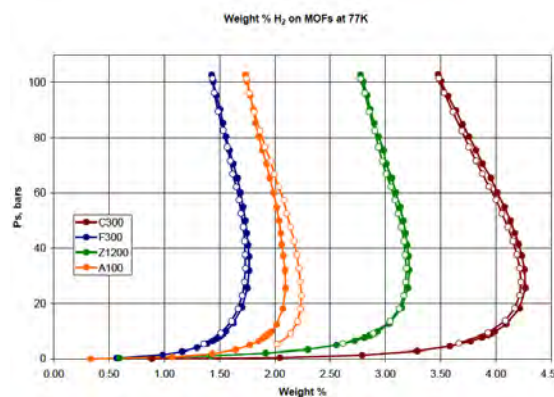


Figure 2: Weight percentage plots of various MOFs analyzed with hydrogen at 77 K.

APPLICATION NOTE 005

of the pores must be included in the calculations. Since the pore size and distribution of these types of materials are not readily available to most users, the excess isotherm will suffice and is commonly reported for adsorption isotherms.

An alternative method to see the storage capacity of materials from the excess isotherm is to view the amount of gas adsorbed as a function of the sample weight. The target weight percentage of hydrogen uptake for storage purposes is between 7% and 8%. Figure 2 shows an overlay of the weight percentage plots based on the isotherms displayed in Figure 1.

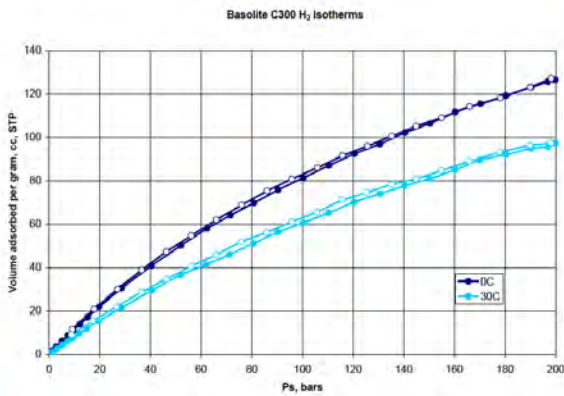


Figure 3: Hydrogen uptake on Basolite C300 at 0 °C (dark blue) and 30 °C (light blue).

Since the Basolite C300 adsorbed the most hydrogen at 77 K, it was also analyzed at two additional temperatures. For one analysis, an ice bath was used to maintain the sample at 0 °C. For the second, a recirculating water vessel was used to maintain the sample temperature at 30 °C. For these two experiments, the sample was dosed with hydrogen to pressures up to 200 bar, the full extent of the pressure range obtainable with the HPVA. The excess isotherms are shown in Figure 3 and the weight percentage plots in Figure 4.

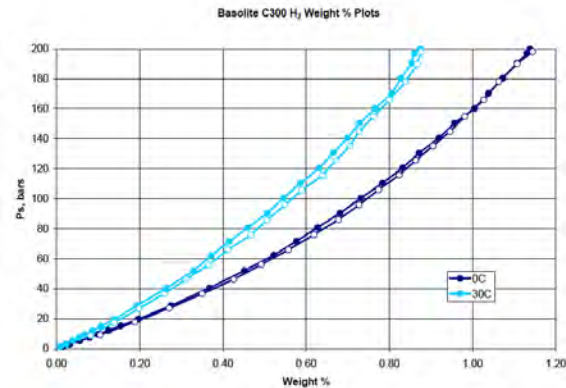


Figure 4: Weight percentage plots of hydrogen on Basolite C300 at 0 °C (dark blue) and 30 °C (light blue).

When reviewing the data in Figures 1 through 4, it is clear that the HPVA is a powerful tool for evaluating the hydrogen storage potential in MOFs and other microporous powders. The HPVA, with its wide temperature range (from cryogenic to 500 °C) and its ability to dose up to 200 bar of pressure, is perfect for analyzing samples under extreme conditions while providing accurate data.

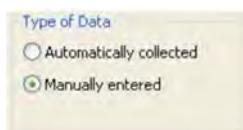
Calculating Isothermic Heats of Adsorption from HPVA Data Using MicroActive

An update in version 3.0 of Micromeritics' MicroActive software allows for pasting HPVA II data into MicroActive sample files. This feature is extremely useful for fitting data to various isotherm models and for calculating isothermic heats of adsorption from isotherms measured at differing temperatures. The following instructions explain how to paste HPVA II data into MicroActive and use the sample files to calculate heats of adsorption:

1. Version 22.0.9 of the HPVA II Excel macro automatically prints columns of data with appropriate headers for pasting into MicroActive. Activate this function by selecting "Edit" from the "HPVA Options" menu. Check the "Print MicroActive Data" box and click OK.



2. When an isotherm report is generated the MicroActive data is located at the bottom of the spreadsheet. Copy the two columns of data, including the two column headers labeled "Absolute Pressure (mbar)" and either "Quantity Adsorbed (cm³/g STP)" or "Quantity Adsorbed (mmol/g)"
3. Open MicroActive. Create a new sample file by choosing "Open" from the "File" menu. Enter a unique file name with the extension ".SMP" and click "Open." Click "Yes" when asked to create the file.
4. Select "Advanced" from the drop down menu located at the bottom of the SMP file window. Select the "Sample Description" tab. Locate "Type of Data" and select "Manually entered."

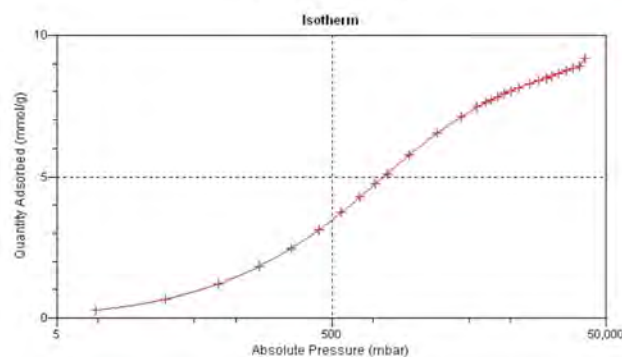
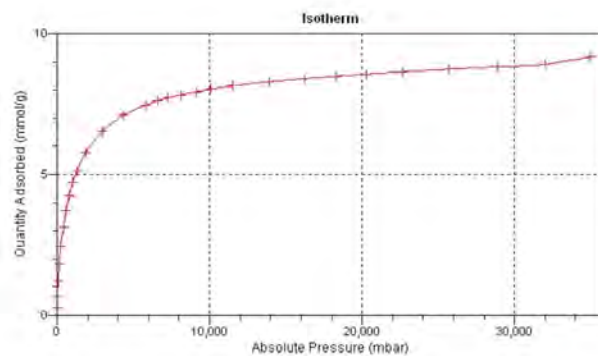


5. New options will appear in the drop down menu located at the bottom of the SMP file window. Select "Isotherm" and a blank graph will appear.

6. Click "p° and T..." and enter the analysis temperature. Saturation pressure for condensable adsorbates can be entered if plotting isotherms as a function of relative pressure is desired. If the adsorbate is in the supercritical state ignore the saturation pressure and isotherm data should only be viewed as a function of absolute pressure. Click "OK" to save changes.

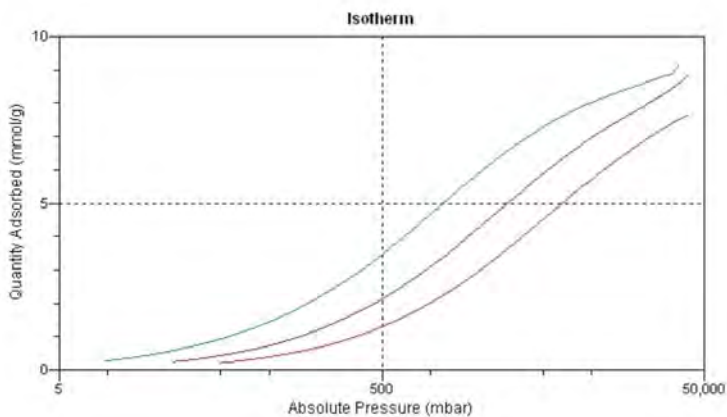


7. Select "Absolute Pressure" or "Relative Pressure" to reflect how the data should be plotted.
8. Click "Paste." The isotherm data will be automatically plotted on an absolute scale and a logarithmic scale.



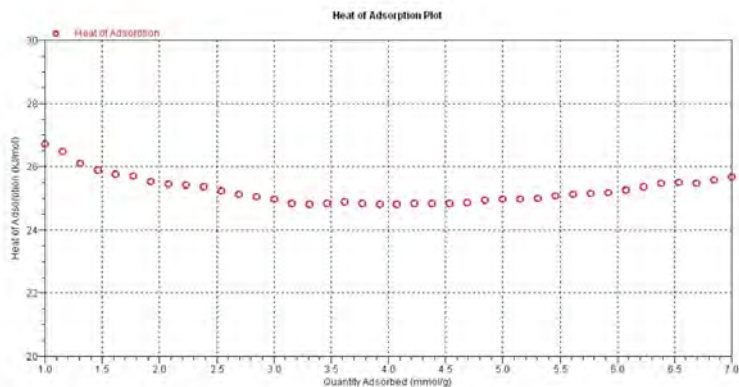
APPLICATION NOTE 006

- Click "Save" in the bottom left corner of the SMP file window to update progress.
- Repeat steps 2-9 for additional isotherms at different temperatures. At least two temperature isotherms are needed for isosteric heats of adsorption calculations.



- From the "Reports" menu select "Heats of Adsorption..."
- Click "Add Samples..." and select the sample files previously created.

- Heat of Adsorption will be plotted as a function of Quantity Adsorbed per gram. Click "Edit Quantities..." to insert a range of quantities adsorbed. For best results, the entered adsorption range should be covered by every isotherm.



Rathole Stability Analysis for Aerated Powder Materials

By: Dr. Kerry Johanson Material Flow Solutions, Inc.

NOTICE: This is the author's version of a work accepted for publication by Elsevier. Changes resulting from the publishing process, including peer review, editing, corrections, structural formatting and other quality control mechanisms, may not be reflected in this document. Changes may have been made to this work since it was submitted for publication. A definitive version was subsequently published in Powder Technology, Vol. 141, 17 April 2004, Pages 161-170, doi:10.1016/j.powtec.2004.02.004.

Abstract:

Forty years ago Jenike and Johanson developed the flow-no-flow equations used to predict stability of bulk solid structures in silos and hoppers. These equations were developed into a theory that has been used to design process equipment to handle cohesive materials. The basis of the theory is a limiting stress state analysis of a bulk material forming a cylindrical pipe (rathole) around or an arch across the hopper outlet. Reliable process operation requires that these two cohesive obstructions be avoided to achieve proper flow of bulk materials through process equipment. Today, industry uses a variety of flow aid devices to overcome these stable flow structures. One such device is aeration pads which are used to maintain fluidization of fine powders and decrease cohesive behavior of bulk materials. Alternatively, air blasters can inject a given quantity of gas into the bulk material creating large transient gas pressure gradients that may destroy these cohesive structures in process equipment. It is important to note that air blasters may destroy cohesive structures provided they are placed in close enough proximity to the stable rathole and with sufficient frequency along the axis of the bin or around the bin perimeter. Although these aeration techniques work, a full understanding of the reason is lacking. Currently, both the placement and required number of these flow aid devices are based on practical experience and not sound theoretical principles. This paper addresses this knowledge void by adding the gas pressure gradient terms to the rathole stability analysis performed by Jenike, thus extending the flow-no-flow rathole analysis to aerated conditions.

Key Words: rathole, slope stability, cohesion, unconfined yield strength, aeration

Introduction:

Processing and handling of fine materials is often difficult. These materials sometimes behave as cohesive masses. However, the addition of air often creates a condition wherein bulk materials exhibit less cohesive tendencies. One example of using aeration to overcome cohesive flow problems is the use of air pads in flat-bottom ash silos to keep material in a flowable condition. Standard rules of thumb suggest that a minimum of 15% of the silo bottom should be covered with air pads to maintain ash in a flowable state. Air flow should be used during filling and maintained during storage. Since a sound theory of cohesive aerated behavior does not exist, current bulk solids practitioners' err on the side of safety and often recommend that the entire bottom be fluidized with the hope that more aeration will provide some safety margin for design. The placement of these pads is more art than science and the amount of air injected is empirical and based on past experience. If the injection system fails, the material within the silo loses entrained gas and cohesive ratholes result. The relationship between rathole stability and degree of aeration is not well understood. This paper addresses a theoretical approach for stable rathole formation in aerated hoppers and bins. It is an extension of the critical rathole stability criteria initially proposed by Jenike [1].

Two conditions that must be satisfied for trouble free process operations using powder materials are that the outlet must be large enough to overcome cohesive arching of bulk materials and that the active flow channel must be larger than the critical rathole dimension. The Jenike arching criteria equations [1] [2] are often used to compute the arching tendency. Alternatively, the arching index approach [3] is used to compute critical arching dimensions. However, reliable flow of bulk material from process equipment also requires that the induced flow channel be large enough to prevent the formation of stable ratholes. Jenike also developed a limiting stress state analysis for prediction of critical rathole diameters in funnel flow bins. This method has been used with moderate success over the last 40 years to provide a conservative estimate of the critical rathole diameter. However it does have some limitations.

APPLICATION NOTE 013

This paper attempts to address one of these limitations.

Both the arching and rathole conditions must be overcome to assure reliable flow. This paper focuses on only the rathole tendency of bulk powders and deals directly with the influence of aeration on the ability of a powder material to form a stable rathole. It will leave the formation of arches in aerated material to some future work. It should be noted that, quite often, in funnel flow bins the critical rathole dimension is the controlling factor in successful handling system operation. The rathole flow-no-flow criteria states that the active flow channel induced in the material must be greater than the critical rathole dimension for reliable flow to occur. The question then arises as to how this critical diameter changes during powder aeration. Two things are required to determine the effect of aeration on cohesive flow obstructions. The relationship between aeration and cohesive flow properties must be established and the stability of cohesive structures under aeration conditions must be understood.

Recent work by Barletta [4], Johanson and Barletta [5], and Kline et. al. [6] makes measurement of unconfined yield strength as a function of aeration possible. These aerated flow property measurements can be used to predict critical rathole dimensions for aerated process equipment. Their work suggests there is a relationship between aeration and unconfined yield strength. However, this effect does not become a dominant issue until the gas pressure gradient acting in the powder approaches the weight density of the bulk powder.

From a theoretical point of view Hill and Cox [7] analyzed the limiting stability rathole equations but did not include gas pressure terms. There is limited discussion in their paper about the validity of their new critical rathole dimension predictions and they neglected to add the gas pressure gradient terms. Hence, their analysis can not handle aerated materials. The following paper addresses the rathole stability in aerated conditions and presents an analysis similar to the one proposed by Jenike, except it includes gas pressure gradient terms.

Derivation of the critical rathole equations

The rathole derivation as defined by Jenike is a critical slope stability calculation and assumes a perfectly plastic limit analysis. The governing equation is called the equilibrium equation and is simply the equation of motion with the acceleration terms omitted (see Eq. 1).

$$\nabla \cdot \underline{\tau} = \gamma \underline{g} - \nabla P \quad (1)$$

This results in the following vector component equations when expressed in cylindrical coordinates see Figure 1.

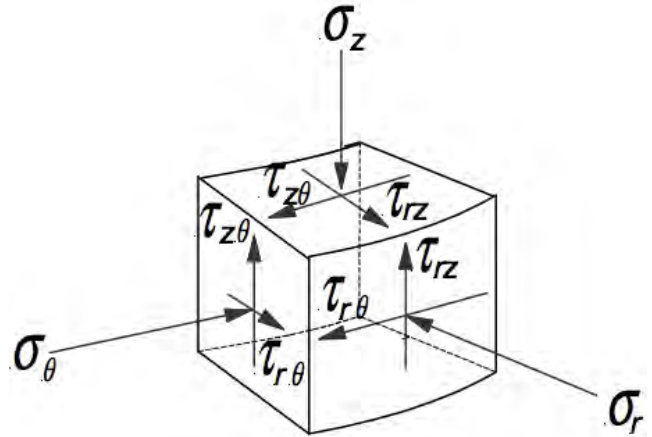


Figure 1: Definition of stress components

$$\frac{1}{r} \cdot \frac{\partial(r \cdot \sigma_r)}{\partial r} + \frac{1}{r} \cdot \frac{\partial(t_{r\theta})}{\partial \theta} - \frac{\sigma_\theta}{r} + \frac{\partial(t_{rz})}{\partial z} = -\frac{\partial P}{\partial r} + \gamma \cdot g_r \quad (2)$$

$$\frac{1}{r} \cdot \frac{\partial(r \cdot t_{rz})}{\partial r} + \frac{1}{r} \cdot \frac{\partial(t_{\theta z})}{\partial \theta} + \frac{\partial(\sigma_z)}{\partial z} = -\frac{\partial P}{\partial z} + \gamma \cdot g_z \quad (3)$$

Normal stress in the θ -direction is assumed to equal the major principal stress in accordance with the Har Von Karman hypothesis, which states that the hoop stress in bulk material is equal to either the major or minor principal stress. This assumption implies that the shear stresses $\tau_{r\theta}$ and $\tau_{\theta z}$ equal zero. The critical rathole dimension for a given piece of process equipment should depend on the strength evaluated at the greatest solids contact stress in the equipment. Janssen [8] analyzed the stresses in cylindrical silos and found an asymptotic relationship for the stress as a function of the axial coordinate. In a silo, the largest solids stress occurs far below the top material surface. At this location, the Janssen stress profile produces a condition where the normal stress σ_z is constant with bed depth. Hence, the terms $M\sigma_z/Mz$ and $M\tau_{rz}/Mz$ equal zero. These assumptions result in the simplified Eq. 4 and Eq. 5.

$$\frac{1}{r} \cdot \frac{\partial(r \cdot \sigma_r)}{\partial r} - \frac{\sigma_\theta}{r} = -\frac{\partial P}{\partial r} \quad (4)$$

$$\frac{1}{r} \cdot \frac{\partial(r \cdot t_{rz})}{\partial r} = -\frac{\partial P}{\partial z} + \gamma \cdot g_z \quad (5)$$

APPLICATION NOTE 013

These equations are transformed using the scale variable proposed in the original rathole analysis. This transformation relates the radial position to a new variable η as given by Eq. 6 and Figure. 2.

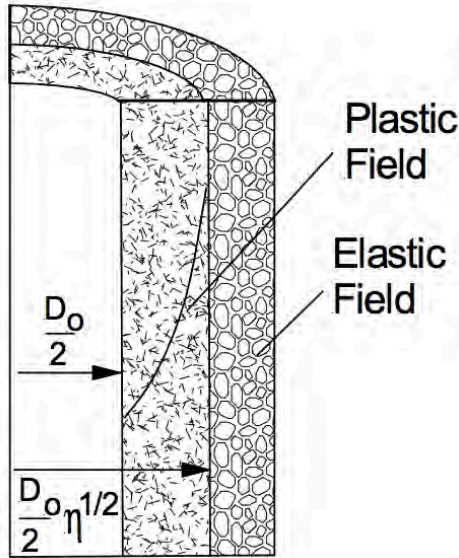


Figure 2: Rathole schematic

$$r = \frac{1}{2} \cdot \eta^{1/2} \cdot D_0 \quad (6)$$

The new rathole stability equations become the following:

$$\frac{d\sigma_r}{d\eta} + \frac{\sigma_r - \sigma_\theta}{2 \cdot \eta} = - \frac{\partial P}{\partial r} \cdot \frac{D_0}{4 \cdot \eta^{1/2}} \quad (7)$$

$$\frac{dt_{rz}}{d\eta} + \frac{t_{rz}}{2 \cdot \eta} = \left[\gamma \cdot g_z - \frac{\partial P}{\partial r} \right] \quad (8)$$

They are similar to the equations originally derived by Jenike, but include gas pressure gradient terms. Eq. 8 can be integrated directly, subject to the boundary condition of zero shear stress at the rathole surface and nearly constant gas pressure gradient in the axial direction, to yield Eq. 9 describing the shear stress as a function of radial position away from the rathole surface.

$$t_{rz} = \frac{1}{4} \cdot \left[\gamma \cdot g_z - \frac{\partial P}{\partial z} \right] \cdot D_0 \cdot \frac{(\eta-1)}{\eta^{1/2}} \quad (9)$$

Eq. 7 and Eq. 8 can not be solved directly, since the number of unknown variables exceeds the number of vector component equations. A constitutive equation relating the normal stresses σ_θ and σ_r is required in order to provide closure to this system of equations.

The concept of a perfect plastic material provides the necessary closure equations. When stress levels reach a critical value, yield will occur. The perfectly plastic assumption uses the stress state at the point of yield as the stress state for all plastic flow conditions. Obviously, this only applies to the condition of incipient flow or yield. Such an assumption can not hope to predict flow behavior between the incipient flow and continual deformation conditions. Consequently, the model derived from these equations may predict the incipient failure of a rathole, but will not give any information describing the flow after initiation. This limitation of the theory is acceptable for this rathole stability analysis since the goal of this work is to predict the incipient failure of a rathole. The yield locus then becomes the constitutive equation required for closure of the equation of motion. The yield locus is the collection of shear stress (τ) normal stress points (σ) that describe incipient failure of a bulk material subjected to a prescribed compaction stress. Figure 3 shows a typical yield locus. The bold line represents the collection of all stress states that will result in yield of the bulk material. This line terminates at a stress condition given by the largest Mohr circle. All failure conditions on the yield locus arise from subjecting the material to the compaction stress state described by this termination Mohr circle and then shearing the preconditioned bulk material at a lower stress state. There is an unique yield locus for each compaction stress state. A linear approximation to this yield locus provides the constitutive equation required for closure of Eqs. 7 and 8. This relationship allows the stress tensor components to be expressed as a function of the mean stress. It is also a function of the direction between the major principal stress and coordinate axis.

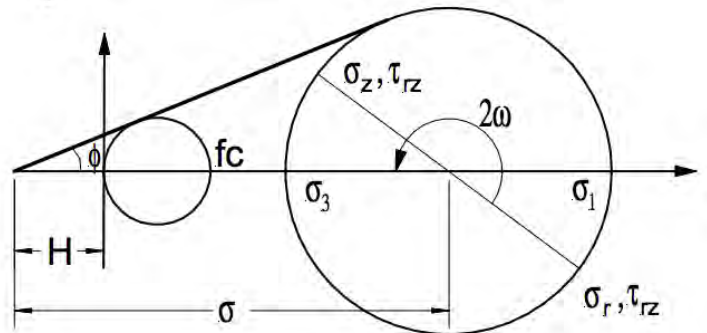


Figure 3: Definition of limiting stress state for rathole analysis

APPLICATION NOTE 013

This definition is identical to the limiting state constitutive equation used by Jenike in his original rathole analysis. It is important to note that the average stress defined in this figure is measured from the apex of the yield locus and not from the origin. This results in Eqs. 10 through 13 for the stress equations.

$$\sigma_r = \sigma \cdot [1 - \sin(\phi) \cdot \cos(2\omega)] + \frac{fc}{2} \cdot \frac{\sin(\phi) - 1}{\sin(\phi)} \quad (10)$$

$$\sigma_z = \sigma \cdot [1 + \sin(\phi) \cdot \cos(2\omega)] + \frac{fc}{2} \cdot \frac{\sin(\phi) - 1}{\sin(\phi)} \quad (11)$$

$$t_{rz} = \sigma \cdot [\sin(\phi) \cdot \sin(2\omega)] \quad (12)$$

$$\sigma_\theta = \sigma \cdot [1 + \sin(\phi)] + \frac{fc}{2} \cdot \frac{\sin(\phi) - 1}{\sin(\phi)} \quad (13)$$

Eq. 9 can be substituted back into Eq. 8 to yield a relationship between η and τ_{rz} .

$$\frac{2 \cdot \sigma \cdot \sin(\phi) \cdot \sin(2\omega) \cdot \frac{d\omega}{d\eta} + \sin(\phi) \cdot \cos(2\omega) \cdot \frac{d\sigma}{d\eta} - \frac{1}{2} \cdot \frac{1 + \cos(2\omega)}{\eta}}{\sigma \cdot \sin(\phi)} = - \frac{\frac{\partial P}{\partial r} \cdot \frac{D_0}{4 \cdot \eta^{1/2}}}{\sigma \cdot \sin(\phi)} \quad (16)$$

$$\frac{\frac{\partial P}{\partial r} \cdot \frac{D_0}{4 \cdot \eta^{1/2}}}{\sigma \cdot \sin(\phi)} = \frac{\frac{\partial P}{\partial r} \cdot \sin(2\omega)}{(\eta - 1) \cdot \left[\gamma \cdot g - \frac{\partial P}{\partial z} \right]} \quad (17)$$

The right side of Eq. 16 can be modified by using the integrated shear stress Eq. 9 and the Mohr circle definition for the shear stress in Eq. 12. This yields Eq. 17 and eliminates the mean stress term from the right side of Eq. 16. This allows

$$\frac{\partial t_{rz}}{\partial \eta} = t_{rz} \cdot \frac{\eta + 1}{\eta \cdot (\eta - 1)} \quad (14)$$

Eq. 14 can then be combined with the Mohr stress yield conditions to provide a relationship between the mean stress (σ) and principal stress direction angle (ω).

$$\frac{1}{\sigma} \cdot \frac{d\sigma}{d\eta} + 2 \cdot \frac{\cos(2\omega)}{\sin(2\omega)} \cdot \frac{d\omega}{d\eta} - \frac{(\eta + 1)}{2 \cdot \eta \cdot (\eta + 1)} = 0 \quad (15)$$

Eq. 15 provides a means of relating mean stress to the principal stress direction. It arises from the solution of the axial equation of motion subject to the simple boundary conditions and assumptions outlined above. The radial component of the equation of motion can also be expressed as a function of mean stress (σ) and principal stress direction (ω). This can be done by substituting Eqs. 10 through 13 into Eq. 7 to yield Eq. 16.

complete separation of the mean stress and principle stress direction derivatives and leads to Eq. 18, which describes the change of principle stress direction (ω) with respect to the dimensionless radial coordinate (η).

$$\frac{d\omega}{d\eta} = \frac{\sin(2\omega)}{4} \cdot \frac{[-\eta - 1 + 2 \cdot \eta \cdot \sin(\phi) \cdot \cos(2\omega) - \sin(\phi) + 2 \cdot \eta \cdot A \cdot \sin(2\omega) \cdot \sin(\phi)]}{\eta \cdot (\eta - 1) \cdot [\sin(\phi) - \cos(2\omega)]} \quad (18)$$

$$A = \frac{\frac{\partial P}{\partial r}}{\frac{\partial P}{\partial z} - \gamma \cdot g_z} \quad (19)$$

APPLICATION NOTE 013

This differential equation must be bounded within the limits of integration to produce physically realizable solutions. Therefore, an analysis of the extreme points of this equation will yield limits on the principal stress direction angle. The denominator can become unbounded if $\sin(\varphi)$ equals $\cos(2\omega)$. This results in Eq. 20 describing the maximum limit of principal stress direction angle.

$$\omega = \frac{\pi}{4} - \frac{\varphi}{2} \quad (20)$$

The numerator must also vanish at this value of ω to maintain a bounded solution. This yields a relationship between the dimensionless coordinate (η), dimensionless gas pressure gradient term (A), and internal friction angle (φ) (Eq. 21). The dimensionless coordinate η_{\max} is the largest possible radial position that can create a plastic stress field given a rathole diameter of D_0 .

$$\omega = \frac{1}{2 \cdot \sin(\varphi) - 1 + \frac{A \cdot 2 \cdot \cos(\varphi) \cdot \sin(\varphi)}{1 + \sin(\varphi)}} \quad (21)$$

The maximum radius of the plastic field is then given by Eq. 22.

$$r = \frac{D_0}{2} \cdot \eta_{\max}^{1/2} \quad (22)$$

Now at the surface of the rathole, η approaches 1, ω approaches 0, and σ_1 approaches the unconfined yield strength f_c . This implies the following relationship between unconfined yield strength (f_c) and average stress level (σ).

$$2 \cdot \sigma \cdot \sin(\varphi) = f_c \quad (23)$$

However, from the solution of the shear stress differential equation average stress can be related to the rathole diameter (D_0).

$$\frac{\sin(2\omega)}{\eta - 1} = \frac{1}{4} \frac{\left[\gamma \cdot g_z - \frac{\partial P}{\partial z} \right] \cdot D_0}{\eta^{1/2}} \quad (24)$$

Eq. 23 and Eq. 24 can be combined to yield a relationship between the rathole diameter and the direction of major principal stress near the rathole surface (Eq. 25).

$$D_0 = \lim \left[2 \cdot f_c \cdot \frac{\sin(2\omega)}{\eta - 1} \cdot \frac{\eta^{1/2}}{\gamma \cdot g_z - \frac{\partial P}{\partial z}} \right] \quad (25)$$

L'Hospital rule must be used to evaluate this limit, resulting in the following equation for the rathole diameter.

$$D_0 = \frac{4 \cdot \frac{d\omega(1)}{d\eta} \cdot f_c}{\gamma \cdot g_z - \frac{\partial P}{\partial z}} = \frac{G \cdot (\varphi, A) \cdot f_c}{\gamma \cdot g_z - \frac{\partial P}{\partial z}} \quad (26)$$

It is obvious from this equation that the derivative of the major principal stress direction, with respect to the dimensionless radial coordinate evaluated at the surface of the rathole ($\eta=1$), is required to determine a maximum limit to the critical rathole diameter. The $G(\varphi, A)$ term defined above is four times the derivative of the principal stress direction with respect to the dimensionless radial coordinate (η). It is similar to the $G(\varphi)$ term derived by Jenike, but includes gas pressure gradient terms. This derivative can be obtained by integrating Eq. 18 subject to the boundary condition $\eta=\eta_{\max}$ at $\omega=\pi/4 - \varphi/2$. Because of the complexity of the differential equation, integration must be done numerically. The integration proceeds backwards from the boundary condition at η_{\max} and terminates at $\eta=1$. The derivative of the principal stress direction angle (ω) with respect to dimensionless radial coordinate (η) evaluated at $\eta=1$ is then used to compute the critical rathole diameter. As a first approximation, gas pressure gradient terms are assumed constant. This is not strictly true and there will be some variation with both radial and axial position in the bin.

A more accurate solution should involve the combined numerical solution of the limiting rathole equations along with the equations of motion describing gas flow through powder. However, the analysis provided in this paper can provide a first approximation to rathole stability in aerated process equipment. Figure 4 shows a typical solution to the differential equation.

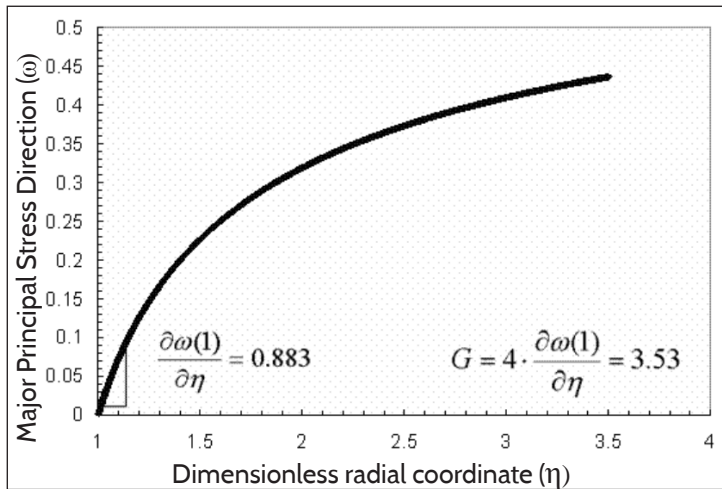


Figure 4: Typical solution for aerated rathole equation

This integration can be repeated for various values of (A) and internal angle of friction (ϕ) resulting in a new relationship for the $G(\phi, A)$ function that includes gas pressure gradient terms (Figures 5 and 6). It is important to note that the radial component of the gas pressure gradient is responsible for rathole destabilization. The larger this gas pressure gradient, the more unstable the rathole becomes. The axial gradient term actually causes the rathole to be more stable by decreasing the effective gravitational forces acting on the rathole.

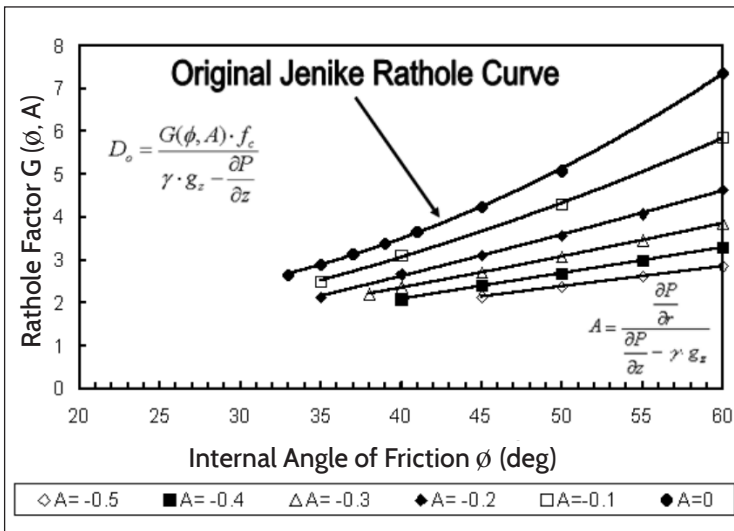


Figure 5: Jenike G factor as a function of internal friction angle (ϕ) at various dimensionless gas pressure gradients (A)

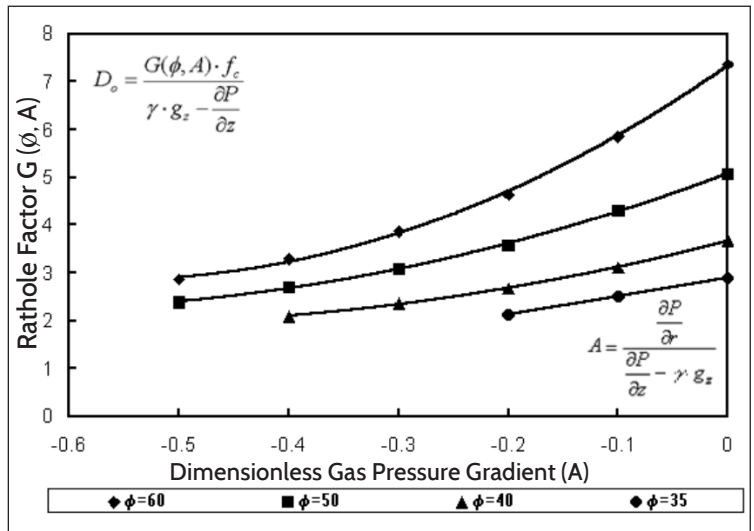


Figure 6: Jenike G factor as a function of dimensionless gas pressure gradient (A) at several internal friction angles (ϕ) between 35E and 60E

Knowledge of the pressure gradients in a bin is required to compute an estimate to the critical rathole dimension. In reality, these gradients are functions of spatial coordinates. This is especially true of the radial pressure gradient. However, an estimate of this radial pressure gradient is obtained by assuming the gas pressure field can be approximated from the solution of a steady state Laplace equation describing permeable materials. If the gas is incompressible, the governing equation is described by Eq. 27.

$$\nabla^2 P = 0 \quad (27)$$

If the gas is subject to isothermal compression, then Eq. 28 applies.

$$\nabla^2 P^2 = 0 \quad (28)$$

For the purposes of this paper, Eq. 27 will be used. If the pressure gradient in the z-direction is constant and the pressure gradient in the θ -direction is small, then Eq. 27 can be expressed simply as a function of the radial coordinate resulting in Eq. 29.

$$\frac{1}{r} \cdot \frac{\partial P}{\partial z} \left[r \cdot \frac{\partial P}{\partial z} \right] = 0 \quad (29)$$

APPLICATION NOTE 013

Normally the gas injection devices used to prevent ratholes are mounted at the bin wall surface. This can be approximated by a constant pressure boundary condition at the bin wall. The pressure at the rathole surface equals the atmospheric pressure. Therefore, Eq. 29 is subject to two constant pressure boundary conditions given in Eq. 30 and Eq. 31.

$$P = P_{\text{atm}} + \Delta P \quad \text{at } r = R_{\text{wall}} \quad (30)$$

$$P = P_{\text{atm}} \quad \text{at } r = R_0 \quad (31)$$

This results in an analytical solution for the gas pressure as a function of radial position (Eq. 32). That solution will yield an equation for the radial gas pressure gradient (Eq. 33) showing an increase in the pressure gradient at the rathole surface.

$$P = \left[\frac{\ln\left(\frac{r}{R_0}\right) - \ln\left(\frac{r}{R_{\text{wall}}}\right)}{\ln\left(\frac{R_{\text{wall}}}{R_0}\right)} \right] \cdot P_{\text{atm}} + \frac{\ln\left(\frac{r}{R_0}\right)}{\ln\left(\frac{R_{\text{wall}}}{R_0}\right)} \cdot \Delta P \quad (32)$$

$$\frac{\partial P}{\partial r} = \frac{1}{r \cdot \ln\left(\frac{R_{\text{wall}}}{R_0}\right)} \cdot \Delta P \quad (33)$$

This can be combined with the definition of the dimensionless radial coordinate (η) given in Eq. 6 and substituted into the dimensionless pressure gradient term (A) found in Eq. 19 to yield a new dimensionless pressure gradient term that depends on the spatial coordinate and the size of the rathole relative to bin diameter (Eq. 34).

$$A(\eta, D_o, D_{\text{wall}}) = \frac{\left[\frac{2 \cdot \frac{\Delta P}{D_{\text{wall}} - D_o}}{\eta^{1/2} \cdot \frac{D_o}{D_{\text{wall}} - D_o} \cdot \ln\left(\frac{D_{\text{wall}}}{D_o}\right)} \right]}{\frac{\partial P}{\partial z} - \gamma \cdot g_z} \quad (34)$$

The new A-value can be used in Eq. 18 to yield a new solution to the rathole equations that incorporates a variable radial pressure gradient. The solution of this equation can then be used in the standard rathole equation. The only difference is that the right side of Eq. 26 now depends on the critical rathole diameter and requires an iterative solution to compute the rathole dimension (Eq. 35).

$$D_o = \frac{G[\phi, A(\eta, D_o, D_{\text{wall}})] \cdot f_c}{\gamma \cdot g_z - \frac{\partial P}{\partial z}} \quad (35)$$

Figure 7 shows the new G-function for the case of an internal angle of friction of 40 degrees as a function of the ratio D_{wall}/D_o and the overall average gas pressure gradient.

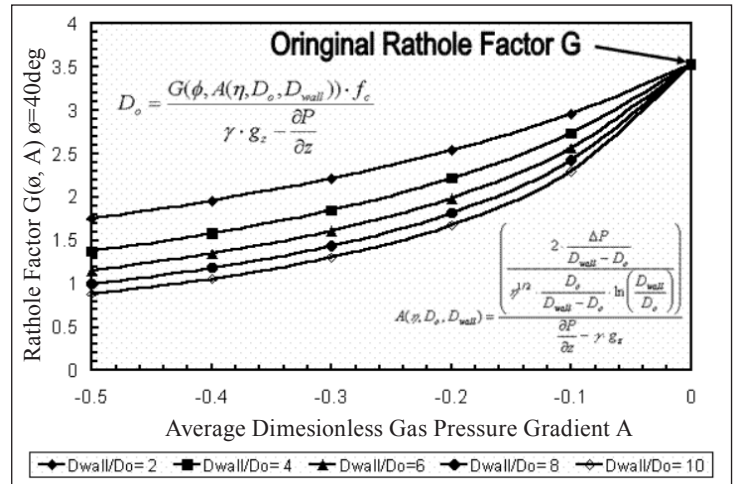


Figure 7: Jenike G-factors for an internal friction angle (ϕ) of 40E as a function of gas pressure gradient at various ratios of bin diameter (D_{wall}) to critical rathole diameter (D_o), D_{wall}/D_o .

The last piece of information required to compute the critical rathole condition in aerated material is an estimate of the unconfined yield strength at aerated conditions and evaluated at solids contact stresses in the process equipment. As indicated previously, researchers have developed testers that measure these aerated cohesive properties as a function of solids contact stresses. These aerated flow functions can be used to estimate the aerated unconfined yield strength needed for this rathole analysis. However, the solids stress in the aerated equipment

APPLICATION NOTE 013

must be known to determine the critical strength value for the rathole analysis. A Janssen analysis of a cylinder with gas effects could be used to estimate the solid contact stresses in a silo. Consider a differential slice of bulk material in a silo (Figure 8).

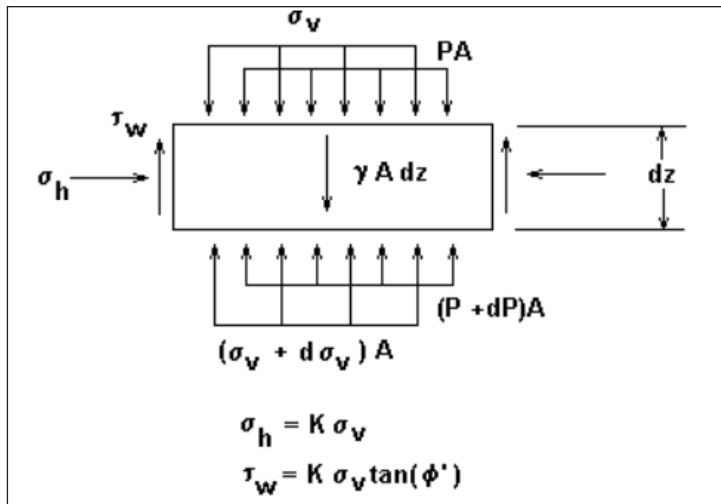


Figure 8: Janssen analysis on aerated material

The forces acting on this differential slice include the solids contact stresses, gas pressures, wall friction, and weight of the material within the slice. A force balance on this differential element results in differential Eq. 36.

$$\frac{d\sigma_v}{dz} + \left[\frac{4 \cdot K \cdot \tan(\phi_w)}{D} \right] \cdot \sigma_v = \gamma \cdot g_z - \frac{\partial P}{\partial z} \quad (36)$$

If the gradient in the axial direction is nearly constant, this differential equation can be integrated subject to a zero stress boundary condition at the top material surface to yield Eq. 37 describing the variation of stress as a function of axial distance from the top of the silo.

$$\sigma_v = \frac{\left[\gamma \cdot g_z - \frac{\partial P}{\partial z} \right] \cdot D}{4 \cdot K \cdot \tan(\phi_w)} \cdot \left[1 - \exp\left(-\frac{4 \cdot K \cdot \tan(\phi_w)}{D} \cdot z \right) \right] \quad (37)$$

This stress level could be evaluated at an axial position (z) equal to the height of the silo to determine an estimate of the solids contact stress for evaluation of the critical rathole diameter in silo geometries. This equation for the solid stress profile in the axial direction assumes that the gas pressure profile is linear along the height of the silo. For conditions where the axial gas pressure gradient varies with time, the most positive axial gas pressure gradient should be used to produce the more conservative solids contact stress for rathole calculations. Eq. 37 should not be used in situations where the gas pressure gradient varies significantly with axial position. It should also be noted that gas pressure gradients in excess of the unit weight density will predict negative solids contact stresses. If this situation occurs, the gas pressure gradient is large enough to cause fluidization of the bulk material provided it is free flowing, or to develop channels with cohesive materials. In either case, the operation mode deviates from the homogenous contact bed conditions inherent in the Janssen stress field assumptions. The solids contact stress should be artificially set equal to zero along the length of the rathole. The procedure for computing the critical rathole dimension in aerated equipment is as follows:

- Estimate the axial gas pressure in the silo.
- Estimate the maximum solids contact stress in the silo with this gas pressure gradient. An accurate approximation to these stresses will require solving both the equations of motion for the gas and solid along with the continuity equations. A Janssen analysis with gas pressure gradient terms may provide an estimate of the critical stress level in the bin.
- Estimate the radial gas pressure gradient in the silo near the rathole surface.
- Estimate the strength of the bulk material at the maximum value of the aerated solids contact stress using the results of the aerated strength test.
- Estimate the $G(\phi, A)$ function from Figure 4 or 6 using the axial and radial estimates of the gas pressure gradients. (A) is the dimensionless gas pressure gradient term which includes the axial and radial gas pressure gradients.
- Use the above equations to compute the critical rathole diameter for the particular geometry.

A numerical example may help to illustrate this procedure. Consider the simple case where the local gas pressure gradients are approximately constant. Please note that this condition may not be the exact condition in aerated bins. Actual pressure

APPLICATION NOTE 013

gradients will depend on the position in the silo. Suppose the conditions and flow properties given in Table I apply to the silo.

Table I: Flow properties and conditions for rathole calculation example

| Property or Aeration Condition | Numerical Value |
|---|-----------------------|
| Bulk density (γ) | 960 kg/m ³ |
| Radial gas pressure gradient (MP/Mr), (MP/Mr / $\gamma g = 0.4$) | 3.76 kPa/m |
| Axial gas pressure gradient (MP/Mz), (MP/Mz / $\gamma g = 0.05$) | 0.47 kPa/m |
| Internal friction angle (ϕ) assumed to be constant and not a function of gas pressure gradient or solid contact stress | 40 degrees |
| Wall friction angle on silo wall (ϕ_w) | 20 degrees |
| Silo Diameter (D) | 5 meters |
| Silo Height (z) | 15 meters |
| Silo Janssen K-ratio | 0.4 |

One of the important conclusions of previous work done by Barletta [4], Johanson and Barletta [5], and Kline et. al. [6] is that the unconfined yield strength does not change much if the pressure gradient is below some critical value near the fluidization limit. This implies that cohesive flow properties in slightly aerated conditions could be approximated by the measured flow properties in non-aerated conditions. However, this is not true for conditions near fluidization and at conditions in converging conical funnel flow geometries. Thus, for the purposes of this example, the influence of aeration on the critical rathole dimension in cylindrical geometries and pressure gradients less than those required for fluidization will be investigated. The procedure could be applied to more complex situations but the additional complexity would cloud the clarity of this example. Suppose, for the sake of example, that the aerated unconfined yield strength could be expressed as a function of major principal stress described in Figure 9.

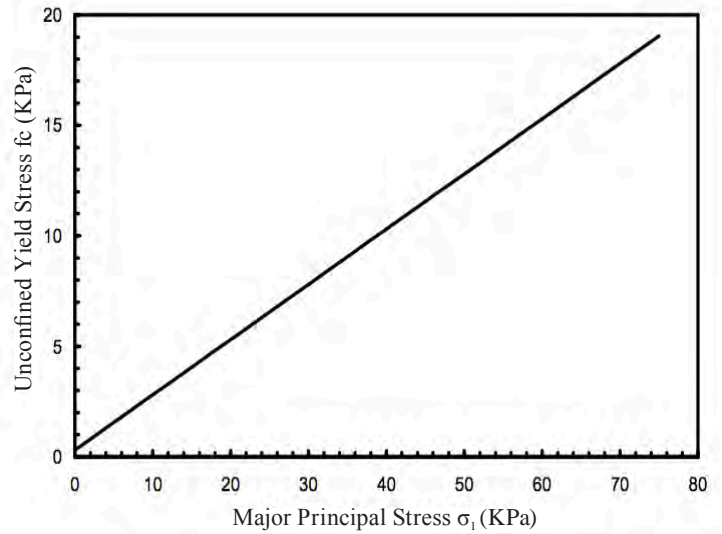


Figure 9: Flow function of aerated material for example rathole calculations

The first step in the procedure above is to estimate the solids stress in the silo using Eq 37. This analysis suggests that the flow properties for rathole analysis should be evaluated at a stress of 63.4 kPa. It is important to point out that this stress is an estimate of the largest major principal stress in the silo over the storage and filling history for the particular silo. This aerated stress would apply for the case where aeration was used on the silo during filling to keep material in a flowable condition. It would not apply to the case where the silo was filled and the aeration system was then turned on in an intermittent mode. The overall maximum solids stress for the intermittent or on-demand gas injection condition would be closer to the non-aerated stress conditions. In fact, processes that use aeration to control the flowability of bulk materials have observed that flow problems arise if the material within the silo becomes deaerated just once. These cohesive deaerated materials are then very difficult to re-aerate and result in persistent rathole problems. It is hoped that this paper will help explain some of these industrial observations.

Once the maximum stress state in the aerated silo is determined the critical strength for rathole calculation can be evaluated using the flow function for the particular aeration condition. In this simple example, the effect of small to moderate gas pressure gradient on the critical rathole dimension are examined and the flow function that applies is the non-aerated condition given in Figure 9. This implies that at a solids stress level of 63.4 kPa the critical strength value for stable rathole formation equals 16.1 kPa. The last step in this

APPLICATION NOTE 013

simplified calculation of aerated critical rathole dimension is to determine the dimensionless gas pressure gradient ratio (A) as given by Equation 19 for constant gradient conditions. This pressure gradient ratio (A) equals -0.421 for the conditions given in Table 1. Figure 6 can then be used to determine the critical rathole factor G used to compute the critical rathole dimension from Equation 26. The entire procedure then yields 3.73 m for the aerated critical rathole dimension. The corresponding critical rathole dimension for non-aerated conditions is 6.59 m suggesting that the assumed aeration conditions for this example case will decrease the rathole tendency to almost half the value of the non-aerated rathole dimension. Thus, controlling the aeration to conditions in this example bin could significantly reduce the size of the active flow channel needed to overcome stable rathole formation. It is important to point out that in this example the critical rathole dimension for non-aerated conditions was greater than the diameter of the bin. This implies that steps must be taken to expand the active flow channel to the full bin diameter to prevent stable rathole formation. If aeration is used then mass flow must only be induced up to the 3.73 m diameter and partial mass flow designs with controlled aeration could be used. This may produce some cost savings in the required bin design.

A similar analysis could be done for the case where gas pressure gradients are a function of radial position. In this case, equation 34 should be used for a calculation of the dimensionless gas pressure gradient (A). In this situation, the A term depends on the critical rathole diameter and will require iteration using equations 34 and 35 to obtain a solution to the critical rathole diameter.

A parametric study of the influence of pressure gradients on rathole stability can be done using the example data in Table 1 and Figure 9 to show the qualitative behavior including gas pressure gradient terms in the rathole limiting stress state equations. Figure 10 shows the expected behavior using the example data. The rathole reduction factor is found by dividing the computed rathole dimension from the analysis above by the standard nonaerated critical rathole dimension from the Jenike method. The strength values needed for this analysis were taken from the example flow function given in Figure 9. This figure indicates that rathole stability can decrease to about 60% of the non-aerated value depending on the radial and axial pressure gradients.

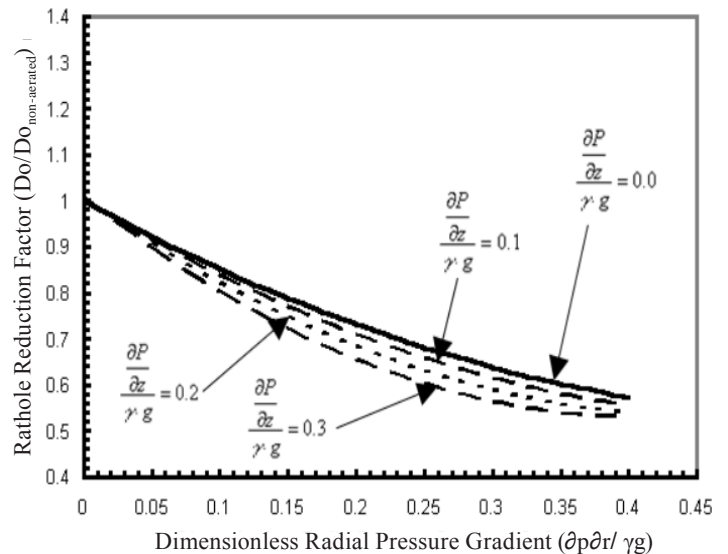


Figure 10: Rathole reduction factor as a function of radial and axial gas pressure gradient using example parameters given in Table 1 and assuming constant gas pressure gradients and the flow function behavior given in Figure 9

Conclusions

The rathole analysis presented in this paper extends the Jenike analysis to aerated conditions. The resulting theory predicts a decrease in the critical rathole diameter as gas pressure gradients acting in the negative r-direction increase. This is intuitively reasonable since the support of ratholes originates in the z-direction. Normal stresses perpendicular to this direction can provide additional body forces required to fail these circumferential cohesive arches (i.e. ratholes). However, increasing the gas pressure gradient in the z-direction will increase the stability of the rathole. This occurs because the upward acting axial gas pressure gradient partially supports the material weight making the material behave as if it were lighter than expected. If the cohesion is the same then lighter material will produce smaller solids contact stresses and result in less stress available to break or destabilize ratholes. The net result is to create more stable ratholes with axial gas counter-flow. Flow aid devices designed to maximize radial gas pressure gradients may overcome rathole problems provided they are placed close to the rathole free surface. This paper provides some preliminary theoretical guidance in using aeration devices to overcome stable rathole formation in process equipment. It is hoped that this work can be refined through Experimental confirmation and industrial observation of rathole stability which will be a subject of future work.

APPLICATION NOTE 013

Nomenclature:

A Dimensionless pressure gradient body force ratio.

D Bin diameter as a function of axial position

D_o Critical rathole diameter

D_{wall} Cylindrical bin diameter

f_c Unconfined yield strength

$G(\varphi, A)$ Critical rathole G factor

H The projected linear yield locus normal tensile stress

K Janssen k-value ratio of stress normal to the wall to the vertical stress in the axial direction. Typically equals 0.4

P Gas pressure

P_{atm} Gas pressure at rathole surface

ΔP Difference between gas pressure at bin wall and gas pressure at rathole surface

r Radial position

R_o Radial position of rathole surface

R_{wall} Radial position of bin wall

γ Powder bulk density

η Dimensionless radial position

η_{max} Maximum value of the dimensionless radius that will produce a stable plastic field

φ Internal friction angle

φ_w Wall friction angle

σ_r Normal stress on the plane perpendicular to the radial direction in a cylindrical coordinate system

σ_θ Normal stress on the plane perpendicular to the θ -direction in a cylindrical coordinate system

σ_z Normal stress on the plane perpendicular to the axial direction in a cylindrical coordinate system

σ Mean limit stress

σ_1 Major principal stress

σ_3 Minor principal stress

σ_v Average vertical stress for Janssen analysis

σ_h Stress normal to cylinder wall for Janssen analysis

τ_{rz} Shear stress on the plane perpendicular to the radial direction acting in the axial direction in a cylindrical coordinate system

$\tau_{r\theta}$ Shear stress on the plane perpendicular to the radial direction acting in the θ -direction in a cylindrical coordinate system

$\tau_{\theta z}$ Shear stress on the plane perpendicular to the θ -direction acting in the axial direction in a cylindrical coordinate system

τ_w Shear stress on the wall for Janssen analysis

ω Angle between the minor principal stress and the r-coordinate direction

Acknowledgment:

The author would also like to acknowledge the financial support of the Engineering Research Center (PERC) for Particle Science and Technology at the University of Florida, the National Science Foundation NSF Grant #EEC-94-02989, and the Industrial Partners of the PERC.

APPLICATION NOTE 013

References:

[1] Jenike, A.W. Gravity flow of bulk solids. Bulletin108, Utah Engineering Station, 1961

[2] Drescher A. Analytical Methods in Bin Loads Analysis, Elsevier; New York, 1991

[3] Johanson J.R., Flow Indices in the Prediction of Powder Behavior, Pharmaceutical Manufacturing International, pp 159-164, 1995

[4] Barletta D., Discharge of fine granular materials from aerated hoppers, Dottorato Di Ricerca In Ingegneria Chimica, University of Salerno, 2002

[5] Johanson K.D. and Barletta D., The Influence of Air Counter-Flow Through Powder Materials on the Measurement of Unconfined Yield Strength, Proceedings of the 4th International Conference for Conveying and Handling of Particulate Solids, 2003

[6] Klein, J., Höhne, D. and Husemann, K. The influence of air permeation on the flow properties of bulk solids. Chem. Eng. Technol. 26 139-146, 2003

[7] Hill, J.M. and Cox, G.M., Cylindrical cavities and classical rat-hole theory occurring in bulk materials, Int. J Numer. Anal. Meth. Geomech., 24:971-990, 2000

[8] Janssen, H. A. Versuche über getreidedruck in silozellen. Z. Ver.Dt. Ing. 39 1045- 1049, 1895

Using Dynamic Image Analysis to Measure Fiber Particles

Analysis of fiber particles requires numerous measurement parameters to fully qualify their true shape.

Introduction

Automated image analysis has been developed to provide users with a more accurate measurement of their particles. For many years, particle size analyzers have rendered results with the assumption that all measured particles are spherical. However, in many applications, the circularity of particles can affect both performance and flowability in manufacturing. In some cases, for example, measuring surface smoothness can impact how well abrasives perform.

Those in industry who have realized that the irregularity of their particles impact both manufacturability and efficacy have resorted to microscopy for shape analysis. Manual microscopy, by its very nature, is a slow and tedious method for particle analysis and becomes impractical to analyze a large number of particles. Therefore, the end-user potentially is left with a poor representation of the sample. This makes microscopy acceptable for obtaining a general idea of particle shape, but is unacceptable when using particle shape analysis as a means to control a process.

One raw material which lends itself to be ideally measured by shape analysis is fibers. Fiber particles are used in a vast array of applications from adding strength to building materials to making effective filtration media.

In all cases where raw fibers are used, there has been an expressed need to know the fiber length, width, and aspect ratio, as well as the curl of the fiber. Particle analysis results expressed in equivalent spherical diameter do not come close to giving the user critical information about their fibers, and how they will perform in their final state. Measuring such particles with manual microscopy is also impractical in a quality control environment where fast and representative analysis is required.

Figure 1 shows a typical fiber in the sample analyzed using the Particle Insight Dynamic Image Analyzer from Particulate Systems.



Figure 1: Fiber sample used for analysis.

Analysis of this fiber sample with a conventional particle size analyzer assumes all particles are spheres, and reports minimal information; in this instance, a size of 112.1 μm .

Analysis of the same fiber sample using the Particle Insight Image analyzer, a proper-shape analyzer with fiber-shape measures, can yield much more information on a high population of particles in just minutes.

The measurement of fiber length and width is calculated along with the aspect ratio, which is simply the length divided by the width. Another measurement that can be calculated is the fiber curl, a fractional measure that is equal to 1 for a straight fiber. The smaller the fiber curl value, the greater degree of curvature

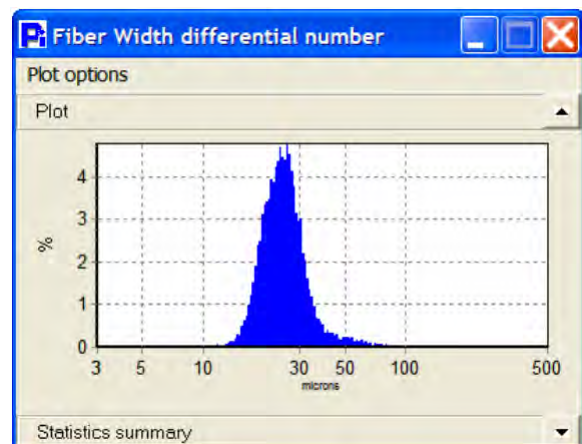


Figure 2: Indicates the width of these fibers were rather uniform in nature. A total of 10,000 particles was analyzed in 149 seconds.

APPLICATION NOTE 001

the fiber has. This can be very useful in making determinations of how fibers will interact with each other in a production process. These measurements are summarized below:

Fiber Length: 449.9 μm
Fiber Width: 22.7 μm
Fiber Aspect Ratio: 19.82
Fiber Curl: 0.984

Figures 2 through 5 provide additional data statistics as indicated in the figure captions.

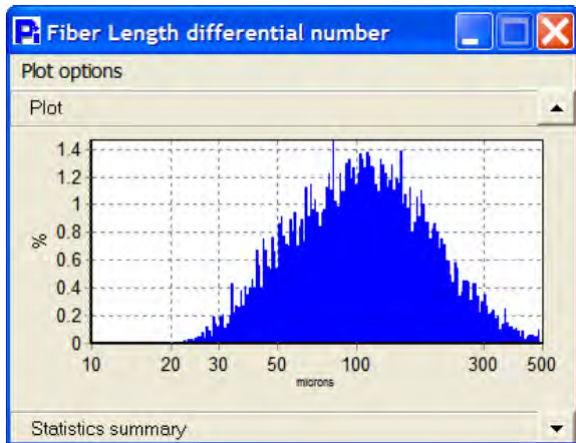


Figure 3: Shows the average length of the fibers to have a mean of 123 μm with a standard deviation of 74.8 μm .

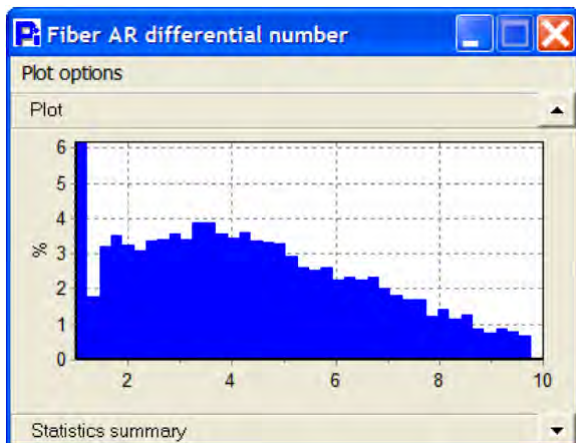


Figure 4: Although the width of the fibers is well controlled, the length is not. As a result, the aspect ratio results are broad. Here the aspect ratio shows a mean of 4.450 with a standard deviation of 2.262.

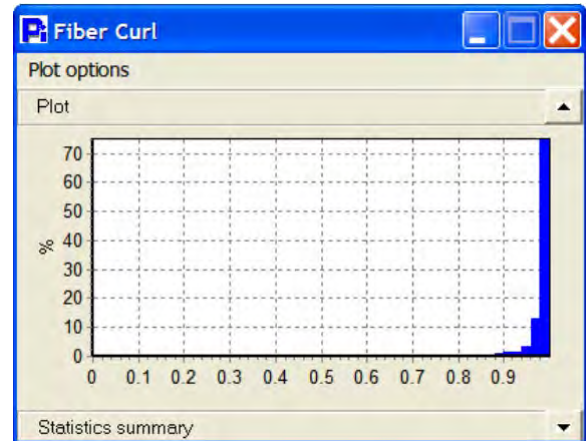


Figure 5: The mean fiber curl is 0.97 with a mode fiber curl of 0.99. This clearly indicates that the population of fibers is mostly non-curved.

Conclusion

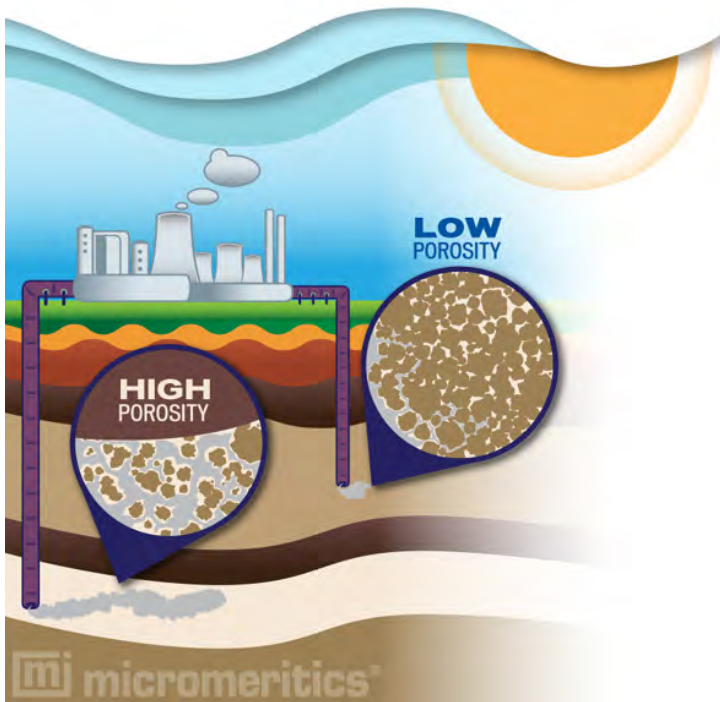
It is important to select a particle size analyzer that can properly analyze the parameters that are important. As can be seen, measuring a fiber with the assumption that they are spherical in shape may not be the most accurate method for quantification. Size, in this case, was not enough to give the user a true and accurate measure of the fibers. In the case of the fiber samples in this application, it was much more revealing to use the four fiber-specific measures to gain a better understanding of the particles and, possibly, in their manufacturing process. It is also very practical to use one or more of these fiber-specific measures as a quality control specification given that the analysis is accurate, fast, and can measure thousands of particles in seconds.

Instruments Aid in Research Aimed at Sequestration of Carbon Dioxide Greenhouse Gas

The combustion of fossil fuels for energy has steadily increased the concentration of greenhouse gases in the earth's atmosphere. Of the numerous trace gases, carbon dioxide is a major component making up the majority of these emissions. Carbon dioxide sequestration involves the capture and secure storage of not only existing amounts of CO₂ in the atmosphere, but emitted CO₂ as well. Since the Kyoto Protocol, concerns over combustion gas emissions have received a great deal of attention.

There are numerous energy-related approaches to managing CO₂ that include several carbon free energy sources (e.g. nuclear, solar, wind, geothermal, and biomass energy). Scientists are also searching for ways to increase the efficiency of energy conversion so that smaller amounts of fossil fuel energy are required for the same energy output. However, although promising, these alternatives currently have a relatively small effect on current fossil fuel demand and usage. Fossil fuels continue to supply the overwhelming majority of the world's energy consumption. Increasing energy demands, the lag in converting to alternative energy sources, the global economic dependence on fossil fuels, and its relative low cost and high availability mean that fossil fuel consumption will likely continue for decades to come. As a result, there is a large amount of scientific research focused on effective methods to remove large amounts of carbon dioxide from the atmosphere and industrial emission sources, and store it safely.

A number of researchers now believe that sequestration of carbon dioxide in deep geological formations shows much promise as a long-term solution for safely storing CO₂ that is captured through cleanup efforts. The basic idea involves compressing captured CO₂ into a dense fluid and injecting it into a porous deep geological formation, where the rising CO₂ fluid is sealed beneath a layer of impermeable cap-rock. Years of experience in the United States with natural gas storage, injecting CO₂ for enhanced oil recovery (EOR), Enhanced Coal Bed Methane recovery (ECBM), and the injection of acid gases into saline geological structures have provided an incentive to pursue this promising theory. The U.S. Department of Energy, led by the NETL and Regional Carbon Sequestration Partnerships (RCSP) in partnership with industry and academia, is pursuing a CO₂ Sequestration Research, Development, and Demonstration Program. Field tests are currently taking place throughout the U.S. and Canada. Storage areas being investigated include depleted oil and gas reservoirs, unminable coal seams, and deep saline formations. Many of these formations have contained



APPLICATION NOTE 014

naturally stored carbon dioxide, other gases, and fluids for millions of years and are believed to have the potential to store many years of human-generated CO₂. In addition, in the last fifteen years, three large-scale CO₂ storage projects in Norway (1996), Canada (2000), and Algeria (2004), have begun operations and reported no safety or health-related incidents.

Even though these formations have the theoretical potential to store human-generated CO₂, it is estimated that annually over a billion metric tons must be sequestered in order to make a significant reduction. Many factors have to be studied prior to determination and full-scale implementation of appropriate sequestration sites. Factors such as proper engineering design and monitoring, hydrologic-geochemical-geomechanical processes that govern the long-term storage of carbon dioxide in the subsurface need to be understood. Research scientists require methods to characterize geological materials that help determine the value of the formation as a reservoir.

Since 1962, Micromeritics has supplied analytical tools that determine porosity and surface area, critical measurements needed for the study of potential CO₂ sequestration sites. Surface area and mercury porosimetry instruments have been used as necessary tools to characterize the sealing and fluid-transport properties of fine-grained sedimentary rocks under the pressure and temperature conditions of geological carbon dioxide. Pore volume measurements help predict the capacity of a formation. Pore size is an important variable in determining the rate at which CO₂ will flow through the formation while filling. Micromeritics' AutoPore Mercury Porosimeter has been used to determine the sealing capacity and pore-throat aperture size distribution

on reservoir core samples. Fluid transport experiments can be complemented by the combination of B.E.T. specific surface area data collected on Micromeritics' ASAP 2020 Accelerated Surface and Porosimetry System and mercury porosimetry data. These experiments help reveal significant changes in the transport properties and sealing efficiency of the samples. The ASAP 2020 is also an ideal tool for measuring both micropore and mesopore distributions in coal, therefore providing valuable information for ECBM studies.

Micromeritics' ASAP 2050 Xtended Pressure Sorption Analyzer and Particulate Systems' HPVA-100 High Pressure Volumetric Analyzer are ideal instruments for evaluating the storage capacity of CO₂ sorbents at high pressures. The ASAP 2050 is a high-resolution instrument that provides capacity as a function of storage pressure for vacuum to 10 bar. The HPVA extends the characterization to 100 or 200 bar. Both the ASAP 2050 and HPVA allow researchers to evaluate materials under real-world conditions.

International governments, with the aid of the scientific community, must find a way to eliminate the excess CO₂ in our atmosphere generated from the burning of fossil fuel. Preliminary data suggest the sequestration of CO₂ in geologic formations presents a promising solution. The goal of storing massive amounts of CO₂ depends partially on a number of physical characteristics needed for research on each of many geological formations. Micromeritics' expertise and its innovative materials characterization instrumentation have already been, and will continue to be, instrumental in providing important measurements required for carbon dioxide sequestration projects.

AIR PERMEABILITY: A NEW (OLD) TECHNIQUE FOR PARTICLE SIZE MEASUREMENT

By: Frank J. Venskytis, Independent Consultant. Clayton, NC

Abstract:

The permeability of air through a packed powder bed has been used for many years to measure particle size, via pressure measurements converted to surface area and subsequent conversion to particle size. Instruments using this method have been used extensively in the refractory metals industry due to their fast and easy operation.

Older instruments using this technique suffer from poor precision due to uncertain control of compaction forces and the lack of accurate pressure measurement. Thus, older instruments have fallen out of use in recent years, and are no longer available or supported. Newer instruments have now surfaced that provide precise control of compaction forces and accurate pressure measurement, exhibiting much better precision.

This presentation describes the air permeability method and compares the precision of the newer instruments with older ones, outlining how the newer instruments can be useful. Comparison with other particle size analysis methods is also presented.

Introduction:

For many years, the permeability of air through a bed of packed powder has been used to measure powder specific surface area, converting the measured surface area into a particle size based on assumed geometry and material density. Indeed, the refractory metals industry has relied on air permeability measurements of particle size* for over 50 years, because of the quick and easy operation of instruments using this technique. In fact, many specifications of metal and carbide particle size have been written based on these measurements. Problems have arisen, however, due to the poor precision of the instruments used, where material that is measured to be within the particle size specification limits is actually out of spec, and vice versa. Recent developments in instrument technology, as described below, may be able to minimize these problems.

It should be noted that no measurement technique actually measures the particle size of a powder, which is almost always

a distribution of a range of particle sizes, in various shapes. All measurement methods rely on some other characteristic that can be related to particle size, and usually express their results in terms of an “equivalent spherical diameter” based on those characteristics. Thus, many standard test methods for particle size contain the following cautionary caveat¹ :

Reported particle size measurement is a function of both the actual dimension and/or shape factor as well as the particular physical or chemical properties of the particle being measured. Caution is required when comparing data from instruments operating on different physical or chemical parameters or with different particle size measurement ranges. Sample acquisition, handling, and preparation can also affect reported particle size results.

Nevertheless, these “particle size” measurements can be very useful in a relative sense for estimating the particle size of many powder materials, including metal powders and their compounds like carbides and oxides. The measurement methods can be the basis for particle size specifications when the precision and variability of the measurements are taken into account, if the variability is not too large.

Particle Size Measurement by Air Permeability:

The air permeability method of particle size measurement has the advantage of being fast and easy to perform, taking just a few minutes without a great deal of sample preparation. In this method, a quantity of powder equal to 1 cm³ of actual solid material (sample mass numerically equal to the density of the material) is packed to a specified force in a tube of known inside diameter. The porosity of the powder bed is then measured by means of the height of the powder column, thereby measuring the total (apparent) volume of the powder bed and comparing that to the 1 cm³ of material in the tube. Air is then passed through the powder bed at a specified pressure, and the transmitted pressure is measured. The specific surface area of the powder is then determined using

APPLICATION NOTE 015

the Kozeny-Carman equation², which relates the surface area to the porosity and the pressure drop through the compacted powder. The “average particle size” can then be determined from a simple relation of surface area to particle size:

$$d = 6 / \rho S \quad (1)$$

where:

d = the average particle diameter in μm

ρ = the density of the powder material in g/cm^3

S = the specific surface area of the powder material in m^2/g , and

6 = a factor which converts the units of d to μm .

Old Method:

The older methods of air permeability particle size measurement, typified by the Fisher Sub-Sieve Sizer† instrument (Figure 1), use analog estimation techniques to arrive at an average particle size.



Figure 1: Fisher Sub-Sieve Sizer³

† The Fisher Sub-Sieve Sizer is no longer commercially available, nor is it supported with parts and service. Some instruments are still being used, especially in the refractory metals industry.

The packing force in this instrument is applied using a “needle-scale” torque wrench, or one that is “clickable”, stopping and releasing the force when the specified torque is reached. The input pressure is controlled by means of an observed bubbling rate in a water standpipe at the back of the instrument (viewed through the hole at the upper left of the instrument).

Figure 2 shows a closer look at the chart on the Fisher Sub-Sieve Sizer:

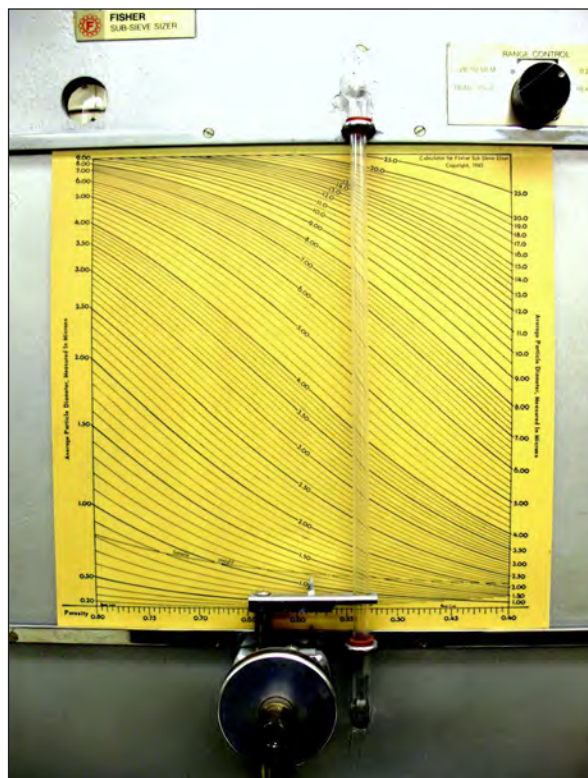


Figure 2: Fisher Sub-Sieve Sizer Particle Size Chart³

The chart shows curves representing the calculation of the average particle diameter via the Kozeny-Carman equation and Equation (1). The sample height is also read from the chart by aligning the point of the arrow on the metal crossbar with the nearly-horizontal “Sample Height” line near the bottom, by sliding the chart to the left or right. The average particle diameter (often called the “Fisher Number”) is then read from the chart by aligning the metal crossbar with

APPLICATION NOTE 015

the bottom of the water meniscus in the glass standpipe (a measure of the transmitted pressure) and reading the line closest to the pointer tip (or interpolating between lines).

It is quite obvious that poor precision can arise from all these “eyeball” estimations:

1. The packing force is unreliable because of the variability of operating and reading the torque wrench.
2. The bubble rate is not a very precise measure of pressure.
3. The sample height, and thus the porosity, is very difficult to estimate - just a slight difference in aligning the pointer with the sample height line of the chart can result in a large difference in porosity. That shift then affects the position of the chart lines in relation to the pressure standpipe and the pointer when measuring the transmitted pressure.
4. It is very difficult to locate the bottom of the meniscus in the standpipe.
5. It is very difficult to read the position of the pointer with respect to the chart lines, depending greatly on the angle of view, the eyesight of the viewer, and the skill of the operator in interpolation.

New Method

The new method of air permeability particle size measurement is performed by an instrument called the Subsieve AutoSizer (Figure 3).



Figure 3: Subsieve AutoSizer (SAS)

This new instrument makes use of all-digital control and measurement:

1. The packing force is controlled by calibrated pressure transducers.
2. The sample height is measured by the precise position of a piston that does the compaction, thus accurately determining the porosity.
3. The input pressure is accurately and precisely controlled, also by calibrated pressure transducers.
4. The transmitted air pressure is measured accurately and precisely by calibrated, traceable pressure transducers.
5. The Kozeny-Carmen equation is used directly to calculate the surface area from the porosity and transmitted pressure.
6. Equation (1) is used to directly calculate the average particle diameter.

Precision:

Because of the more precise control and measurement capabilities of the newer method, its test variability would be expected to be lower. Figure 4 shows a comparison of the new method's repeatability precision with that of the old method. There it can be seen that the new method does indeed show a lower repeatability interval⁵ - a measure of the single-instrument, single-operator variability of the measurement^{6,7} - across the entire range of measured particle sizes.

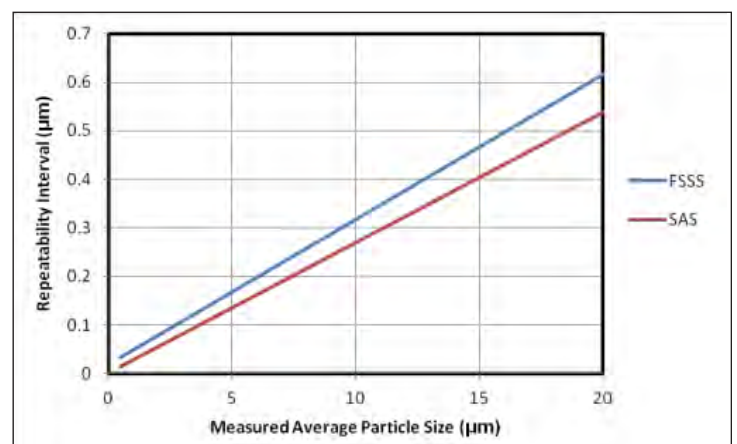


Figure 4: Repeatability Comparison^{5,8}

Figure 5 shows a similar comparison with regard to reproducibility – a measure of the between instruments, between-laboratories variability^{6,7}. Here the reproducibility interval is clearly lower for the new method.

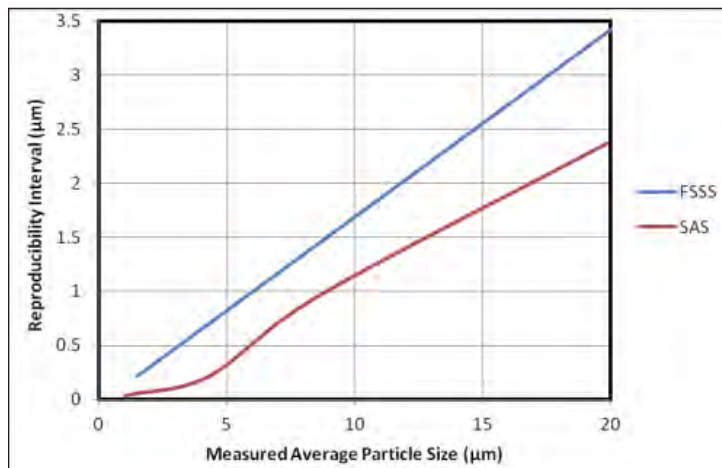


Figure 5: Reproducibility Comparison^{5,10}

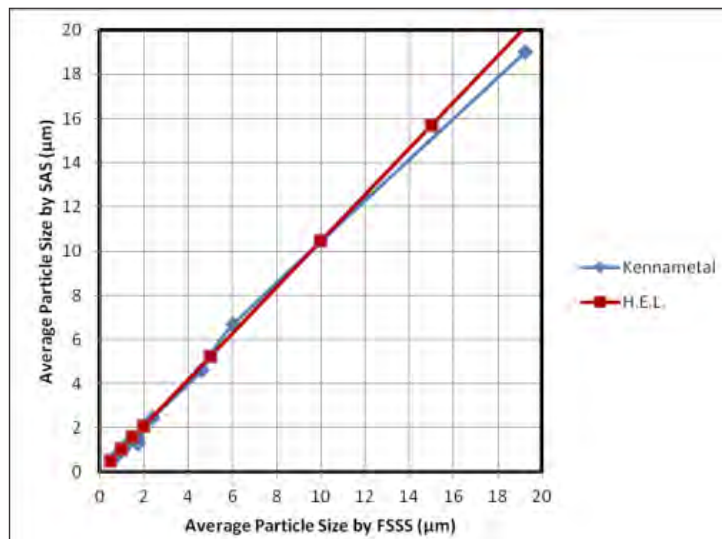


Figure 6: Comparison of Results from Old (FSSS) and New (SAS) Methods^{8,9}

In Figure 6, a comparison of particle size results shows a nearly 1:1 relationship between the old and new methods in two different sets of data, indicating that the new method is a suitable replacement for the old with regard to measured average particle size.

Comparison With Other Methods:

Figure 7 shows a preliminary comparison of the new method with laser diffraction particle size analysis. Although the absolute values of particle size differ, the correlation is quite good. Note that the correlation is logarithmic, not surprising as particle size distributions measured by laser diffraction tend to be log normal distributions; thus, a technique that measures only an average particle size might be expected to produce results that are logarithmically related to the laser diffraction distribution.

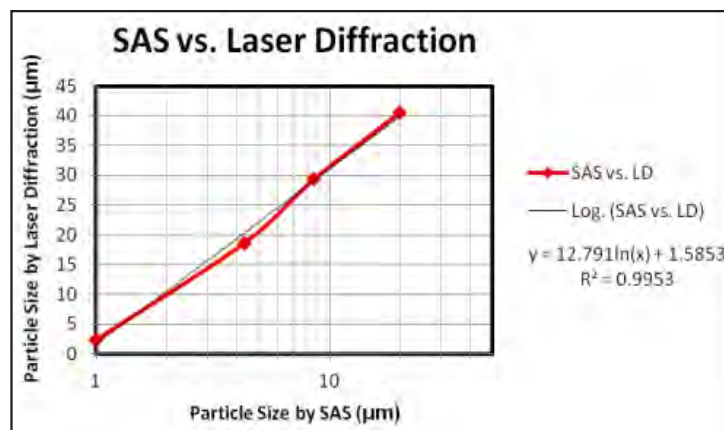


Figure 7: Comparison of the New Method with Laser Diffraction Particle Size Analysis¹⁰

The differences here serve to point out what was mentioned earlier: that different particle size measurement methods, based on different physical and chemical principles, can produce different results. A likely reason for the large differences here is related to dispersion of the powder: This preliminary comparison was done on tungsten powder, which has a tendency to bind finer particles together into relatively large, strongly-bound, multi-particle agglomerates. Standard procedure when analyzing these materials for primary particle size is to gently mill the powders to break up the agglomerates¹¹, followed by ultrasonic treatment in a surfactant solution to keep the primary particles dispersed¹². This procedure was not followed in this preliminary comparison.

Summary and Conclusion:

Table 1 summarizes how the intermediate measurements are determined and their method of application. There it is quite obvious that the new method should be superior to the old in precise and accurate application of forces and pressures, and in obtaining more reliable results. The new method's superior precision is borne out by Figures 4 and 5.

APPLICATION NOTE 015

| Measurementw Parameters | Old Method | New Method |
|-------------------------|---|---|
| Packing Force | Needle-Scale Torque Wrench | Calibrated Digital Pressure Transducers |
| Input Pressure | Visually-Timed Bubble Rate | Calibrated Digital Pressure Transducers |
| Sample Height | Visual Alignment with Sample Height Curve on Chart | Position of Piston |
| Transmitted Pressure | Visually Estimated Level of Meniscus in Standpipe | Calibrated Digital Pressure Transducers |
| Particle Size | Visual Alignment and Interpolation of Curves on Chart | Direct Calculation |

Table I: Determination and Application of Intermediate Measurement Parameters

Since the introduction of the new method, several standard test methods have been revised and written to include the new technique:

- MPIF Standard 32, Methods for Estimating Average Particle Size of Metal Powders Using Air Permeability¹³
- ASTM B330, Standard Test Methods for Estimating Average Particle Size of Metal Powders and Related Compounds Using Air Permeability⁵
- ASTM C721, Standard Test Methods for Estimating Average Particle Size of Alumina and Silica Powders by Air Permeability¹⁴
- ASTM E2980, Standard Test Methods for Estimating Average Particle Size of Powders Using Air Permeability¹⁵
- ISO 10070, Metallic powders – Determination of envelope-specific surface area from measurements of the permeability to air of a powder bed under steady-state flow conditions¹⁶

MPIF 32, ASTM B330, and ASTM C721 now include the new method, but continue to include the old method, as several of the older instruments are still in use throughout

the world. ASTM E2980 is a general standard that specifies only the new method, and as such can be used for many different classes of materials, including organic materials. ISO 10070 is currently in the process of revision, and will continue to include the old method, as well as some even older methods that are probably no longer used.

The new air permeability technique has been shown to be a viable and more precise method for estimating the particle size of powder materials. Although the method cannot give any indication of the full particle size distribution of a powder, it can be useful for assessing the relative particle sizes of a particular powder material produced in a broad range of sizes; for example, tungsten and tungsten carbide. The new air permeability technique can be used for many different classes of materials, such as ceramics, pigments, and even pharmaceutical drugs. The new method can be especially useful in production control and quality control of metal powders, where particle size specifications can now be written with confidence in their applicability, avoiding the confusion stemming from the poor precision of the old method.

Future Work:

Considerably more work needs to be done to further evaluate the precision of the new air permeability method on a wider range of materials (here only tungsten was used), on a broader range of particle sizes, and in multiple unrelated laboratories. Work also needs to be done to compare the new method with other particle size analysis techniques, including but not limited to laser diffraction, using better dispersion methods to yield particle size results that are not only correlatable, but closer in absolute size.

Acknowledgements:

The author is indebted to Joe Tauber of Kennametal for much of the precision and comparison data; to Wen Gao and John Miller of Global Tungsten & Powders for helpful discussions and information about the Fisher SubSieve Sizer; to Tony Thornton of Micromeritics for support of the standards revisions mentioned here; and to Max Groom and Pat Wommack of Micromeritics, Particulate Systems, for precision and comparison data, and support of this work.

APPLICATION NOTE 015

References:

1. Various ASTM Standards, including E1617, "Standard Practice for Reporting Particle Size Characterization Data" and E2651, "Standard Guide for Powder Particle Size Analysis", Annual Book of ASTM Standards, Volume 14.02, 2015, ASTM International, West Conshohocken, PA.
2. P.C. Carman, J.Soc.Chem.Ind., 57, p 225 (1938).
3. Wen Gao, 2015, Global Tungsten & Powders Corporation, Towanda, PA, private communication.
4. "Micromeritics Limited Subsieve AutoSizer", Micromeritics Instrument Corporation, <http://www.particulatesystems.com/products/Micromeritics-Limited-Subsieve-AutoSizer-SAS.aspx>
5. ASTM Standard B330, "Standard Test Methods for Estimating Average Particle Size of Metal Powders and Related Compounds Using Air Permeability", Annual Book of ASTM Standards, Volume O2.05, 2015, ASTM International, West Conshohocken, PA.
6. ASTM Standard E456, "Standard Terminology Relating to Quality and Statistics", Annual Book of ASTM Standards, Volume 14.02, 2015, ASTM International, West Conshohocken, PA.
7. ASTM Standard E691, "Standard Practice for Conducting an Interlaboratory Study to Determine the Precision of a Test Method", Annual Book of ASTM Standards, Volume 14.02, 2015, ASTM International, West Conshohocken, PA.
8. J. P. Tauber, 2015, Kennametal Inc., Latrobe, PA, private communication.
9. Hazard Evaluation Laboratory, Subsieve AutoSizerBrochure, 2012, HEL Ltd., Hertfordshire, UK.
10. Max Groom, 2016, Micromeritics Instrument Corporation, Norcross, GA, private communication.
11. ASTM Standard B859, "Standard Practice for De-Agglomeration of Refractory Metal Powders and Their Compounds Prior to Particle Size Analysis", Annual Book of ASTM Standards, Volume O2.05, 2015, ASTM International, West Conshohocken, PA.
12. ASTM Standard B821, "Standard Guide for Liquid Dispersion of Metal Powders and Related Compounds for Particle Size Analysis", Annual Book of ASTM Standards, Volume O2.05, 2015, ASTM International, West Conshohocken, PA.
13. MPIF Standard 32, "Methods for Estimating Average Particle Size of Metal Powders Using Air Permeability", Standard Test Methods for Metal Powders and Powder Metallurgy Products, 2016, Metal Powder Industries Federation, Princeton, NJ.
14. ASTM Standard C721, "Standard Test Methods for Estimating Average Particle Size of Alumina and Silica Powders by Air Permeability", Annual Book of ASTM Standards, Volume 15.02, 2015, ASTM International, West Conshohocken, PA.
15. ASTM Standard E2980, "Standard Test Methods for Estimating Average Particle Size of Powders Using Air Permeability", Annual Book of ASTM Standards, Volume 14.02, 2015, ASTM International, West Conshohocken, PA.
16. ISO Standard 10070, "Metallic powders – Determination of envelope-specific surface area from measurements of the permeability to air of a powder bed under steady-state flow conditions", 1991, International Organization for Standardization, Geneva, Switzerland.

Review of New Segregation Measurement Technique

By: Dr. Kerry Johanson Material
Flow Solutions, Inc.

Abstract

Segregation in industrial settings is responsible for a significant amount of lost product due to poor quality issues. In the pharmaceutical industry, segregation of the active ingredient is a critical problem that can lead to loss of life or physical harm if not closely monitored and controlled. Therefore, finding a way to control or predict segregation is critical to optimizing product design or to mitigate quality issues with bulk powders and granules. Obviously, the best way to handle segregation is to create a product consisting of a mixture of key ingredients that does not tend to separate when subjected to typical stimulus in handling processes and distribution networks. While this is the best alternative, it is often difficult to fully achieve in practice. One of the needs to accomplish this goal is to find a method of easily characterizing a mixture to measure segregation potential. This paper addresses that need. It describes an automated methodology used to measure segregation and evaluates that method for consistency, repeatability, and correlation to previous methods. The method first forms a pile of material in a controlled manner and then uses reflectance spectrum to differentiate between components in a mixture along the pile. The method of computing the concentrations and segregation intensities from reflectance measurements is presented. Repeat experiments are done to determine the expected error of the method. This error is found to be within 7% from test to test for a badly segregating material and within 0.5% for a moderately segregating material. The method also uses a complex data acquisition scheme and numerical analysis of large amounts of data. We measured the error of the data collection and subsequent numerical analysis and found the error for computation to be within 0.3%. We compared this to other manual methods and found good correlation to these methods of segregation measurement generating data within 7.8% of other methods.

Key words: Segregation, Spectral analysis, product quality, quality by design

Introduction

Currently, the pharmaceutical industry relies on one of two formulation routes to mitigate segregation of granular feed stocks. The first methodology is dry blending and is by far the simpler route. In dry blending, individual ingredients are mixed to form dry blends which are packed into tablets and capsules. The second methodology is wet granulation. In wet granulation, raw ingredients are combined with liquid, granulated to form large sized particles, dried to remove binding liquid, sized to assure quality product, and packed in tablets and capsules. There is almost always a recycle step in a wet granulation phase which complicates the process and batch inventory management. In addition, wet granulation can cause unwanted reactions that affect drug quality. Dry blend is simplest, but more prone to segregation. Wet granulation is more costly and complex, but less sensitive to segregation. If possible, pharmaceutical companies will choose the simpler process. Therefore, a tool to determine the potential segregation problems of dry blends is needed. The methodology presented in this paper addresses the specific need in typical dry blend processes and it is hoped that the tool and methodology can be extended to potential segregation measurement in wet granulation processes as well. In addition, the tool and method described can be applied to the food, chemical, cosmetic, paint, powdered metals, and ceramic industries.

Segregation is a mechanistic phenomenon. Therefore, it is useful to understand the magnitude of segregation, measure the pattern, and if possible infer the cause. Segregation is also a multi-component phenomenon where one component may have one or several causes of segregation. For this purpose, a small review of some of the causes of segregation may be instructive. The following is a short list of some common segregation mechanisms:

Sifting

Fines may sift through a matrix of coarse particles during handling. This mechanism requires that the void space between adjacent particles be large enough to permit fine

particle to pass through. Generally, this requires a particle size difference of about 3:1 [1]. Inter-particle motion is also required to provide a means of exposing empty voids spaces to fine particles [2]. The fines must also be free flowing enough to prevent arching between adjacent particles and the void spaces must be empty enough to accept fine particles [3]. In general, this type of segregation produces a radial pattern as material forms a pile in process equipment [4]. The fines accumulate near the pile charge point and decrease in concentration toward the edge of the pile.

Angle of repose differences

Two materials may have different angles of repose. Thus, when these two materials flow down a pile they essentially create overlapping piles where the material with the steepest repose angle accumulates near the top of the pile while the material with the flattest repose angle accumulates near the pile edge [5]. Generally, there is a distribution of these two materials along the pile's surface. Repose angle differences of about 2 degrees can result in significant segregation [2]. Material of different particle sizes can possess sufficient difference in repose angles to cause this type of segregation. However, particle size difference is not a prerequisite angle of repose segregation and materials of the same size can separate via this mechanism. In addition, your process must also generate piles during handling or processing to cause this type of segregation.

Air entrainment

The mixture may contain fines that are small enough to be carried by air currents in the handling system [6]. These fines drop out of the air stream when gas velocities decrease below the entrainment velocity. This causes separation of fines and coarse in handling systems. The fines generally deposit near the container walls. This type of segregation requires a source of air currents in process equipment. This source of air can come from free fall of a compressible material. When the falling stream impacts the material level, the entrained air is pushed out of the interstitial pores and carries the fine particles in the resulting dust cloud. This segregation typically causes a radial pattern during pile formation, but the fines are at the bottom of the pile and not the top [2].

Impact fluidization

If the mixture is fine enough, then air trapped in the interstitial voids can cause material to fluidize. As a large particle drops into this fluidized layer, momentum causes the large particles to penetrate this fluid layer, resulting in a top-to-bottom segregation of fine and coarse particles [2]. This mechanism requires a source of air and the ability of the bulk material to hang onto entrained air for a moderate amount of time.

Any materials can separate due to any difference in particle scale properties provided that the handling system can induce a stimulus that enhances that type of particle separation. For example, surface friction differences can cause angle of repose segregation, but only if piles are formed in process equipment. The fall height and material flow rate change the amount of entrained gas in the material and strongly influence air entrainment. But, this will only be important in a process that is subject to large free fall distances. This suggests that any viable segregation tester must have the ability to vary both feed and pile formation conditions to be able to correlate with reality. Some segregation testers inject an arbitrary amount of gas that is often much greater than would be present in any real gravity feed process, and then measure a segregation potential of fines versus coarse based on this stimulus [7]. Such a segregation method has no ability to predict reality. To be valuable, a segregation method should at least approximate the type of stimulus in typical handling processes and provide some means of controlling this stimulus to allow for matching process operations (i.e. the test method should subject the material to the same or similar behavior found in filling containers in typical systems). This then becomes the first judgment criteria for a viable segregation methodology.

Another need is to have a segregation method that can measure more than just two components. Real mixtures are comprised of multiple components. Current segregation analysis methods focus on measurement of just two components, typically fines and coarse [8] [9] [10]. The tool and methodology presented and reviewed in this paper will consider simultaneous segregation potential measurement of a mixture comprised of up to 6 components. This limit is somewhat arbitrary and could be extended to a greater number of components. However, data from mixtures of up to 6 component has been evaluated at present. Not all available data will be presented

here since the goal of this paper is to introduce and validate the robustness of the method. Thus, the ability for the method to be generally applied to more than two components is an important criterion for a robust segregation analysis method.

Another need for any measurement system to be successful is that the method should produce results that do not change and are consistent within a reasonable error range. Both the overall calculations in segregation pattern and segregation intensity for each component should be reasonably robust. Thus, robustness and consistency is the third criterion for a viable segregation methodology.

Finally, where possible the new methodology should be compared to at least one previous methodology to assure reasonable correlation. It is not required that the new methodology match exactly with previous methods since each method can give slightly different results. For example, there are dozens of particle size measurement techniques which presumably measure the same thing. However, none of these methods measure precisely the same particle size distribution. The same can be said of segregation potential measurements; the segregation potential measurement from technique to technique will not necessarily fall on top of each other. However, they should be reasonably close. Thus, the final criterion is that the test methodology should correlate with other measurements and at least measure the same trends.

Method and Materials

The new methodology consists of filling a container with a representative sample of product in such a way as to induce segregation similar to what one might find in a typical handling

process, then measuring the segregation pattern using an optical technique, and computing the segregation magnitude and intensity from the measured segregation pattern (Figure 1). Each of these criteria will be examined for this new methodology and, where possible, quantitative judgments be made on how well the new test method satisfies the criteria.

The following basic procedure was used to measure the segregation pattern of multi-component mixtures. Only the general steps are presented here; the details of each step are found below as well as details of the calculations required.

1. Feed the mixed material into the segregation slice model bin at a controlled flow rate and preset fall height (as discussed above).
2. Record the top position of the pile and the bottom of the pile (see Figure 3).
3. Determine the active measurement zone by taking measurements of the mixture parallel to the pile and at a depth of 6 mm from the top surface (see Figure 3).
4. Record the overall average concentration of key components in the mixture.
5. Measure the average spectrum of each pure component in the mixture.
6. Select a view port size for segregation measurements of mixture placed in segregation slice model bin.
7. Select the number of view port areas to examine along the pile and then select the number of spectral measurement points to acquire per view port.
8. Measure the average spectrum of the mixture material in a view port for all the view port areas desired along the pile.
9. Use the spectra of the key components, the overall average concentrations of the mixture, and the spectra of the mixture collected along the pile to compute the local concentrations of key components along the pile.
10. Use the concentration profiles to compute segregation intensity numbers for each key component.

While the above procedure is general in nature, the details of each step allow the user to obtain reliable

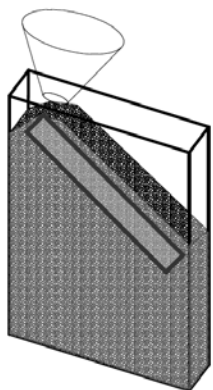


Figure 1. Schematic of segregation tester

Dump material into box and observe the change in color intensity along the pile as measured just below the top surface of the pile (rectangle section).

These changes in color intensity are an indication of differences in either chemical composition or in particle size and can be used to estimate the segregation of key components in the system.

APPLICATION NOTE 016

data. The reasons for each procedural choice will be explained so the reader will know what procedural details are important to successful data collection.

The first detail to be considered is control of the filling procedure to mimic or relate to behavior in a typical process. There are two process situations to consider when using segregation test data to predict process behavior. One general case is the static segregation pattern created when a material fills a process container. The second general case is segregation that arises in a dynamic operation condition. For example, does the test data predict segregation that may be present in a rotary shell blender as piles are formed and re-formed? Likewise, does the segregation test data correlate to the particle separation that may occur in a fluid bed?

We will consider the static condition where material free falls into a container at a given rate. Consider what happens in this case from a physics standpoint. A collection of particles falls into a container. These particles tend to spread as they accelerate. They may travel as a stream or they may travel as individual particles. In either case, the falling material entrains air in the surrounding area as it falls. If material travels as a stream, then it impacts the pile at a velocity near that given in equation 1.

$$1) V_{\max_{pile}} = \sqrt{2 \cdot h \cdot g}$$

This initial velocity free fall velocity depends on the distance of the fall (h). However, if the solid's flow rate is small, then the free fall stream spreads and the velocity of impact depends on the terminal velocity based on air drag (equation 2). In this case, the initial impact velocity is a function of the effective particle size (Dp), density of solid particles (ρ_s), density of the air (ρ_{air}) and viscosity of the air (μ_{air}). The actual impact velocity will be somewhere in between. Velocity increases as per equation 1 until it reaches the terminal velocity in equation 2.

$$2) V_{\min_{pile}} = \left(\frac{2 \cdot g \cdot (\rho_s - \rho_{air}) \cdot D_p^{5/3}}{15 \cdot \rho_{air}^{1/3} \cdot \mu_{air}^{2/3}} \right)^{3/4}$$

In addition, the impacting material has associated kinetic energy. When material impacts the surface, the surface can compact and deform plastically. If this compaction is excessive, then the strain energy required to accomplish this compression will influence the kinetic energy of the free fall and reduce the velocity. We assume that loss of strain energy

due to compaction with typical materials will be negligible. Thus, we deal only with the drag forces slowing the particle free fall velocities. We assume that, when particles hit the pile, they slid down the pile at the velocity compatible with friction angles of material sliding on material. The velocity (V_{pile}) traveling down a pile of length (L) is shown in equation 3.

$$3) V_{pile} = \sqrt{V_{impact}^2 + 2 \cdot g \cdot L \cdot (\tan(\theta_r) - \tan(\phi)) \cdot \cos(\theta_r)}$$

This velocity depends on the pile slope angle (θ_r) and the effective friction of material flowing down the pile (ϕ). If the friction angle is greater than the pile slope angle, the velocity down the pile slows and eventually stops. In fact, the stopping distance can be computed using the equation above (see equation 4).

$$4) L = \frac{-V_{impact}^2}{2 \cdot g \cdot (\tan(\theta_r) - \tan(\phi)) \cdot \cos(\theta_r)}$$

For the case of non terminal velocity flow, the distance traveled down the pile is given by equation 5 and shows a linear relationship between distance traveled down a pile and fall height.

$$5) L = \frac{-2 \cdot h}{2 \cdot (\tan(\theta_r) - \tan(\phi)) \cdot \cos(\theta_r)}$$

This implies a linear scale relationship between drop height and distance traveled on a pile for the process and small scale segregation test hopper for non terminal velocity flow in a process. For terminal velocity behavior, the scale relationship between the lab scale experiment and process geometry can be computed by equation 6.

$$6) L = \frac{-\min(V_{\max_{pile}}, V_{\min_{pile}})^2}{2 \cdot g \cdot (\tan(\theta_r) - \tan(\phi)) \cdot \cos(\theta_r)}$$

In either case, there exists a scale relationship between the process and small scale segregation test hopper. The simple analysis described above suggests that two main variables, namely free fall height and solids flow rate, are important in scaling between lab and full scale conditions. For terminal flow conditions, some information about particle size will also be required. Therefore, the segregation tester must have, as a minimum set of scale parameters, the ability to adjust both flow rate and fall height. To accomplish this, the tester was outfitted with a vibratory feed system attached to an extendable platform. The position of the feeder can be raised

APPLICATION NOTE 016

and lowered using this extendable platform. The vibration control can vary the flow rate into the segregation test hopper.

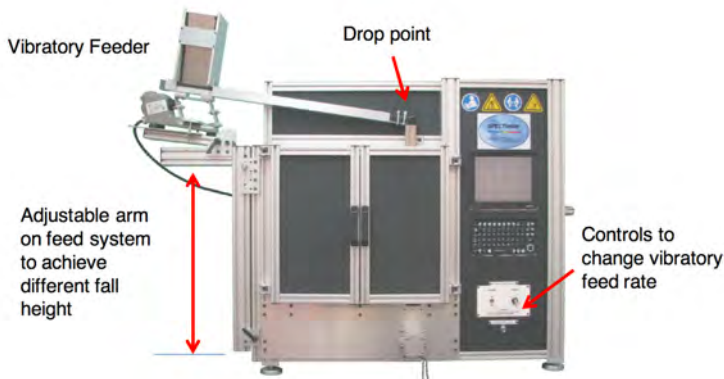


Figure 2. Segregation tester flow control

The second detail involves properly feeding material to be analyzed into the instrument. A feed tube directs material into the slice model to form the pile (Figure 2). The vibratory feeder pan/tube is flat on the bottom, is just as wide as the slice model and directs the flow into the segregation measurement chamber. This is a critical part of the feed design. As material exits the vibratory feeder, it does so in a sheet or solids particle curtain that distributes the particles across the feeder tube and supplies a consistent flow to the entire width of the segregation slice box. This builds the pile without any radial pile effects. The hopper feeder tube is positioned such that the top of the pile formed in the segregation test cell is at one wall of the segregation test cell (Figure 3). The pile surface is a plane that forms on one side of the segregation test cell or slice model. Filling the cell in this fashion produces the same pattern at the front surface of

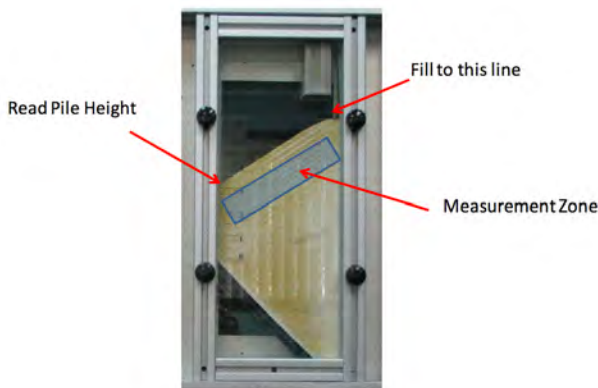


Figure 3. Segregation test hopper

the slice model bin as on the back surface of the slice model bin. Past researchers [11] discovered that wall effects in slice model bins with powders and granular material require that models be 25 mm or wider to prevent wall induced banding.

Banding can also naturally occur with slightly cohesive materials as they form a pile. Cohesive materials build up the pile and then periodically cascade down the pile, sifting during the cascade event and producing layers of fines and coarse [12]. This is a natural phenomenon that is part of real systems. Feeding material into the slice model where the walls are close together causes the same banding behavior. The tester must measure real segregation events and not tester induced events. Therefore, the segregation test cell width was limited to a minimum 25 mm to limit the occurrence of banding in the segregation test bin.

The segregation bin measurement zone is positioned parallel to the pile surface at a depth of about 6 mm below the top surface of the pile. The pile is observed through an optical glass plate at the back of the test cell with a standard fiber optic reflectance probe angled at 45 degrees to reduce the spectral reflectance of the glass surfaces. It is assumed that the entire zone parallel to the pile surface is representative of the average material placed in the tester.

It was discovered through trial and error that, for badly segregating materials, segregation may be more prevalent at the end of emptying the feed hopper. This effect occurred in the last 11% of the emptying cycle for material in the feed bin. To assure a representative sample in the segregation test cell, the feed hopper must be filled in small piles to minimize the segregation in this bin. Flow into the tester segregation test cell should be stopped when the level in the feed bin is 30% empty (or to the indicated fill line on the test cell). Thus, we avoided conditions that would cause segregation due to feed bin operation.

To confirm the consistency of segregation from back to front we filled a slice model made of glass end walls with a poorly segregating material and captured an image of the back and front material surfaces to determine how closely these images agreed using standard gray scale image correlation algorithms [13] [14]. We computed the average gray scale as a function of dimensionless radius from the top of the pile and used this data to compute a regression coefficient. The computed regression coefficient for this analysis is $r = 0.971$ ($r^2 = 0.942$) which suggest that 5.7% of deviation between

these curves is due to random uncontrolled events and 94.3% of the deviation is due a linear relationship between these curves. A regression coefficient of 0.971 is a strong positive coefficient, suggesting that Figure 4 shows reasonable agreement between the front and back segregation profiles and providing evidence that the controlled feed method and observation of the side of the pile can relate to segregation in real systems as the pattern measured on either side of the segregation test cell is effectively the same. We must still prove that observations measured at the side correlate well with volume based concentrations measured across the test cell. Additional evidence is presented below when segregation profiles measured with the new test technique are compared to alternate manual segregation test measurements incorporating the concentrations based on volume in the test cell.

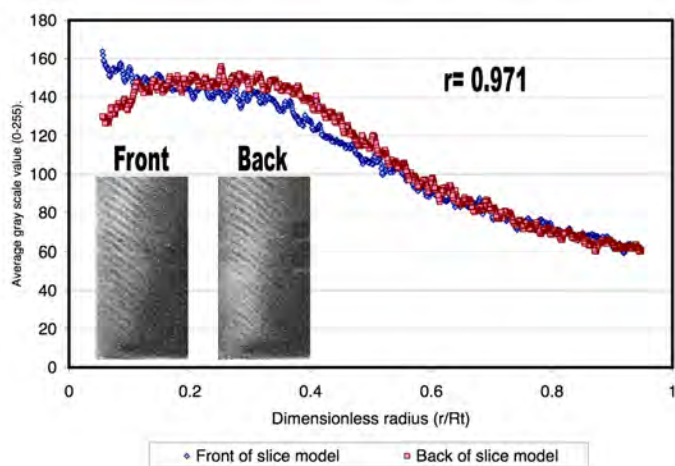


Figure 4. Correlation between front and back segregation pattern

Controlling flow behavior into a slice model, along with the ability to control both the feed rate and drop height, suggests that the segregation tester can be tuned to approximate process fill behavior. The data from this tester should also have applicability in dynamic segregation where segregation in blenders that form piles or inter-particle shear takes place. However, this test technique may not have applicability to conditions where the bulk material is fluidized and segregation is caused by the act of fluidization. The current filling methodology must be modified to accomplish this task.

The next detail in the methodology is to measure reflectance spectra of the mixture along the pile and the pure components and use this data to compute the concentration profile of key components down the pile. However, a discussion of the theory behind these measurements and calculations will prove useful.

Theory/calculation

Multi-component Segregation Theory and Measurement

To be of value, the measurement technique must be able to quantify segregation patterns for more than two ingredients. Literature is full of examples and theories outlining the segregation of bimodal mixtures. These measurements and the theories developed from these measurements are over simplified. If the component of interest does not deposit in one location, then another component increases its concentration to make up the difference. When three or more components are added to the mix (multi-component) the situation becomes much more complex. It is possible that two components segregate relative to each other, but adding additional components expands the potential interactions significantly. Theories describing this complex situation must allow for this possibility. Likewise, the measurement technique must be able to easily measure the segregation pattern of three or more components. If the subject of segregation modeling is to move forward, the measurement of multi-component segregating systems is at the heart of the discovery process. The author's contention is that sometimes the modeling leads the measurement, and other times the measurement leads and points the direction for the mathematical modeling. However, both are required in order to make significant forward steps in understanding a scientific topic. Very little is being done in the area of multi-component segregation theory largely due to the lack of an instrument capable of easily measuring segregation potential of multi-component systems. The following analysis presents a general method of measuring multi-component segregation potential. Several assumptions and simplifications have been made as a means of making the calculations and measurement simpler. At the heart of these measurements are the evaluation and use of reflectance spectra. The examples presented in this paper to validate the technique use reflectance spectra in the visible as well as near infrared (NIR) wavelengths.

A basic discussion of reflectance spectral measurements may be useful to the reader. If diffuse light of a given wavelength shines on a sample of particles, all at a known distance from the probe, the intensity of the light reflected back depends on three primary interactions. First, the particles can disperse the light based on simple light scattering. In this case the brightest intensity is caused by the finest particles. Second, if the particles contain colored pigment or chemicals that preferentially absorb a given wavelength of light, then

APPLICATION NOTE 016

the light being reflected back is only that which was not absorbed by certain pigment or chemicals. A surface looks red because all light hitting the surface except the red light is absorbed. The intensity of a reflectance spectrum, then, is a function of the chemical and pigment makeup in the measurement zone. Finally, in some cases, light absorbed activates bond in a particular chemical, absorbing photonic energy and converting it into photonic energy of a different wavelength. This is the basic principle involved in fluorescence. The analysis presented assumes that fluorescence is not a major effect in the systems studied. Thus, intensity of a reflectance spectrum is a function of the particle size and the pigments or chemical in the observation zone.

A reflectance spectrum also depends on the distance to the target. Non-laser light expands at some angle as it emits from the source. The intensity of the light reaching the target depends on the distance from the source and follows an r square law. When light hits the target it is usually reflected back in a diffuse manner. Thus, not all of the reflected light is captured by the reflectance probe, even if none of it is chemically absorbed

Consider the case of a powder material surface placed against an optical glass plate. The distance to target depends on the position of the particle surface relative to the plate surface. The probe may be at a prescribed distance from the optical plate, but the target is the particle on the other side of the plate. If the light shines on the particle directly against the plate, then the intensity of light is a maximum value. If the light hits a particle between the voids of the particle pressed against the plate, then the intensity of the reflectance spectrum is lower. When measuring a reflectance spectrum of a powder there will be variations in spectral intensity due to particle size distribution effects. A single reflectance measurement is not sufficient to determine the average reflectance spectrum of the powder. Therefore, we must average multiple spectra to obtain a representative spectrum value.

An integral part of the measurement process using this technique is the basic assumption that all data collected by spectral measurements is for material that has a known average concentration of key components. Simply put, all spectral data collected - when averaged together - represents the spectrum of a consistent mixture made of the specified concentrations of the key components. These average concentrations (step 4) are required for the calculation of the concentrations

in the mixture. They aid in the calibration of the spectral information to convert the measured spectra to concentrations. Correctly identifying the expected concentration of any given component in the mixture is a critical detail.

In step 5, pure components are placed in the component trays in a loose packed condition (Figure 5). Care is taken during this procedure to fill the component trays by scooping material into the tray using side-to-side motion to avoid a single pile in the center of the tray. The object of this filling process is to present to the optical glass a representative sample in terms of particle size. Thus, the trays were filled with minimal segregation. As pointed out above, a single measurement is not sufficient to characterize the average spectrum of any pure component. The probe measurement area is about 2.0 mm and ten measurements are taken at offsets of 1.2 mm to assure some overlap of spectral measurements. All ten spectra are averaged. The averaged spectra represents the spectral fingerprint of each pure component in the system. Care is taken to avoid measurements near the component tray edge or top of the component tray. It is critical that the probe measurement position for the material in the component trays be at the same distance as the measurement position for the mixture. This is done by calibrating the distance between the probe and the optical glass. The final calibration is done by placing a homogeneous reflective surface on the glass in each measurement area (segregation bin and pure component trays areas) and adjusting the intensity of the signal to be uniform at each measurement location.

Fill the component trays

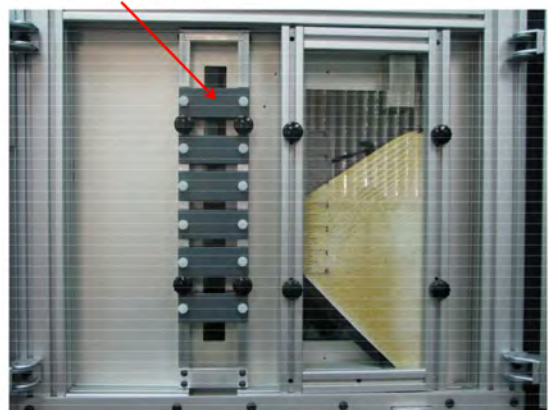


Figure 5. Filling the component trays

APPLICATION NOTE 016

Detail six requires identification of the smallest representative size that describes the segregation event(s) with the material of interest. Segregation measurement is a scale issue. The size of the chosen viewport should be large enough to contain a representative number of particles, yet small enough that differences in local compositions are not lost in the averaging scheme (Figure 6). In general, when no clear banding or pattern is observed, then selecting the view port to be at least 10 times the average particle size limits the error between consistent view ports to below 1%. If banding exists, then the view port must be large enough to cover two banding periods. If there is no clear cut way to assign the viewport, then several view ports should be selected and calculations performed using all of the view port sizes. The ideal view port size is found by plotting the segregation intensity factors as a function of viewport size. The measured segregation intensity factors converge to a consistent value when the view port size is large enough (Figure 7). Figure 7 shows that sand with an average particle size of 1500 microns requires a view ports size of about 4500 microns in order to reach a stable segregation intensity. This does not mean the view port must be exactly three times the average particle size because particle size, shape, banding and segregation pattern formation are all reasons that the view port may need to be changed.

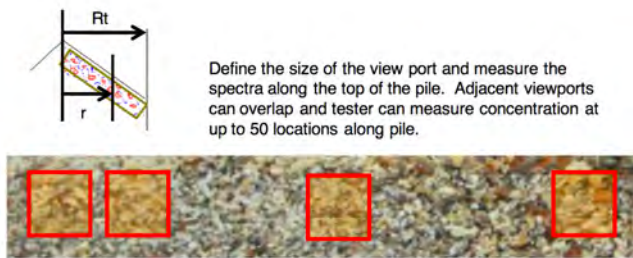


Figure 6. Typical measurement zone along pile top surface

Steps 7 and 8 require the acquisition of a spectrum for the mixture at each location of interest. The probe measurement zone is about 2.0 mm in diameter. Ideally, adjacent measurements should touch or overlap. This implies that a 12 mm viewport should have about 36 measurements (six on each side) to assure a good coverage. If the viewport is 10 mm, then 25 measurements (five on each side) would be sufficient. The selection of the number of measurements in each view port is an optimization issue. Larger measurement increments require some acquisition time, but will give a better result. A view port greater than 14 mm would require more than 49 measurements to be averaged to keep the optimal coverage. Taking 49 measurements at 50 locations along the pile requires about 30 minutes to acquire data and perform the required calculations.

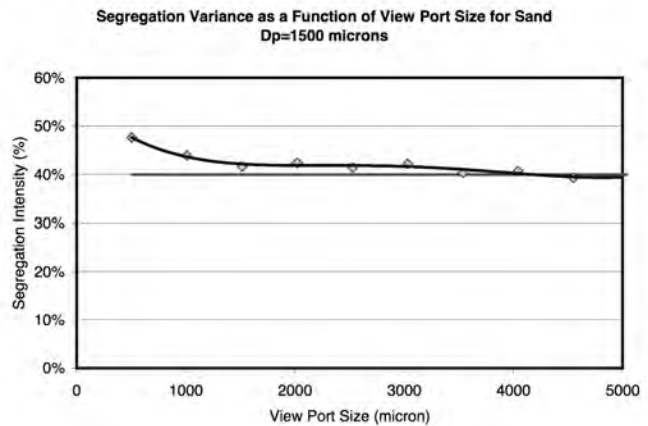


Figure 7. Segregation variance as a function of view port for sand mixture $D_p=1500$ micron

The next detail involves the decision regarding the type of spectrum used in the mixture analysis. This ninth step requires a spectral mixing law sufficiently general to be used for all types of materials.

One option is to use the complete reflectance intensity spectra, adjusted for black balance, the first derivative, or the second derivative of that complete intensity spectra. The intensity can be scaled relative to another intensity spectrum of one of the pure components. This enhances the differences between the peaks from different components. One advantage of using the second derivative is that the second derivative of the NIR or visible spectra removes most of the spectral information due to particle size and other influences that could affect the spectra intensity. The result is a signal that contains much of the chemical or color difference information with little particle size effects. Even in this case, there is still some influence of particle size and other effects. Thus, we used a spectral mixing methodology that includes the effect of particle size, particle orientation, and the filling of voids between the coarse particles. If the particles were spherical and all the same size, then there would be no optical difference between the particles in the mixture and pure particles placed in the component trays. In this special case, the mixture spectral intensity $FS_{mix}(\lambda)$ would be a simple linear combination of the spectral intensity of pure components ($FS_i(\lambda)$) based on the local fraction ($x_{fi,j}$) of each component. However, smaller particles fill the voids between coarse particles, creating a shadow effect for the coarse particles. These fine particles within the voids occupy a proportionally greater percent of area than the volume fraction would suggest. This indicates that a linear combination of pure spectra will not account for the mixture spectra. The mixture spectra will bias toward the fine materials. Likewise,

APPLICATION NOTE 016

if one component is a flake, then the orientation of particles relative to the glass will determine how much area the spectral probe sees. There are other size and shape effects that can bias the spectral area probe sees for any one component. Instead of creating a robust model to account for all of these potential probe view effects, a weighting factor is added to the additive spectra law to account for the probe measurement area effects. There is a unique weighting factor for each component. In reality this weighting factor is a matrix or tensor because there is a weighting factor for each component and potentially for each particle size. For the purposes of this work, it was assumed that the weighting factors are dependant only on the components. With this simplifying assumption, the spectral additive equation can be modeled by adding a weighting factor for component i (W_i) to the linear combination of spectra (equation 7).

$$7) \quad FS_{mix_j}(\lambda) = \sum_i W_i \cdot x_{f_{i,j}} \cdot FS_i(\lambda)$$

Equation 7 represents the computed spectrum for the j th position on the pile. There will be one of these equations for every position measured on the pile. An error function (equation 8) was defined as the sum of the square difference between the measured spectra ($F_{mix_i}(\lambda)$) and the computed spectra ($FS_{mix_i}(\lambda)$) for all the spectra measured along the pile.

$$8) \quad Error = \sum_j (FS_{mix_j}(\lambda) - F_{mix_j}(\lambda))^2$$

The goal is to minimize the error function given in equation 8. However, there are several other constraints that must be met for the optimal solution to be valid. At each point on the pile the fractional concentrations of the components must sum to 1.0 (equation 9). Likewise, all fractional concentration values must be between 0.0 and 1.0 (equations 10 and 11).

$$9) \quad 1 = \sum_i W_i \cdot x_{f_{i,j}} \quad \text{for all } j$$

$$10) \quad x_{f_{i,j}} > 0 \quad \text{for all } i \text{ and } j$$

$$11) \quad x_{f_{i,j}} > 1 \quad \text{for all } i \text{ and } j$$

Finally, the average of all fractional concentrations for each component in the system must equal the total overall mixture concentration (x_{ftot_i}) equation (12).

$$12) \quad x_{ftot_i} = \frac{\sum_j W_i \cdot x_{f_{i,j}}}{npts} \quad \text{for all } i$$

Equation 8 provides the target optimization function. Equations 9 through 12 provide the equations and constraints to be solved to generate the local concentrations of key components along the pile. All of these equations must be solved together.

Spectral mixing methods used by other researchers fall into one of two categories. Some methods [15] [16] [17] measure the spectrum of the pure compound and store this information in a data base of spectral fingerprints. Cross correlation techniques are used to compare these database spectra to new spectra and the percent of match or correlation between the new spectra and the database spectra indicates the likelihood that the new spectra is identical to a spectra in the data base. If several mixtures of spectra are in the data base, then this method can be used to approximate the concentration of the new mixture by statistical correlation with similar mixtures.

Other spectral mixing methods [18] [19] [20] observe the spectra of a prescribed mixture and focus on variation of spectra with change in one component. The spectra of samples containing various known concentrations of the key component of interest are recorded. Usually, a particular wavelength or band of wavelengths that shows a lot of intensity variation with the component of interest is used to create a least squares curve describing the relationship between the concentration and the spectral intensity. Once this relationship is defined, then the mixture spectrum is analyzed and the intensity in the wavelength band of interest is used to convert the intensity to a concentration of key components. If multiple concentrations are needed, then multivariate least squares analysis needs to be employed to compute the other concentrations from the spectral data.

The reflectance spectral signal is a function of light absorbed by the chemical species and light dispersed or scattered by the particle size of the observed surface. This relationship was first postulated using the Kubelka-Munk theory [21] [22] of reflectance of films or sheets. The net result is that reflectance is a function of the ratio (K/S) of the absorption coefficient (K) and the scattering coefficient (S). The fact that reflectance is a function of the ratio of these two coefficients complicates the analysis, for one must de-convolute this ratio to take into account the effect of particle size (scattering) and chemical composition (absorption). However, if the system of interest is governed primarily by one coefficient or the other,

APPLICATION NOTE 016

then a mono-modal relationship will exist between either absorption and reflectance or scattering and reflectance.

Results and Discussion

The tester compares the computed intensity curve with the actual measured curve and adjusts the weighting factors and local fractions at all measured locations along the pile to minimize error between the two curves. In addition, the method used to solve this set of equations is a non-linear least squares optimization with constraints used in NI LabView®. This is a standard solution technique that combines the constraints and data in the same matrix and solves for all of the concentration and weight factors together [23]. It is assumed that the total collected data represent the average material placed in the tester. This provides a method of simplifying the calculations. Normally, an NIR or visible spectral measurement requires that the spectra of several known concentrations of components in a mixture be entered in the NIR or visible unit to act as calibration spectra to “train” the instrument. The spectra of these various concentrations would normally be used to generate a regression plot between concentration and spectral intensity at some key wavelength of light. In this new method the spectra of the pure components and the fact that the overall average concentration is known provides the means of training the instrument. The complication is that all the spectral data is required to compute the concentration data requiring the solution of a very large number of simultaneous equations. The software takes into account all the spectra and then, using least squares correlation techniques, determines the best guess of the concentration of key components. The result is a measurement of concentration of key ingredients along the length of the pile for all measurement points along the pile (Figure 8).

There is not another method that currently measures the segregation profile of multi-component mixtures, so comparison data in the literature is lacking. However, seven mixture systems were studied to ascertain if the segregation pattern was similar to manual segregation patterns measured in similar tests. These manual segregation tests were done by filling a slice model with a mixture, carefully tipping the slice model backward, removing the front plate to expose the material in the slice model, sectioning the top of the pile into 5 or 6 sections and manually measuring the concentrations of key components in each sample collected along the pile. This procedure was repeated for seven different systems containing between two and five components. This manual

segregation method was compared to the spectral segregation method described above. The data from the new spectral segregation tester was measured at more points along the pile than could be collected using the manual method. Thus, the data was grouped and averaged over appropriate dimensionless radius values to compute points comparable to the data measured using the manual method. One such data set is presented in Figure 8, describing segregation of three types of bird seed. There is very good agreement between the manual measured points and the concentration points generated from the spectral segregation method.

Based on the complete set of data generated from this validation method, the standard deviation was estimated to be 2.6%. This suggests that the new methodology approximates other methods of measuring segregation with reasonable accuracy, indicating that the spectral method described above can be used to accurately estimate segregation concentration profiles of complex mixtures.

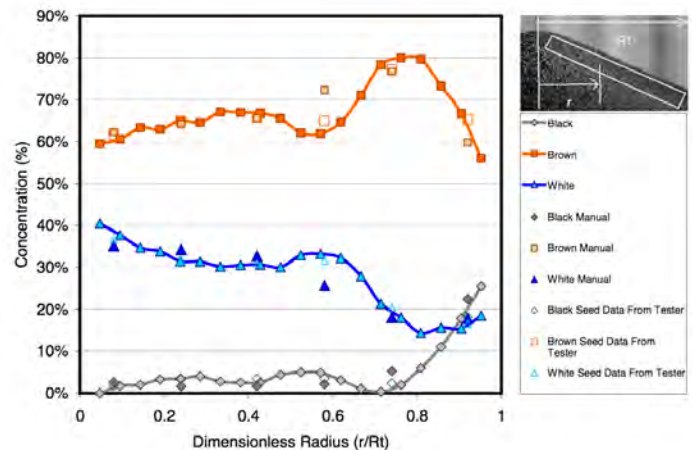


Figure 8. Segregation variance compared with alternate method of measuring segregation for a mixture of three bird seeds

If the measurement method is to be of value, the segregation measurement procedure must be reproducible. Repeatability should be reasonable, even with very easily segregating material. A protocol to test this repeatability sensitivity was done using the segregation measurement procedure outlined above. A set of three free flowing sands of different size and color were mixed. This mixture was introduced into the tester three distinct times and the procedure followed to generate the concentration profiles (Figures 9 and 10). Twenty

APPLICATION NOTE 016

samples along the pile were analyzed and the deviation off of the average for these three tests was measured. This experiment suggests that, based on a three sigma estimate, the error caused by repeated measurement is about 7.0% for a material that is highly sensitive to segregation. Other data was used with a material that was less prone to segregation and found that the repeated measurement error for that case was 0.5%. Thus the repeated measurement error for this new technique was bound between 0.5% and 7.0%. Figure 10 indicates that there may be some spatial variation effects in the error of the test. However, this could also be due to the nature of the segregation pattern. The data suggests that this spectral segregation test method using controlled filling reproduces segregation patterns with reasonable accuracy.

It is also important that the calculation method used to compute the concentration profiles be reliable. To test reliability, the mixture of three sands was placed in the tester and the concentration profile was measured for this same pattern three times (Figures 11 and 12). The repeated solution of these concentration profiles indicates that based on three sigma deviation, the measurement error for a material that was very sensitive to segregation was 0.3%.

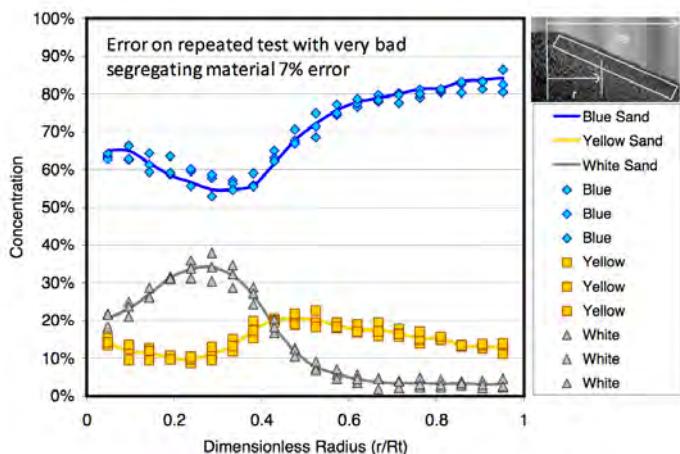


Figure 9. Segregation variance due to repeated tests using spectral segregation measurement

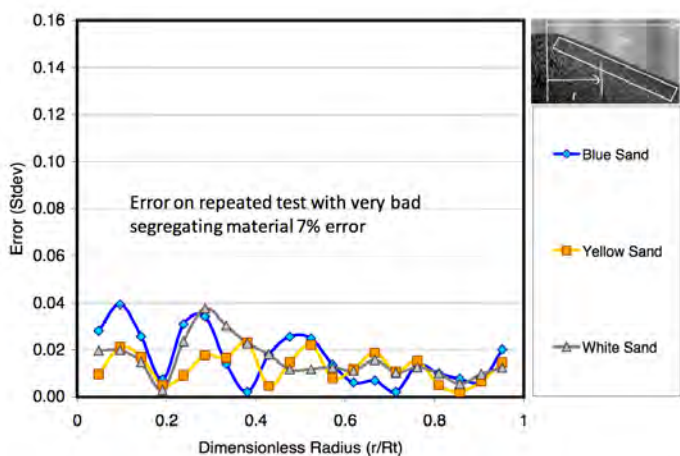


Figure 10. Segregation variance due to repeated tests as a function of radial position using spectral segregation measurement

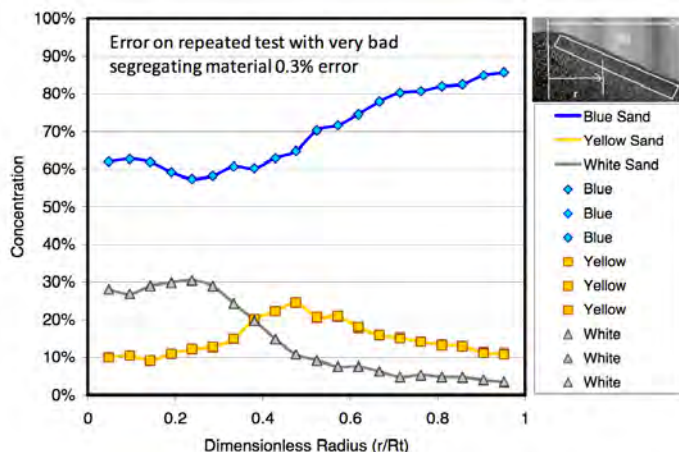


Figure 11. Segregation variance due to repeated calculations of a segregation pattern using spectral segregation measurement

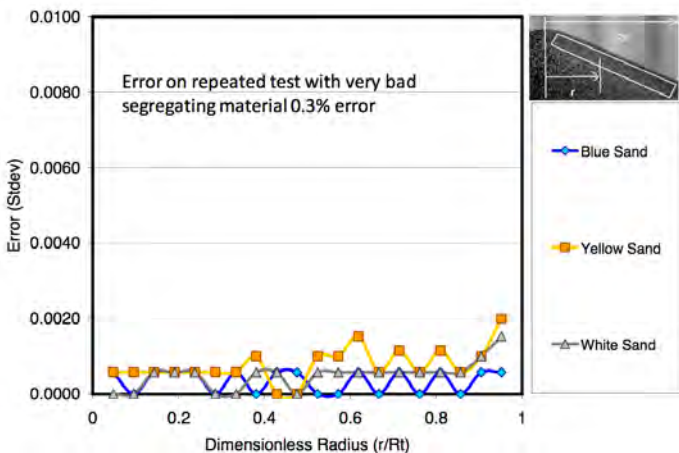


Figure 12. Segregation variance due to repeated calculations of a segregation pattern as a function of radial position using spectral segregation measurement

References

1. Kerry Johanson, Chris Eckert, Dev Ghose, Millorad Djomlija, and Mario Hubert, Quantitative measurement of particle segregation mechanisms, *Powder Technology* Volume 159, Issue 1, 2 November 2005, Pages 1-12
2. Jerry Johanson, Solids segregation: causes and solutions, *Powder and Bulk Engineering*, August 1988
3. J. M. Ottino, and D. V. Khakhar, Fundamental research in heaping, mixing, and segregation of granular materials: challenges and perspectives, *Powder Technology*, Volume 121, Issues 2-3, 26 November 2001, Pages 117-122
4. Anjani K. Jha, and Virendra M. Puri, Percolation segregation of binary mixtures under periodic movement, *Powder Technology*, Available online 7 May 2009, doi:10.1016/j.powtec.2009.04.013
5. Y. L. Ding, R. Forster, J. P. K. Seville, and D. J. Parker, Segregation of granular flow in the transverse plane of a rolling mode rotating drum, *International Journal of Multiphase Flow*, Volume 28, Issue 4, April 2002, Pages 635-663
6. Are Dyrøy, Morten Karlsen, Gisle G. Enstad, Sunil de Silva, A system for the reduction of air current segregation in silos, *Handbook of Powder Technology*, Volume 10, 2001, Pages 623-630
7. Fluidization Segregation Tester U.S. Patent 6,487,921 B1 ASTM Standard D6941-03
8. Y.R. He, H.S. Chen, Y.L. Ding, and B. Lickiss, Solids Motion and Segregation of Binary Mixtures in a Rotating Drum Mixer, *Chemical Engineering Research and Design* Volume 85, Issue 7, 2007, Pages 963-973
9. Shu-San Hsiau, Jing-I Wang, Segregation processes of a binary granular mixture in a shaker, *Advanced Powder Technology*, Volume 10, Issue 3, 1999, Pages 245-253
10. D. V. Khakhar, Ashish V. Orpe, J. M. Ottino, Continuum model of mixing and size segregation in a rotating cylinder: concentration-flow coupling and streak formation, *Powder Technology*, Volume 116, Issues 2-3, 23 May 2001, Pages 232-245
11. Stuart B. Savage, *Disorder and Granular Media*, edited by D. Bideau and A. Hansen (1993) North-Holland, Amsterdam, p.255
12. Makse, H. A., P. Cizeau and H. Eugene Stanley, Possible Stratification Mechanism in Granular Mixtures, (1997) volume 78, number 17 *Physical Review Letters* 28 April 1997
13. M.A. Sutton, J.-J. Orteu, H. W. Schreier, *Image Correlation for Shape, Motion and Deformation Measurements*, Springer; 2009 edition (April 22, 2009)
14. T.J. Keating, P.R. Wolf, and F.L. Scarpace, "An Improved Method of Digital Image Correlation," *Photogrammetric Engineering and Remote Sensing* 41(8):993-1002,(1975)
15. Núria Martínez-Carreras, Andreas Krein, Thomas Udelhoven, Francesc Gallart, Jean F. Iffly, Lucien Hoffmann, Laurent Pfister, Desmond E. Walling, A rapid spectral-reflectance-based fingerprinting approach for documenting suspended sediment sources during storm runoff events, *Journal of Soils and Sediments*, April 2010, Volume 10, Issue 3, pp 400-413
16. J. Ricardo Lucio-Gutiérrez, J. Coello, Application of near infrared spectral fingerprinting and pattern recognition techniques for fast identification of *Eleutherococcus senticosus*, *Food Research International*, Volume 44, Issue 2, March 2011, Pages 557-565
17. Yunzhao Wu, Jun Chen, Junfeng Ji, Peng Gong, Qilin Liao, Qingjiu Tian, Hongrui Ma, A Mechanism Study of Reflectance Spectroscopy for Investigating Heavy Metals in Soils, *Journal: Soil Science Society of America Journal - SSSA*, vol. 71, no. 3, 2007
18. Liu, W., Baret, F., Gu, X., Tong, Q., Zheng, L., & Zhang, B. (2003). Evaluation of methods for soil surface moisture estimation from reflectance data. *International Journal of Remote Sensing*, 24, pp. 2069-2083
19. Kathleen A. Martin, Direct measurement of moisture in skin by NIR spectroscopy *J. Soc. Cosmet. Chem.*, 44, 249-261 (September/October 1993)
20. Wallis, I.R., Foley, W.J., 2003. Independent validation of near-infrared reflectance spectroscopy as an estimator of potential food intake of *Eucalyptus* foliage for folivorous marsupials. *Aust. J. Zool.* 51: 1-4
21. Li Yang, Björn Kruse, Revised Kubelka-Munk theory. I. Theory and application, *Journal of The Optical Society of America A-optics Image Science and Vision - J OPT SOC AM A-OPT IMAGE SCI*, vol. 21, no. 10, 2004
22. Bruce Hapke, *Theory of Reflectance and Emittance Spectroscopy*, Cambridge University Press; 1st Pbk. Ed edition (February 17, 2005)
23. Philip E. Gill, *Practical Optimization*, Academic Pr (October 1981)

Taste the Difference—A New Method of Measuring Segregation: Steak Seasoning, a Case Study

By: Dr. Kerry Johanson Material
Flow Solutions, Inc.

Abstract

Bulk solid processing generally fails due to one of three problems. The material may hang-up in the system, the material flow rate cannot be controlled by volumetric feeders, or the material segregates during handling and processing creating quality problems. The focus of this paper will be diagnosing and solving segregation problems. There is a significant lack in the ability to measure segregation especially when dealing with more than two components. Almost all bulk solid mixtures are a combination of at least three or more materials; yet our ability to measure and mitigate segregation tendencies in multi-component mixtures is significantly below our ability to create these mixtures. There is a critical need for segregation testers that can estimate the segregation profiles of mixtures of multiple components. This paper presents a method to measure the segregation potential of a mixture comprised of multiple components using spectral methods. Steak seasoning with five components was chosen as a case study mixture to show the effects of segregation in multi-component systems. Changing the physical characteristics of just one component in the system can often affect segregation of several components in the system. This study shows how changing just the size of the salt component affects at least two other components.

Key Words: Segregation, Sifting, Angle of Repose, Reflectance Spectra

Introduction

There are two uses for segregation data. Engineers may wish to use the segregation data to optimize product design creating a product with minimal segregation. Engineers may also wish to modify the processing to minimize the effect of segregation in their plant packaging process or handling facility. In either case, the segregation pattern, segregation mechanism, and magnitude of segregation are key parameters in process or product design recommendations.

Bulk segregation can occur due to a variety of mechanisms [1,2]. Finer particles sift down through a matrix of coarse particles [3], separating as they slide down a pile. Air currents generated by free fall carry fines to regions in the bin where gas velocities decrease enough to precipitate particles [4]. Differences in repose angles can cause materials to slide down the pile at different velocities, creating a separation of materials based on particle friction characteristics [5,6,7]. In order to mitigate the segregation issues existing with bulk materials, it is necessary to understand the mechanisms causing segregation as well as the magnitude of the segregation. It is also valuable to know the pattern of segregation in process vessels. Attempting to cure a segregation problem caused by air entrainment of fines requires modifying the amount of air entrained in the free falling solid. However, modifying the free fall height will not affect segregation caused by sifting.

One problem with current segregation testers is that they do not relate well to the process. Any two or three materials can segregate if there is a difference in properties and the mixture is subject to enough external stimuli. Adding enough fluidization gas will separate materials of different densities, even though these extreme conditions may not occur in the actual process. The real question to be answered is: will the mixture segregate when exposed to a feed behavior similar to that present in the process? Therefore, any measurement of segregation tendency should have three key elements. First, the feed should be controlled so as to allow the measured segregation to be scalable to process conditions. Second, the pattern of the segregation should be included as part of the mechanism in order to predict the expected concentration leaving process equipment. Finally, the magnitude of the segregation should be quantified to provide guidance in determining if the mechanism is actually a potential problem in the process.

Segregation Measurement Device and Procedure

The ideal segregation test would be to, first, feed material into a small container in a manner similar to

the actual process conditions. Then, section the pile at many (15 to 50) distinct points and, finally, measure concentration of key components in a small amount of material collected at these points. This procedure would yield enough information about the segregation magnitude, mechanism, and pattern of multi-component materials to be useful in process and product design.

In the past researchers have fed bulk materials onto a pile, sectioned a conical pile into annular sections, and performed chemical or size analysis on the material collected in each annular section [8, 9]. This is a long and tedious method which results in only a very few measurements collected along the pile. Plant personnel often use thieves to sample piles in process equipment. This method also yields only a few measurements along the pile and disturbs the surface, thereby changing the segregation pattern. Others measure segregation pattern by placing material in a funnel flow hopper and then discharging the hopper, collecting the output stream and measuring the quality of the mixture by chemical composition or particle size [10, 11]. This convolutes the segregation with the flow pattern from a particular hopper or bin. Unless the bin design in the tester is precisely the same as the bin design in the process, there is no guarantee that the composition during discharge from the tester will be similar to that found in the actual process. Additionally, the cohesive properties of the bulk material can impede flow from the segregation tester hopper, even though hang-ups may not occur in the process with the same material.

It is the author's contention that it is better to measure the segregation pattern from the pile formation segregation tester then compute the velocity pattern from flow properties. Once the segregation pattern and velocity profile are known, the composition of material leaving the hopper can be estimated. This method possesses the added benefit that, once the segregation pattern is measured, the concentration output from any series of general bins, hoppers, and other process equipment can be computed to yield the segregation effect on the entire process. Thus, this methodology provides a powerful tool to predict and mitigate segregation problems in feed systems and not just within a single bin or hopper.

The majority of real process mixtures contain more than two components. However, quite often segregation studies

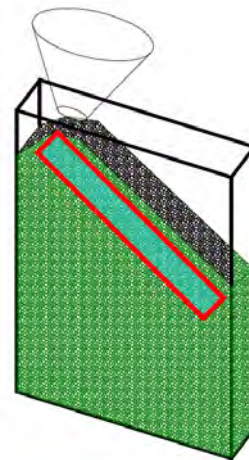
are done only for two component combinations [12-19]. This is done because analysis for multiple materials is difficult and time consuming. The interaction of two materials is usually simple and follows predictable rules. One example of a simple rule is that the fines fill the voids. In a two component system this causes finer particles to concentrate at the top of the pile. Simple rules applied to two component system generally result in predictable behavior.

The real challenge is to predict what happens in systems with multiple components subject to one or more segregation mechanism. Some researchers have formulated models that incorporate multi-particle effects [20 - 22]. In multi-particle flows, simple rules may not apply. The segregation pattern of a mixture containing more than two components is significantly more complex due to interaction of multiple sets of particles. Sometimes this can lead to predictable patterns. For example, materials with differing repose angle will generally concentrate in order of their repose angle along a pile surface with the flattest repose angle at the bottom of the pile and the steepest at the top. However, suppose that a material is subject to both angle of repose segregation and sifting segregation. Increasing the local concentration of fines increases the local repose angle on the pile, causing a material that was not previously segregating to separate from the bulk because of local repose angle differences. Likewise, partially filling the voids between particles with the right size particle can create a smoother surface that can facilitate segregation of other materials in the mixture as they slide down a pile. Changing one component often affects the segregation profile of all the materials in the mixture. In any event, the ability to measure the segregation pattern of a mixture with multiple components is critical to understanding the segregation behavior of that mixture.

Figure 1. Schematic of segregation tester

Dump material into box and observe the change in color intensity along the pile as measured just below the top surface of the pile (rectangle section).

These changes in color intensity are an indication of differences in either chemical composition or in particle size and can be used to estimate the segregation of key components in the system.



APPLICATION NOTE 017

One way to gain access to the pile cross-section is to fill a slice model with material and observe the segregation pattern through the side of the slice model using optical techniques (Figure 1).

Observation of segregation through the sides of a slice model will be biased to the optical pattern that exists at

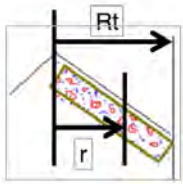


Figure 2. Measurement zone along pile top surface

Define the size of the view port and measure the spectra along the top of the pile. Adjacent viewports can overlap and tester can measure concentration at up to 50 locations along pile.



the wall of the segregation tester. Therefore, care must be taken when loading the tester to assure a representative sample is visible through the side of the tester. Filling the tester across the width of the slice model will distribute the material to the tester wall, creating a uniform material across the tester. Limiting the thickness of the slice model will also help with distribution of representative material to the tester wall. Extremely thin slice models are subject to banding due to wall effects that would not be present in wider slice models. For typical materials, this limits the slice model to a minimum of approximately 25 mm thick.

Reflectance spectroscopic methods can be employed to measure subtle differences in color. Since we are dealing with a discrete particle system, multiple measurements are required to determine the average concentration within a given view-port. Segregation measurement is also a scale issue. The size of the chosen view-port should be large enough to contain a representative number of particles, yet small enough that differences in local compositions are not lost in the averaging scheme. The ideal segregation tester will allow the user to change the size of the view-port, as well as the number of measurements within the view-port, to accomplish segregation measurement.

Based on the principles addressed above, a novel segregation tester (Figure 3) was created to measure the segregation pattern of various materials. The tester consists of a vibratory



Figure 3. Segregation tester used in experiment showing the variable speed vibratory feed system and the pile formed in the tester for analysis (note right door is open to expose the segregation hopper)

feed system to control the rate and fall height of material fed into the tester slice model. The back of the slice model is made of glass so the reflectance probe can view the side of the pile. This probe is connected to an x-z stage that moves to observe any portion of the slice model hopper.

The light from this probe is fed to a spectrophotometer, which generates spectra of the material in the view-port area. There are also up to six component trays that contain the pure components materials and be viewed with the spectrophotometer. The front of the test unit is opened during filling and closed during spectral measurement. The black glass doors are designed to keep ambient light from influencing the spectral imaging results.

For the purposes of demonstrating the use of the tester as a means of providing product design recommendations, the material selected was steak seasoning which consists of five components of different size, shape, and color. Let's suppose that there is freedom to select one of three grades of salt for use as one of the components in the seasoning mixture. The question to be answered is: what grade of salt gives the most uniform mixture and is least sensitive to segregation issues? Steak seasoning consisting of 47% salt, 28% minced garlic, 19% black pepper, 2% red pepper, and 4% dill seed was used in this experiment. The following procedure was used in the generation of steak seasoning segregation data.

1. Create a mixture of steak seasoning using one of three possible grades of salt.
2. Feed this mixture into the segregation tester slice model at a rate of 1.5 lit/min through a drop height of 152 mm inches.
3. Place salt, garlic, black pepper, red pepper, and dill seed in the individual component measurement trays and

APPLICATION NOTE 017

measure the reflective spectral response of each material for 1825 wavelengths between 420 nm to 850 nm.

4. Select a measurement zone that is parallel to the pile surface and positioned 20 mm below the top surface of the pile.
5. Select the view-port to be a square 15 mm by 15 mm and measure the spectra of 36 (a 6x6 matrix) distinct points within this view-port. Average these 36 values to create an average spectral reading of the material within the selected view-port.
6. Select 20 points along the pile to measure the average view-port spectra (total 720 complete spectral measurements per pile).
7. Using the spectra of the pure components and the average mixture spectra along the pile, compute the concentration of the pure components from numerical spectral de-mixing techniques. This will give the concentration of the different materials along the pile as a function of radial distance to the pile's edge.
8. Repeat steps 1 through 7 for each salt grade used.

Figure 4 shows the averaged spectra of the five components used in the mixture. Notice the different peaks at various wavelengths. The garlic and salt have similar spectra. The dill seed and black pepper are similar, and the red pepper has a unique spectra. These average spectra were created by filling the component holders with pure materials and averaging 10 individual spectral images of each pure component. These pure component spectra include the effect of surface texture, color and particle size. The spectra also are affected by particle orientation. If the particles were spherical and all the same size, then there would be no optical difference between the particles in the mixture and pure particles placed in the component trays. In this case, the mixture spectral intensity $F_{mix_j}(\lambda)$ would be a simple linear combination of the spectral intensity of pure components ($F_i(\lambda)$) based on the local fraction ($x_{i,j}$) of each component (equation 1).

$$1) \quad i x_j(\lambda) = \sum_i x_{i,j} \cdot F_i(\lambda)$$

However, in this case the smaller particles fill the voids between coarse particles, creating a shadow effect for the coarse particles. These fine particles within the voids occupy a proportionally greater percent of area than the volume fraction would suggest. This indicates that a linear combination of pure spectra will not account for the mixture spectra. The

mixture spectra will be more biased towards the fine materials. This effect can be modeled by adding a weighting factor (W_i) to the linear combination of pure spectra (equation 2).

$$2) \quad F_{mix_j}(\lambda) = \sum_i W_i \cdot x_{i,j} \cdot F_i(\lambda)$$

Figure 5 contains a list of the computed optical weighting factors for the steak seasoning. The tester compares the computed intensity curve with the actual measured curve and adjusts the weighting factors and local fractions to minimize the error between the two curves. The data in Figure 5 shows the actual measured intensity at one point in the tester and the computed weighted spectral combination for steak seasoning using the overall spectral weighting factors. There is good agreement between the measured curve and the computed weighted linear combination.

The error between the computed spectra using weighted spectral averaging and the actual measured spectra

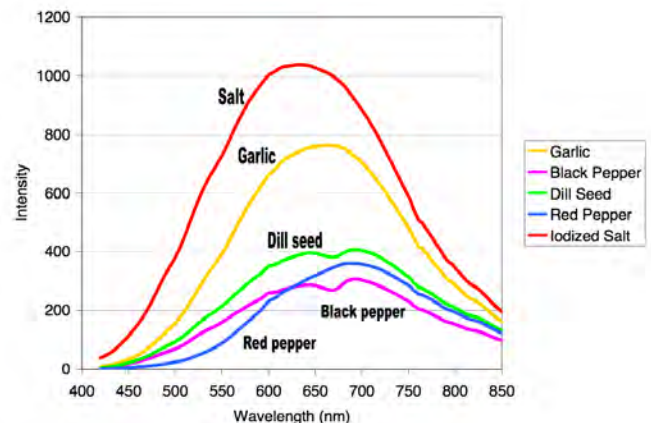


Figure 4. Spectra of steak seasoning components

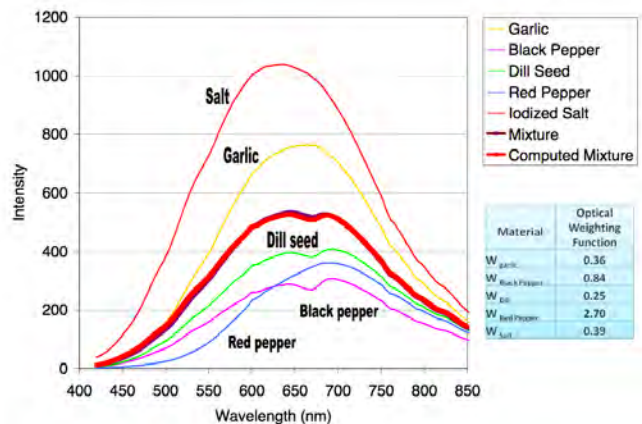


Figure 5. Sample mixture spectra resulting in a composition of 27.1% Garlic, 19.7% Black pepper, 4.0% Dill seed, 2.0% Red pepper, and 47.2% iodized Morton® salt

APPLICATION NOTE 017

from the reflectance probe was minimized to obtain the local concentrations of spices in the steak seasoning mixture. This gave concentration profile data for each of salt grades as shown in Figures 6 through 8.

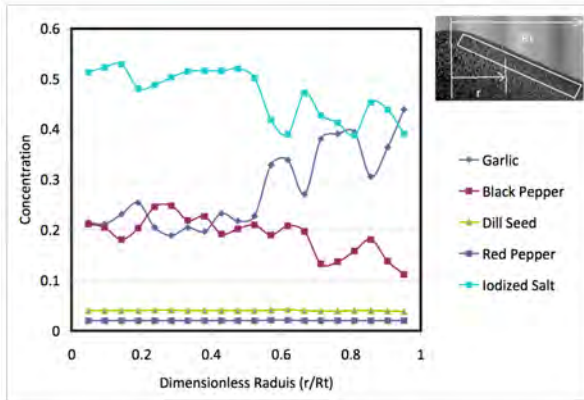


Figure 6. Segregation Test results for steak seasoning with iodized salt

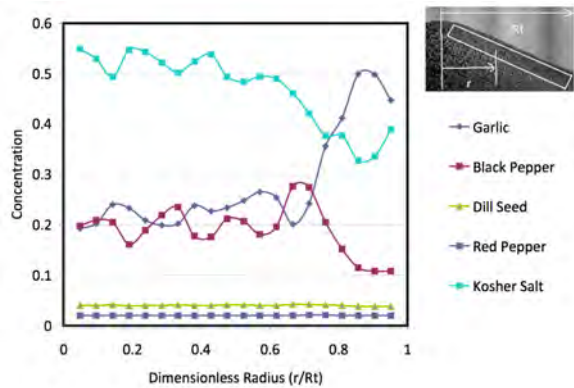


Figure 7. Segregation Test results for steak seasoning with kosher salt

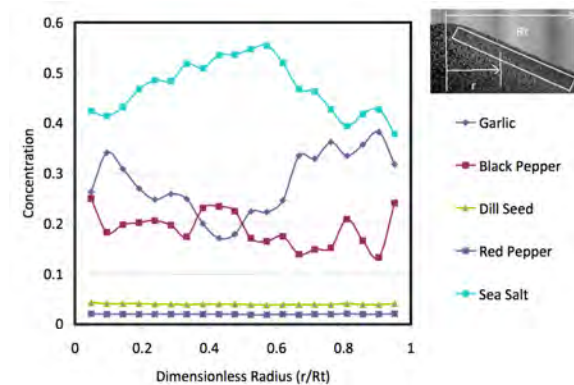


Figure 8. Segregation Test results for steak seasoning with sea salt

The dill seed and red pepper show no signs of segregation. However the garlic, salt and black pepper exhibit some interesting interaction. The iodized salt has the finest particle size of all the salts used and is subject to sifting segregation with both garlic and pepper. However, there is also some angle of repose segregation between black pepper and garlic. The finer salt accumulates near the top of the pile while the garlic accumulates at the bottom of the pile. However, making the salt particle size larger (kosher salt) actually increases the segregation magnitude. Apparently the angle of repose segregation of the coarser particles creates more segregation than does sifting segregation.

There is another way of representing the segregation occurring in a bulk material that helps characterize the pattern of segregation (Figure 9 through 11). One can compute the cumulative concentration of various compounds in the mixture and normalize them by dividing by the average concentration of each component. This cumulative data can be plotted against the radial dimension. All cumulative concentration data would vary from 0 to 1 over the radial distance down the pile. A uniform material then yields a straight line between 0 and 1. Any deviation off of this line would indicate segregation. A positive deviation off of this line indicates accumulation near the top of the pile. A negative deviation off of this line indicates accumulation toward the bottom of the pile. The overall deviation from this line is a quantitative measure of segregation. Figures 9 through 11 suggest that the worst segregation occurs with the kosher salt. The least segregating salt is the sea salt. This reduces the overall segregation of all components.

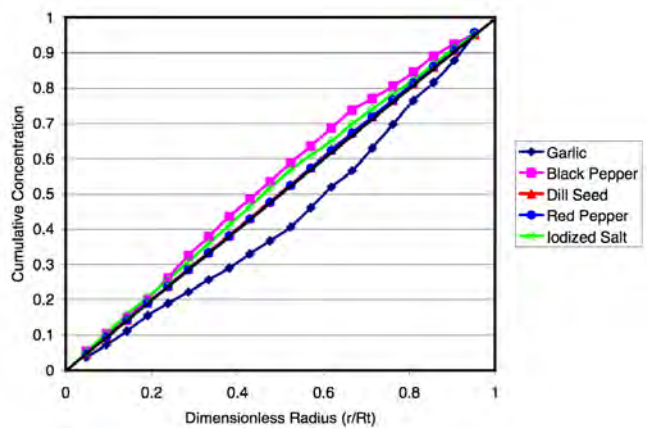


Figure 9. Cumulative steak seasoning distribution as a function of radial dimension for iodized salt

APPLICATION NOTE 017

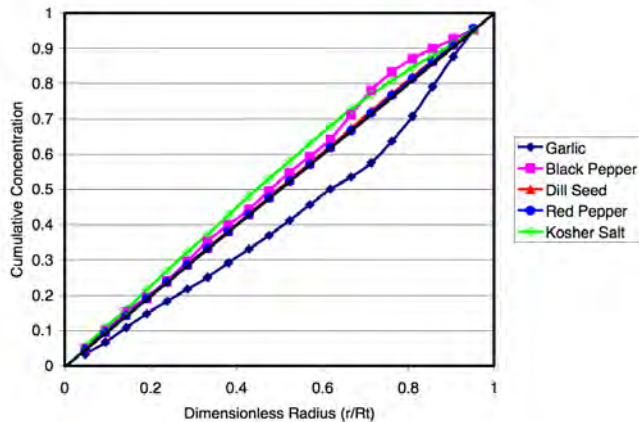


Figure 10. Cumulative steak seasoning distribution as a function of radial dimension for kosher salt

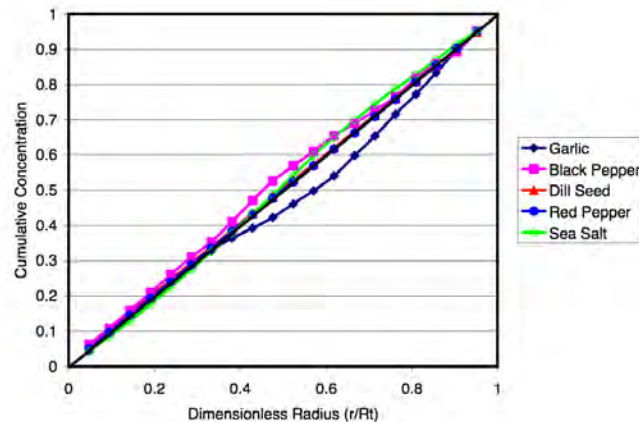


Figure 11. Cumulative steak seasoning distribution as a function of radial dimension for sea salt

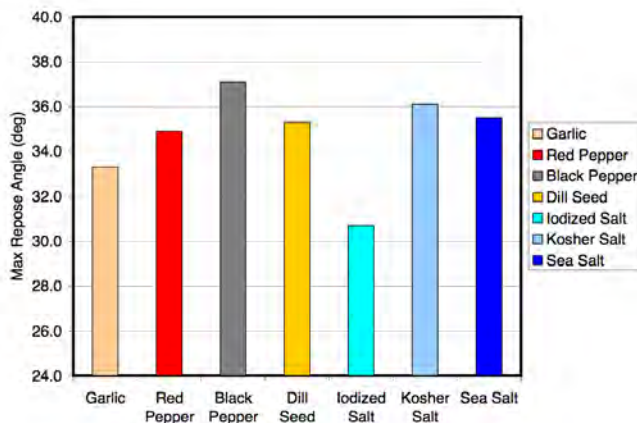


Figure 12. Angle of repose for steak seasoning components.

We also measured 6 repose angles for each of these materials and selected the maximum repose angle to be representative of the bulk material (see Figure 12). If repose angle were the only mechanism of segregation with this material then the materials should segregate in order of repose angle down the pile. The top of the pile should be rich in black pepper, followed by dill seed, then red pepper, garlic and finally iodized salt. However the reality is that the red pepper and dill seed do not segregate. This is likely due to the low percentage of these materials in the mix. There is not enough particulate material to effectively form a unique repose angle and the repose angle of these two ingredients are close to the median response angle. Thus, there is little driving force to cause these two materials to segregate. The black pepper has the largest repose angle and it always show a positive deviation from the cumulative concentration plots indicating that black pepper accumulates near the top of the pile. This is validated by the repose angle measurements. However, the repose angle data would suggest that the salt should accumulate at the bottom of the pile. In reality the segregation tests indicate that iodized salt accumulates at the top of the pile. This is due to the fact that the iodized salt has a finer particle size and will also sift down through the void of coarse particles depositing near the pile top. Thus, the angle of repose driving force and the sifting segregation driving force oppose each other decreasing the overall segregation of salt. However, Kosher salt has some fine particles that can promote sifting and the angle of repose of Kosher is close to that of black pepper. Thus both the angle of repose driving force and the sifting driving force promote salt accumulation at the top of the pile. This is validated by the results of the segregation tester which shows Kosher salt as the worst material to use for steak seasoning mixture. The sea salt repose angle is similar to the dill and red pepper angle and is a little smaller than the kosher salt repose angle. The particle size of the sea salt is larger than the kosher salt so both the angle of repose segregation driving force and the sifting segregation driving force decrease making the sea salt the optimal salt to use for steak seasoning.

It is obvious from the analysis above that this novel segregation tester plays an important role in product design. It can provide guidance in product selection when multiple segregation mechanisms are significant. It is important to point out that the optimal mixture still exhibits some segregation, but it is the best that can be done subject to the constraint of only changing one material. Further work could be done to optimize

APPLICATION NOTE 017

the segregation profile by changing other components. Each segregation test requires about 10 minutes to perform. Thus, in one to two hours an engineer can determine the optimal steak seasoning mixture, whereas previous methods have taken days or weeks to gather the necessary data. This segregation tester can reduce the time required to generate optimal product recommendations using lab scale batches. It is a powerful tool to understanding segregation of bulk materials.

Nomenclature

| | |
|----------------------|--|
| $F_{mix_j}(\lambda)$ | reflectance spectral intensity of the mixture in the tester as a function of wavelength |
| $F_i(\lambda)$ | reflective spectral intensity of the pure component as a function of wavelength |
| r | radial position from the top of the pile to the point of interest |
| R_t | radial dimension of the bottom of the pile |
| W_i | optical weighting factors for each particle based on all data measure on the pile |
| $x_{i,j}$ | fraction of the i^{th} pure component at the j^{th} position on the pile |
| λ | wavelength of light |

Conclusions

The new spectral method of measuring segregation presented above is a valuable tool for enhancing product design. This test method provides an easy way to measure the potential segregation behavior of prospective or current mixtures. The measured segregation tendencies can then be used to optimize the mixture by selecting the right components for combination. This should facilitate the production of new materials using lab scale quantities.

An important side note is that segregation of multi-component mixtures is often due to multiple segregation mechanisms. The tester can identify up to four prominent segregation mechanisms in addition to particle size and chemical composition. It also shows the influence of the segregation of one component on other components in the system. The segregation potentials of all components are inter-related, and changing one component often changes the segregation potential of all components in the system – usually in a complex way. Observing these details is possible since the tester measures many concentration points, providing valuable information and allowing the user to obtain more segregation features than traditional segregation testing will allow.

It is clear that this tester is valuable for successful product design. However, the fact that segregation magnitude is dependent on changes in one product, and that these differences can be measured, means that the tester can also be used to provide quality control information in the plant. A sample of material can be obtained from the plant and placed in the tester. This tester then measures the segregation of material and compares this with the segregation potential of an ideal mixture. Small changes in either the size or shape of single components will cause subtle differences in the measured segregation potential and segregation pattern. One of the keys to successful process control is the ability to directly measure the influence of key properties on critical bulk behavior. Wherever possible, direct measurements of critical process behavior should be used as the control variable. In other words, if product segregation is a key process behavior to control, then it is much more advantageous to measure segregation directly than measure wall friction angle and cohesion and infer segregation behavior. This tester allows direct measurement of product segregation.

References

1. Jerry Johanson, "Solids segregation: causes and solutions," Powder and Bulk Engineering, August 1988
2. J. M. Ottino, and D. V. Khakhar, "Fundamental research in heaping, mixing, and segregation of granular materials: challenges and perspectives," Powder Technology, Volume 121, Issues 2-3, 26 November 2001, Pages 117-122
3. Anjani K. Jha, and Virendra M. Puri, "Percolation segregation of binary mixtures under periodic movement," Powder Technology, Available online 7 May 2009, doi:10.1016/j.powtec.2009.04.013
4. Are Dyrøy, Morten Karlsen, Gisle G. Enstad, Sunil de Silva, "A system for the reduction of air current segregation in silos," Handbook of Powder Technology, Volume 10, 2001, Pages 623-630
5. Y. L. Ding, R. Forster, J. P. K. Seville, and D. J. Parker, "Segregation of granular flow in the transverse plane of a rolling mode rotating drum," International Journal of Multiphase Flow, Volume 28, Issue 4, April 2002, Pages 635-663
6. D. V. Khakhar, Ashish V. Orpe, J. M. Ottino, "Continuum model of mixing and size segregation in a rotating cylinder: concentration-flow coupling and streak formation," Powder Technology, Volume 116, Issues 2-3, 23 May 2001, Pages 232-245
7. Florence Cantelaube, Daniel Bideau, Stéphane Roux, "Kinetics of segregation of granular media in a two-dimensional rotating drum," Powder Technology, Volume 93, Issue 1, September 1997, Pages 1-11
8. S. Massol-Chaudeur, H. Berthiaux, , and J. Dodds, "The Development and Use of a Static Segregation Test to Evaluate the Robustness of Various Types of Powder Mixtures," Food and Bioproducts Processing, Volume 81, Issue 2, June 2003, Pages 106-118
9. D. McGlinchey, "Quantifying segregation in heaps: an experimental study," Powder Technology, Volume 145, Issue 2, 27 July 2004, Pages 106-112
10. William R. Ketterhagen, Jennifer S. Curtis, Carl R. Wassgren, and Bruno C. Hancock, "Modeling granular segregation in flow from quasi-three-dimensional, wedge-shaped hoppers," Powder Technology, Available online 3 July 2007, doi:10.1016/j.powtec.2007.06.023
11. Thomas Baxter, James Prescott, "Process Development, Optimization, and Scale-up: Powder Handling and Segregation Concerns," Developing Solid Oral Dosage Forms, 2009, Pages 637-665
12. Shu-San Hsiau, Jing-I Wang, "Segregation processes of a binary granular mixture in a shaker," Advanced Powder Technology, Volume 10, Issue 3, 1999, Pages 245-253
13. Y.R. He, H.S. Chen, Y.L. Ding, and B. Lickiss, "Solids Motion and Segregation of Binary Mixtures in a Rotating Drum Mixer," Chemical Engineering Research and Design, Volume 85, Issue 7, 2007, Pages 963-973
14. David Elya, Sai Chamarthy and M. Teresa Carvajal, "An investigation into low dose blend uniformity and segregation determination using NIR spectroscopy," Colloids and Surfaces A: Physicochemical and Engineering Aspects, Volume 288, Issues 1-3, 5 October 2006, Pages 71-76
15. Nicholas Christakis, Pierre Chapelle, Nadezhda Strusevich, Ian Bridled, John Baxter, Mayur K. Patel, Mark Cross, Ugur Tüzün, Alan R. Reed and Michael S.A. Bradley, "A hybrid numerical model for predicting segregation during core flow discharge," Advanced Powder Technology, Volume 17, Issue 6, 2006, Pages 641-662
16. Kunio Shinohara, and Boris Golman, "Particle segregation of binary mixture in a moving bed by penetration model," Chemical Engineering Science, Volume 57, Issue 2, January 2002, Pages 277-285
17. Sanjay Puri, Hisao Hayakawa, "Segregation of granular mixtures in a rotating drum," Physica A: Statistical Mechanics and its Applications, Volume 290, Issues 1-2, 1 February 2001, Pages 218-242
18. Guy Metcalfe, Mark Shattuck, "Pattern formation during mixing and segregation of flowing granular materials," Physica A: Statistical Mechanics and its Applications, Volume 233, Issues 3-4, 1 December 1996, Pages 709-717
19. Paul Meakin, Remi Jullien, "Simple models for two and three dimensional particle size segregation," Physica A: Statistical Mechanics and its Applications, Volume 180, Issues 1- 2, 1 January 1992, Pages 1-18
20. Kunio Shinohara, Boris Golman, Takahumi Nakata, "Size segregation of multicomponent particles during the filling of a hopper," Advanced Powder Technology, Volume 12, Issue 1, 2001, Pages 33-43
21. Kerry Johanson, Chris Eckert, Dev Ghose, Millorad Djomlija, and Mario Hubert, "Quantitative measurement of particle segregation mechanisms," Powder Technology, Volume 159, Issue 1, 2 November 2005, Pages 1-12
22. V. N. Dolgunin, A. A. Ukolov, "Segregation modeling of particle rapid gravity flow," Powder Technology, Volume 83, Issue 2, May 1995, Pages 95-103

Why is Understanding Segregation Mechanisms so Important?

By: Dr. Kerry Johanson Material Flow Solutions, Inc.

In process design, the solution to a segregation problem can be attacked from two angles. The process can be modified to accommodate segregation patterns caused by the various mechanisms or changes can be made to the process to reduce the cause of segregation. In either case, understanding segregation mechanisms is critical to developing robust processes to handle segregating materials.

Materials segregate when handled for a variety of reasons. Many solids flow practitioners quickly identify the potential for fine material to sift through the matrix of coarse particles as material slides down a pile. Indeed, sifting segregation is a predominant cause of separation during handling of differently sized particles. This mechanism usually results in a radial segregation pattern where fines accumulate near the center of a pile while the coarse material is predominately at the pile's edge (see Fig 1). However, severe sifting segregation can cause a top-to-bottom segregation pattern where the fines are beneath the coarse particles. This is especially true if inter-particle motion is induced within the material by some external means such as vibration. Typically, particle size differences greater than three to one are enough to produce significant sifting segregation problems.

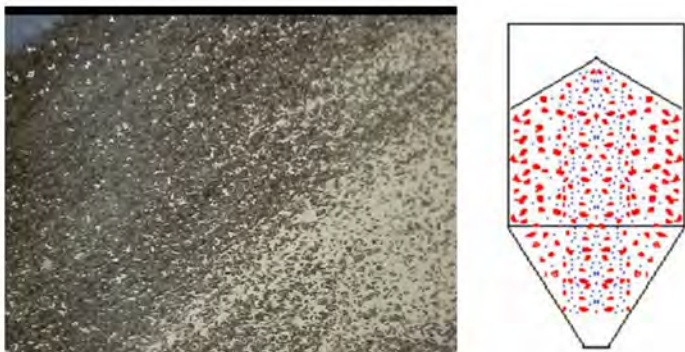


Fig 1. Typical sifting segregation profile on pile

Sifting segregation is by no means the only mechanism to cause separation of particulate material during handling. Some particles have differences in inter-particle friction and thus form piles with different repose angles. Formation of piles

within process equipment causes the less frictional particle to slide further down the pile accumulation at the pile's edge. This mechanism results in a radial segregation pattern. Materials with an angle of repose difference of more than 2 degrees can show significant repose angle segregation. The figure below illustrates segregation of fine and coarse fractions of roofing granules due to angle of repose. In this case, the particle size difference between the fines and coarse is only about 30% so sifting is not possible. The repose angles are only 2 degrees different and are the cause of significant segregation.

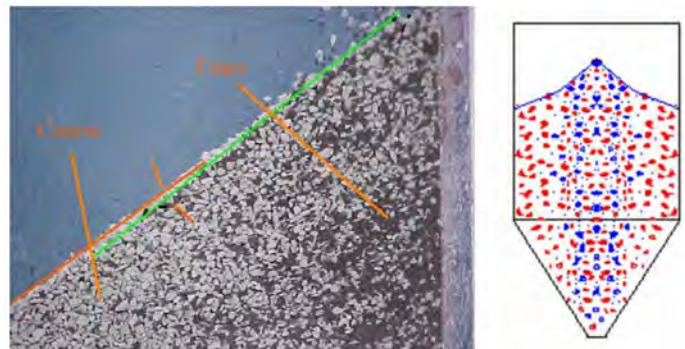


Fig 2. Typical repose angle segregation

Air currents caused during filling may carry fine material to regions where the air currents decrease sufficiently to deposit the fine material. This air entrainment segregation can produce a radial pattern or a side to side pattern depending on the position of the inlet and the geometry of the vessel. Generally, fines accumulate near process vessel walls with this segregation. Figure 3 shows a typical profile for air entrainment segregation where the fines accumulate near the wall. However, it is important to point out that this figure also shows the result of sifting segregation where the fines accumulate near the drop point. Figure 3 also indicates that several segregation mechanisms can occur at the same time producing a complex overall segregation pattern. If the bulk material is very fine and compressible, then it may become fluidized during filling of a process vessel. This fluidization is not persistent as it would be in a fluid bed where there is an external source of air. The material begins to lose its entrained air

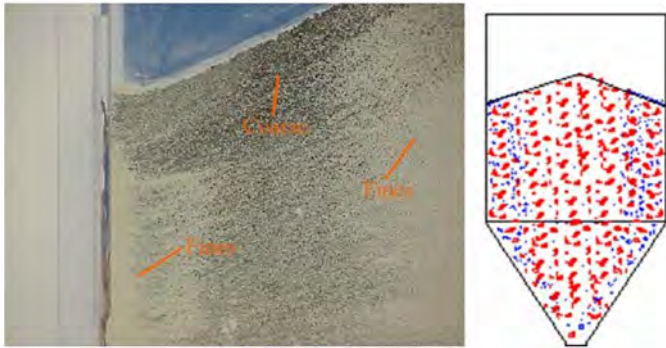


Fig 3. Typical air entrainment segregation

soon after completion of the filling process. However, these materials retain their fluid-like behavior for several minutes or even hours. Coarse particles entering the bin during this time can impact on this fluidized material and penetrate the top layer of fluidized solid before coming to rest below the top surface. This results in a top-to-bottom separation of particles in the bulk mixture, thereby creating layers of fines and coarse (see Fig 4).



Fig 4. Typical impact fluidization segregation

Many solid flow practitioners promote the concept that mass flow will always solve a segregation problem. This is a short-sited view. The flow pattern within a given piece of process equipment must be matched with the segregation profile to achieve a process that will minimize segregation during handling. For example, suppose that the material segregated by impact fluidization forming layers when placed in a bin or a hopper. Placing a typical step mass flow hopper on this bin would not help the segregation, but would significantly enhance the separation of bulk materials. The uniform velocity induced by a typical well designed

mass flow bin would cause the coarse to exit, followed by the fines, making the segregation problem worse.

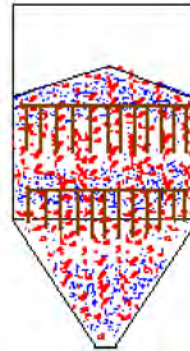


Fig 5. Mass flow velocity profile with impact fluidization segregation profile

Uniform Velocity

Leads to More Segregation during discharge

Conversely, a radial segregation pattern will be helped by converting the bin to mass flow. Material will leave the bin as it entered the hopper. There will be a segregation profile across the outlet, but at least the material at each cross-section will be the correct consistence. If better mixing than this is required, additional in-line blenders should be added to the process to achieve blend consistency.

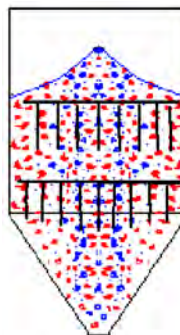


Fig 6. Mass flow profile with radial segregation pattern

Uniform Velocity

Leads to Less Segregation during discharge

In conclusion, knowing the segregation mechanism as well as the flow profiles in your process equipment is critical to solving potential segregation problems. Simple tests can be performed to measure the magnitude and type of segregation occurring in your systems. Flow properties can also be measured to determine the flow patterns in your process equipment. Using this information, a reliable solution to complex segregation problems can be designed to put you back on track for quality production.

Segregation Properties of Heart Healthy Medication

1.0 Segregation – An Introduction

There are two uses for segregation data. Engineers may use segregation data to optimize product design, creating a product with minimal segregation tendency. Engineers may also wish to modify the processing to minimize the effect of segregation in their plant packaging process or handling facility. In either case, the segregation pattern, segregation mechanism, and magnitude of segregation are key parameters required for process or product design.

Segregation occurs through several mechanisms. Identification of the primary segregation cause and the segregation pattern produced through handling is critical to prevent de-mixing of the final detergent mixture during handling and packaging. Any property difference between materials can cause separation of critical material components. However, there are five common causes of segregation problems in typical handling systems.

Sifting:

Fines may sift through a matrix of coarse particles during handling. This mechanism requires that the void space between adjacent particles be large enough to permit fine particle to pass through. Generally, this requires a particle size difference of about 3:1. Inter-particle motion is also required to provide a means of exposing empty void spaces to fine particles. The fines must also be free flowing enough to prevent arching between adjacent particles and the void spaces must be empty enough to accept fine particles. In general, this type of segregation produces a radial pattern as material forms a pile in process equipment. The fines accumulate near the pile charge point and decrease in concentration toward the edge of the pile.

Angle of repose differences:

Two materials may have different angles of repose. Thus, when these two materials flow down a pile they essentially create overlapping piles where the material with the steepest

repose angle accumulates near the top of the pile while the material with the flattest repose angle accumulates near the pile edge. Generally, there is a distribution of these two materials along the pile's surface. Repose angle differences of about 2 degrees can result in significant segregation. Material of different particle sizes can possess sufficient difference in repose angles to cause this type of segregation. However, particle size difference is not a prerequisite angle of repose segregation and materials of the same size can separate via this mechanism. In addition, your process must also generate piles during handling or processing to cause this type of segregation.

Air entrainment:

The mixture may contain fines that are small enough to be carried by air currents in the handling system. These fines drop out of the air stream when gas velocities decrease below the entrainment velocity. This causes separation of fines and coarse in handling systems. The fines generally deposit near the container walls. This type of segregation requires a source of air currents in process equipment. This source of air can come from free fall of a compressible material. When the falling stream impacts the material level, the entrained air is pushed out of the interstitial pores and carries the fine particles in the resulting dust cloud. This segregation typically causes a radial pattern during pile formation, but the fines are at the bottom of the pile and not the top.

Impact fluidization:

If the mixture is fine enough, then air trapped in the interstitial voids can cause material to fluidize. As a large particle drops into this fluidized layer, momentum causes the large particles to penetrate this fluid layer, resulting in a top-to-bottom segregation of fine and coarse particles. This mechanism requires a source of air and the ability of the bulk material to hang onto entrained air for a moderate amount of time.

Percolation:

A fluidized layer of material can lose its entrained air as it sits stationary in a container that was just filled. Percolation forces air up through the bulk material. Generally, this process forms fissures in the bulk material where the gas escapes. The local velocity in these fissures is relatively high and can entrain fine particles in the process, causing top-to-bottom segregation. This results in the size separation of fluidizable material with wide particle size distributions.

It is critical to identify the cause of segregation to avoid processing that will induce the problem. It is also necessary to know the pattern of segregation in order to provide a means of re-mixing material, if required. Understanding the segregation mechanism will also help in determining what must be done to the material to create a product that is less likely to segregate.

2.0 Segregation Testing Results - Background

In the past researchers have fed bulk materials onto a pile, sectioned a conical pile into annular sections, and performed chemical or size analysis on the material collected in each annular section. This is a long and tedious method which results in only a very few measurements collected along the pile. Plant personnel often use thieves to sample piles in process equipment. This method also yields only a few measurements along the pile and disturbs the surface, thereby changing the segregation pattern. Other researchers measure the segregation pattern by placing material in a funnel flow hopper and then discharging the hopper, collecting the output stream and measuring the quality of the mixture by chemical composition or particle size. This method convolutes the segregation with the flow pattern from a particular hopper or bin. Unless the bin design in the tester is precisely the same as the bin design in the process, there is no guarantee that the composition during discharge from the tester will be similar to that found in the actual process. In addition, the cohesive properties of the bulk material can impede flow from the segregation tester hopper, even though hang-ups may not occur in the process with the same material.

One problem with current segregation testers is that they do not relate well to the process. Any two or three materials can segregate if there is a difference in properties and the mixture is subject to enough external stimuli. For example adding enough fluidization gas will separate materials of different densities, even though these extreme conditions

may never occur in the actual process. The real question to be answered is: will the mixture segregate when exposed to a feed behavior similar to that present in the process? Therefore, any measurement of segregation tendency should have three key elements. First, the feed should be controlled so as to allow the measured segregation to be scalable to process conditions. Second, the pattern of the segregation should be included as part of the measurement in order to predict the expected concentration leaving process equipment. Finally, the magnitude of the segregation should be quantified to provide guidance in determining if the mechanism is actually a potential problem in the process. Ideally we would like the concentrations based on chemical components in the mixture.

2.1 Relation of Test Results to Process

Let's identify the key attribute that must be controlled or measured to make segregation measurements scalable to process conditions. For simplicity, we will assume that material simply falls from a mechanical conveyor into the process vessel. Material entering the process typically free-falls from some fall height at some process velocity. It is important to note that, in this case, the dynamic effects caused by particle rebound or sliding down the pile scale linearly with the geometry of the process equipment (Figure 1). The same cannot be said of the case where gas is carried with the input stream. However, similar models can be created for this case and a scale law developed. For the purpose of this report, and because the segregation data is for simple comparison, we will assume little or no gas effects during the filling of a typical pharmaceutical process. The small scale segregation tester can then be run at a constant drop rate and fall height. We deposited material in a slice model, forming half a pile, at a rate of about 1 lit/min. The free fall dimension was set to be 0.57 times the diameter or width of the receiving bin. It is important to note that the full diameter of the receive bin in the process would correspond to twice the width of the slice mode bin in the tester since the slice model was filled on one side. For a typical 1.5-meter wide bin this would correspond to a drop of about 0.85 meters.

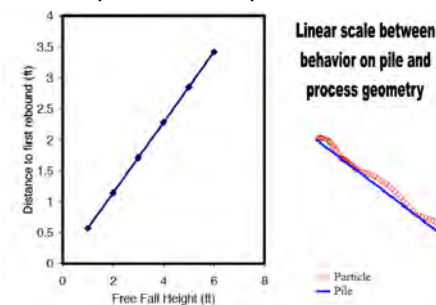


Figure 1. Typical rebound of free fall particles down pile surface

2.2 Segregation Pattern

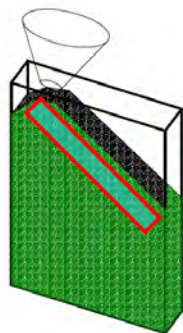
The pattern of segregation requires that segregation be measured by analyzing spatial concentration data. This spatial analysis always has a sample size or view port associated with it. It must be decided beforehand what volume of material represents a reasonable segregation basis. The view port must contain enough particles to be statistically relevant. If that volume occupies only one or two particles, then any segregation measurements are doomed to failure since the segregation measurement volume cannot represent an average sample. If that sample volume is the same as the bin size, then every segregation measurement will represent the global average concentration placed in the process vessel. The proper segregation volume should be chosen somewhere in between.

Obviously, these spatial segregation measurements require access to some spatial view of the material after it has segregated due to initial process filling. One way to gain access to the cross section of a pile is to fill a slice model with material and observe the segregation pattern through the side of the slice model using optical techniques (Figure 2).

Figure 2. Schematic of segregation tester

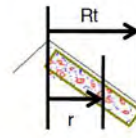
Dump material into box and observe the change in color intensity along the pile as measured just below the top surface of the pile (rectangle section).

These changes in color intensity are an indication of differences in either chemical composition or in particle size and can be used to estimate the segregation of key components in the system.



Observation of segregation through the sides of a slice model will be biased to the optical pattern that exists at the wall of the segregation tester. Therefore, care must be taken when loading the tester to assure a representative sample is visible through the side of the tester. Filling the tester across the width of the slice model will distribute the material to the tester wall, creating a uniform material across the tester. Limiting the thickness of the slice model will also help with the distribution of representative material to the tester wall. However, one should be aware that extremely thin slice models are subject to banding due to wall effects that would not be present in wider slice models. For typical materials, this limits the slice model to a minimum of approximately 25 mm thick.

Reflectance spectroscopic methods can be employed to measure subtle differences in color. Since we are dealing with a discrete particle system, multiple measurements are required to determine the average concentration within a given viewport. Segregation measurement is also a scale issue. The size of the chosen viewport should be large enough to contain a representative number of particles, yet small enough that differences in local compositions are not lost in the averaging scheme (Figure 3). We defined the tester view port area as 1.27 cm square and averaged 36 sample readings within the view port area. We moved the viewport to collect data at about 30 points along the length of the pile at a position that was about 1.27 cm below the top surface of the pile as indicated in the schematic in Figure 2.



Define the size of the view port and measure the spectra along the top of the pile. Adjacent viewports can overlap and tester can measure concentration at up to 50 locations along pile.



Figure 3. Measurement zone along pile top surface

If the spectra of the pure components are known, and the spectra of the mixture in different, view port boxes along the pile are known then pure component spectra can be used to compute the concentration of the components along the length of the pile. One drawback of this technique is that good data requires many spectral measurements collected at multiple points along the pile. Manually collecting this data is tedious and time consuming. Therefore, an automatic instrument was constructed to control the feed, obtain the pure component spectra, and measure spatial concentration profiles for spectral measurements (Figure 4).



Figure 4. SPECTester used in Segregation Analysis

2.3 Results of SPECTester Analysis

The segregation pattern and data is given in Figures 5 through 7. The concentrations are plotted as a function of dimensionless radius. A radius of 0 is the top of the pile and a radius of 1.0 is the bottom of the pile. This profile shows moderate segregation of the API and significant segregation of active B and inert C ingredients, as indicated by the segregation intensity (Figure 7). In the same Figure, active A and inert A ingredients show moderate segregation. Active A, active B, and inert C ingredients tend to accumulate at the top of the pile, while the inert A ingredient accumulates at the bottom of the pile (Figure 5). API tends to accumulate at the top of the pile and near the bottom of the pile. Measurements indicate that active B and inert C ingredients are the worst acting for segregation. Additionally, the API exhibits sufficient segregation tendency to be a real problem in production. This type of profile is indicative of angle of repose segregation. However, API may be segregating due to two mechanisms. Some of these inert ingredients that show significant segregation do not need to be well mixed with the mixture to maintain a good product. However, the API segregation is large enough that dry formation processes will need to be monitored carefully to ensure good (uniform) product formation. This mixture must be placed in a well designed handling system to assure that it remains mixed after the blending step before it is tableted.

Sometimes the segregation trend is easier to see if viewed from a cumulative concentration point of view. We can sum, or integrate, the fraction of any component along the pile and normalize it relative to the actual average concentration of that component along the pile (Figure 6). If there is no segregation, then this procedure would show a straight line passing through the point (0,0) and (1,1) when plotted against dimensionless radius. A positive deviation off this line indicates accumulation near the top of the pile. A negative deviation off this line indicates accumulation toward the bottom of the pile. An s-shaped curve indicated accumulation at both top and bottom. The magnitude of the deviation off this line indicates the percent deviation from the mean concentration for any one component. The reason for plotting segregation in this manner is to relate the segregation profile to the deviation from the mean or average concentration. These plot provide a quick way to view how bad the segregation is from a mean concentration point of view while giving you a feel of the type of segregation occurring.

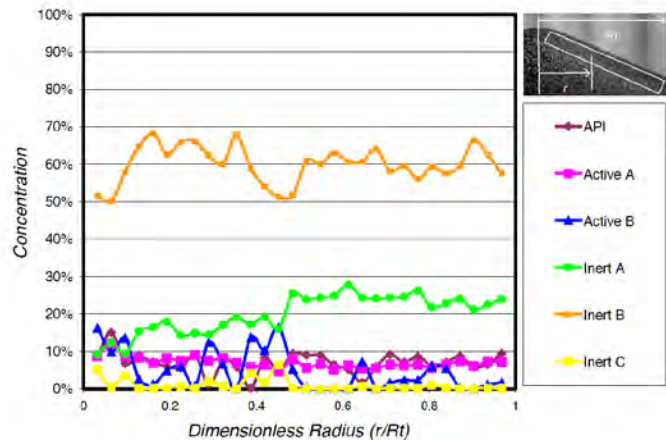


Figure 5. Radial segregation profile for Heart Healthy Medication

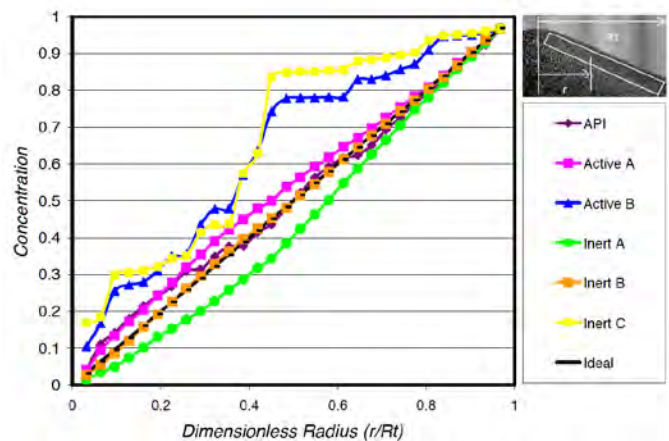


Figure 6. Cumulative radial segregation profile for Heart Healthy Medication

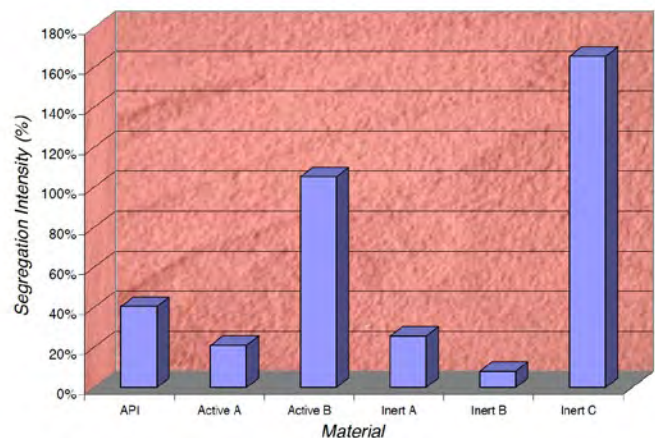


Figure 7. Segregation Intensity for Heart Healthy Medication

Segregation Properties of Household Powdered Cleanser

1.0 Segregation – An Introduction

There are two uses for segregation data. Engineers may use segregation data to optimize product design, creating a product with minimal segregation tendency. Engineers may also wish to modify the processing to minimize the effect of segregation in their plant packaging process or handling facility. In either case, the segregation pattern, segregation mechanism, and magnitude of segregation are key parameters required for process or product design.

Segregation occurs through several mechanisms. Identification of the primary segregation cause and the segregation pattern produced through handling is critical to prevent de-mixing of the final detergent mixture during handling and packaging. Any property difference between materials can cause separation of critical material components. However, there are five common causes of segregation problems in typical handling systems.

Sifting:

Fines may sift through a matrix of coarse particles during handling. This mechanism requires that the void space between adjacent particles be large enough to permit fine particle to pass through. Generally, this requires a particle size difference of about 3:1. Inter-particle motion is also required to provide a means of exposing empty void spaces to fine particles. The fines must also be free flowing enough to prevent arching between adjacent particles and the void spaces must be empty enough to accept fine particles. In general, this type of segregation produces a radial pattern as material forms a pile in process equipment. The fines accumulate near the pile charge point and decrease in concentration toward the edge of the pile.

Angle of repose differences:

Two materials may have different angles of repose. Thus, when these two materials flow down a pile they essentially

create overlapping piles where the material with the steepest repose angle accumulates near the top of the pile while the material with the flattest repose angle accumulates near the pile edge. Generally, there is a distribution of these two materials along the pile's surface. Repose angle differences of about 2 degrees can result in significant segregation. Material of different particle sizes can possess sufficient difference in repose angles to cause this type of segregation. However, particle size difference is not a prerequisite angle of repose segregation and materials of the same size can separate via this mechanism. In addition, your process must also generate piles during handling or processing to cause this type of segregation.

Air entrainment:

The mixture may contain fines that are small enough to be carried by air currents in the handling system. These fines drop out of the air stream when gas velocities decrease below the entrainment velocity. This causes separation of fines and coarse in handling systems. The fines generally deposit near the container walls. This type of segregation requires a source of air currents in process equipment. This source of air can come from free fall of a compressible material. When the falling stream impacts the material level, the entrained air is pushed out of the interstitial pores and carries the fine particles in the resulting dust cloud. This segregation typically causes a radial pattern during pile formation, but the fines are at the bottom of the pile and not the top.

Impact fluidization:

If the mixture is fine enough, then air trapped in the interstitial voids can cause material to fluidize. As a large particle drops into this fluidized layer, momentum causes the large particles to penetrate this fluid layer, resulting in a top-to-bottom segregation of fine and coarse particles. This mechanism requires a source of air and the ability of the bulk material to hang onto entrained air for a moderate amount of time.

Percolation:

A fluidized layer of material can lose its entrained air as it sits stationary in a container that was just filled. Percolation forces air up through the bulk material. Generally, this process forms fissures in the bulk material where the gas escapes. The local velocity in these fissures is relatively high and can entrain fine particles in the process, causing top-to-bottom segregation. This results in the size separation of fluidizable material with wide particle size distributions.

It is critical to identify the cause of segregation to avoid processing that will induce the problem. It is also necessary to know the pattern of segregation in order to provide a means of re-mixing material, if required. Understanding the segregation mechanism will also help in determining what must be done to the material to create a product that is less likely to segregate.

2.0 Segregation Testing Results - Background

In the past researchers have fed bulk materials onto a pile, sectioned a conical pile into annular sections, and performed chemical or size analysis on the material collected in each annular section. This is a long and tedious method which results in only a very few measurements collected along the pile. Plant personnel often use thieves to sample piles in process equipment. This method also yields only a few measurements along the pile and disturbs the surface, thereby changing the segregation pattern. Other researchers measure the segregation pattern by placing material in a funnel flow hopper and then discharging the hopper, collecting the output stream and measuring the quality of the mixture by chemical composition or particle size. This method convolutes the segregation with the flow pattern from a particular hopper or bin. Unless the bin design in the tester is precisely the same as the bin design in the process, there is no guarantee that the composition during discharge from the tester will be similar to that found in the actual process. In addition, the cohesive properties of the bulk material can impede flow from the segregation tester hopper, even though hang-ups may not occur in the process with the same material.

One problem with current segregation testers is that they do not relate well to the process. Any two or three materials can segregate if there is a difference in properties and the mixture is subject to enough external stimuli. For example adding enough fluidization gas will separate materials of different densities, even though these extreme conditions

may never occur in the actual process. The real question to be answered is: will the mixture segregate when exposed to a feed behavior similar to that present in the process? Therefore, any measurement of segregation tendency should have three key elements. First, the feed should be controlled so as to allow the measured segregation to be scalable to process conditions. Second, the pattern of the segregation should be included as part of the measurement in order to predict the expected concentration leaving process equipment. Finally, the magnitude of the segregation should be quantified to provide guidance in determining if the mechanism is actually a potential problem in the process. Ideally we would like the concentrations based on chemical components in the mixture.

2.1 Relation of Test Results to Process

Let's identify the key attribute that must be controlled or measured to make segregation measurements scalable to process conditions. For simplicity, we will assume that material simply falls from a mechanical conveyor into the process vessel. Material entering the process typically free-falls from some fall height at some process velocity. It is important to note that, in this case, the dynamic effects caused by particle rebound or sliding down the pile scale linearly with the geometry of the process equipment (Figure 1). The same cannot be said of the case where gas is carried with the input stream. However, similar models can be created for this case and a scale law developed. For the purpose of this report, and because the segregation data is for simple comparison, we will assume little or no gas effects during the filling of a typical pharmaceutical process. The small scale segregation tester can then be run at a constant drop rate and fall height. We deposited material in a slice model, forming half a pile, at a rate of about 1 lit/min. The free fall dimension was set to be 0.57 times the diameter or width of the receiving bin. It is important to note that the full diameter of the receive bin in the process would correspond to twice the width of the slice mode bin in the tester since the slice model was filled on one side. For a typical 1.5-meter wide bin this would correspond to a drop of about 0.85 meters.

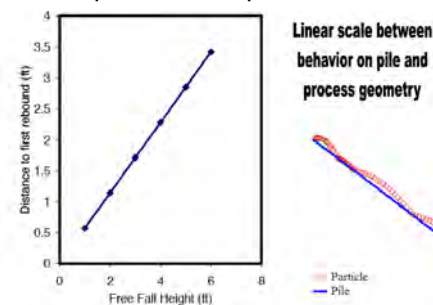


Figure 1. Typical rebound of free fall particles down pile surface

2.2 Segregation Pattern

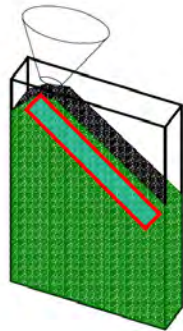
The pattern of segregation requires that segregation be measured by analyzing spatial concentration data. This spatial analysis always has a sample size or view port associated with it. It must be decided beforehand what volume of material represents a reasonable segregation basis. The view port must contain enough particles to be statistically relevant. If that volume occupies only one or two particles, then any segregation measurements are doomed to failure since the segregation measurement volume cannot represent an average sample. If that sample volume is the same as the bin size, then every segregation measurement will represent the global average concentration placed in the process vessel. The proper segregation volume should be chosen somewhere in between.

Obviously, these spatial segregation measurements require access to some spatial view of the material after it has segregated due to initial process filling. One way to gain access to the cross section of a pile is to fill a slice model with material and observe the segregation pattern through the side of the slice model using optical techniques (Figure 2).

Figure 2. Schematic of segregation tester

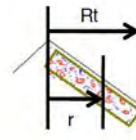
Dump material into box and observe the change in color intensity along the pile as measured just below the top surface of the pile (rectangle section).

These changes in color intensity are an indication of differences in either chemical composition or in particle size and can be used to estimate the segregation of key components in the system.



Observation of segregation through the sides of a slice model will be biased to the optical pattern that exists at the wall of the segregation tester. Therefore, care must be taken when loading the tester to assure a representative sample is visible through the side of the tester. Filling the tester across the width of the slice model will distribute the material to the tester wall, creating a uniform material across the tester. Limiting the thickness of the slice model will also help with the distribution of representative material to the tester wall. However, one should be aware that extremely thin slice models are subject to banding due to wall effects that would not be present in wider slice models. For typical materials, this limits the slice model to a minimum of approximately 25 mm thick.

Reflectance spectroscopic methods can be employed to measure subtle differences in color. Since we are dealing with a discrete particle system, multiple measurements are required to determine the average concentration within a given viewport. Segregation measurement is also a scale issue. The size of the chosen viewport should be large enough to contain a representative number of particles, yet small enough that differences in local compositions are not lost in the averaging scheme (Figure 3). We defined the tester view port area as 1.27 cm square and averaged 36 sample readings within the view port area. We moved the viewport to collect data at about 30 points along the length of the pile at a position that was about 1.27 cm below the top surface of the pile as indicated in the schematic in Figure 2.



Define the size of the view port and measure the spectra along the top of the pile. Adjacent viewports can overlap and tester can measure concentration at up to 50 locations along pile.



Figure 3. Measurement zone along pile top surface

If the spectra of the pure components are known, and the spectra of the mixture in different, view port boxes along the pile are known then pure component spectra can be used to compute the concentration of the components along the length of the pile. One drawback of this technique is that good data requires many spectral measurements collected at multiple points along the pile. Manually collecting this data is tedious and time consuming. Therefore, an automatic instrument was constructed to control the feed, obtain the pure component spectra, and measure spatial concentration profiles for spectral measurements (Figure 4).



Figure 4. SPECTester used in Segregation Analysis

2.3 Results of SPECTester Analysis

The segregation pattern and data is given in Figures 5 through 7. The concentrations are plotted as a function of dimensionless radius. A radius of 0 is the top of the pile and a radius of 1.0 is the bottom of the pile. This profile shows significant segregation of surfactant, as indicated by the segregation intensity (Figure 7). Further, surfactant tends to segregate heavily toward the bottom of the pile (Figure 5). It is interesting to note that the main active ingredient does not show much propensity to segregate. However, the surfactant shows a major propensity to segregate. The segregation pattern suggests that both angle of repose and sifting are potential causes of particle segregation with this mixture. The main active ingredient may be filling the voids between the other particles in the mixture, forming a well graded blend that is insensitive to segregation. Conversely, the surfactant shows a large propensity to accumulate at the bottom of the pile. This is an example of complex segregation patterns when dealing with mixtures of more than two ingredients. Inert A material is interacting mostly with the surfactant to induce segregation, but this sub-mixture (the combination of inert A and surfactant) does not show much segregation potential with the main active ingredient. Thus, a formulator would only need to optimize the segregation with the sub-mixture to reduce the overall segregation of this mix.

Sometimes the segregation trend is easier to see if viewed from a cumulative concentration point of view. We can sum, or integrate, the fraction of any component along the pile and normalize it relative to the actual average concentration of that component along the pile (Figure 6). If there is no segregation, then this procedure would show a straight line passing through the point (0,0) and (1,1) when plotted against dimensionless radius. A positive deviation off this line indicates accumulation near the top of the pile. A negative deviation off this line indicates accumulation toward the bottom of the pile. An s-shaped curve indicated accumulation at both top and bottom. The magnitude of the deviation off this line indicates the percent deviation from the mean concentration for any one component. The reason for plotting segregation in this manner is to relate the segregation profile to the deviation from the mean or average concentration. These plot provide a quick way to view how bad the segregation is from a mean concentration point of view while giving you a feel of the type of segregation occurring.

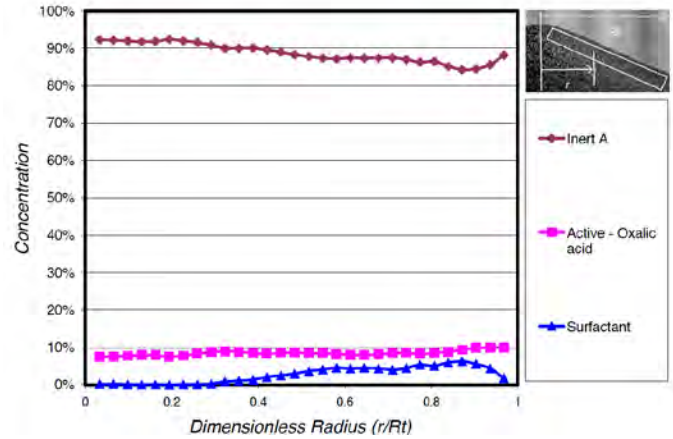


Figure 5. Radial segregation profile for Household Powdered Cleanser

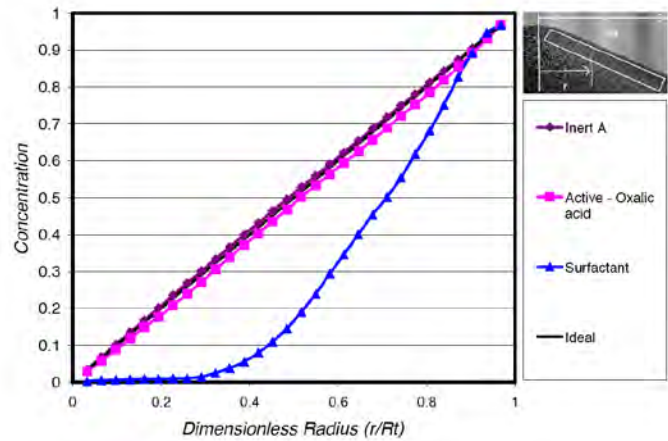


Figure 6. Cumulative radial segregation profile for Household Powdered Cleanser

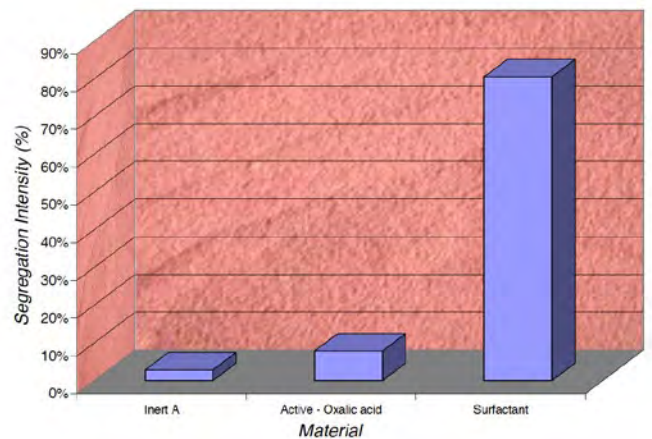


Figure 7. Segregation Intensity for Household Powdered Cleanser

Segregation Properties of Laundry Detergent with Brightener

1.0 Segregation – An Introduction

There are two uses for segregation data. Engineers may use segregation data to optimize product design, creating a product with minimal segregation tendency. Engineers may also wish to modify the processing to minimize the effect of segregation in their plant packaging process or handling facility. In either case, the segregation pattern, segregation mechanism, and magnitude of segregation are key parameters required for process or product design.

Segregation occurs through several mechanisms. Identification of the primary segregation cause and the segregation pattern produced through handling is critical to prevent de-mixing of the final detergent mixture during handling and packaging. Any property difference between materials can cause separation of critical material components. However, there are five common causes of segregation problems in typical handling systems.

Sifting:

Fines may sift through a matrix of coarse particles during handling. This mechanism requires that the void space between adjacent particles be large enough to permit fine particle to pass through. Generally, this requires a particle size difference of about 3:1. Inter-particle motion is also required to provide a means of exposing empty void spaces to fine particles. The fines must also be free flowing enough to prevent arching between adjacent particles and the void spaces must be empty enough to accept fine particles. In general, this type of segregation produces a radial pattern as material forms a pile in process equipment. The fines accumulate near the pile charge point and decrease in concentration toward the edge of the pile.

Angle of repose differences:

Two materials may have different angles of repose. Thus, when these two materials flow down a pile they essentially

create overlapping piles where the material with the steepest repose angle accumulates near the top of the pile while the material with the flattest repose angle accumulates near the pile edge. Generally, there is a distribution of these two materials along the pile's surface. Repose angle differences of about 2 degrees can result in significant segregation. Material of different particle sizes can possess sufficient difference in repose angles to cause this type of segregation. However, particle size difference is not a prerequisite angle of repose segregation and materials of the same size can separate via this mechanism. In addition, your process must also generate piles during handling or processing to cause this type of segregation.

Air entrainment:

The mixture may contain fines that are small enough to be carried by air currents in the handling system. These fines drop out of the air stream when gas velocities decrease below the entrainment velocity. This causes separation of fines and coarse in handling systems. The fines generally deposit near the container walls. This type of segregation requires a source of air currents in process equipment. This source of air can come from free fall of a compressible material. When the falling stream impacts the material level, the entrained air is pushed out of the interstitial pores and carries the fine particles in the resulting dust cloud. This segregation typically causes a radial pattern during pile formation, but the fines are at the bottom of the pile and not the top.

Impact fluidization:

If the mixture is fine enough, then air trapped in the interstitial voids can cause material to fluidize. As a large particle drops into this fluidized layer, momentum causes the large particles to penetrate this fluid layer, resulting in a top-to-bottom segregation of fine and coarse particles. This mechanism requires a source of air and the ability of the bulk material to hang onto entrained air for a moderate amount of time.

Percolation:

A fluidized layer of material can lose its entrained air as it sits stationary in a container that was just filled. Percolation forces air up through the bulk material. Generally, this process forms fissures in the bulk material where the gas escapes. The local velocity in these fissures is relatively high and can entrain fine particles in the process, causing top-to-bottom segregation. This results in the size separation of fluidizable material with wide particle size distributions.

It is critical to identify the cause of segregation to avoid processing that will induce the problem. It is also necessary to know the pattern of segregation in order to provide a means of re-mixing material, if required. Understanding the segregation mechanism will also help in determining what must be done to the material to create a product that is less likely to segregate.

2.0 Segregation Testing Results - Background

In the past researchers have fed bulk materials onto a pile, sectioned a conical pile into annular sections, and performed chemical or size analysis on the material collected in each annular section. This is a long and tedious method which results in only a very few measurements collected along the pile. Plant personnel often use thieves to sample piles in process equipment. This method also yields only a few measurements along the pile and disturbs the surface, thereby changing the segregation pattern. Other researchers measure the segregation pattern by placing material in a funnel flow hopper and then discharging the hopper, collecting the output stream and measuring the quality of the mixture by chemical composition or particle size. This method convolutes the segregation with the flow pattern from a particular hopper or bin. Unless the bin design in the tester is precisely the same as the bin design in the process, there is no guarantee that the composition during discharge from the tester will be similar to that found in the actual process. In addition, the cohesive properties of the bulk material can impede flow from the segregation tester hopper, even though hang-ups may not occur in the process with the same material.

One problem with current segregation testers is that they do not relate well to the process. Any two or three materials can segregate if there is a difference in properties and the mixture is subject to enough external stimuli. For example adding enough fluidization gas will separate materials of different densities, even though these extreme conditions

may never occur in the actual process. The real question to be answered is: will the mixture segregate when exposed to a feed behavior similar to that present in the process? Therefore, any measurement of segregation tendency should have three key elements. First, the feed should be controlled so as to allow the measured segregation to be scalable to process conditions. Second, the pattern of the segregation should be included as part of the measurement in order to predict the expected concentration leaving process equipment. Finally, the magnitude of the segregation should be quantified to provide guidance in determining if the mechanism is actually a potential problem in the process. Ideally we would like the concentrations based on chemical components in the mixture.

2.1 Relation of Test Results to Process

Let's identify the key attribute that must be controlled or measured to make segregation measurements scalable to process conditions. For simplicity, we will assume that material simply falls from a mechanical conveyor into the process vessel. Material entering the process typically free-falls from some fall height at some process velocity. It is important to note that, in this case, the dynamic effects caused by particle rebound or sliding down the pile scale linearly with the geometry of the process equipment (Figure 1). The same cannot be said of the case where gas is carried with the input stream. However, similar models can be created for this case and a scale law developed. For the purpose of this report, and because the segregation data is for simple comparison, we will assume little or no gas effects during the filling of a typical pharmaceutical process. The small scale segregation tester can then be run at a constant drop rate and fall height. We deposited material in a slice model, forming half a pile, at a rate of about 1 lit/min. The free fall dimension was set to be 0.57 times the diameter or width of the receiving bin. It is important to note that the full diameter of the receive bin in the process would correspond to twice the width of the slice mode bin in the tester since the slice model was filled on one side. For a typical 1.5-meter wide bin this would correspond to a drop of about 0.85 meters.

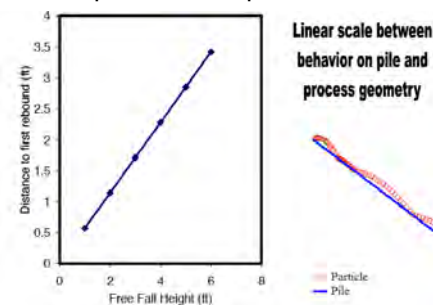


Figure 1. Typical rebound of free fall particles down pile surface

2.2 Segregation Pattern

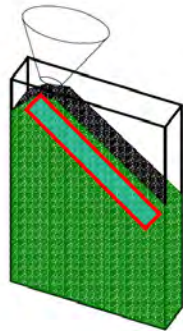
The pattern of segregation requires that segregation be measured by analyzing spatial concentration data. This spatial analysis always has a sample size or view port associated with it. It must be decided beforehand what volume of material represents a reasonable segregation basis. The view port must contain enough particles to be statistically relevant. If that volume occupies only one or two particles, then any segregation measurements are doomed to failure since the segregation measurement volume cannot represent an average sample. If that sample volume is the same as the bin size, then every segregation measurement will represent the global average concentration placed in the process vessel. The proper segregation volume should be chosen somewhere in between.

Obviously, these spatial segregation measurements require access to some spatial view of the material after it has segregated due to initial process filling. One way to gain access to the cross section of a pile is to fill a slice model with material and observe the segregation pattern through the side of the slice model using optical techniques (Figure 2).

Figure 2. Schematic of segregation tester

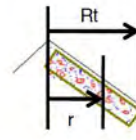
Dump material into box and observe the change in color intensity along the pile as measured just below the top surface of the pile (rectangle section).

These changes in color intensity are an indication of differences in either chemical composition or in particle size and can be used to estimate the segregation of key components in the system.



Observation of segregation through the sides of a slice model will be biased to the optical pattern that exists at the wall of the segregation tester. Therefore, care must be taken when loading the tester to assure a representative sample is visible through the side of the tester. Filling the tester across the width of the slice model will distribute the material to the tester wall, creating a uniform material across the tester. Limiting the thickness of the slice model will also help with the distribution of representative material to the tester wall. However, one should be aware that extremely thin slice models are subject to banding due to wall effects that would not be present in wider slice models. For typical materials, this limits the slice model to a minimum of approximately 25 mm thick.

Reflectance spectroscopic methods can be employed to measure subtle differences in color. Since we are dealing with a discrete particle system, multiple measurements are required to determine the average concentration within a given viewport. Segregation measurement is also a scale issue. The size of the chosen viewport should be large enough to contain a representative number of particles, yet small enough that differences in local compositions are not lost in the averaging scheme (Figure 3). We defined the tester view port area as 1.27 cm square and averaged 36 sample readings within the view port area. We moved the viewport to collect data at about 30 points along the length of the pile at a position that was about 1.27 cm below the top surface of the pile as indicated in the schematic in Figure 2.



Define the size of the view port and measure the spectra along the top of the pile. Adjacent viewports can overlap and tester can measure concentration at up to 50 locations along pile.



Figure 3. Measurement zone along pile top surface

If the spectra of the pure components are known, and the spectra of the mixture in different, view port boxes along the pile are known then pure component spectra can be used to compute the concentration of the components along the length of the pile. One drawback of this technique is that good data requires many spectral measurements collected at multiple points along the pile. Manually collecting this data is tedious and time consuming. Therefore, an automatic instrument was constructed to control the feed, obtain the pure component spectra, and measure spatial concentration profiles for spectral measurements (Figure 4).



Figure 4. SPECTester used in Segregation Analysis

2.3 Results of SPECTester Analysis

The segregation pattern and data is given in Figures 5 through 7. The concentrations are plotted as a function of dimensionless radius. A radius of 0 is the top of the pile and a radius of 1.0 is the bottom of the pile. This profile shows significant segregation of both blue dots and brightener, as indicated by the segregation intensity (Figure 7). The detergent base tends to accumulate at the top of the pile while blue dots and brightener accumulate at the bottom of the pile (Figure 5). Measurements indicate that the blue dots are the worst acting ingredient for segregation. This profile is indicative of angle of repose segregation. This suggests that the formation of piles during filling of any equipment downstream of the mixing unit and before the packing step should be minimized.

Sometimes the segregation trend is easier to see if viewed from a cumulative concentration point of view. We can sum, or integrate, the fraction of any component along the pile and normalize it relative to the actual average concentration of that component along the pile (Figure 6). If there is no segregation, then this procedure would show a straight line passing through the point (0,0) and (1,1) when plotted against dimensionless radius. A positive deviation off this line indicates accumulation near the top of the pile. A negative deviation off this line indicates accumulation toward the bottom of the pile. An s-shaped curve indicated accumulation at both top and bottom. The magnitude of the deviation off this line indicates the percent deviation from the mean concentration for any one component. The reason for plotting segregation in this manner is to relate the segregation profile to the deviation from the mean or average concentration. These plot provide a quick way to view how bad the segregation is from a mean concentration point of view while giving you a feel of the type of segregation occurring.

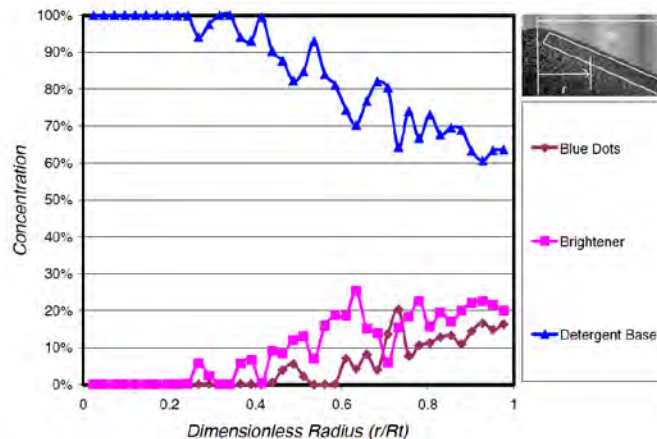


Figure 5. Radial segregation profile for laundry detergent with brightener

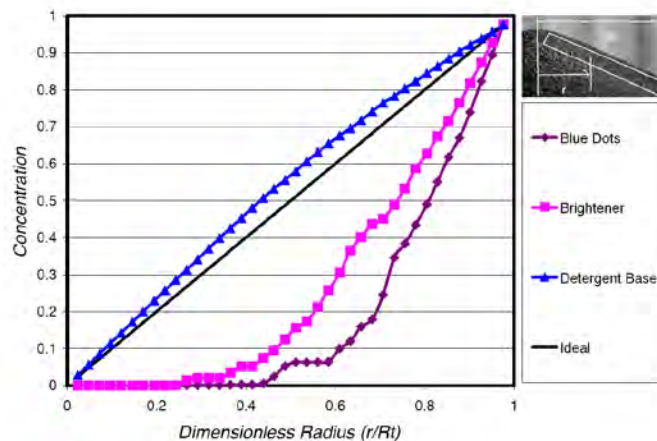


Figure 6. Cumulative radial segregation profile for laundry detergent with brightener

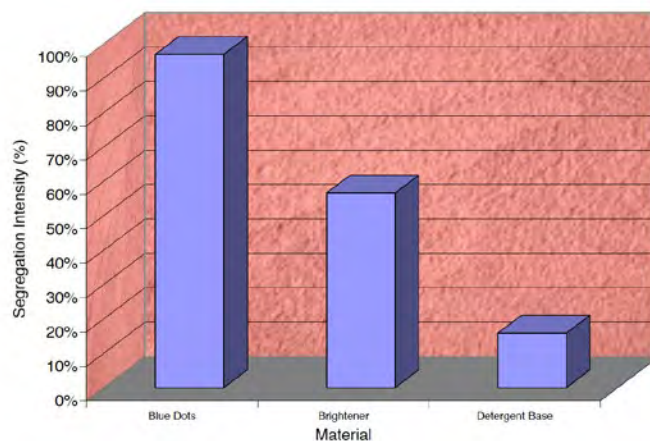


Figure 7. Segregation Intensity for laundry detergent with brightener

Segregation Properties of Tri-Color Sand Mixture

1.0 Segregation – An Introduction

There are two uses for segregation data. Engineers may use segregation data to optimize product design, creating a product with minimal segregation tendency. Engineers may also wish to modify the processing to minimize the effect of segregation in their plant packaging process or handling facility. In either case, the segregation pattern, segregation mechanism, and magnitude of segregation are key parameters required for process or product design.

Segregation occurs through several mechanisms. Identification of the primary segregation cause and the segregation pattern produced through handling is critical to prevent de-mixing of the final detergent mixture during handling and packaging. Any property difference between materials can cause separation of critical material components. However, there are five common causes of segregation problems in typical handling systems.

Sifting:

Fines may sift through a matrix of coarse particles during handling. This mechanism requires that the void space between adjacent particles be large enough to permit fine particle to pass through. Generally, this requires a particle size difference of about 3:1. Inter-particle motion is also required to provide a means of exposing empty void spaces to fine particles. The fines must also be free flowing enough to prevent arching between adjacent particles and the void spaces must be empty enough to accept fine particles. In general, this type of segregation produces a radial pattern as material forms a pile in process equipment. The fines accumulate near the pile charge point and decrease in concentration toward the edge of the pile.

Angle of repose differences:

Two materials may have different angles of repose. Thus, when these two materials flow down a pile they essentially

create overlapping piles where the material with the steepest repose angle accumulates near the top of the pile while the material with the flattest repose angle accumulates near the pile edge. Generally, there is a distribution of these two materials along the pile's surface. Repose angle differences of about 2 degrees can result in significant segregation. Material of different particle sizes can possess sufficient difference in repose angles to cause this type of segregation. However, particle size difference is not a prerequisite angle of repose segregation and materials of the same size can separate via this mechanism. In addition, your process must also generate piles during handling or processing to cause this type of segregation.

Air entrainment:

The mixture may contain fines that are small enough to be carried by air currents in the handling system. These fines drop out of the air stream when gas velocities decrease below the entrainment velocity. This causes separation of fines and coarse in handling systems. The fines generally deposit near the container walls. This type of segregation requires a source of air currents in process equipment. This source of air can come from free fall of a compressible material. When the falling stream impacts the material level, the entrained air is pushed out of the interstitial pores and carries the fine particles in the resulting dust cloud. This segregation typically causes a radial pattern during pile formation, but the fines are at the bottom of the pile and not the top.

Impact fluidization:

If the mixture is fine enough, then air trapped in the interstitial voids can cause material to fluidize. As a large particle drops into this fluidized layer, momentum causes the large particles to penetrate this fluid layer, resulting in a top-to-bottom segregation of fine and coarse particles. This mechanism requires a source of air and the ability of the bulk material to hang onto entrained air for a moderate amount of time.

Percolation:

A fluidized layer of material can lose its entrained air as it sits stationary in a container that was just filled. Percolation forces air up through the bulk material. Generally, this process forms fissures in the bulk material where the gas escapes. The local velocity in these fissures is relatively high and can entrain fine particles in the process, causing top-to-bottom segregation. This results in the size separation of fluidizable material with wide particle size distributions.

It is critical to identify the cause of segregation to avoid processing that will induce the problem. It is also necessary to know the pattern of segregation in order to provide a means of re-mixing material, if required. Understanding the segregation mechanism will also help in determining what must be done to the material to create a product that is less likely to segregate.

2.0 Segregation Testing Results - Background

In the past researchers have fed bulk materials onto a pile, sectioned a conical pile into annular sections, and performed chemical or size analysis on the material collected in each annular section. This is a long and tedious method which results in only a very few measurements collected along the pile. Plant personnel often use thieves to sample piles in process equipment. This method also yields only a few measurements along the pile and disturbs the surface, thereby changing the segregation pattern. Other researchers measure the segregation pattern by placing material in a funnel flow hopper and then discharging the hopper, collecting the output stream and measuring the quality of the mixture by chemical composition or particle size. This method convolutes the segregation with the flow pattern from a particular hopper or bin. Unless the bin design in the tester is precisely the same as the bin design in the process, there is no guarantee that the composition during discharge from the tester will be similar to that found in the actual process. In addition, the cohesive properties of the bulk material can impede flow from the segregation tester hopper, even though hang-ups may not occur in the process with the same material.

One problem with current segregation testers is that they do not relate well to the process. Any two or three materials can segregate if there is a difference in properties and the mixture is subject to enough external stimuli. For example adding enough fluidization gas will separate materials of different densities, even though these extreme conditions

may never occur in the actual process. The real question to be answered is: will the mixture segregate when exposed to a feed behavior similar to that present in the process? Therefore, any measurement of segregation tendency should have three key elements. First, the feed should be controlled so as to allow the measured segregation to be scalable to process conditions. Second, the pattern of the segregation should be included as part of the measurement in order to predict the expected concentration leaving process equipment. Finally, the magnitude of the segregation should be quantified to provide guidance in determining if the mechanism is actually a potential problem in the process. Ideally we would like the concentrations based on chemical components in the mixture.

2.1 Relation of Test Results to Process

Let's identify the key attribute that must be controlled or measured to make segregation measurements scalable to process conditions. For simplicity, we will assume that material simply falls from a mechanical conveyor into the process vessel. Material entering the process typically free-falls from some fall height at some process velocity. It is important to note that, in this case, the dynamic effects caused by particle rebound or sliding down the pile scale linearly with the geometry of the process equipment (Figure 1). The same cannot be said of the case where gas is carried with the input stream. However, similar models can be created for this case and a scale law developed. For the purpose of this report, and because the segregation data is for simple comparison, we will assume little or no gas effects during the filling of a typical pharmaceutical process. The small scale segregation tester can then be run at a constant drop rate and fall height. We deposited material in a slice model, forming half a pile, at a rate of about 1 lit/min. The free fall dimension was set to be 0.57 times the diameter or width of the receiving bin. It is important to note that the full diameter of the receive bin in the process would correspond to twice the width of the slice mode bin in the tester since the slice model was filled on one side. For a typical 1.5-meter wide bin this would correspond to a drop of about 0.85 meters.

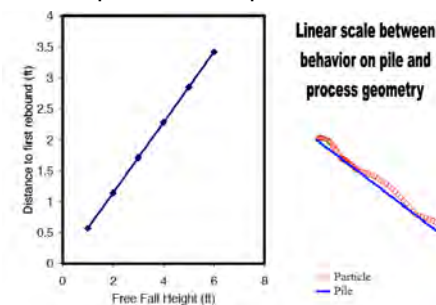


Figure 1. Typical rebound of free fall particles down pile surface

2.2 Segregation Pattern

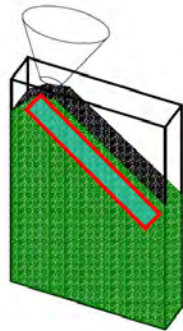
The pattern of segregation requires that segregation be measured by analyzing spatial concentration data. This spatial analysis always has a sample size or view port associated with it. It must be decided beforehand what volume of material represents a reasonable segregation basis. The view port must contain enough particles to be statistically relevant. If that volume occupies only one or two particles, then any segregation measurements are doomed to failure since the segregation measurement volume cannot represent an average sample. If that sample volume is the same as the bin size, then every segregation measurement will represent the global average concentration placed in the process vessel. The proper segregation volume should be chosen somewhere in between.

Obviously, these spatial segregation measurements require access to some spatial view of the material after it has segregated due to initial process filling. One way to gain access to the cross section of a pile is to fill a slice model with material and observe the segregation pattern through the side of the slice model using optical techniques (Figure 2).

Figure 2. Schematic of segregation tester

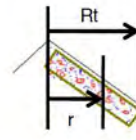
Dump material into box and observe the change in color intensity along the pile as measured just below the top surface of the pile (rectangle section).

These changes in color intensity are an indication of differences in either chemical composition or in particle size and can be used to estimate the segregation of key components in the system.



Observation of segregation through the sides of a slice model will be biased to the optical pattern that exists at the wall of the segregation tester. Therefore, care must be taken when loading the tester to assure a representative sample is visible through the side of the tester. Filling the tester across the width of the slice model will distribute the material to the tester wall, creating a uniform material across the tester. Limiting the thickness of the slice model will also help with the distribution of representative material to the tester wall. However, one should be aware that extremely thin slice models are subject to banding due to wall effects that would not be present in wider slice models. For typical materials, this limits the slice model to a minimum of approximately 25 mm thick.

Reflectance spectroscopic methods can be employed to measure subtle differences in color. Since we are dealing with a discrete particle system, multiple measurements are required to determine the average concentration within a given viewport. Segregation measurement is also a scale issue. The size of the chosen viewport should be large enough to contain a representative number of particles, yet small enough that differences in local compositions are not lost in the averaging scheme (Figure 3). We defined the tester view port area as 1.27 cm square and averaged 36 sample readings within the view port area. We moved the viewport to collect data at about 30 points along the length of the pile at a position that was about 1.27 cm below the top surface of the pile as indicated in the schematic in Figure 2.



Define the size of the view port and measure the spectra along the top of the pile. Adjacent viewports can overlap and tester can measure concentration at up to 50 locations along pile.



Figure 3. Measurement zone along pile top surface

If the spectra of the pure components are known, and the spectra of the mixture in different, view port boxes along the pile are known then pure component spectra can be used to compute the concentration of the components along the length of the pile. One drawback of this technique is that good data requires many spectral measurements collected at multiple points along the pile. Manually collecting this data is tedious and time consuming. Therefore, an automatic instrument was constructed to control the feed, obtain the pure component spectra, and measure spatial concentration profiles for spectral measurements (Figure 4).



Figure 4. SPECTester used in Segregation Analysis

2.3 Results of SPECTester Analysis

The segregation pattern and data is given in Figures 5 through 7. The concentrations are plotted as a function of dimensionless radius. A radius of 0 is the top of the pile and a radius of 1.0 is the bottom of the pile. This profile shows significant segregation of the yellow and white sands, as well as some segregation of blue sand, as indicated by the segregation intensity values (Figure 7). Additionally, blue sand accumulates at the bottom of the pile while white sand accumulates toward the top of the pile. Yellow sand shows a tendency to accumulate toward the center of the pile with a smaller amount of accumulation toward the top of the pile (Figure 5). This segregation pattern is primarily indicative of angle of repose segregation, combined with some sifting segregation. These sands are used to color the grout or cement for specialty decorative slabs and pool decks, etc. If a uniform mixture of these three ingredients were needed to achieve the desired effect, this segregation pattern would suggest that the end user would need to use special mixing equipment and bin designs to maintain consistency of the color.

Sometimes the segregation trend is easier to see if viewed from a cumulative concentration point of view. We can sum, or integrate, the fraction of any component along the pile and normalize it relative to the actual average concentration of that component along the pile (Figure 6). If there is no segregation, then this procedure would show a straight line passing through the point (0,0) and (1,1) when plotted against dimensionless radius. A positive deviation off this line indicates accumulation near the top of the pile. A negative deviation off this line indicates accumulation toward the bottom of the pile. An s-shaped curve indicated accumulation at both top and bottom. The magnitude of the deviation off this line indicates the percent deviation from the mean concentration for any one component. The reason for plotting segregation in this manner is to relate the segregation profile to the deviation from the mean or average concentration. The plot provides a quick way to view how bad the segregation is from a mean concentration point of view while giving you a feel of the type of segregation occurring.

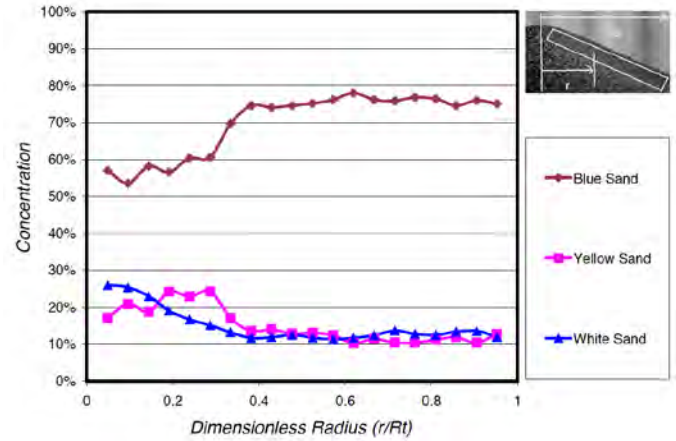


Figure 5. Radial segregation profile for Tri-Color Sand Mixture

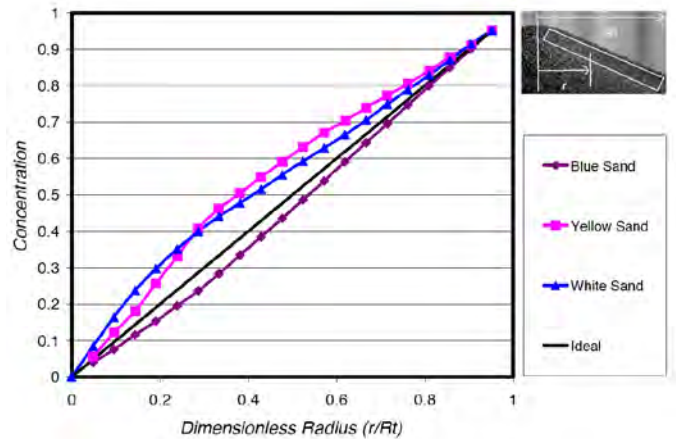


Figure 6. Cumulative radial segregation profile for Tri-Color Sand Mixture

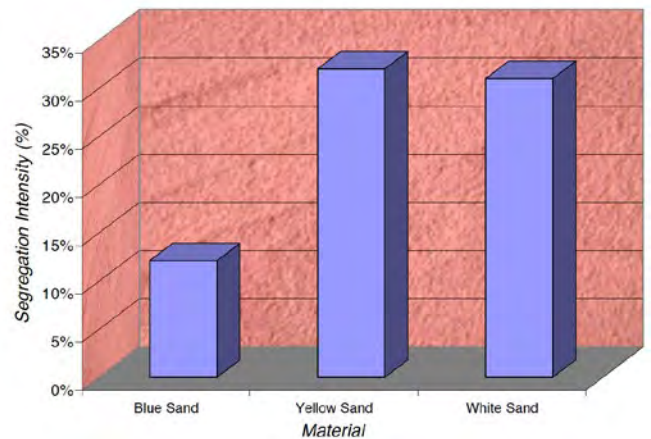
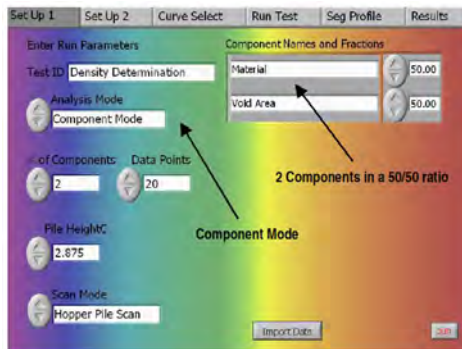


Figure 7. Segregation Intensity for Tri-Color Sand Mixture

Using the SPECTester to Quantify Density (Porosity) of a Mixture

The SPECTester is designed to evaluate and quantify the segregation potential of both individual components, and the entire mixture in a product containing up to six unique components. However, the machine's capability extends to analyzing the density/porosity of any material, regardless of the number of ingredients in the mix. Essentially, when reviewing the pile formed in the test hopper, the SPECTester measures the amount of material present compared to the void space between any/all particles in the pile. In other words - comparing the presence of material to air in the pile, we can determine the density/porosity of the material at specific points in the process. Steps to determine the density (porosity) of a mixture using the SPECTester:

- Using only two component trays, leave the bottom (second) tray empty and fill the top tray with the material mixture.



- Fill the tester hopper in normal fashion, with ~2L of the material to be analyzed.

- On the touch-screen, begin the SPECTester program.

- When the SetUp1 screen appears, enter the name of the Test to be run.

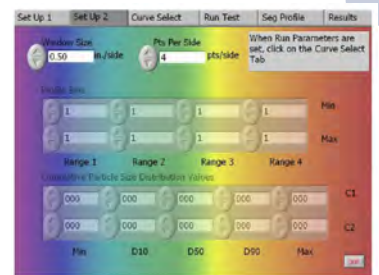
- Select "Component Mode" to acquire density.

- Enter "2" as the number of components.

- And the number of data points to be collected by the SPECTester. We recommend 15 to 20 data points for most materials.

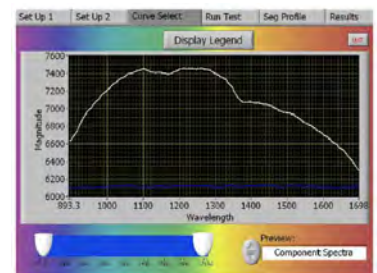
- Referring to the pile height gauge, enter the height of the left side of the material pile.

- Enter the names and percentage of concentration for the two components. The names are arbitrary, to the User preference. However, the percentage concentration of the two components (material and air) should be defined as a 50/50 mixture, or 50% each.



- On the SetUp2 screen, select the standard 0.5 inch window with 4- or 5-sided matrix.

- The CurveSelect screen shows the void (air) spectra as a flat blue line and the material spectra as a white curved line.



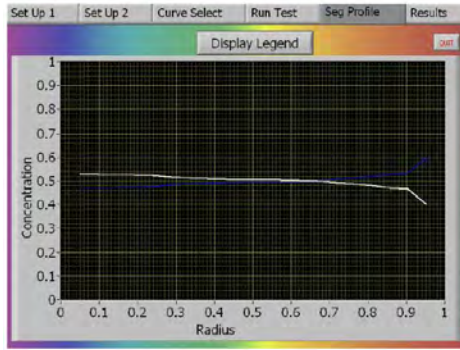
- On the RunTest screen, check all your entered data for accuracy and then click "Get Data." Data collection and analysis will take several seconds to a few minutes.

The segregation profile represents the density/porosity of the mixture at the various locations in the pile, which simulates the process. If density remained constant through the material run, then both the blue and white line would be perfectly horizontal, overlapping one another. Where the white line appears above the 0.5 line, material density is greater. Where the white line appears below the 0.5 line, material density is less and the packaged material may be underweight. Please note that if the process has typical funnel flow hoppers that cause the sides of the bin to empty last, then the material at the very end

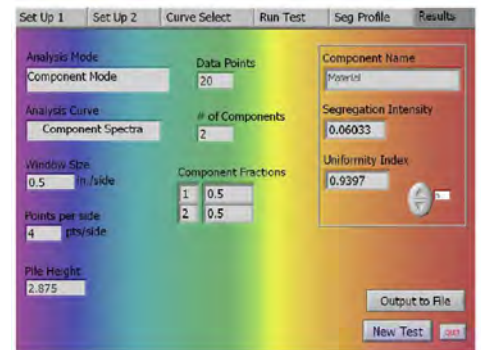
APPLICATION NOTE 023

of the production run is likely to be somewhat out-of-spec, as indicated by the large dip in the density profile.

The number of primary interest on the Results screen is the Material Segregation Intensity number. For the example shown (which corresponds to the segregation profile graph above), the overall density of product through the process is good.



To properly evaluate a material's density using the SPECTester, it is necessary to consider both the Segregation Profile graph as well as the Segregation Intensity Number. Together, these data provide the information necessary to describe the density (or porosity) segregation of a sample mixture.



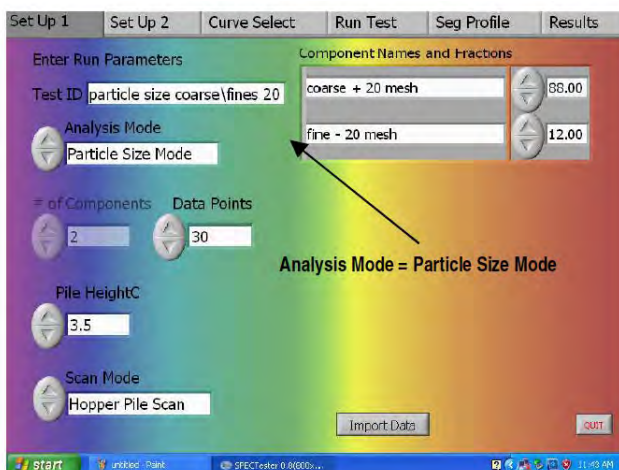
Using the SPECTester to Quantify Segregation by Particle Size

The SPECTester is designed to easily and quickly evaluate and quantify the segregation occurring in a product mixture containing up to six unique components. However, by utilizing a few simple additional steps, the tester can analyze a product made up of variously-sized particles of the same material: in other words, segregation due to particle size. The additional steps include:

be the pure components used in the component trays during the SPECTester's analysis. The material from the riffling step is re-combined and thoroughly mixed to fill the feeder hopper.

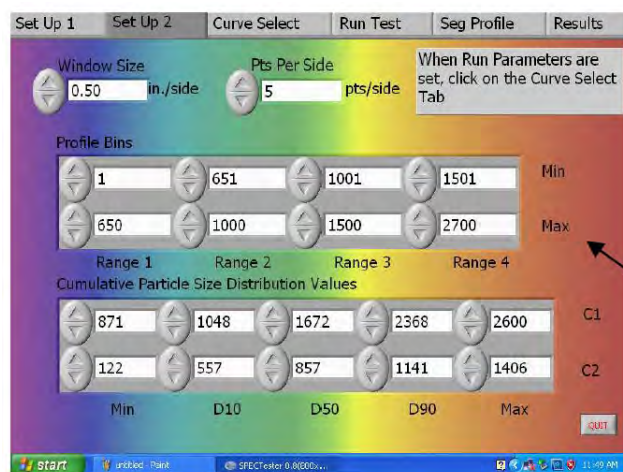
You will need a few additional pieces of industry-standard information.

- Cumulative PSD values (Min, D10, D50, D90 and Max)
- Profile bin values



- Riffle the material to obtain a representative sample - you will need about 2.5 L of material to assure sufficient sample remaining for the SPECTester analysis.
- Take a portion of this sample and sieve it to create two components (coarse and fine).
- Measure the PSD of the coarse and fine and determine the Minimum particle size, D10, D50, D90, and Maximum particle size.
- Using the final sieved sample, determine the % concentration by mass of the coarse and fine particles.

The fines and coarse obtained during this sieving process will



In Component Mode operation, the bottom portion of Setup2 screen is inactive. In Particle Size Mode, the profile bin values, as well as the cumulative PSD values (Min, D10, D50, D90 and Max) values, must be added.

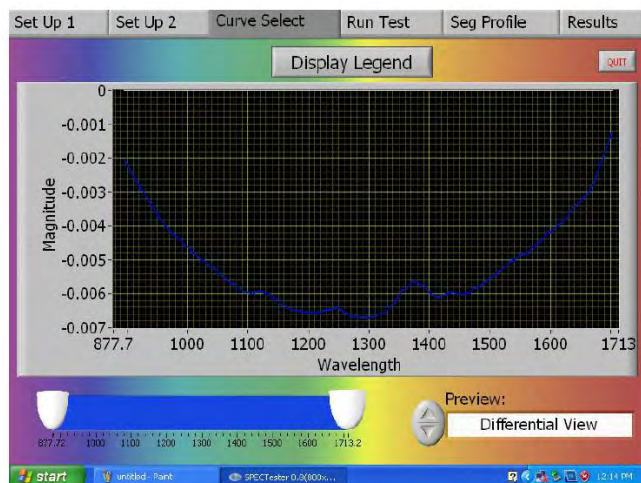
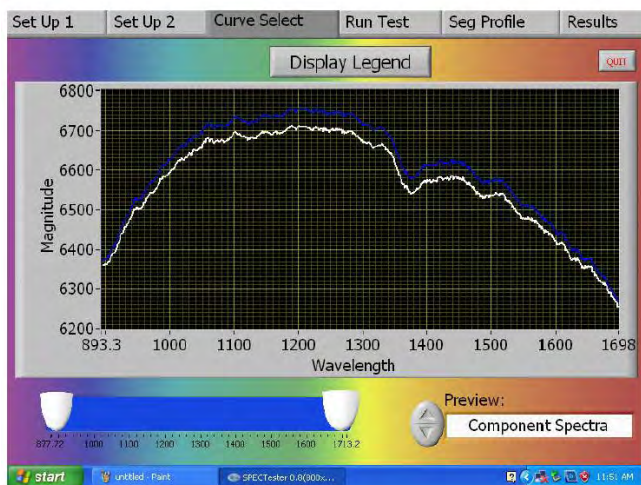
With either component spectra or differential view spectra, the concentration of fines and coarse are computed just as any other pure components in a mixture. The SPECTester uses these fines and coarse concentrations along with the particle size data to estimate the particle size of any particle size bin specified in the Profile Bin values entered in Setup2 screen. For example, four particle size bins were used: PS Bin One (1-650), PS Bin Two (651-1000), PS Bin Three (1001-

APPLICATION NOTE 024

1500) and PS Bin Four (1501-2700). The concentration of each of these sized bins will be plotted as a function of dimensionless radius. You do not have to span the entire PS range with the bin sizes that are entered in setup2 screen.

Component Spectra Preview:

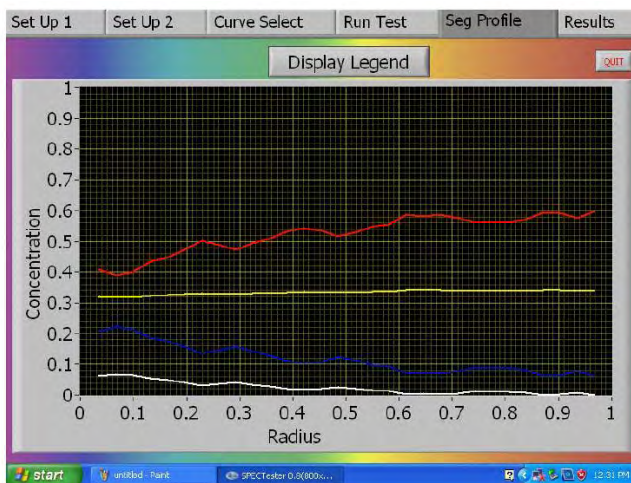
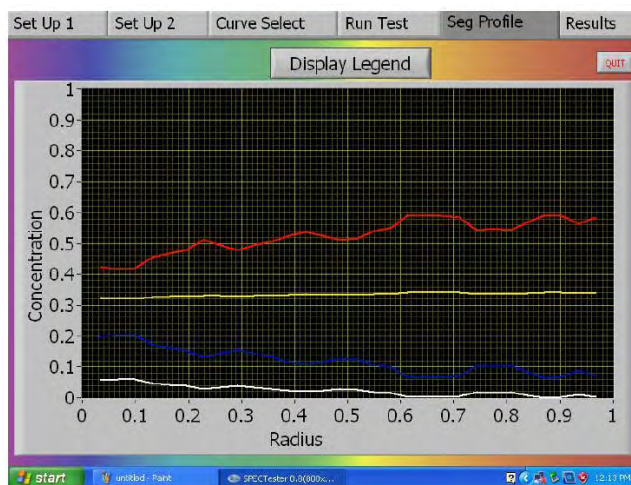
In component spectra mode, the spectral signatures of the fines and coarse are similar. The difference in the spectral signature (as seen by the SPECTester) is due to the difference in intensity of hue resulting from particle size difference. The finer material scatters light more, and will therefore have the more intense spectral signature. Note that the peaks and valleys of the two spectral signatures remain the same.



Differential View Preview:

In differential view mode, the spectral signatures of fines and coarse are dissimilar because the spectral intensity curves are subtracted one from another. The major component spectral intensity curve will be set equal to zero and the other component will be subtracted from that value to give the differential view spectra. In this example case, the coarse particles (major component - white line) show zero intensity and the fines (blue line) are subtracted to give the differential spectra below.

The choice of preview mode is for User's convenience. The resulting segregation profile is essentially the same for either preview mode.



Dynamic Image Analysis of Suspended Liquid Particles

Introduction

In various industries, it is important to measure the size of liquid particles in a suspension. These could be as simple as oil droplets suspended in water or water droplets suspended in oil. There are other instances in pharmaceutical applications where liquid dosages may be encapsulated inside a harder outer shell. In many of these cases, the end user may have a need to determine the size of these globules, the shape, and possibly the concentration. However, the challenge is using an automated technique that can differentiate between a water droplet and an oil droplet as well as to differentiate these particles of interest from other debris as to not impact the concentration measurements.

The most common particle measurement techniques can only differentiate particles based on size. In addition, most of these common techniques will assume all particles are spherical in shape, which for this globule application is an accurate assumption unless there are non-spherical particles, such as debris, that could incorrectly be measured as part of the main population of particles. In addition, some of the more common techniques require supplementary information about the particles as well as the fluid they are suspended in. Parameters such as refractive index may be needed to properly measure particles. Given that globules are of one, or various, refractive indexes and the liquid they are suspended in are of a different refractive index, performing measurements of globules present a challenge using some of the more common particle size measurement techniques. Needless to say, the differentiation between droplet types and debris is also difficult to do with size-only measurement techniques.

Because of this, it is difficult to use the more common techniques to properly measure concentration and to even detect globules suspended in liquid. End users are then limited to use manual microscopy to ensure the particles in question are being identified and measured properly. Microscopy allows the end user to view the particles in

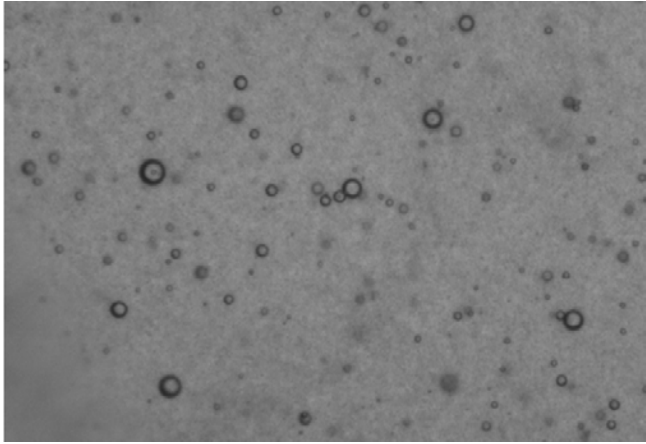
question and to differentiate one type of globule from another visually. In addition, it allows the user to identify debris or other particles that are not globules to ignore them or take action on the fact that they are present in the sample. The problem is that these manual methods tend to be tedious and time consuming. In addition, manual microscopy is not a practical technique for measuring an adequate population of sample to ensure statistical assurance. Microscopy also has a tendency of deforming the sample as it is put on a microscope slide. Something not experienced in Dynamic Image Analysis where globules are allowed to flow freely.

Combining the speed and accuracy of the more common methods with the visual abilities of microscopy has been accomplished with Dynamic Image Analysis. This method enables users to differentiate not only on size, but also on numerous other shape parameters in a high speed automated measurement. Dynamic Image Analysis works on the principle that as particles pass through a detection zone, images are captured and analyzed. ISO 13322-2 is used as the guideline for all Dynamic Image Analysis instruments available on the market today. The key benefit of using Image Analysis for globule measurement is the identification, quantification and differentiation of different particles by using Size, Shape, and Opacity shape measurements. The end user would be able in a single analysis perform a size / shape measurement, have a concentration measurement of each type of particle type present and have thumbnail images of each measured particle. Globules made of different liquids, silicone, water, oil, etc., all tend to be spherical in nature and can have random sizes, but all would have different opacity (darkness) that could be detected and used as a differentiation discriminator of each type of globule. In addition, the presence of debris (non-globules) would also be captured and reported. One additional benefit that Dynamic Image Analysis brings is the ability to show particle thumbnails of each and every measured particle for visual confirmation and identification.

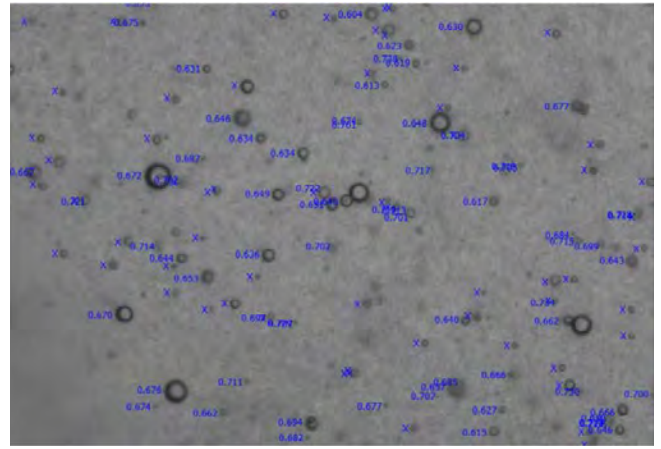
APPLICATION NOTE 025

Experimental #1:

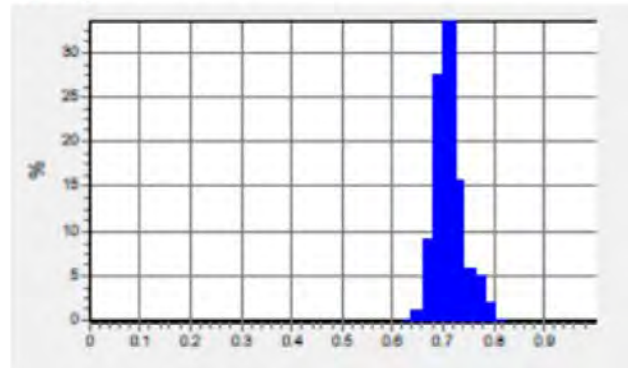
For this experiment the Particle Insight, Particle Shape and Size Analyzer was used to measure an oil sample from an airplane engine. In this case the engine had significant wear and thus resulted in cooling liquid (water based) present in the oil. Below is a single screen capture of the sample analyzed on the Particle Insight.



In a real-time basis, the PI can analyze the particles on the screen and perform 30 shape measurements as well as save the individual particle thumbnail images. As can be seen here, the Particle Insight can eliminate or ignore particles that are out of focus. In this case the measurements shown are for the Opacity of each particle. It is also interesting to point out that water droplets in oil come in different sizes however debris that was also found in this sample was distinguishable by their irregular shapes (lower Circularity values, lower Smoothness values and darker Opacity values). Thousands of particles were measured in a matter of a few minutes. However, because the Particle Insight has no lower limit on concentration detection, even if very few particles were present, the recirculating of the sample would capture any rare event particles.



Opacity



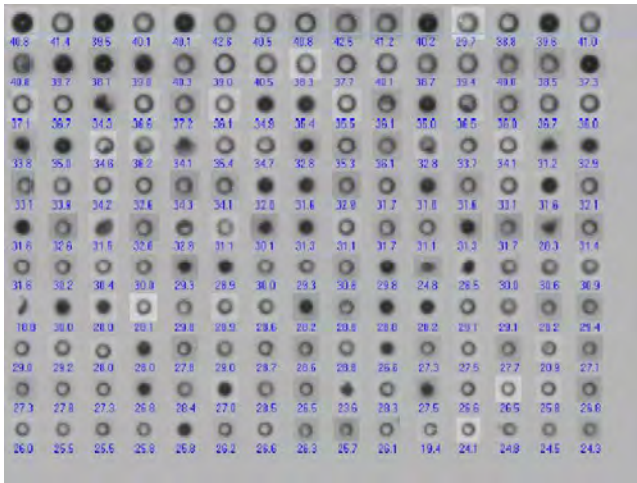
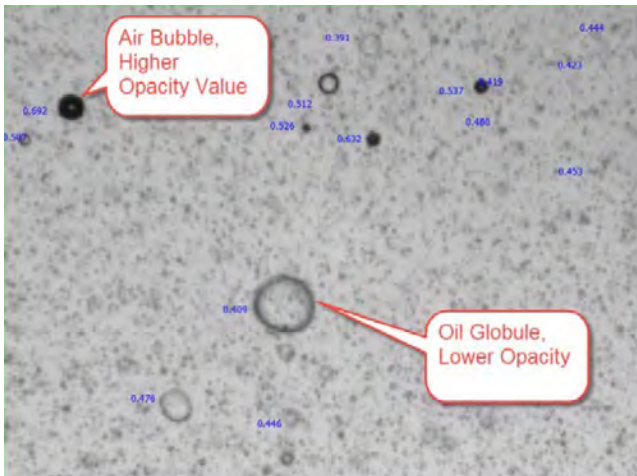
Typical Opacity histogram showing distribution of particles based on how dark they are. Air bubbles and debris tend to have a higher Opacity value than liquid globules.

APPLICATION NOTE 025

Experimental #2:

This next experiment was the detection of oil droplets in water. As can be seen here, there are large oil globules as well as some air bubbles. The easy way for the Particle Insight to differentiate between an oil droplet and an air bubble was using the opacity measurement.

Smaller debris is present as can be seen in the background. The smaller debris can also be measured in real-time or the instrument settings can be adjusted to ignore them.



After analyzing tens of thousands of particles in minutes, the Particle Insight shows all thumbnail images. As can be seen here, lighter round particles are globules while darker round particles are air bubbles and darker irregular particles are debris. Relative concentration of all three populations can be given and important to know

Experimental #3:

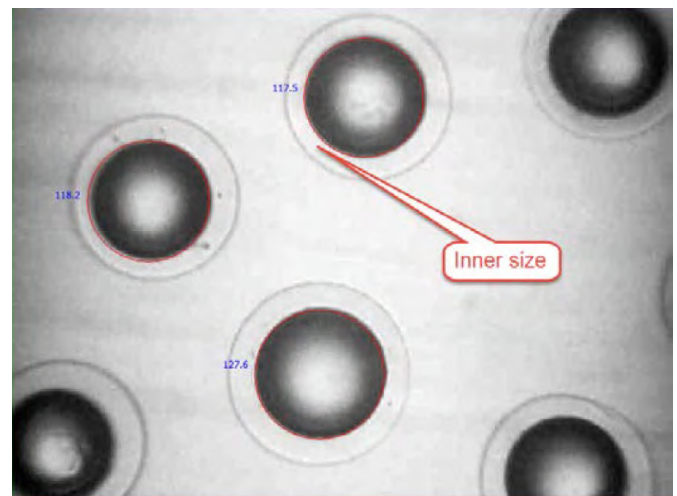
The images below were from a pharmaceutical time-released sample that has an inner globule encapsulated in a hard-outer shell. In this sample the customer was interested in determining the thickness of the coating.

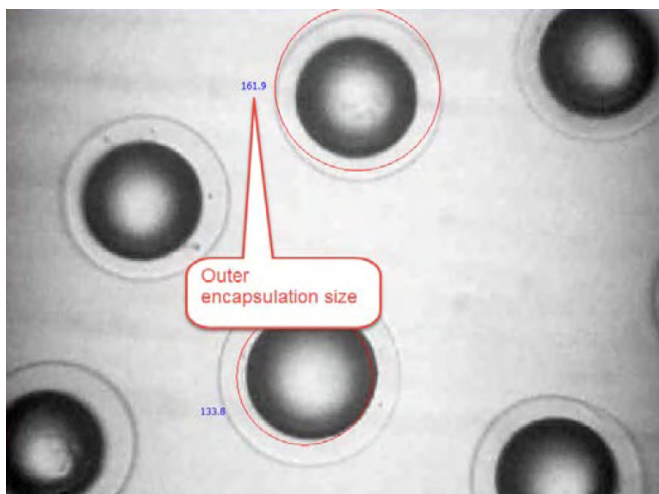
All particle size instruments can measure the inner particle when not coated and report the same size because these are spheres.

After the particles have been coated is where most other particle size instruments have a problem. Because the coating is clear optical instruments like light obscuration and laser diffraction will not be able to exclude the inner particle from the analysis and with the clear coating issue with the suspending liquid can cause the outer shell to disappear. For opaque coatings all particle size instruments will be able to measure the coating.

Dynamic Image Analysis has advantages over the few other instruments that can also measure the clear outer shell and has advantages over sizing opaque coatings.

For clear coatings Dynamic Image Analysis can measure both the inner and outer particles in one analysis, because Dynamic Image Analysis offers the ability to change the dark threshold of image detection. The Particle Insight could perform an automated analysis of the sample analyzing the inner globule particle. Once this analysis was completed, the same sample was then analyzed with a different threshold condition where only the outer ring (the shell) was analyzed for size and shape.





Another advantage Dynamic Image Analysis offers for coatings, clear or opaque, is how uniform the coating is. The coating can be test for circularity, smoothness, uniformity.

Finally for clear coatings the images saved during the analysis can be viewed to see how centered the spheres are in the coatings.

Also if the coated particles are place is a solution that dissolves the coating the images and shape measure will show how evenly the coating dissolves.

Results and discussions:

In all the above experiments the suspension liquid was of different opacities. In the case of the encapsulated globules, the suspension liquid was clear. In the case of the oil samples, the suspension liquid was dark used oil. Regardless of this Dynamic Image Analysis could detect the suspended globule particles. In addition, having the particle thumbnails available enabled us

to ensure that the proper parameters were set to capture the particles in question. In the oil in water and the water/air bubble in oil analysis, there was a clear differentiation in Opacity that enabled us to determine the percentage of water particles present, the percentage of air bubbles present as well as the percentage of debris present in the sample. In this case the end user could determine the health of the equipment where this fluid came from and was then used as a quality control tool to check the stability of the engine from time to time.

In the case of the encapsulated globule, the end user could perform the analysis on a single aliquot of sample. This was a very efficient way to perform the test and did not require the end user to break the outer shell to do a size determination of the inner globule.

Conclusions:

Liquid or globule particles suspended in other liquids would present difficulties for proper detection using typical size measurement techniques. Dynamic Image Analysis has shown to be a valuable tool in the analysis and differentiation of these particle suspensions. In addition, the ability to have particle thumbnails enables a visual validation of the analysis.

How to Use the MCCTC Configuration of the PID EFFI to Perform Pulse Chemisorption Experiments

The MCCTC (Micro Catalyst Characterization and Testing Center) configuration of the PID EFFI is designed to equip the EFFI with the ability to both characterize and perform activity testing of catalysts in-situ. By pairing the MCCTC configuration of the EFFI with a mass spectrometer, the user has a powerful tool that allows them to characterize their catalyst, perform activity testing, and then characterize it again to see how the catalyst surface has changed after being subjected to industrial conditions. One of the characterization techniques employed by the MCCTC option is pulse chemisorption, a method commonly used to measure active metal dispersion. This is made possible because of the inclusion of an extra gas feed via Mass Flow Controller (MFC) and a known volume loop, typically 0.5 cc in volume, used for gas dosing. Here, we will explain the experimental procedure, how to set up the Process@ software of the EFFI to automatically perform the pulse chemisorption experiment, set up the Process Eye software of the MKS Cirrus2 Mass Spec to collect relevant data for the experiment, and how to use MicroActive from Micromeritics to import the mass spec data and calculate results.



Experimental Procedure

For this example, the Platinum-Alumina (Pt-Al) reference material from Micromeritics will be analyzed via pulse chemisorption using pure CO as the active species to fill the known volume loop for dosing. 10% H₂/Ar is used as the feed to reduce the sample and to be the carrier gas during

gas dosing. For this test, 1 g of sample is used but note that because sample mass is an input parameter for calculations, varying quantities of sample can be used for this characterization technique. It is important to keep in mind the quantity of sample; too much sample will adsorb high quantities of gas and will require many gas doses but too little sample will not adsorb enough gas to provide high resolution data. Diluted CO mixtures (CO/He) can be used but will require more doses because of the reduced quantity of the active species in the dosing loop. In addition, H₂ and H₂ mixtures can be used as the active species when paired with an inert carrier feed such as N₂ or He.

Building a Session Table in Process@ to Perform the Pulse Chemisorption Experiment

Process@ gives the user the ability to program an automated experiment by building a session table. Each session is given a finite amount of time and any or all of the system parameters (temperatures, flows, pressure, etc.) can be changed moving from session to session. Moving forward, this document will explain how to build the session table for automatically analyzing the Pt-Al reference material.

Prior to gas dosing, the Pt-Al reference material should be reduced under a flow of 50 ml/min of H₂/Ar while being ramped to 400°C at a rate of 10°C/min. Once 400°C is achieved the sample should be held at this temperature for 30 additional minutes to allow for a complete reduction of the sample. After the reduction is complete the sample should be cooled to room temperature—the fastest way to achieve this is by opening the hot box door. Once the sample has cooled, the mass spec can begin recording and the active species, CO, can be dosed to the sample via the 6-way valve with the known volume loop. The session table should look similar to the one built in Figure 1.

APPLICATION NOTE 026

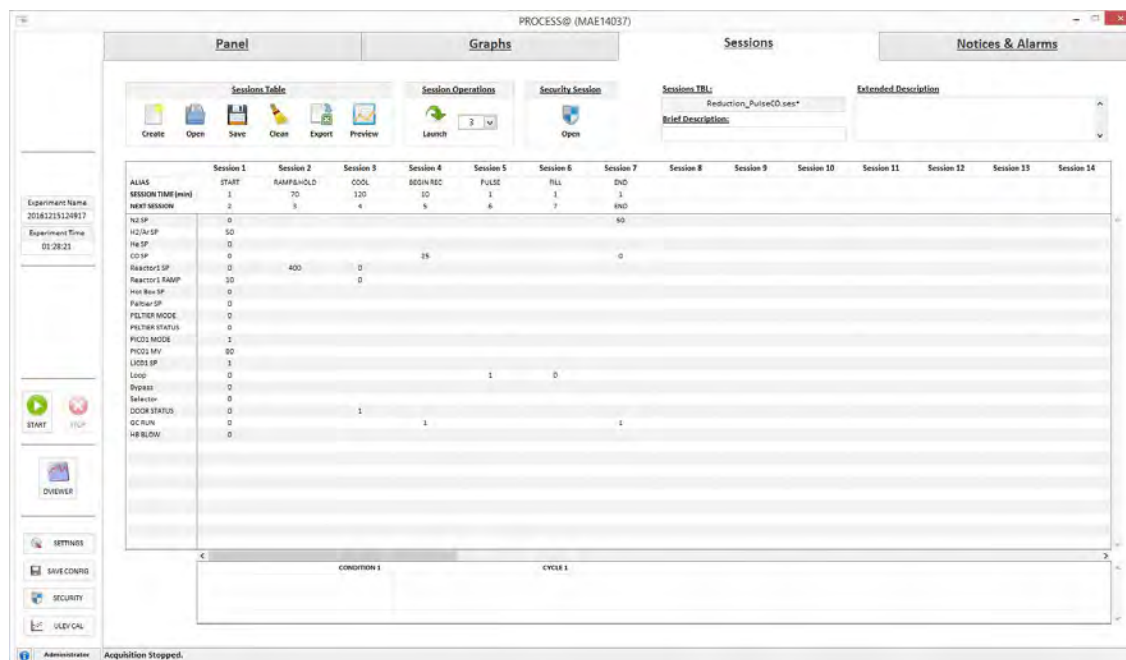


Figure 1: A Process@ session table built to reduce and dose active species onto the catalyst

There are a few items to note in this session table. First, the pressure control valve (PCV) is set to manual operation (PICO1 MODE = 1) and the valve is fully open (PICO1 MV = 80%). This ensures the system will be operating at atmospheric pressure for the duration of the analysis. Second, the door is opened by setting DOOR STATUS to "1". Likewise, when

it is set to "0" it will close. Third, CONDITION 1 is set up in Figure 2. It is designed to save time; even though the system is given 120 minutes to cool to room temperature when the reactor temperature reaches 30°C or below the software will automatically jump to Session 4 to begin the data collection (GC RUN = 1) and move forward with the analysis.

APPLICATION NOTE 026

Sessions 5 and 6 are looped for nine total injections of CO into the carrier stream. Session 5 is used to inject the full loop into the carrier stream (Loop = 1) and Session 6 is used to re-fill the loop (Loop = 0). A time of 1 minute for each of these sessions is sufficient. The nine total injections is achieved via CYCLE 1, seen in Figure 3. To build the cycle, enter "9" in the Repetitions field and select Session 5 and click Include Cycle and then click OK. The final session terminates the analysis and stops the data acquisition by the mass spec (GC RUN = 1). Note that the logic of the software requires the GC RUN parameter to be set to "1" for both starting and stopping. This can be manipulated to the user's advantage where multiple sets of data can be collected at varying times throughout the duration of the analysis by continuing to set the GC RUN parameter to "1". Therefore each odd iteration of setting GC RUN to "1" will begin the collection of data and each even iteration will end the collection of data.

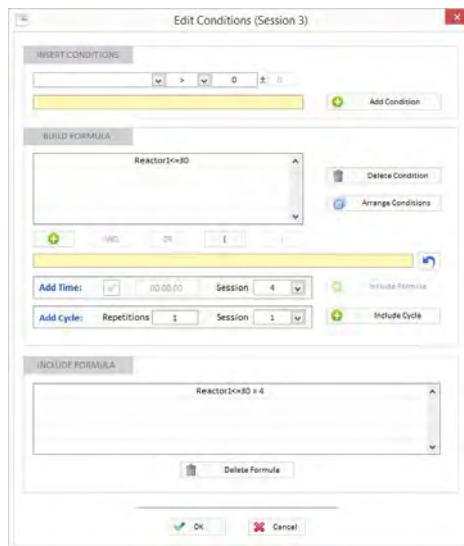


Figure 2: Creating a conditional jump to move the experiment forward once the reactor reaches 30°C

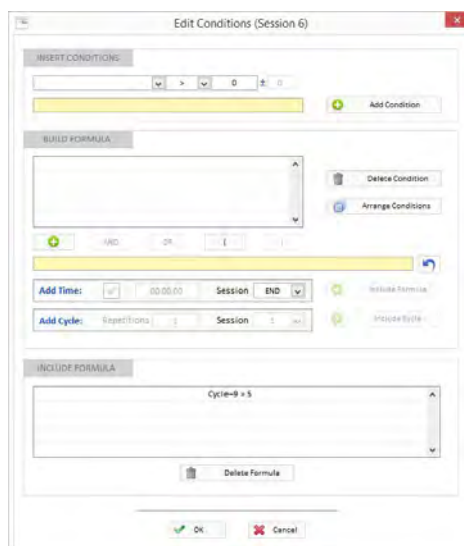


Figure 3: Editing the analysis conditions to include a nine repetition cycle between Session 5 and Session 6

APPLICATION NOTE 026

Creating and Running an Automatic Sequence in Process Eye to Automatically Collect Data

The user can setup Process Eye to automatically collect data when triggered. The digital signal cable between the EFFI and Cirrus2 Mass Spec is the interface used to transmit the trigger signal mentioned in the previous section (GC RUN = 1). With Process Eye open, click Start Create/Edit Recipe and either select an existing recipe from the menu or enter a name for a new recipe as shown in Figure 4 and click OK.

Next, enter the atomic mass of the active species. The Faraday detector is typically used for this application and Skip on Saturation should be selected. Properly configuring the Accuracy setting is critical for generating high resolution results. When this parameter is increased, the reading is more accurate but it requires more time. Likewise, when the parameter is decreased, the reading is less accurate but can be recorded more frequently. For this application choosing an Accuracy setting of "4" is an excellent compromise. The Cycle Time becomes "0.100", meaning that Process Eye will record data every 0.1 seconds. This can be seen in Figure 5. Optionally, the user can click the green plus icon to add additional mass readings for more complex applications but this is not needed for the pulse chemisorption application.

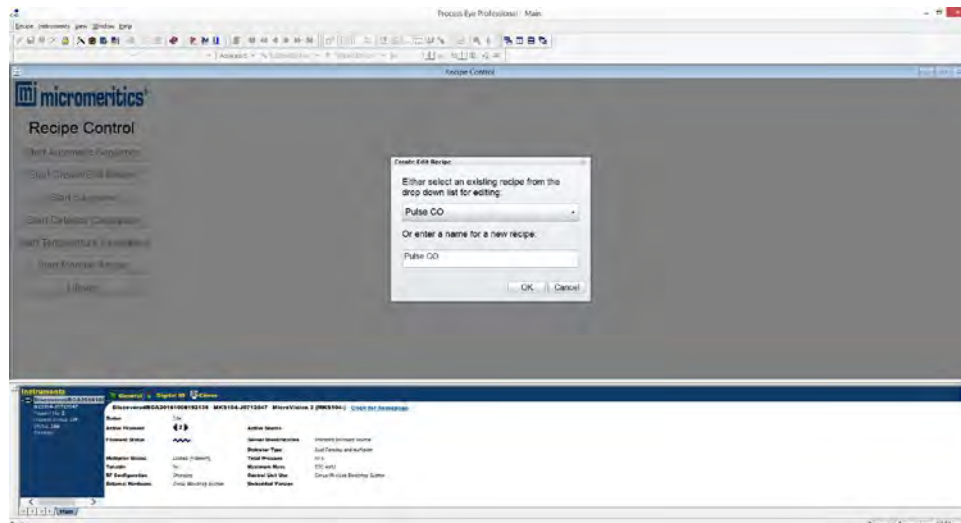


Figure 4: The window which appears when clicking Start Create/Edit Recipe in the Process Eye software

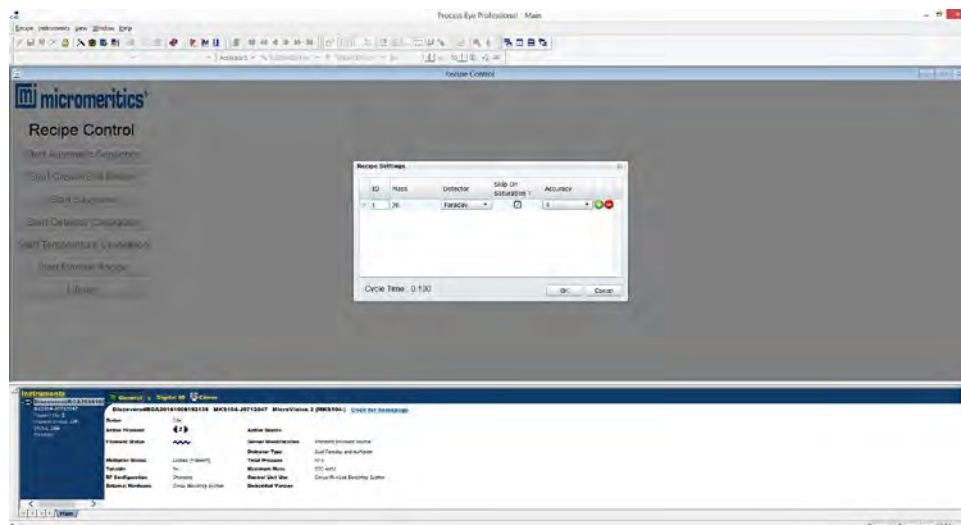


Figure 5: Adjusting the Recipe Settings

APPLICATION NOTE 026

When Start Automatic Sequence is selected, the view seen in Figure 6 will appear. The newly created recipe should be selected from the Recipe Name menu. The string entered into the Save As field will be the name of the new data file created during the analysis. Both Export As Text and Filament Enabled should be selected. When Begin Automatic Sequence is chosen the Process Eye software will begin the automatic sequence and will be ready to receive the trigger signal from the EFFI to begin recording data as seen in Figure 7. Note that for more complex applications multiple recipes can be run in sequence when combined with the multiple trigger signals mentioned in the previous section. If Restart After Sequence Completion is selected then the automatic sequence will run the recipes in an infinite loop that must be stopped by the user by clicking Stop Automatic Sequence or Abort Automatic Sequence.

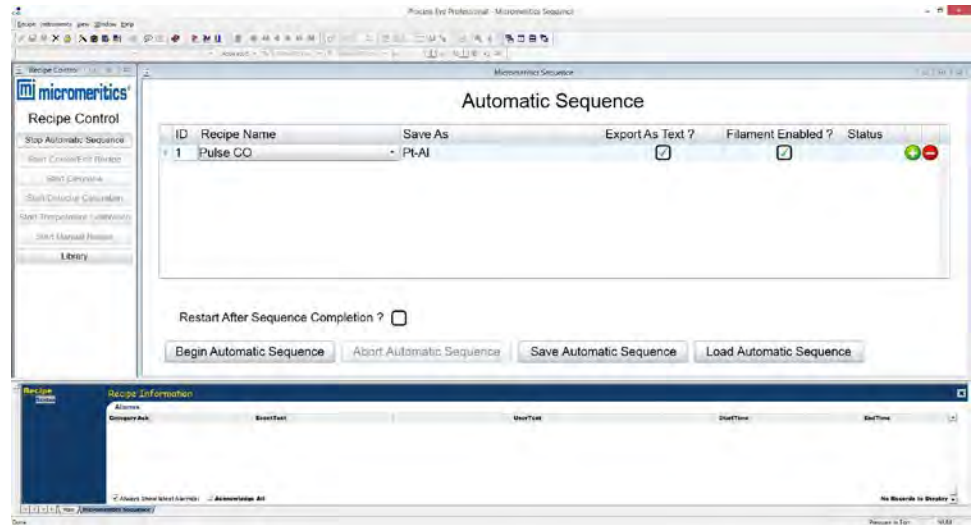


Figure 6: Building the Automatic Sequence in Process Eye

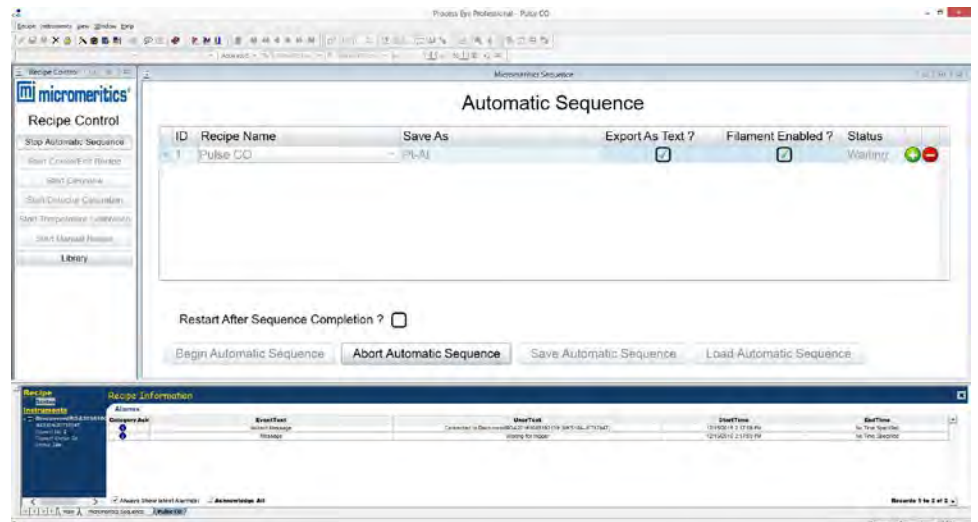


Figure 7: The automatic sequence waiting to receive a trigger signal to begin data acquisition

APPLICATION NOTE 026

Session 4 in the Session Table is when the mass spec is first triggered to begin data acquisition. Its duration is 10 minutes for two reasons. First, it allows the mass spec to establish a steady baseline and second, it allows flushing of the loop with the active species. Once the active species has been injected into the carrier stream the automatic sequence will look similar to Figure 8. Here, the first injection was performed at minute 10. It took about 40 seconds for the active species to travel from the loop, first to the reactor through the catalyst bed and then out the exhaust to the mass spec connection. The first injection should have a smaller peak than the subsequent injections because the catalyst will chemically adsorb some of the active species but note that a logarithmic scale is used by default for the y-axis so the peaks may appear to be the same size. If part of the live data plot disappears, as seen in Figure 8 prior to the 9 minute mark, the data is still successfully being written to the data file. Upon completion of the analysis the second trigger signal will be sent to the mass spec to stop data recording. This will complete the experiment and save the data file in a format that can be imported by MicroActive.

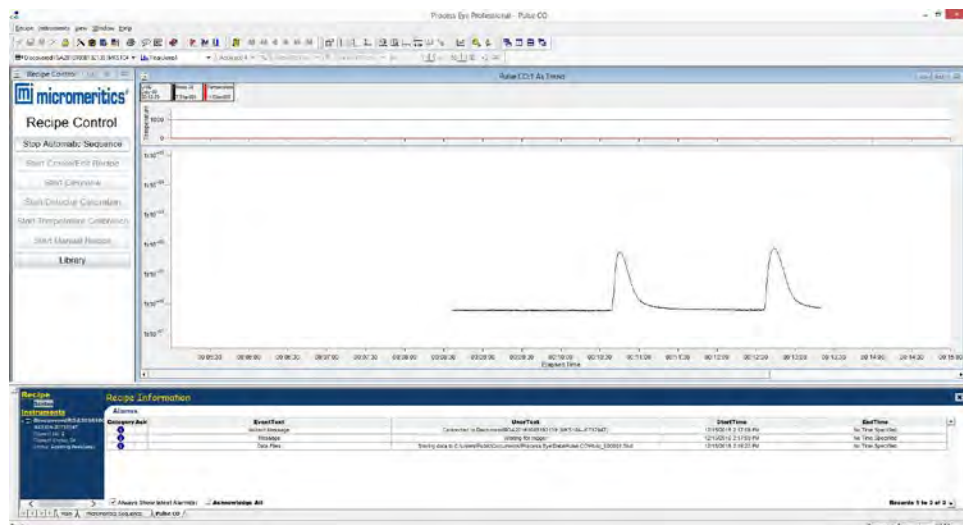


Figure 8: Live recording of data during the pulse chemisorption experiment

APPLICATION NOTE 026

Importing the Mass Spec Data with MicroActive and Calculating Results

Versions 4.04 and newer of MicroActive includes the ability to import mass spec files and use the data for calculations. To do this, select the File menu and select Import... then browse to the Process Eye data folder. Make sure to specify the file type in the bottom right corner; MKS file should be selected for files generated by Process Eye as seen in Figure 9.

When importing data into MicroActive, the user can either add this data to an existing sample file or create a new file. In this example a new file is created. For a new file, enter the sample name, the operator, and sample mass, as seen in Figure 10.

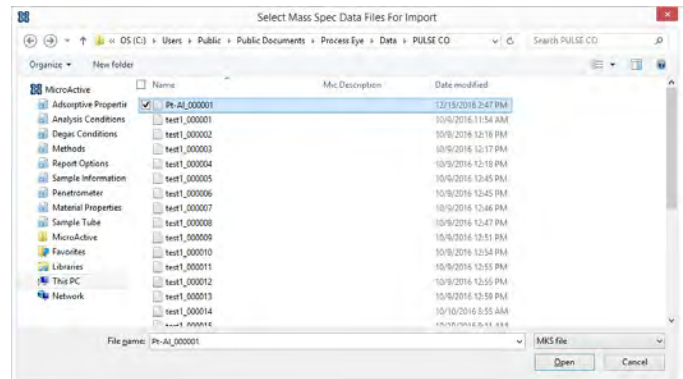


Figure 9: Selecting the mass spec data file to import into MicroActive

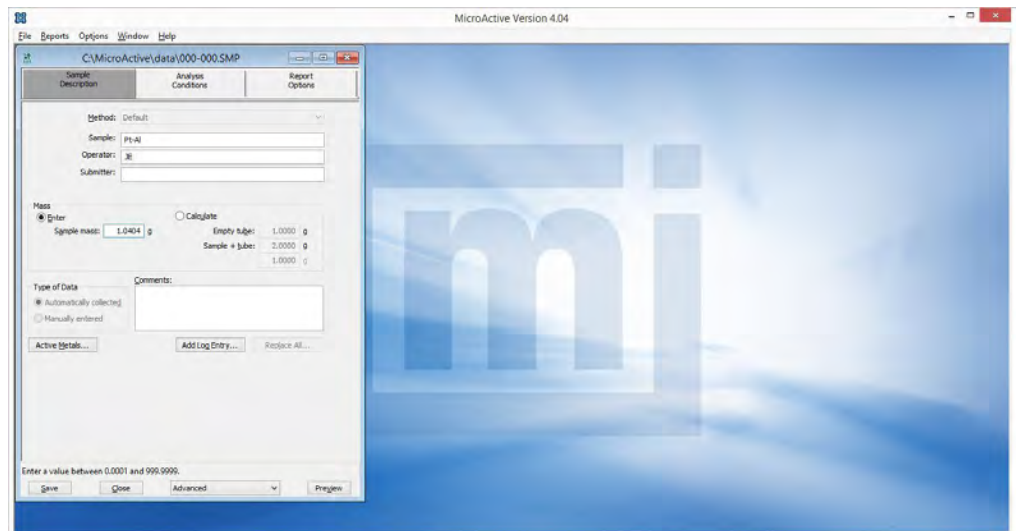


Figure 10: Entering the sample information into the .SMP file

APPLICATION NOTE 026

For a pulse chemisorption experiment, the percentage of active metal (catalyst) in the sample must be specified. This is done by clicking the Active Metals... button. The Pt-Al reference material is 0.5% Platinum—this should be entered as seen in the Active Metals table in Figure 11.

Next, the Analysis Conditions should be entered as seen in Figure 12. Here, the description Mass Spec will already be entered. The Type of analysis should be selected as Pulse Chemisorption. The carrier gas and its flow rate can be entered, but this is optional but useful to have as a reference. The analysis gas must be selected so the proper stoichiometric factor can be applied in calculations. Loop injection should be selected and the calibrated loop volume should be entered. The loop temperature should remain 0.0°C – this will ensure the full entered loop volume entered in the previous step is used in the calculations. Finally, the entered ambient temperature and atmospheric pressure values should remain as defaults.

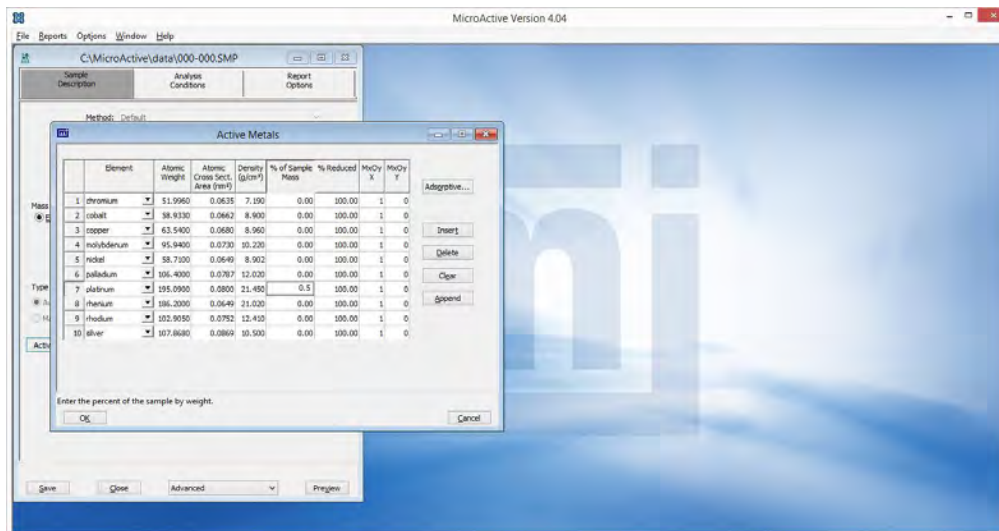


Figure 11: The Active Metals table

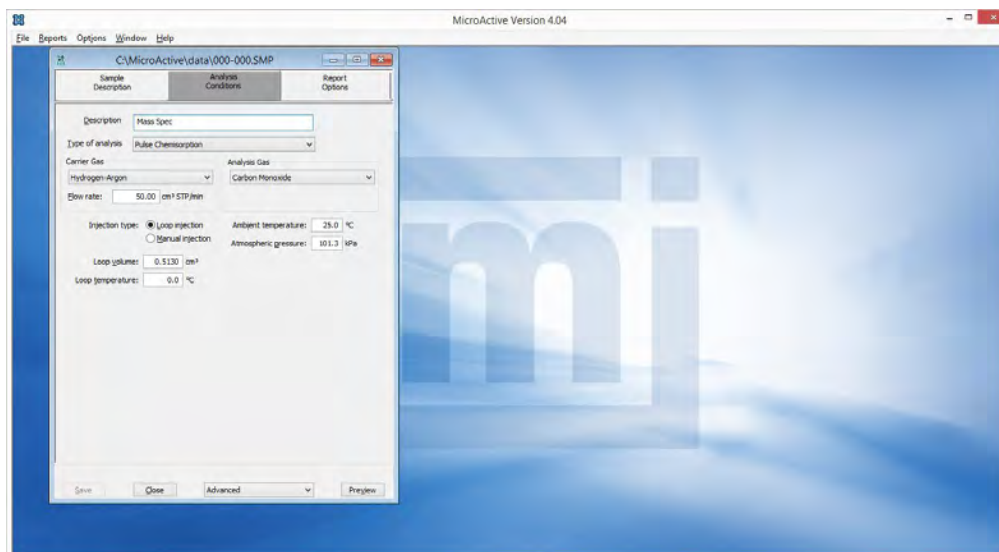


Figure 12: Entering the Analysis Conditions into the sample file

APPLICATION NOTE 026

Pulse Chemisorption should be selected under Report Options. The number of peaks used for saturation can be edited as seen in Figure 13. In this case, the last 5 peaks will be used. When using approximately 1g of the Pt-Al material with a 0.5cc injection loop and pure CO as the active species, adsorption will occur during only the first 2-3 injections. The number of peaks used for saturation should be edited to reflect the analysis conditions.

Once the sample information, analysis conditions, and report options have been edited, Peak Editor–Mass Spec should be selected from the drop-down menu at the bottom of the sample file window. Click Find All Peaks and MicroActive will automatically find and integrate the peaks generated by the gas injections during the experiment. The peak information will be displayed in a table on the left side of the window as seen in Figure 14.

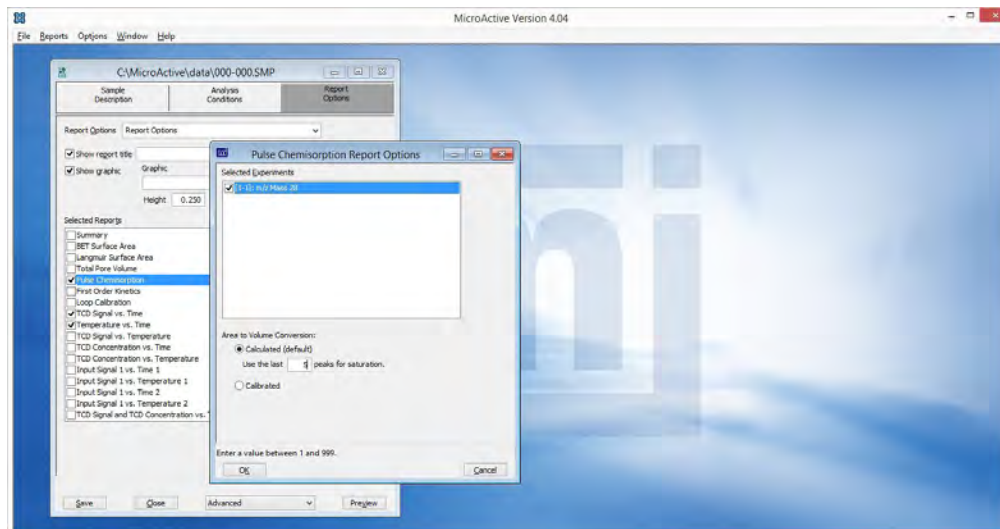


Figure 13: Editing the Pulse Chemisorption Report Options

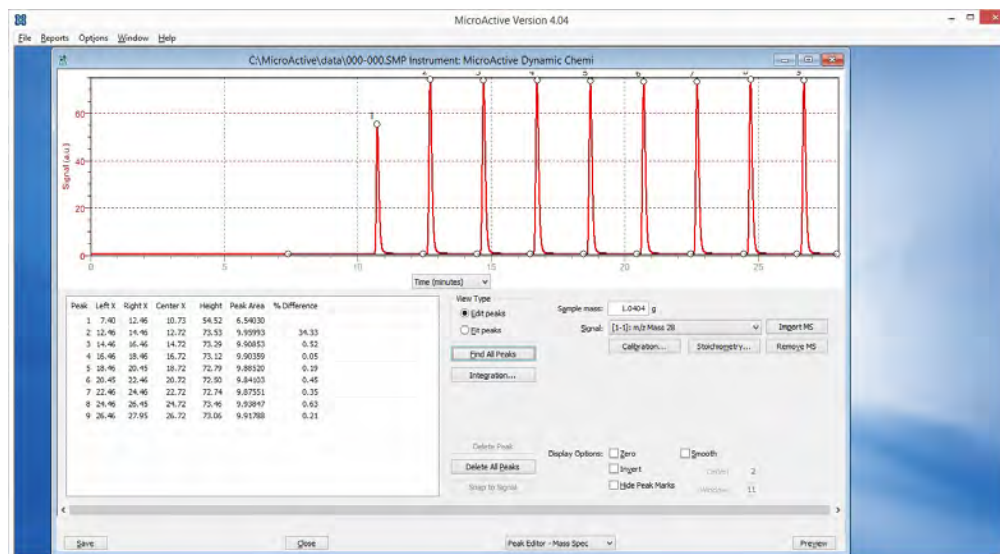


Figure 14: Using the Peak Editor in MicroActive

APPLICATION NOTE 026

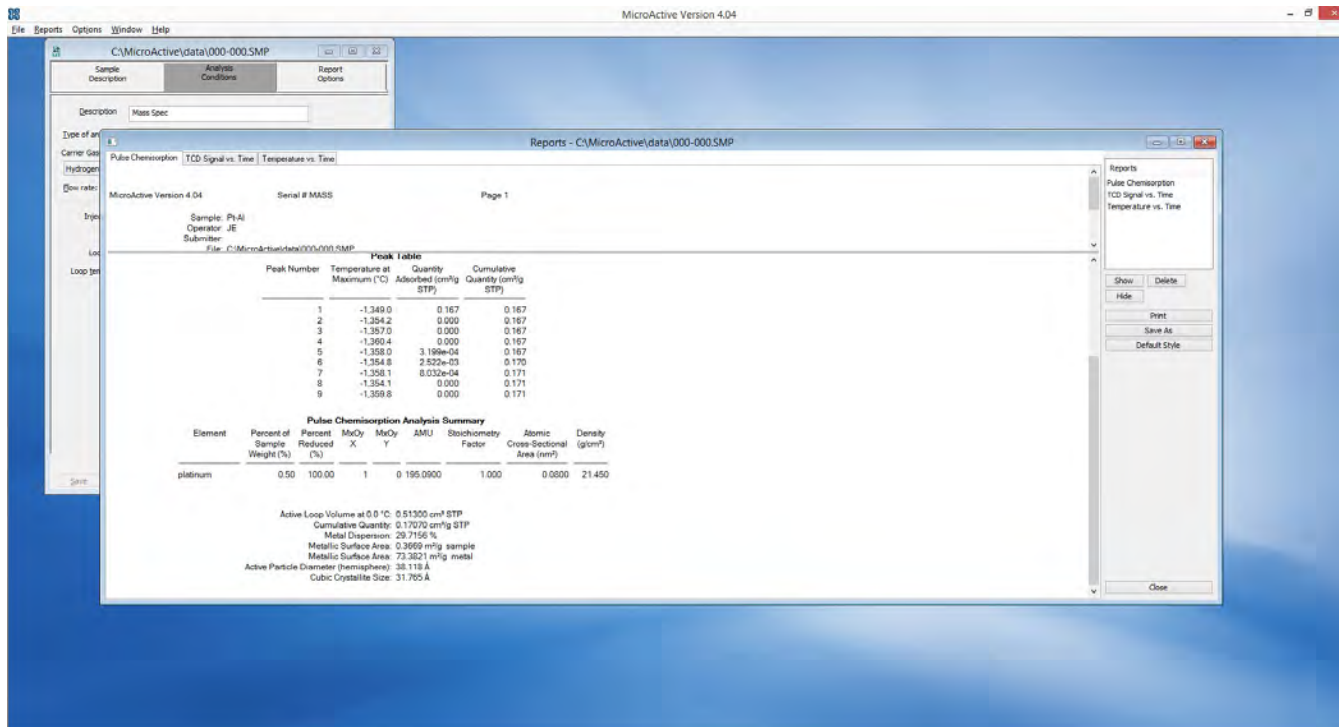


Figure 15: The Pulse Chemisorption report

Click Save and then Preview to generate the pulse chemisorption report. The dispersion will be calculated and reported as seen in Figure 15. Note that the dispersion values will be low if the final sample mass is not entered. The sample

will lose some mass via water loss during the reduction phase of the analysis. The final sample mass can be entered into the analysis file and the report can then be regenerated.

Effect of O₂ Traces in the Carrier Gas on Quantifying the Active Species in Catalysts

Simon Yunes, Justin Hardwick, Pat Wommack and Jason Exley. Micromeritics, Particulates System

Determination of the dispersion of active species on catalysts is a tremendous tool to discover and predict the activity of the catalyst. Thus, dispersion of active species indicate the quantity of active particles located on the surface of a catalyst that are accessible and have a direct contact with the reactant molecules that have to react and produce a new substance. Hence, a correct measurement of the dispersion of the active species predict the activity of the catalyst for a specific catalytic process.

The technique comprises the reduction of the active particles in the catalyst at elevated temperature. Usually Hydrogen is widely used for this task and that could be used as pure hydrogen or a mixture of H₂ balanced inert gas. Upon completion of reduction and the catalyst temperature is brought back to room temperature, the catalyst is then titrated by using a calibrated loop and dosing known amount of active gas, usually is carbon monoxide or hydrogen. Therefore and upon saturation, the amount of adsorbed active gas is being calculated and related to the accessible active species on the surface of the catalyst. This method of titration is by far, the most useful tool to predict the activity of the catalyst.

The problem arises during the removal of the remaining hydrogen on the catalyst after reduction. This task is usually done by flowing an inert gas over the sample at the same reduction temperature. Removal of the remaining H₂ can take some time, could take one hour or sometimes more than that depending of the active particles themselves and their ability to retain H₂. Upon removal of the remaining H₂, the sample temperature is brought back to room temperature having the inert gas still flowing over the sample. If the inert gas being used, contains traces of O₂, will slightly oxidize the freshly produced reduced particles, and hence, change the composition of the accessible particles on the surface that used to determine the dispersion.

Experimental

A 0.5% Pt/Alumina Micromeritics reference material with a 35 percent dispersion plus or minus 5, was considered for the experiments. The sample was first reduced by flowing a 100 ml/min of hydrogen at 400C for one hour. Upon reduction, sample was swept by 100 ml/min of Helium at the reduction temperature for 30 minutes. Then the sample temperature was reduced to room temperature at which pulse of active gas was carried out until saturation. A mass spectrometer Cirrus II was used as a detector to follow the masses involved in the analysis.

The first analysis was carried out after reduction and a complete removal of the remaining hydrogen. Pulse of 0.0513 ml were carried out and signal of mass 2 (H₂) was followed by mass spectrometer to ensure complete saturation of the sample. Figure 1 shows the spectrum of H₂ where one pulse was completely adsorbed while peaks 5 to 9 show complete saturation and were taken into account for the determination of the total amount of H₂ adsorbed. (See table 1)

Following this first analysis, sample was taken back to 400C under the flow of 100 ml/min of helium to remove all adsorbed H₂. A complete removal of H₂ at 400C was followed by the signal of H₂ (mass 2) on the Mass Spectrometer. Right after, the sample was brought to room temperature under the same flow of helium. At this step, a 0.1 ml of air (approximately 0.03ml of oxygen) was injected using a syringe to the carrier gas in order to simulate the presence of traces of O₂ in case of the use of a contaminated Helium in order to see its effect on the dispersion. Figure 2 shows for the same pulse technique, larger amount of H₂ being adsorbed by the sample. In this case, 4 full injections were completely adsorbed by the same sample shown in figure 1. This effect demonstrate that the presence of traces of O₂ in the inert gas used to clean the sample from the remaining H₂ after reduction, will badly alter the dispersion results. In this case the dispersion was inflated by a factor of 3 approximately. (See table 2)

APPLICATION NOTE 030

The same procedure described above was repeated but Carbon Monoxide was used as active gas instead of H₂.

First, the analysis was carried out without the passivation procedure described above. Result of CO chemisorption indicated on figure 3, yield the correct value of the dispersion that is 35 percent plus or minus 5. (See table 3)

Figure 4 shows two spectra corresponding to the CO pulse chemisorption. The above one demonstrates the spectrum

of CO coming from the passivated sample as was done in the case above for hydrogen. A 1/3 of the first pulse was adsorbed while the rest of the peaks indicate saturation.

The below spectrum of figure 4 correspond to mass 44 at indicates the formation of Carbon dioxide while CO being pulsed on an oxidized or passivated sample. The final result of dispersion indicates that the presence of traces of O₂ is responsible for the overestimation of the dispersion on the Micromeritics reference material. (see table 4)

Results of Hydrogen Chemisorption:

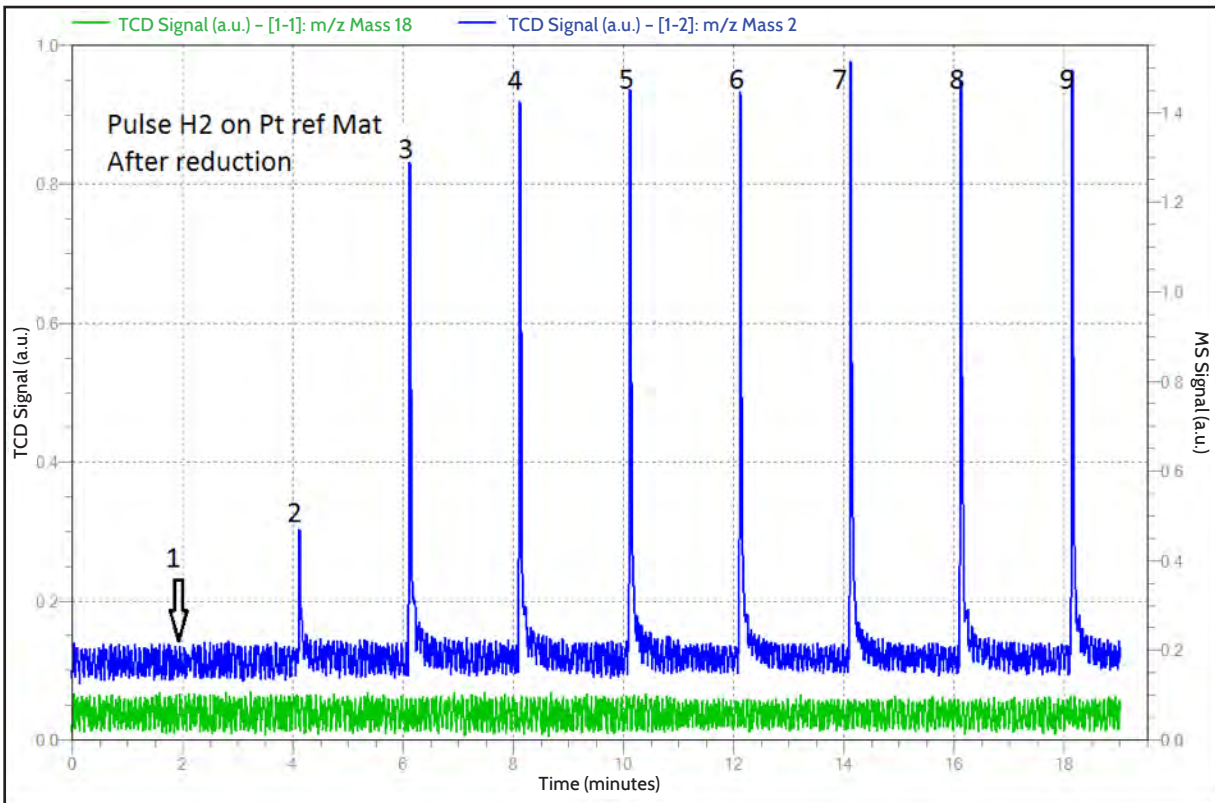


Figure 1: Pulses of H₂ over freshly reduced material

APPLICATION NOTE 030

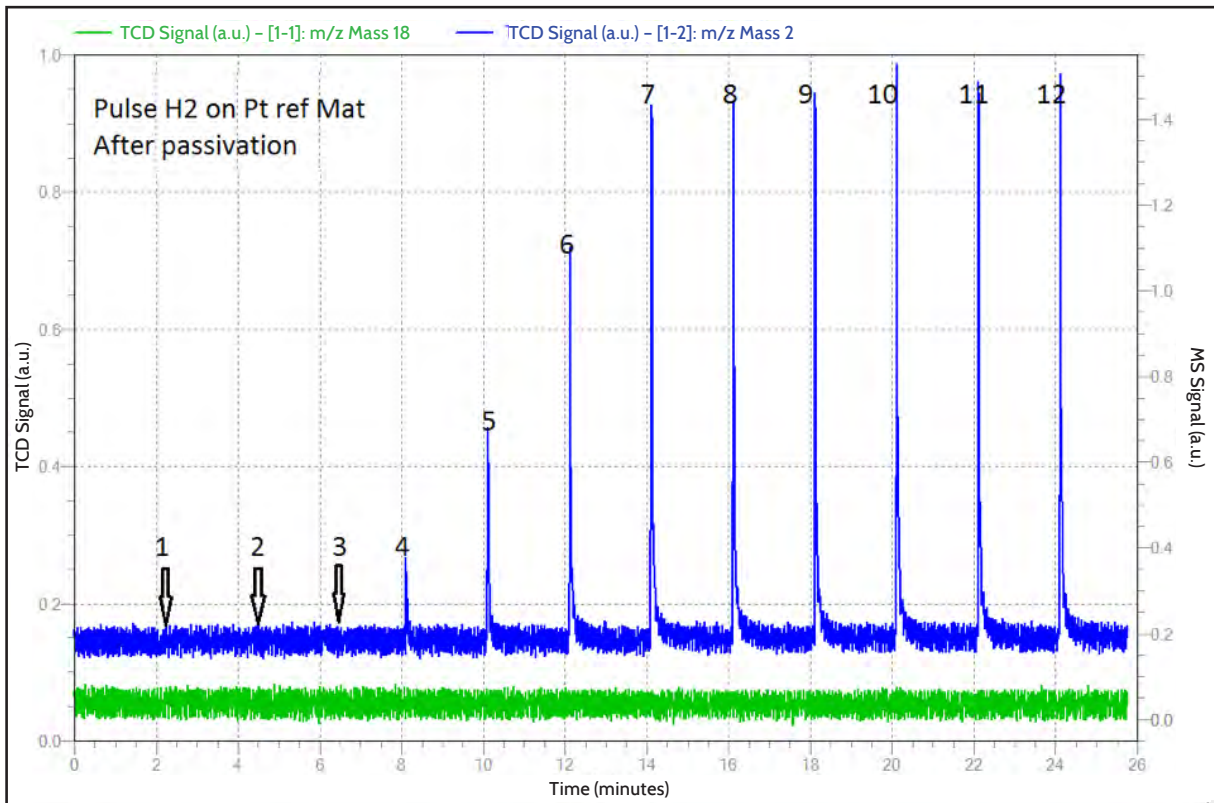


Figure 2: Pulse of H₂ over freshly oxidized material

APPLICATION NOTE 030

Result of quantities adsorbed as well as dispersion for each analysis are shown here below:

| Peak Table | | | | | | | | |
|-------------|-----------------------------|--|--|--|--|--|--|--|
| Peak Number | Temperature at Maximum (°C) | Quantity Adsorbed (cm ³ /g STP) | Cumulative Quantity (cm ³ /g STP) | | | | | |
| 1 | 303.8 | 5.012e-02 | 5.012e-02 | | | | | |
| 2 | 303.0 | 4.095e-02 | 9.107e-02 | | | | | |
| 3 | 302.2 | 7.009e-03 | 9.808e-02 | | | | | |
| 4 | 301.7 | 2.234e-03 | 0.100 | | | | | |
| 5 | 301.1 | 1.236e-03 | 0.102 | | | | | |
| 6 | 300.6 | 1.501e-03 | 0.103 | | | | | |
| 7 | 300.5 | 0.000 | 0.103 | | | | | |
| 8 | 301.0 | 2.130e-03 | 0.105 | | | | | |

| Pulse Chemisorption Analysis Summary | | | | | | | | |
|--------------------------------------|------------------------------|---------------------|--------|--------|----------|----------------------|--|------------------------------|
| Element | Percent of Sample Weight (%) | Percent Reduced (%) | MxOy X | MxOy Y | AMU | Stoichiometry Factor | Atomic Cross-Sectional Area (nm ²) | Density (g/cm ³) |
| platinum | 0.50 | 100.00 | 2 | 0 | 390.1800 | 2.000 | 0.0800 | 21.450 |

Active Loop Volume at 23.0 °C: 0.04732 cm³ STP
 Cumulative Quantity: 0.10518 cm³/g STP
 Metal Dispersion: 36.6195 %
 Metallic Surface Area: 0.4522 m²/g sample
 Metallic Surface Area: 90.4312 m²/g metal
 Active Particle Diameter (hemisphere): 30.932 Å
 Cubic Crystallite Size: 25.777 Å

Table 1: Quantification and measurement of dispersion on the freshly reduced sample determined by H₂ chemisorption

| Peak Table | | | | | | | | |
|-------------|-----------------------------|--|--|--|--|--|--|--|
| Peak Number | Temperature at Maximum (°C) | Quantity Adsorbed (cm ³ /g STP) | Cumulative Quantity (cm ³ /g STP) | | | | | |
| 1 | 303.2 | 5.661e-02 | 5.661e-02 | | | | | |
| 2 | 302.9 | 5.668e-02 | 0.113 | | | | | |
| 3 | 302.0 | 5.642e-02 | 0.170 | | | | | |
| 4 | 301.3 | 5.110e-02 | 0.221 | | | | | |
| 5 | 301.0 | 3.657e-02 | 0.257 | | | | | |
| 6 | 300.4 | 1.951e-02 | 0.277 | | | | | |
| 7 | 300.5 | 2.074e-03 | 0.279 | | | | | |
| 8 | 300.4 | 3.440e-04 | 0.279 | | | | | |
| 9 | 300.6 | 0.000 | 0.279 | | | | | |
| 10 | 300.4 | 0.000 | 0.279 | | | | | |
| 11 | 300.5 | 1.087e-03 | 0.280 | | | | | |
| 12 | 300.6 | 0.000 | 0.280 | | | | | |

| Pulse Chemisorption Analysis Summary | | | | | | | | |
|--------------------------------------|------------------------------|---------------------|--------|--------|----------|----------------------|--|------------------------------|
| Element | Percent of Sample Weight (%) | Percent Reduced (%) | MxOy X | MxOy Y | AMU | Stoichiometry Factor | Atomic Cross-Sectional Area (nm ²) | Density (g/cm ³) |
| platinum | 0.50 | 100.00 | 2 | 0 | 390.1800 | 2.000 | 0.0800 | 21.450 |

Active Loop Volume at 0.0 °C: 0.05130 cm³ STP
 Cumulative Quantity: 0.28039 cm³/g STP
 Metal Dispersion: 97.6212 %
 Metallic Surface Area: 1.2054 m²/g sample
 Metallic Surface Area: 241.0739 m²/g metal
 Active Particle Diameter (hemisphere): 11.603 Å
 Cubic Crystallite Size: 9.669 Å

Table 2: Quantification and measurement of dispersion on the freshly re-oxidized sample determined by H₂ chemisorption

APPLICATION NOTE 030

Results obtained by CO chemisorption:

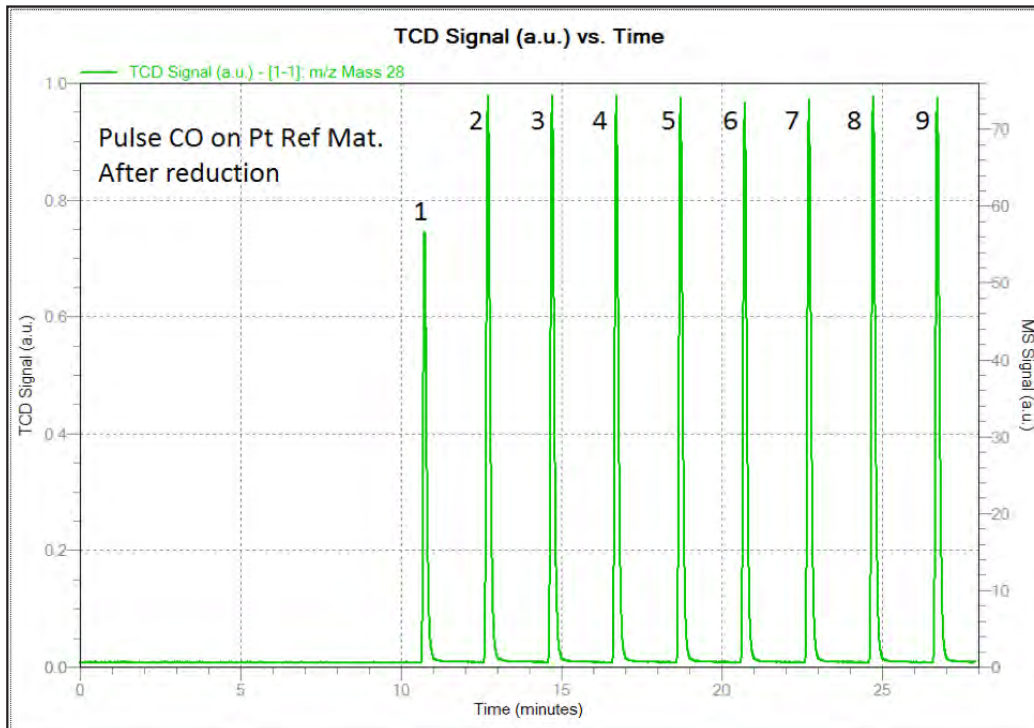


Figure 3: This figure shows the CO pulse chemisorption on the freshly reduced sample

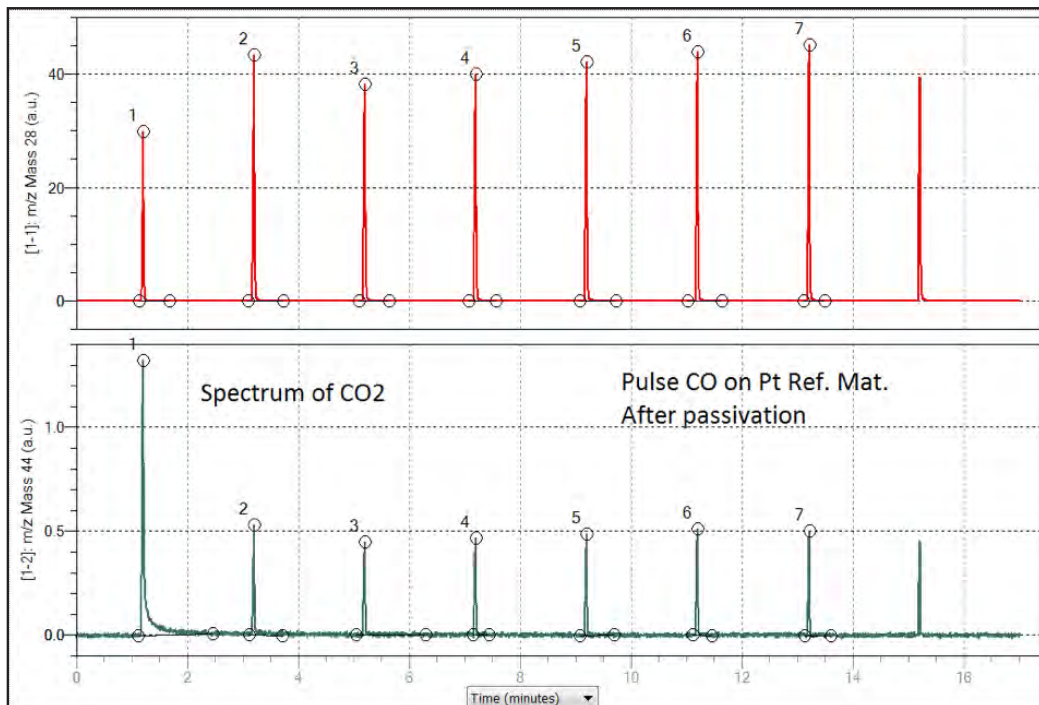


Figure 4: This figure shown the CO pulse chemisorption on the passivated sample (above) while the spectrum below shown the formation of Carbon Dioxide upon each pulse of CO

APPLICATION NOTE 030

| Peak Table | | | | |
|-------------|-----------------------------|--|--|--|
| Peak Number | Temperature at Maximum (°C) | Quantity Adsorbed (cm ³ /g STP) | Cumulative Quantity (cm ³ /g STP) | |
| 1 | -1,622.2 | 0.192 | 0.192 | |
| 2 | -1,627.3 | 0.000 | 0.192 | |
| 3 | -1,630.1 | 0.000 | 0.192 | |
| 4 | -1,633.6 | 0.000 | 0.192 | |
| 5 | -1,631.2 | 1.209e-03 | 0.193 | |
| 6 | -1,628.0 | 4.239e-03 | 0.197 | |
| 7 | -1,631.3 | 2.089e-03 | 0.199 | |
| 8 | -1,627.3 | 0.000 | 0.199 | |
| 9 | -1,633.0 | 0.000 | 0.199 | |

| Pulse Chemisorption Analysis Summary | | | | | | | | |
|--------------------------------------|------------------------------|---------------------|--------|--------|----------|----------------------|--|------------------------------|
| Element | Percent of Sample Weight (%) | Percent Reduced (%) | MxOy X | MxOy Y | AMU | Stoichiometry Factor | Atomic Cross-Sectional Area (nm ²) | Density (g/cm ³) |
| platinum | 0.50 | 100.00 | 1 | 0 | 195.0900 | 1.000 | 0.0800 | 21.450 |

Active Loop Volume at 22.0 °C: 0.47476 cm³ STP
 Cumulative Quantity: 0.19918 cm³/g STP
 Metal Dispersion: 34.6731 %
 Metallic Surface Area: 0.4281 m²/g sample
 Metallic Surface Area: 85.6245 m²/g metal
 Active Particle Diameter (hemisphere): 32.668 Å
 Cubic Crystallite Size: 27.224 Å

Table 3: Quantification and measurement of dispersion on the freshly reduced sample determined by CO chemisorption

| Peak Table | | | | |
|-------------|-----------------------------|--|--|--|
| Peak Number | Temperature at Maximum (°C) | Quantity Adsorbed (cm ³ /g STP) | Cumulative Quantity (cm ³ /g STP) | |
| 1 | 303.7 | 0.263 | 0.263 | |
| 2 | 304.1 | 1.843e-02 | 0.281 | |
| 3 | 303.9 | 1.133e-02 | 0.293 | |
| 4 | 303.4 | 4.573e-03 | 0.297 | |
| 5 | 303.8 | 0.000 | 0.297 | |
| 6 | 302.9 | 0.000 | 0.297 | |
| 7 | 302.4 | 0.000 | 0.297 | |

| Pulse Chemisorption Analysis Summary | | | | | | | | |
|--------------------------------------|------------------------------|---------------------|--------|--------|----------|----------------------|--|------------------------------|
| Element | Percent of Sample Weight (%) | Percent Reduced (%) | MxOy X | MxOy Y | AMU | Stoichiometry Factor | Atomic Cross-Sectional Area (nm ²) | Density (g/cm ³) |
| platinum | 0.50 | 100.00 | 1 | 0 | 195.0900 | 1.000 | 0.0800 | 21.450 |

Active Loop Volume at 22.0 °C: 0.47476 cm³ STP
 Cumulative Quantity: 0.29718 cm³/g STP
 Metal Dispersion: 51.7333 %
 Metallic Surface Area: 0.6388 m²/g sample
 Metallic Surface Area: 127.7546 m²/g metal
 Active Particle Diameter (hemisphere): 21.895 Å
 Cubic Crystallite Size: 18.246 Å

Table 4: Quantification and measurement of dispersion on the freshly passivated sample determined by CO chemisorption

Conclusion

It can be concluded from this work that chemisorption technique is highly sensitive to contamination, especially for the inert gas that is used to remove the excess of hydrogen that remains adsorbed by the sample after reduction.

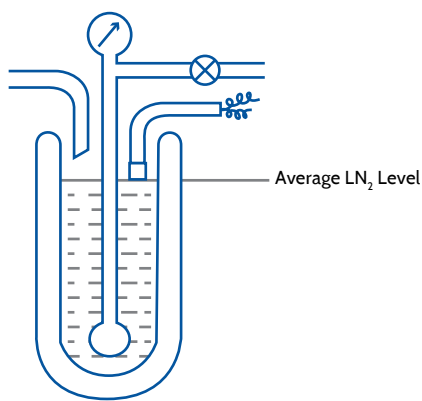
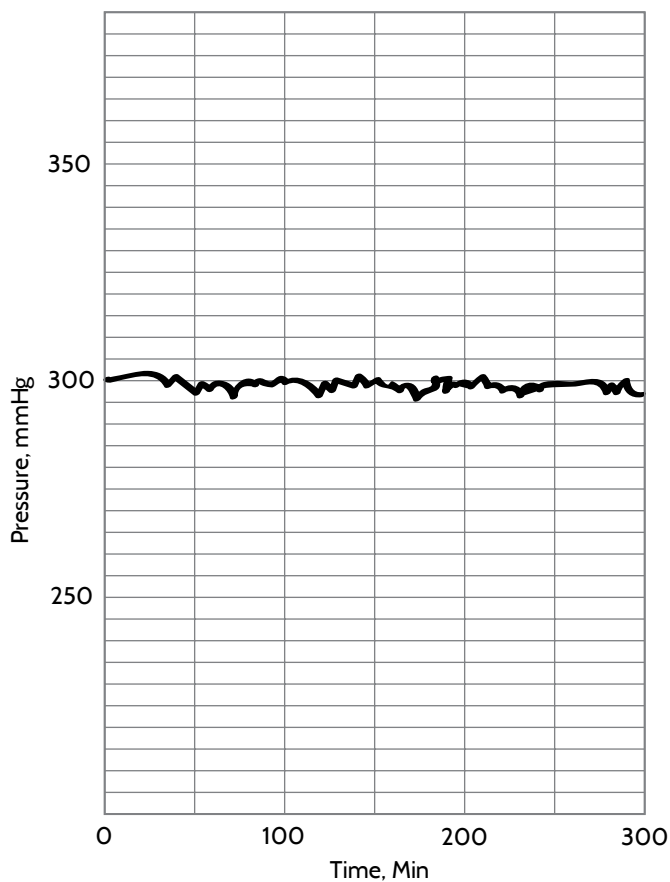
The overestimation of the result will depend on the quantity of contamination existing in the carrier gas. In any case, pure gases are required for a good chemisorption analysis, otherwise, results will not offer any meaning, especially if are related to the activity of the catalyst.

In the case of H_2 chemisorption, a large amount of H_2 is being adsorbed. One part is being adsorbed by the atoms of Platinum, while the large amount of H_2 is being retained or adsorbed by the atoms of O_2 located on the platinum atoms on the surface of the solid. However, it can be affirmed that molecules of H_2 are only adsorbed without reaction as spectrum of water indicates the complete absence of it.

Results from CO chemisorption however, show somehow different results. Carbon Monoxide shows higher activity than H_2 over atoms of Platinum, is capable to remove the O_2 atoms and produce carbon dioxide as has been shown on figure 4 resulting in higher dispersion of the material, table 4.

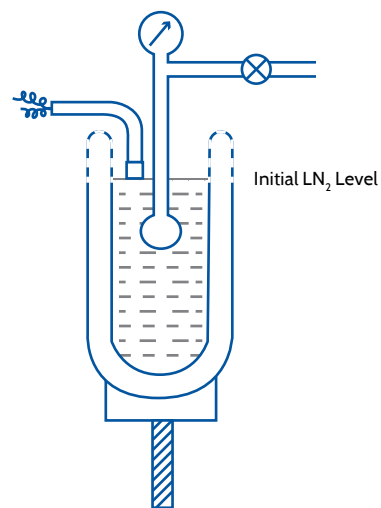
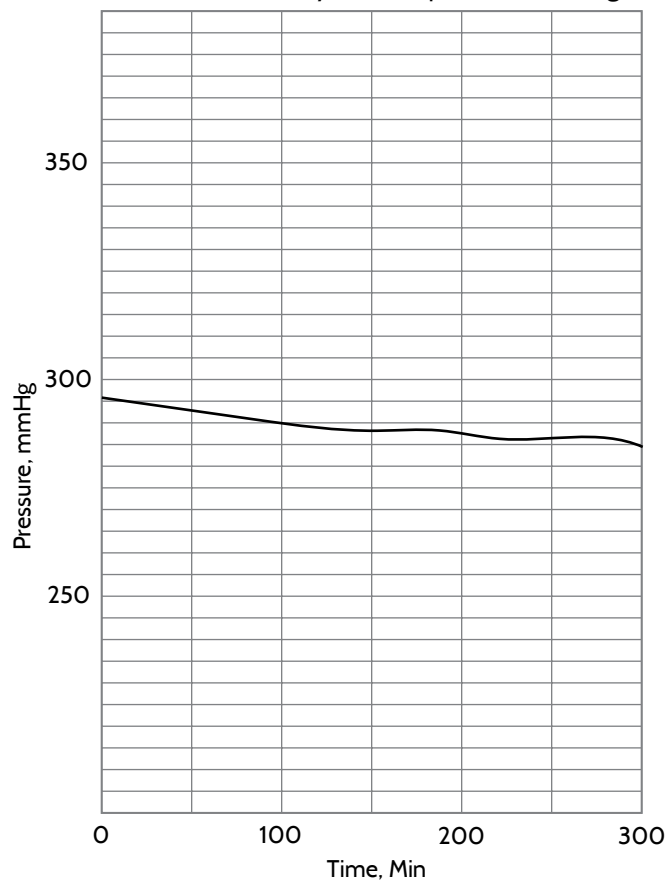
APPLICATION NOTE 167

it does this with minor fluctuations arising due to LN₂ surface disturbances as each increment of new liquid is added. This system accomplishes its intended goal and is attractive for very long analysis time situations. If the time is too long however, ice extracted from the water vapor in the ambient atmosphere will build up choking off access to the entire system. It also requires somewhat expensive peripheral equipment.



Test 2. LN₂ Level Control

Raising the Dewar to compensate for evaporation, as shown by the next diagram, inserts more of the stem leading to the sample and the gas contained in the stem into the expanding cold vapor zone deeper and deeper within the Dewar. This would be expected to produce a decrease in gas pressure, as indeed it does as is revealed by the companion recording.



Test 3. Rising Dewar